Additive Manufacture of Plasma Diagnostic Components
Final Report Phase II

April 16, 2018

Institution:	Woodruff Scientific Inc.
Street Address/City/State/Zip:	4000 Aurora Ave N, Seattle, WA 98103
Principal Investigator:	Dr. Simon Woodruff
Contributors:	James E. Stuber, Morgan J. Quinley, Paul A. Melnik, Paul E. Sieck, Katherine Chun, Trevor Smith, Alexander Card, Sett You, Carlos Romero-Talamás, Will Rivera
Telephone Number:	206-905-9477
Email:	simon@woodruffscientific.com

DOE/Office of Science:	Office of Fusion Energy Sciences
Technical Contact:	Dr. Francis Thio
DOE Award Number:	DE-SC0011858
Consultants/subcontractors:	Dr. Carlos Romero-Talamás, University of Maryland, Baltimore County Prof. Sett You, University of Washington Dr. Ben Utela, Independent consultant Mr. Steven Diesburg, PATH

Executive Summary

There is now a well-established set of plasma diagnostics (see e.g. [3]), but these remain some of the most expensive assemblies in fusion systems since for every system they have to be custom built, and time for diagnostic development can pace the project. Additive manufacturing (AM) has the potential to decrease production cost and significantly lower design time of fusion diagnostic subsystems, which would realize significant cost reduction for standard diagnostics. In some cases, these basic components can be additively manufactured for less than 1/100th costs of conventional manufacturing.

In our DOE Phase II SBIR, we examined the impact that AM can have on plasma diagnostic cost by taking 15 separate diagnostics through an engineering design using Conventional Manufacturing (CM) techniques, then optimizing the design to exploit the benefits of AM. The impact of AM techniques on cost is found to be in several areas. First, the cost of materials falls because AM parts can be manufactured with little to no waste, and engineered to use less material than CM. Next, the cost of fabrication falls for AM parts relative to CM since the fabrication time can be computed exactly, and often no post-processing is required for the part to be functional. We find that AM techniques are well suited for plasma diagnostics since typical diagnostic complexity comes at no additional cost. Cooling channels, for example, can be built in to plasma-facing components at no extra cost. Fabrication costs associated with assembly are lower for AM parts because many components can be combined and printed as monoliths, thereby mitigating the need for alignment or calibration. Finally, the cost of engineering is impacted by exploiting AM design tools that allow standard components to be customized through web-interfaces. Furthermore, we find that concept design costs can be impacted by scripting interfaces for online engineering design tools.

Our commercialization plan is to use AM to develop diagnostics, offering complete systems at substantially lower cost than conventional manufacturing. We seek to demonstrate this technology in fusion applications and then aspire to service a wider scientific instrumentation market worldwide.

Contents

Chapter 1

Introduction

1.1 Measuring plasma performance is a grand challenge

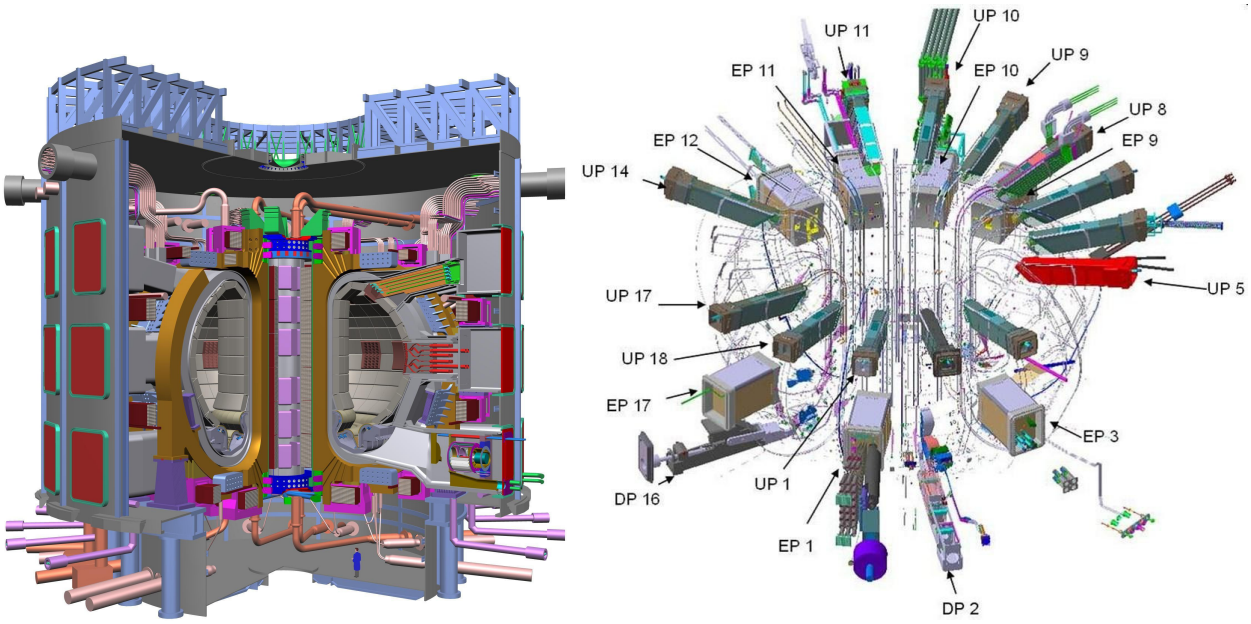

Figure 1.1: a) ITER currently under construction in Cadarace, France. ITER began as a Reagan-Gorbachov initiative in 1985, DT ops now planned for 2027. b) About 50 individual measurement systems will help to control, evaluate and optimize plasma performance in ITER and to further understanding of plasma [4]. These include lasers, X-rays, neutron cameras, impurity monitors, particle spectrometres, radiation bolometers, pressure and gas analysis, and optical fibres.

In the next few years, several major fusion experiments will begin operation [1]. For example, ITER is the largest ever fusion experiment that aims to demonstrate the technological and scientific feasibility of fusion energy. ITER aims to deliver ten times the power it consumes. From 50MW of input power, the ITER machine is designed to produce 500MW of fusion power and aims to be the first fusion experiment to produce net energy. To measure the plasma performance, numerous 'plasma diagnostics' are situated close to the burning plasma (see Fig. 1.1 b)). Diagnostics are sensors that measure all important plasma parameters [3] in order to assess performance, and provide feedback for control systems. The ITER diagnostic system will comprise of about 50 individual measuring systems drawn from the full range of modern plasma diagnostic techniques, including lasers, X-rays, neutron cameras, impurity monitors, particle spec-

trometers, bolometers, pressure and gas analysis, and optical fibres. Some diagnostics must be exposed to extreme environments. Electrostatic probes are designed to enter the plasma. Magnetic probes are usually protected beneath heat shielding. Optical diagnostics have endoscopes to protect most components, but 1st mirrors can be exposed to high temperatures. RF diagnostics will also have horns or antennae close to plasma.

Plasma diagnostics are therefore highly complex (see Fig. 1.2) and require very detailed engineering design for specific applications (highly customized). Because some components are in proximity to the burning plasma, they will degrade over time and require periodic replacement. Complexity is often due to cooling requirements and integration with other systems. Component requirements are constantly evolving due to scientific requirements. Since most fusion diagnostics are experimental (i.e. have never been tried in a fusion environment) they can be viewed as prototypes. There are currently no mass-produced diagnostics, however components are readily available 'off the shelf.'

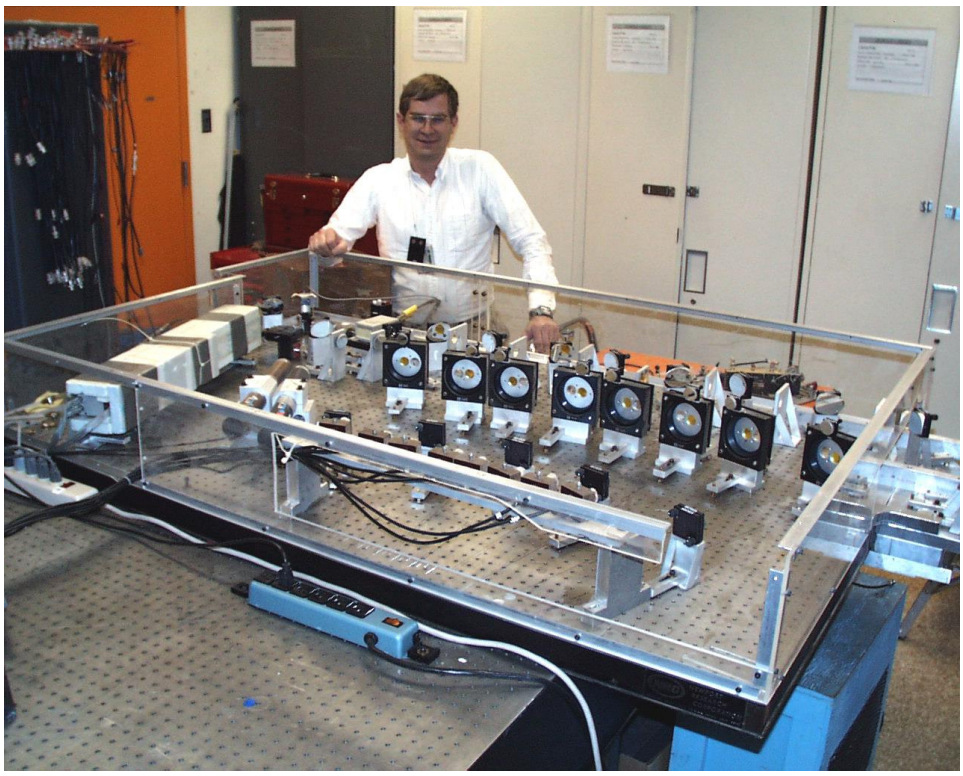

Figure 1.2: An interferometer with 8 chords. On the optical bench (floating on vibration isolation legs) are over 150 separate components - lasers, mirrors, beam splitters, detectors, etc. Benches don't usually see neutrons.

1.2 Fusion environment places stringent demands on materials used in diagnostics

A primary challenge is to interface a burning plasma at 10M degrees Celsius to a room temperature environment. This challenge is being taken up by materials scientists around the world [2]. Materials used in plasma-facing components must withstand high power loads, as high as 5MW/m^2 in steady state (for example in the divertor regions) to 50MW/m^2 in what are termed 'off-normal events' such as plasma disruptions or instabilities that cause local peaking in incident power, which could cause their ablation (low Z preferred) or out-gassing. Components must withstand neutron bombardment: it is expected that radiation damage of

up to 200 displacements per atom (dpa) must be tolerated (expecting 7-20dpa per year - much higher than for fission). Radioactive waste must be minimized by selection of low activation materials. Safety is also a principal concern in the selection of materials. Finally materials selection must be economic.

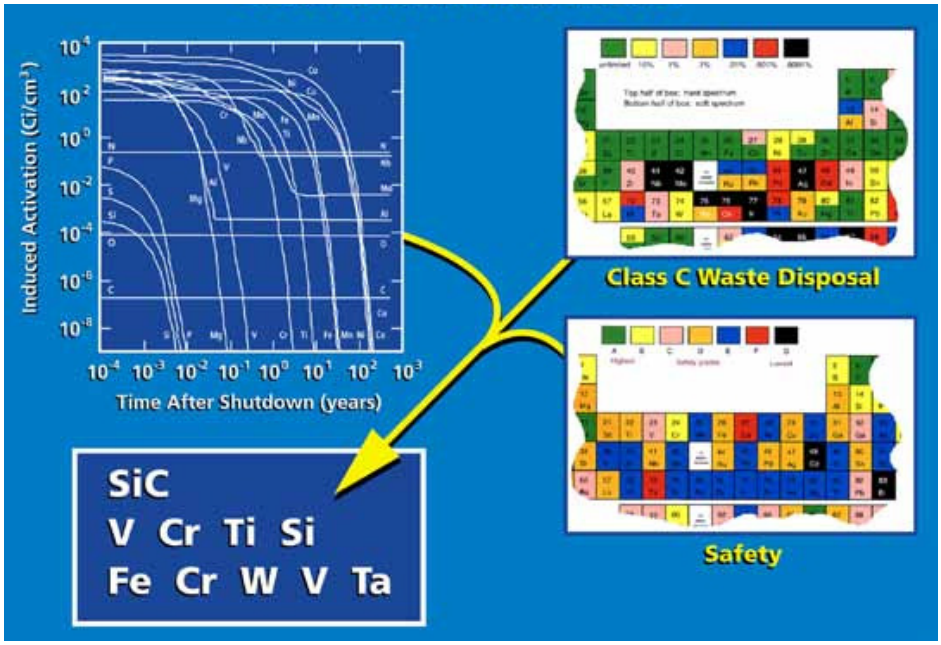

Figure 1.3: Ideal materials must be safe, must minimize rad waste (and be suitable for recycling), and must be economically competitive (high thermal efficiency, acceptable lifetime, reliable).

1.3 Additive Manufacturing (AM) is ideally suited for plasma diagnostics

Serving an initial market for rapid prototyping (since 1980's) AM has evolved to the point that fully functional components (i.e. not just the prototype) can be printed [6]. There are now a diverse set of methods, most of which are patented (though some patents now expiring). The US recognizes potential of this disruptive tech and is preparing (e.g. [5]). It has the benefits of low/no waste (only the material needed in the component is used), low energy (only the energy needed to produce the part is used), and has a predictable machine time (reducing uncertainty in costing). Building objects up layer by layer, instead of cutting away material can reduce material needs and costs by up to 90% [7]. Printing objects as a single piece without welding or bolting makes them both stronger and lighter. The is no extra cost for complexity, printed parts can be functional thereby reducing costs associated with assembly. Print accuracy varies from 100-300 microns (ebeam melting shown schematically in Fig. 1.4) to 25 microns for desktop stereolithography (SLA), and furthermore to submicron (nm) sizes for research systems based on SLA. Most commercial Fused Deposition Modeling (FDM) printers have accuracy within 50 microns. It is expected that the cost of printing will fall and accuracy increase rapidly in coming years as technology is adopted and put into practice.

1.4 Structure of this report

In Chapter 2 we outline the methods, assumptions and procedures for addressing the objectives of our Phase II work. While we proposed to address the work on a diagnostic basis, we have found it more instructive to summarize the findings within the context of a cost model. In Chapter 3 we discuss the results according to

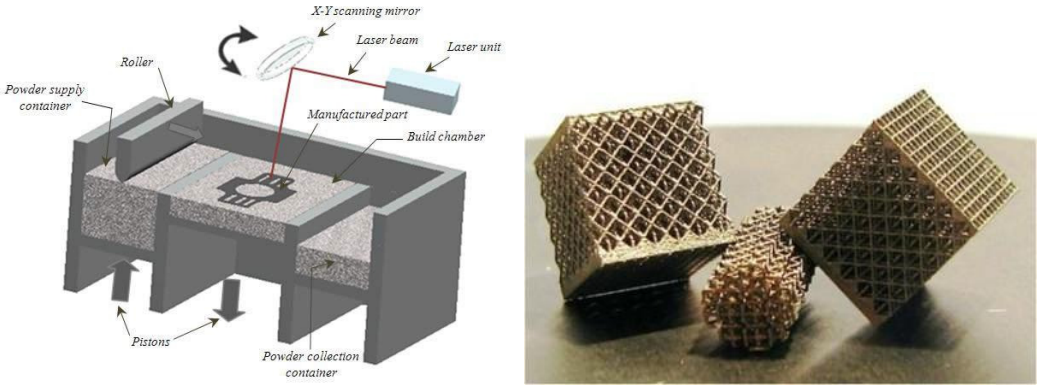

Figure 1.4: a) Method shown here is laser sintering of powder (metals, plastics, ceramics) in which the bed covered with a fine layer (few microns) of material, and a high power laser is scanned over the surface, melting it to the layer below. The bed is lowered, a fresh layer of power is rolled across and process is repeated. b) Complex alumina components, with lattice structure to reduce total volume of materials. Similar components can be printed in metals, and plastics.

the separate cost categories to show how AM impacts costs relative to CM. Chapter 4 contains the conclusions of the Phase II work, and Chapter 5 outlines some recommendations for commercialization.

We include extensive appendices pertaining to all aspects of the work undertaken, including papers and contributions from organizations subcontracted for this work (University of Washington and University of Maryland Baltimore County).

Chapter 2

Methods, Assumptions and Procedures

2.1 Method

The overarching aim of the work was to determine if the use of AM could significantly impact the cost of the diagnostic. We therefore developed a cost model (based mainly on our usual quoting methods) that comprises the labor costs associated with design, fabrication and testing and material costs incurred throughout the process. To compare costs between CM and AM, we performed conventional concept and engineering designs for each separate diagnostic system. The method for design review is mapped out in numerous texts ([8]). The design reviews typically ran for a day and enlisted all collaborators and consultants.

For the Phase I effort, we had to constrain the total number of diagnostics that we could take through this process due to time and cost constraints. We opted to consider pre-existing designs that had a body of literature to support them (see Table 2.1), and this helped to develop both a working engineering model and a bill of materials / components. We then prioritized the list of materials according to cost and sought to determine which components could be produced by AM. There was a two step design process: 1) obtain original functionality of components; 2) optimize full assembly for AM. Where it was helpful to understand costs further, we printed prototypes.

Diagnostic	Example PI	Example Device
Magnetic field coil	Strait [9] [10]	DIII-D (GA)
Magnetic coil array	Strait	DIII-D (GA)
Rogowski coil	Strait	DIII-D (GA)
Calibration jig	Lambert	(KCL)
Langmuir probe		JET (CCFE)
RFEA	Pitts [11]	JET (CCFE)
HeNe interferometer	Kumar	BSE (Caltech)
CO2 interferometer	Carlstrom [12]	DIII-D (GA)
CO2 polarimeter	Akiyama	LHD (NIFS)
Microwave reflectometer	Willis	LDX (Columbia)
Thomson Scattering (Yag)	McLean	SSPX (LLNL)
Thomson Scattering (Ruby)	Golingo	ZAP (UW)
Inverse Compton	Wurden	DIII-D (LANL/GA)
Visible Spectrometer		
Bolometer	Wurden	TFTR (PPPL)
Scintillators	Mishnayot	

Table 2.1: Scope of diagnostics examined for the Phase I study.

2.2 Cost model

We developed a cost model (based on our usual quoting methods), and established a shared spreadsheet on Google Docs for all collaborators to contribute costing information for 15 individual diagnostics. An example of one of the costing exercises is included in the results section (see Fig. 3.5), and most of the costing analyses are included in the appendix for other diagnostics. The costing equation shown in Equation 2.1 consists of labor and materials as direct costs, and we included overhead on labor and materials, which are assumed the same for purposes of this report. A contingency is applied to materials cost. We scaled the costing from 1 to 10 units to determine if there were cost savings that occur with higher unit production.

$$C_{Total} = [(C_{CDR} + C_{EDR} + C_{PDR} + C_{Fab} + C_{Test}) * f_{Labor} + C_{Materials} * f_{Cont} + C_{Ship}] * f_{G\&A} \quad (2.1)$$

where costs are broken into labor, materials and overhead. For labor costs: C_{CDR} is the cost associated with the Physics Design Review; C_{EDR} and C_{PDR} are the costs associated with the Engineering and Product Design Reviews (prelim and final designs); C_{Fab} is the cost of fabrication; C_{Test} is cost of testing. For these roles we have assumed a full time scientist or engineer billing at \$120/hr (fully loaded). Where some tasks require shop or technicians, we have assumed \$90/hr (based on experience in Seattle with local machine shops). For materials costs, $C_{Materials}$ is cost of materials and a contingency factor is applied, f_{Cont} for CM estimating purposes (ignored for this work, since exact material quantities can be computed for AM). Shipping costs, C_{Ship} are ignored for this work, though it should be noted that one can utilize local manufacture to reduce these to near zero. Overhead is computed in terms of labor, f_{Labor} and a general and administrative cost, $f_{G\&A}$. Note that we are calculating the cost of components and assemblies that will require periodic service and replacement - for example a plasma-facing mirror may well require replacement after a number of hours, which over the life of the experiment could become a principal cost of the diagnostic. We ignore these costs for now, and bracket the subject for discussion later. We are also ignoring costs associated with learning the intricacies of working with new manufacturing techniques (we strongly advise not buying a printer and instead using a printing service). The primary question we sought to answer in the context of the cost model was: $C_{Total\,AM} << C_{Total\,CM}$? (AM = Additive Manufacture, CM = Conventional Manufacture).

2.3 Out-gas testing: component testing in vacuum

In order to determine if we could further impact cost of materials, we are considering the plating of non-metallic components to reduce outgassing, and tested the outgas characteristics in the University of Maryland test stand (shown in Fig. 2.1). The test stand includes mass spectrometry equipment in a chamber capable of achieving ultra high vacuum (UHV), and was recently upgraded to achieve lower baseline vacuum levels as well as allow for faster turnaround times between test samples. The chamber contains one roughing pump, one turbomolecular pumps, and an ion pump that can be isolated with gate valves. A mass spectrometer capable of measuring masses up to 200 amu (ExTorr, Model XT200) with partial pressure resolution up to 10^{-10} Torr. A quick-access port allows test parts to be exchanged in and out of the chamber without having to bring the entire chamber up to atmospheric pressure. This equipment has been upgraded to include outgassing measurements at heated conditions with powers greater than 100 kW/m^2. A heater plate specially built for this purpose is shown in Fig. 2.2. We are currently upgrading to test part immersion in glow discharge plasmas. A large displacement translation stage will allow a sample to be placed at varying distances from heat and plasma sources without interruption of mass spectrometry or UHV conditions. Results from outgas testing can be found in publications in the appendix.

2.4 Functionality testing: component testing in situ

Throughout the prototyping stage, we worked with the University of Washington to test functionality of AM components in situ. In other words we installed AM component prototypes into functioning diagnostics. The lab commissioned a number of diagnostics including a spectroscopic tomographic diagnostic to measure

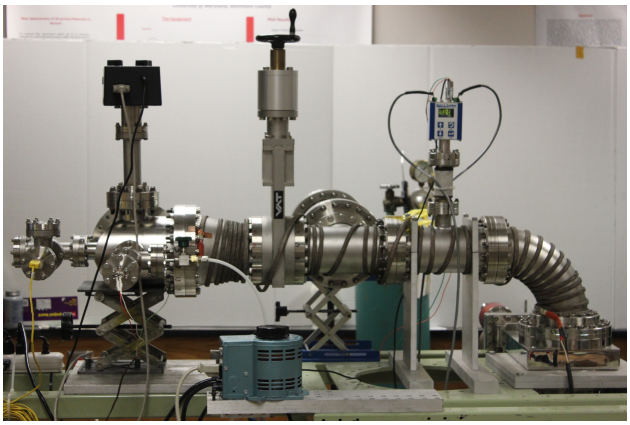

Figure 2.1: UMBC test facility: flexible configuration for surface testing, mass spectrometry and out-gas testing.

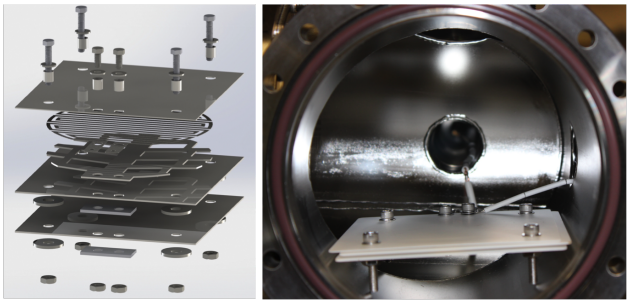

Figure 2.2: Heater plate inside the UMBC test facility.

3D plasma velocities in closed volumes, interferometers, retarding grid energy analyzers, and magnetics. Analysis of these components can be found in the appendix.

Chapter 3

Results and Discussion

3.1 Costs of Fabrication, C_{Fab}

Costs of 3D printing are compared with CM (CNC mill, lathe, drill press, etc). One primary advantage of AM is that complexity adds very little cost when compared to CM. In general AM is less expensive than CM for complex parts. AM also allows pre-assembly and printing of monolithic parts that impact assembly costs. AM allows fabrication of parts that are impossible to engineer with CM. Energy efficient processes and less material waste reduces overall costs. C_{Fab} is reduced by up to 90% in some cases.

3.1.1 C_{Fab} example: Magnetic coils

We considered the DIII-D case shown in Fig. 3.1, consists of alumina rods mounted on Inconel substrate with MgO insulated coaxial turns that form the coil. We sought to optimize the design for AM by removing most of the assembly and developing a modular coil design with turns (of arbitrary cross-section) that could be printed in metal and post-processed with a ceramic coating, thereby replacing a multi-material assembly with 2 step AM piece. Modular design of AM coil allows various magnetic coil configurations - Rogowskis and linear arrays can be built up by printing many of the same component, and arranging in a linear array. Pancake coils, saddle coils, or any coil with complex geometry can be printed at significantly lower costs. C_{Fab} impacted by up to 90% in components and full assembly. In summary, the cost of magnetic subsystems can be significantly impacted by choice of monolithic modular coil design that can then be replicated to produce other diagnostic functionality. The AM process removes the requirement for time-consuming assembly.

3.1.2 C_{Fab} example: Calibration jig

An example of a calibration jig consisting of a Helmholtz coil with 150 turns of 24AWG wire on each spool is shown in Fig. 3.2. Magnetic calibration proceeds by placing a pick-up coil into a known magnetic field. In this case, the jig is designed for a 6mm diameter coil form to be inserted along the axis hole. A second diametric hole is provided for calibration of coils mounted perpendicular to the first set. The design of the jig proceeded by development of a monolith, which was then split into three components (after numerous fails) for printing locally using FDM printer, before sending monolith off to a plastic powder sintering printer. Finally the component engineering design was scripted (see section below) so that .stl files could be written when the user specifies a minimum set of constraints. In summary, the principal costs associated with the design of the calibration jig were not associated with the printing at all, but rather with the winding of the coils (fabrication of winding jig, and set up). Initially, we considered the printing of coils with conductive media per printed PCBs, although this technology is not yet sufficiently mature (see section below on C_{Fab} relating to circuits).

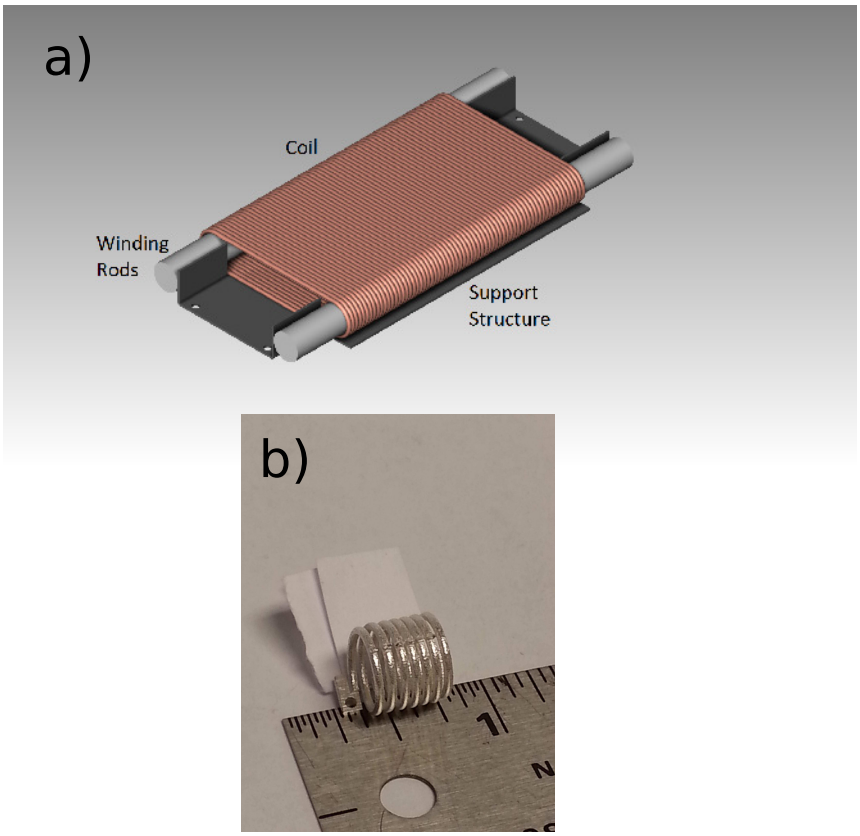

Figure 3.1: a) Strait design; b) our monolithic printing of modular magnetic coil in silver (cost $30) - other materials and techniques are available that significantly impact cost.

3.1.3 C_{Fab} example: Langmuir probe head

An engineering design of an alumina probe head based on existing JET / TCV designs [] was developed. The 1" diameter piece had 5 vertical through holes, one diametric hole at the base, then three angled cuts (which ordinarily would be milled). All edges were given a small radius. Quotes for SLM of the head were obtained for $650. Next we added the WSI logo and a cooling channel in the base and requoted - quotes came back the same. Relative to conventional manufacture (milling a 1" rod), the costs are comparable for the simpler case. We considered other Langmuir probes and heads: those that usually use ceramic (alumina, boron nitride, etc) tubes were less expensive to manufacture conventionally, and it was only when complexity was needed that the AM techniques were less costly. In summary, the cost of Langmuir probe heads can be be impacted if the head is sufficiently complex. The probe head is only one of many components in the assembly, and so the overall cost impact is small if only a single probe head is required. If multiple heads are required (as is the case if the diagnostics are being placed between tiles), then AM can strongly impact C_{Fab} by up to 80%.

3.1.4 C_{Fab} example: Retarding Grid Energy Analyzer (RGEA)

The initial design point we considered was that of Pitts [11] for a probe head to be used in JET (see Fig. 3.4). The assembly entailed almost 30 separate components and multiple grids, with a single orientation. The main components that could be printed were the ceramic head and the grids - however not inexpensively (sub micron printing is possible in metals although comes at a cost). A new design emerged in discussion with UW that served to increase views. Fig. 3.4 shows the AM-optimized head with multiple viewing angles. In summary, the cost of fabrication of the probe head becomes attractive if the complexity is increased, giving

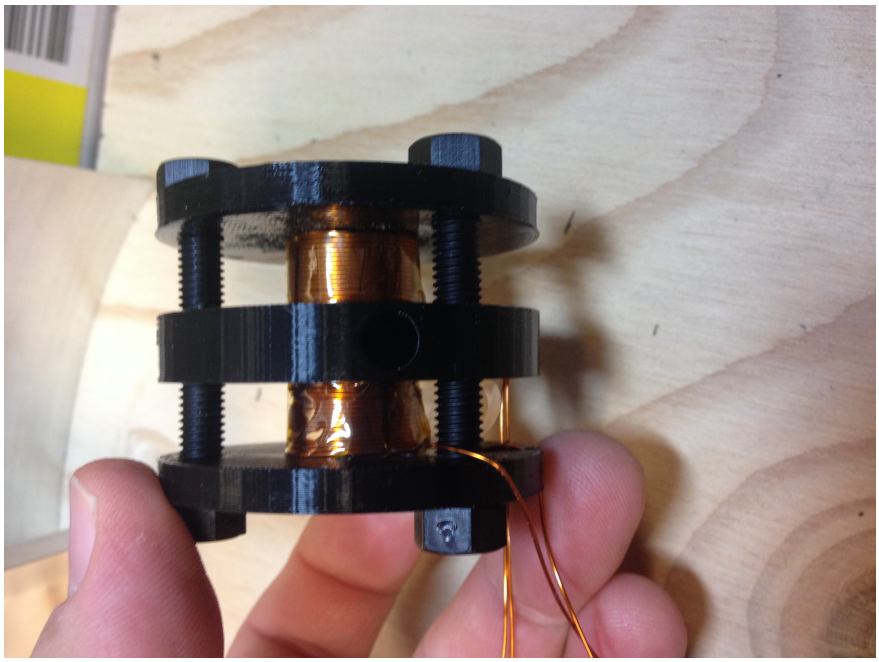

Figure 3.2: HH coil calibration jig

rise to new possibilities in probe head design and new measurements. The discussion of this diagnostic (and the Langmuir head) lead to the consideration of one of the principal component costs, namely high voltage feedthroughs: the material transition from conducting metal to ceramic would be game changing if possible (although given disparate melting points and thermal coefficients, this technology is still in R&D). In summary, C_{Fab} can be impacted significantly for some components in the assembly for conventional design, however, the possibility of unconventional design opens up a range of new measurement options, at seemingly no extra cost.

3.1.5 C_{Fab} example: HeNe and CO2 interferometers

We developed the design of a HeNe based on Kumar, a CO2 interferometer based on Carlstrom [12]. We developed a bill of materials (HeNe example is shown in Fig. 3.5) for all of the system components and sorted according to cost. Note that most optomechanical components can be printed in plastic for use in interferometers, polarimeters, and other optical-bench diagnostics (see also Thomson and inverse Compton in next sections). These components will not typically see neutrons, and so the material requirements are not stringent (except for providing alignment). Although lenses are now available for AM, these are not yet at a sufficient quality (transmission is low) for use in optical diagnostics. For sake of rigor, we spent some time developing components with the same functionality but reduced cost (laser mounts, beam-splitter mounts, linear actuators, posts, mirror mounts, breadboard, etc) which was instructive insofar as it provided detailed information of cost at the component level, and allowed the substantiation of cost reduction. However, we realized even before writing the Phase I application that the advantage AM is not in replication of existing functionality, but in optimization of the design that allows for increase in complexity and reduction in size. This subject is explored more in the section below on Testing costs. In summary, C_{Fab} impacted by up to 99% in some components, but only 20% in full assembly due to printable components being only a fraction of the total cost.

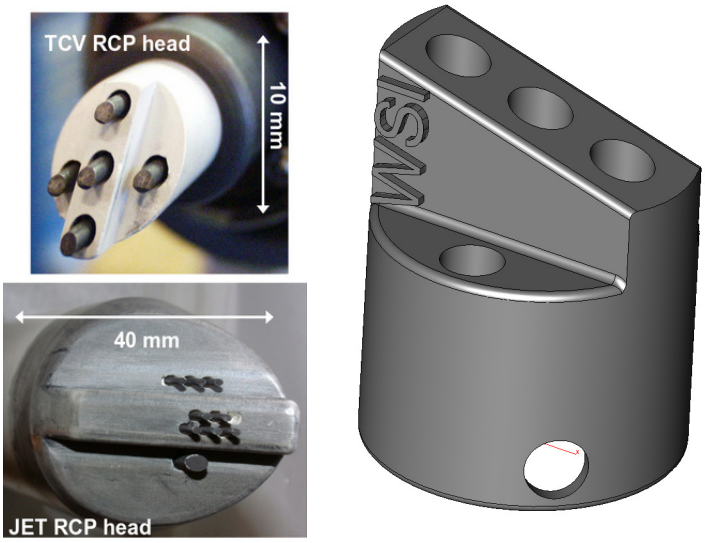

Figure 3.3: Alumina Langmuir probe head (modeled after JET / TCV multi-tip Langmuir probe head - left) with cooling channels and WSI logo.

3.1.6 C_{Fab} example: Profile Thomson Scattering

We considered two Thomson designs - the Ruby laser version at UW, and the YAG version that was developed by Carlstrom for DIII-D and SSPX. We broke down costs for each system in a similar manner to the interferometers and determined which components could examined for AM. All of the optomechnical components fall in that category, as well as beam dumps, baffles, structural support, mounts for optical components (including fibers and collection optics). We examined the use of 3D printing for collection optics, although this technology is not sufficiently mature (transmission coefficients are too low (see offerings by LuxExcel)), and post-processing lenses with blooms is the principle cost in the optics. It is a technology that we will watch, and possibly weigh in on for Phase II, since the surface quality in printing is now sufficient for lenses to be printed for spectacles. In summary C_{Fab} can be impacted in the same categories as for interferometry with the addition of a set of sub-components that would be printed in metal.

3.1.7 C_{Fab} example: Bolometer

We developed the design of an IR imaging bolometer based on Wurden. The bolometer consists of a foil target behind a pixel mask and a pinhole camera. An IR camera is used to image the target foil's temperature rise, allowing for a multi-channel bolometer (see Fig. 3.7). The nosecone of the pinhole camera is placed close to the plasma, and is therefore exposed to large heat fluxes. Cooling channels allow the bolometer to operate in more extreme environments, but add costs in CM. With AM, the added complexity does not add significant cost to the manufacturing process. Additionally, the bolometer can be printed as one monolithic construction, reducing assembly costs. Fig. 3.7 shows a monolithic design with embedded cooling channels suitable for AM. C_{Fab} is impacted by up to 80% in some components, but only 10% in full assembly (the IR camera is still a major component of the total cost)

3.1.8 C_{Fab} Circuits

We examined 3D circuit printing state of the art to see if there were viable applications for plasma diagnostics. Currently, 3D circuit printing technology is not very mature; the technology has one main development: 2D printing with inkjet deposition of silver nitrate and ascorbic acid leaving tracks of silver (http://www.cartesianco.com/product/the-argentum/). This method provides track sizes that are useful for ICs, is able to print on many substrates, and tracks smallest printing on standard circuit substrates.

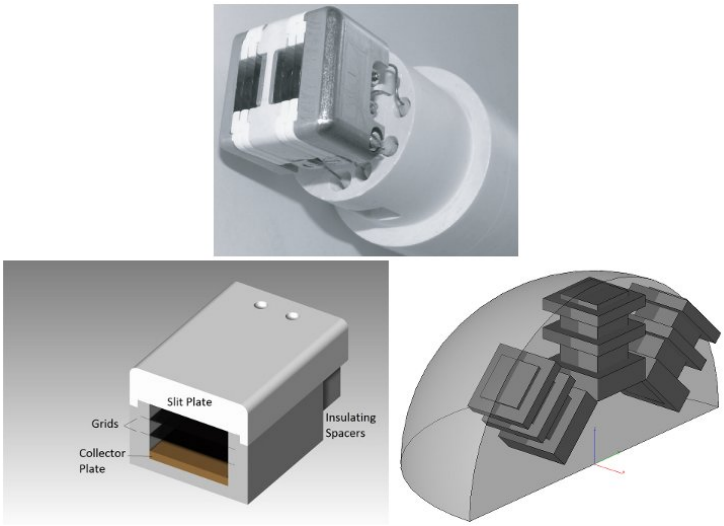

Figure 3.4: Alumina RGEA head for JET, and our version as well as a multi-direction head.

However, silver layers are 5x more resistive than copper tracks, and it is largely an experimental effort. Cost is roughly $1000 for a 1st generation circuit printer. Common electronic components are not yet ready to be additively manufactured, so any circuit which is 3D printed still requires assembly. In summary, AM circuit printing is not quite at the professional production level. Looking forward to a Phase II, the technology will be followed closely for new innovations (http://www.voxel8.co/).

One area where AM could be impactful is enclosures. It can be difficult to source a proper enclosure for circuitry and installation often requires extra machining for connections. Designing custom enclosures for AM is straightforward and could be partially scripted. Cost of materials is low for plastic enclosures. Fig. 3.8 shows an example custom enclosure for a switch and SMA connectors designed by WSI for a Helmholtz coil.

3.2 Costs of Engineering Design, C_{EDR}

The engineering design stage takes a physics concept and produces a full set of engineering drawings, and a bill of materials to hand off to shop for fabrication. This stage can entail some deep FEM thermal and mechanical stress analysis. The cost of performing the appropriate level of engineering design can be considerable - for AM the emphasis is placed on modeling the component ahead of sending to the printer. Small variations in commonly used parts can be scripted. Monolithic designs can be taken straight from physics models. C_{EDR} can be impacted by 100% in most cases - after the first complete design is scripted then costs associated with customization of the design should be zero.

C_{EDR} impacted by scripted Engineering Design Tools that are available for free from major developers of 3D technology. Many diagnostics contain parts which are common to all diagnostics of that type or only vary by certain parameters. For example, the design of a mirror mount might only vary by the size of the mirror. For these types of diagnostics it is possible to script the engineering design in order to reduce costs. To demonstrate, we have developed scripts which produce a CAD file for three parts: a mirror mount, an optical post, and a Helmholtz Coil former. The script is hosted on a web server–potentially for use by a customer–and uses ABFab3D to generate a CAD file. ABFab3D is licensed under the LGPL. Each part has a set of possible inputs, such as height, outer radius, mounting screw type, etc. These inputs cover the range of most user needs for these types of parts. Once the user inputs the desired parameters, they can generate the CAD file. The CAD file is then sent to WSI for review and manufacture. Fig. 3.9 shows the interface

Components	#	Cost per	CM Cost 1	AM Cost 1
Kumar thesis				
Mirror mounts, posts, misc mechanical hardware	30	200	6000	300
Table with vibration isolation	1	5000	5000	200
NI 6133	1	3200	3200	3200
AO Isolator	1	2800	2800	2800
Acoustic optic cell	1	2300	2300	2300
Misc RF components	1	2000	2000	2000
4mW linearly polarized HeNe Laser 25cm cavity length	1	1290	1290	1290
2 axis rotation mount for AO modulator	1	1000	1000	1000
Power supplies	2	500	1000	1000
Beam expander	1	950	950	950
Half wave plate	2	425	850	850
Fringe counting electronics	1	600	600	600
Flat mirrors	5	80	400	400
Detector Mercury Cadmium Telluride Detectors	1	300	300	300
BS	1	200	200	200
Sapphire windows	2	80	160	160
Spherical mirror (4m)	1	100	100	100
Iris	1	100	100	100
SUBTOTAL			28050	17550
CONTINGENCY			5610	3510
TOTAL MATERIALS			**33660**	**21060**
LABOR COSTS	**Time**	**Cost/hour**	CM **Cost**	AM Cost
0. CDR	8	180	1440	0
1. Engineering Design	8	180	1440	0
2. Procurement	8	100	800	0
3. Fabrication				
--Component layout in side lab	40	120	4800	0
--Alignment of all components	40	120	4800	0
--Calibration of the detectors	40	120	4800	120
--Testng with movement	40	120	4800	0
--Installation onto the main experiment	40	120	4800	2400
--Fab fringe-counting circuit	8	120	960	960
--Testing of the circuit	12	120	1440	960
--Software development for phase counting	40	120	4800	0
--Routing cables to DAQ	4	120	480	480
TOTAL LABOR			**35360**	**4440**
TOTAL			**69020**	**25500**

Figure 3.5: Cost breakout of a HeNe interferometer per Kumar for CM and AM. In yellow are the components that we examined for cost reduction by AM.

for generating scripted designs of an optical mount. Fig. 3.10 shows various configurations of a Helmholtz coil former and a mirror mount, all generated with scripts.

Design labor costs are significantly reduced with the use of scripting. Writing the script initially takes time on the order of designing a part, but each successive part designed using a script takes minutes to design instead of hours. A expensive skilled design engineer is not needed to run the script. The library currently in use, ABFab3D, is somewhat limited in its operations and is only suitable for simple parts. More complicated diagnostics could still have reduced design costs by utilizing more powerful CAD scripting tools, such as Solidworks macros. Using scripting to design common parts for diagnostics has the potential to drastically cut costs in engineering design.

3.3 Costs of Testing, C_{Test}

Usually after sub-assemblies have been fabricated, the next step to to obtain a signal from the diagnostic that makes sense to the experimentalist. This process can be drawn out depending on the experience of

Figure 3.6: a) Interferometer mirror mounts: $190 store bought vs $2.86 printed (raw materials); b) mount installed in interferometer.

the experimentalist (for this analysis, we have assumed professional level scientist, not students). It follows therefore that any pre-assembly (for example removing time spent on alignment) will reduce costs. For AM the balance is struck between monolithic designs and sufficient degrees of freedom (DoF) to tune assy (e.g. provide fine alignment of optical components). Optimization of these costs occurs by specifying narrow tolerances in the print stage. We have found that it is possible to print multiple optical component in a monolithic structure that preserves their alignment (see Fig. 3.11). The method for developing this was to discuss with experimentalist at UW which components on their HeNe optical bench had been 'locked down' - i.e. had been positioned and will unlikely be moved again for subsequent operation of the diagnostic. During the initial shake-down of the diagnostic, the components on the bench will move multiple times as the desired response is obtained. The three components identified both fit into the print bed of our PLA FDM printer and utilized components for which pre-exiting designs existed, so the design time was short. We took a photo from above, and set up the optical alignment in the CAD drawing before printing. In printing, we encountered warping of the plastic component due to uneven cooling, and so brought the part up to temperature and let it cool throughout (this sort of careful attention to process is required throughout 3D printing if you own a printer: we strongly advise against buying a printer at this stage). Still, we were able to recover the functional component. So, while the cost of the components was impacted (removing 3 $190 mirror mounts, posts and clamps), the major cost savings are to be obtained in the testing stage, which could entail multiple hours optimizing the positions of the mirrors before locking them down (at $120/hr this adds up quickly). Each separate diagnostic has it's own associated C_{Test}: this can be impacted by up to 100% for magnetics, 50-60% for optical diagnostics (by eliminating many DoF).

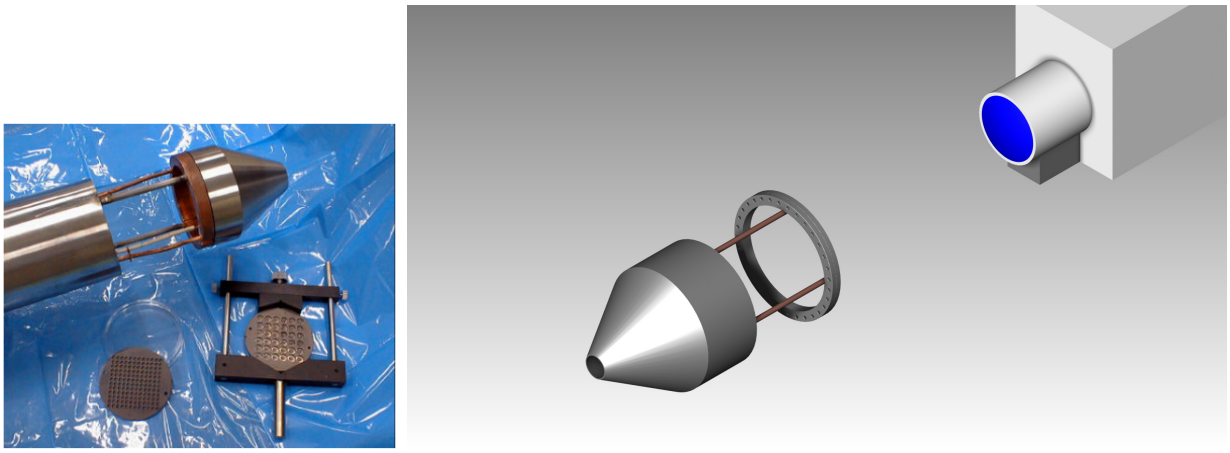

Figure 3.7: IR camera head for bolometer, conventional assembly and monolithic AM design.

3.4 Costs of Concept Design, C_{CDR}

Usually in a concept design review for a plasma diagnostic, an experienced physicist (or team of physicists) examines a measurement and bridges the gap between the measurement and the diagnostic tool using first principles and literature on recent experiments. For all conventional diagnostics, textbooks and a large body of literature are an invaluable resource for this process. By building off of basic physics, statistics models, and data (synthetic or real), a concept design review can include a S:N ratio, typical geometric parameters involved in physical experiment, explanations of the calculations, assumptions, and corrections, and graphs that display typical outputs of the desired measurement over time and/or space. Our scripts were developed using octave, and are thoroughly annotated with references and labels of input parameters that can be changed by the customer to reflect a customized measurement device, such as HeNe/CO2 interferometers, Rogowski coils, etc. As such, a web-based form can be used to constrain the online scripted EDR, and C_{CDR} can be zero after first iteration.

In this way, we have researched and developed scripts for the following five plasma diagnostic subjects:

1. Magnetics (Rogowski Coils, Magnetic Pick-Up Coils, B-dot probes, Saddle Coils, Pancake Coils, Solenoidal Loops) [9, 52, 53]
2. Electrostatics (Langmuir Probes) [54]
3. Refractive Index (CO2 interferometer with synthetic data) [55, 56, 57, 12]
4. Scattering (Thomson Scattering, Laser Inverse Compton Scattering) [61, 62, 63, 64]
5. Spectroscopy [67, 68, 69, 40]

All of the scripts have been made available online [14], and will be updated should errors be discovered.

3.5 Costs of Materials, C_{Mat}

Only the amount of material needed for a part is paid for in most 3D printing cost models, so there is little to no waste. Parts can be made hollow or latticed to reduce amount of material, but retaining strength (further analysis is warranted). Table 3.1 shows the materials available for 3D printing that are also of use for fusion systems: almost all common materials (metals, ceramics and plastics) can now be used for AM. The most useful technique for fusion components is direct metal laser sintering or melting using electron beams or lasers. C_{Mat} is impacted up to 99% - see specific case examples in next sections.

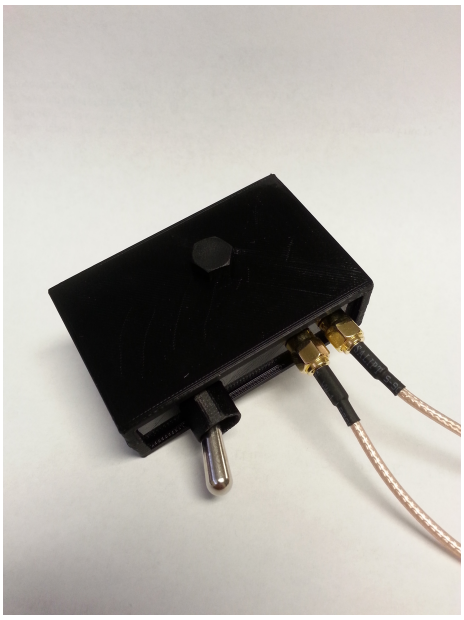

Figure 3.8: 3D Printed electronics enclosure designed by WSI

One important aspect of 3D printing is the possibility of printing with multiple materials, and use of post-processing to coat inexpensive materials for use in new applications and environments and for modifying surfaces. The use of nickel plating of vacuum-components manufactured with conventional plastics was investigated as part of the Phase I activity. The components are shown in Fig. 3.13 - printed ABS plastic components, one plated with a few microns of nickel, and the outgas results are shown also. In the first results from this new facility, is seen that water pressure is higher for the uncoated part.

3.6 Costing summary

Table 3.2 summarizes the cost reduction we have found for the various diagnostics in this Phase I study. This costing analysis should be taken as a preliminary examination - it is clear that cost savings can be made in some diagnostics (such as magnetic systems, and in particular those that are not exposed to neutrons or high power loadings, or even UHV vacuum conditions), the cost savings for diagnostics in the R&D phase are not so apparent. For example, there is only a small amount of literature on the Laser Inverse Comtpon Scattering diagnostic, and development of a complete CDR is more difficult in these cases. However, we found that across the board, costs could be significantly impacted by use of AM and more complete design of each diagnostic that optimizes for cost seems warranted.

3.7 Progress in understanding outgassing of AM-produced metal components

We concentrated at on studying laser-sintered components since there has been little reported data on outgassing of this type of AM metal components, and this is the most common AM method for metals. Additionally, we have found that AM commercial suppliers are reluctant to reveal all parameters used in production, making it difficult to create a solid scientific understanding of outgassing and surface properties of AM metals. We started by analyzing outgassing AM samples of several common materials, and compared them with published data, seen in Table 3.3: Aluminum, which for laser sintering is designated as ALSI10, exhibited a similar final pressure as Al-6061; PH1 was three orders of magnitude higher in pressure than SS-304; and AM Inconel seemed to be absorbing humidity (and thus lowering ΔP) even days after vacuum

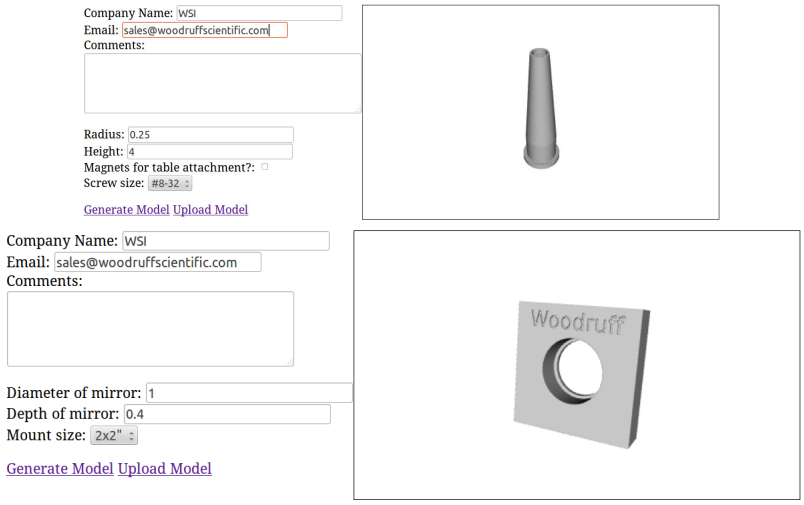

Figure 3.9: Scripted example of a mirror post: possible inputs are length, post diameter, or mounting screw type. Scripted example of a mirror mount: possible inputs are mirror diameter, depth, and size of mount.

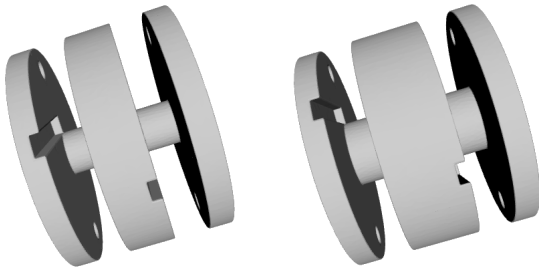

Figure 3.10: Scripted example of a Helmholtz coil former with various parameters.

pumping was started. For all of these results ΔP and Θ are with respect to background with no samples taken at the UMBC test chamber. Note that these samples were not heated.

Motivated by the present results, we have started our own database, using our own hardware for consistency and reproducibility, of outgassing for various materials for conventionally produced metals, as well as the most similar AM metals corresponding to each metal. Moreover, we have carried out electron microscopy and surface analyses of AM metal samples to understand the differences in outgassing rates with respect to conventional materials. One of these materials is IN718, which was also used for the measurements displayed in Table 3.3. A micrography of IN718 is shown in Fig. 3.14. Note that the surface is clearly non-uniform, and contains many voids and inclusions which we speculate are responsible for initial rapid outgassing, as well as for adsorption of humidity after long times in the vacuum chamber. Heating the samples alleviates the adsorption issues, but the non-uniformity of the surface (and presumably of the volume) is of concern given once the materials are exposed to high-temperature plasmas and neutrons.

Further analysis using x-ray back-scattering of the areas indicated in Fig. 3.14 also show that the non-uniformity occurs in the concentration of materials. Figure 3.15 shows the x-ray spectra for the two different regions. At this point, we are unsure if non-homogeneous composition is an issue (although is highly likely), and is subject of continued investigation.

Another issue that we found from x-ray spectrometry is that the composition by weight reported for the powder metal used in laser sintering does not match our surface measurements. For example, when scanning the entire area shown in Fig. 3.14 we found that the Ni content was 28% by weight, whereas the advertised Ni content for the powder that the manufacturer used for our sample is 50 - 55% by weight. We believe that

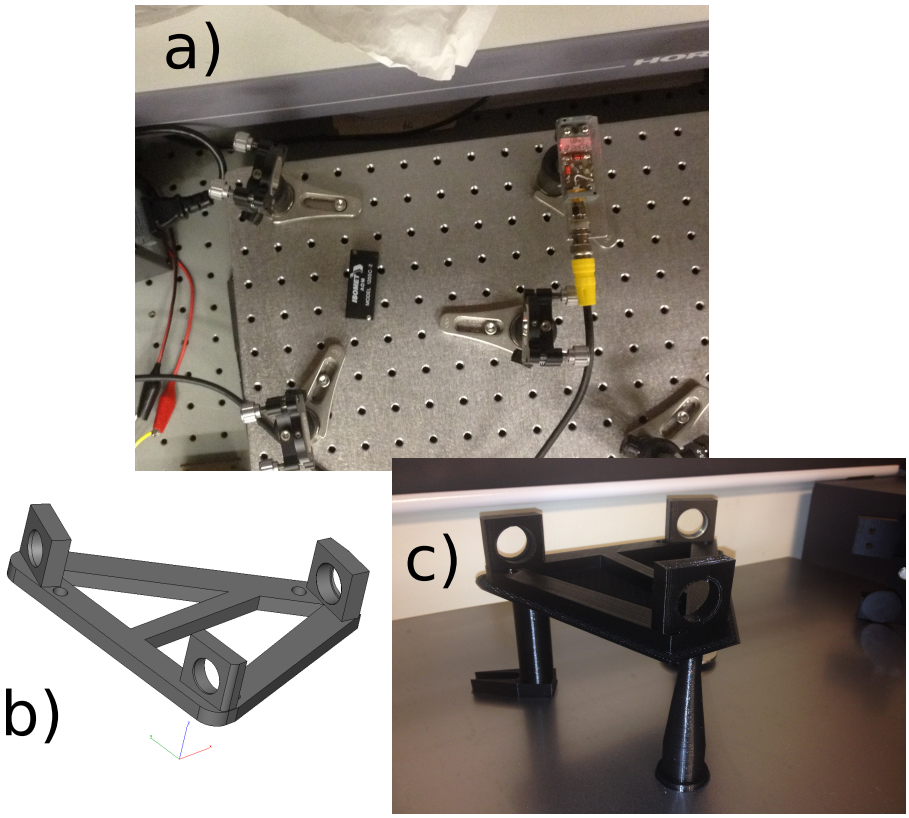

Figure 3.11: a) original interferometer components; b) pre-aligned monolithic mirror mounts; c) printed monolithic assy

a more controlled AM process coupled to post-processing of the parts will make them better compatible to UHV conditions and high-temperature plasma reactors.

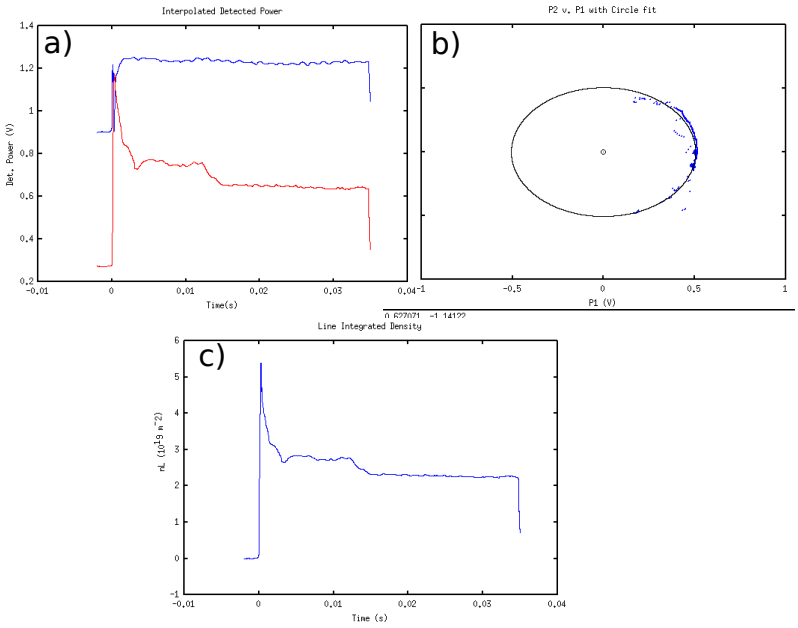

Figure 3.12: a) data from two separate detectors; b) fitting of data in phase plot; c) reconstruction of plasma density.

Material	UHV / HV / LV	Method
1. Metals		
Stainless steel	UHV	DMLS
Tungsten	UHV	DMLS
Vanadium	UHV	SLS
OFHC Copper	UHV	SLS
Titanium	UHV	DMLS
Aluminum	UHV	DMLS
Indium	HV	DMLS
Molybdenum	UHV	DLS
Chromium	UHV	SLS
Tantalum	UHV	SLS
Gold	UHV	DLS
Niobium	UHV	DMLS
Cusiltin	UHV	DMLS
Inconel	UHV	DMLS
Glidcop	UHV	DMLS
2. Ceramics		
Macor	UHV	
Boron nitride	UHV	
Alumina	UHV	FDM / DLS
Borosilicate glass	HV	
Quartz	HV	
3. Plastics		
PEEK	HV	SLM/FDM
Vespel polyimide	HV	?
Delrin	V	FDM/SLM

Table 3.1: Materials used in fusion environment, their vacuum rating (UHV is Ultra High Vacuum, typically in the 10^{-9}Torr range, and the AM technique (DLS/DLM - Direct Laser Sintering or Melting, FDM - Fused Deposition Modeling, SLA - Stereo Lithography

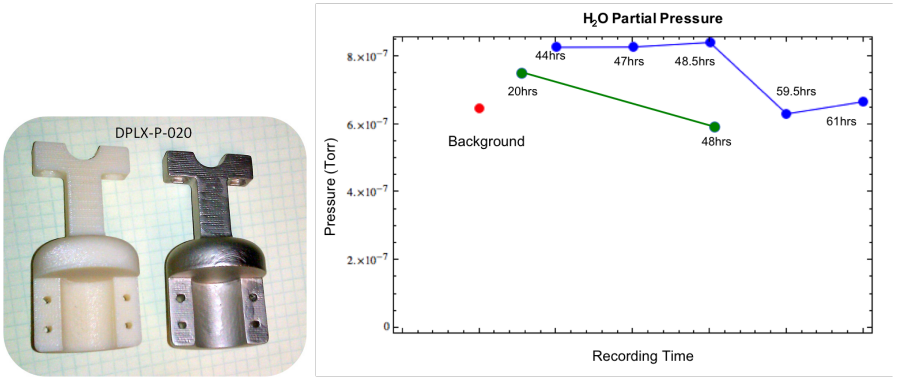

Figure 3.13: Outgas data from the UMBC test stand showing the effects on partial pressure for an uncoated ABS plus component against a nickel plated ABS plus component - base pressure can be lowered but post-processing of plastics (at least in this simple test) does not get us to UHV regimes.

Diagnostic	C_{Total}	C_{CDR}	C_{EDR}	C_{PDR}	C_{Fab}	C_{Test}	C_{Mat}
Magnetic field coil	0.06	0	0	0.1	0.1	0.1	0.1
Magnetic coil array	0.062	0	0	0.1	0.1	0.1	0.1
Rogowski coil	0.062	0	0	0.1	0.1	0.1	0.1
Calibration jig	0.14	0	0	0.1	0.5	0.1	0.1
Langmuir probe	0.35	0	0	0.1	0.5	1	0.9
RFEA	0.35	0	0	0.1	0.5	1	0.9
HeNe interferometer	0.71	0	0	0.1	0.9	0.2	0.9
CO2 interferometer	0.72	0	0.2	0.1	0.9	0.2	0.9
CO2 polarimeter	0.72	0	0.2	0.1	0.9	0.2	0.9
mm interferometer	0.73	0	0.2	0.1	0.9	0.2	0.9
Thomson Scattering	0.85	0.1	0.9	1	0.9	0.2	0.95
Inverse Compton	0.92	1	1	1	0.9	1	0.9
Spectrometer	0.49	0	0.1	0.1	1	1	0.95
Bolometer	0.59	0	0	1	0.7	1	0.95
Scintillator	0.33	0	0	0.1	0.1	1	0.9

Table 3.2: Cost breakout of diagnostics produced with AM relative to CM costs

Specimen	ΔP (Torr)	Θ (Torr-liters/s-cm^2)	Compare to	Θ (Torr-liters/s-cm^2)
ALSI10	2.19e-8	2.19e-8	AL-6061	2.5e-8 (after 10h in vac.)
PH1	1.73e-8	1.29e-8	SS-304	8e-11 (after 44h in vac.)
IN718	-8.34e-9	-6.30e-9	Inconel-625	2e-9 (after 20 h in vac.)

Table 3.3: Comparison between AM metals tested at UMBC and similar tests reported in E. A. Moshey, PPPL Technical Report No. 82-001 Rev. A, 15 Feb. 1982.

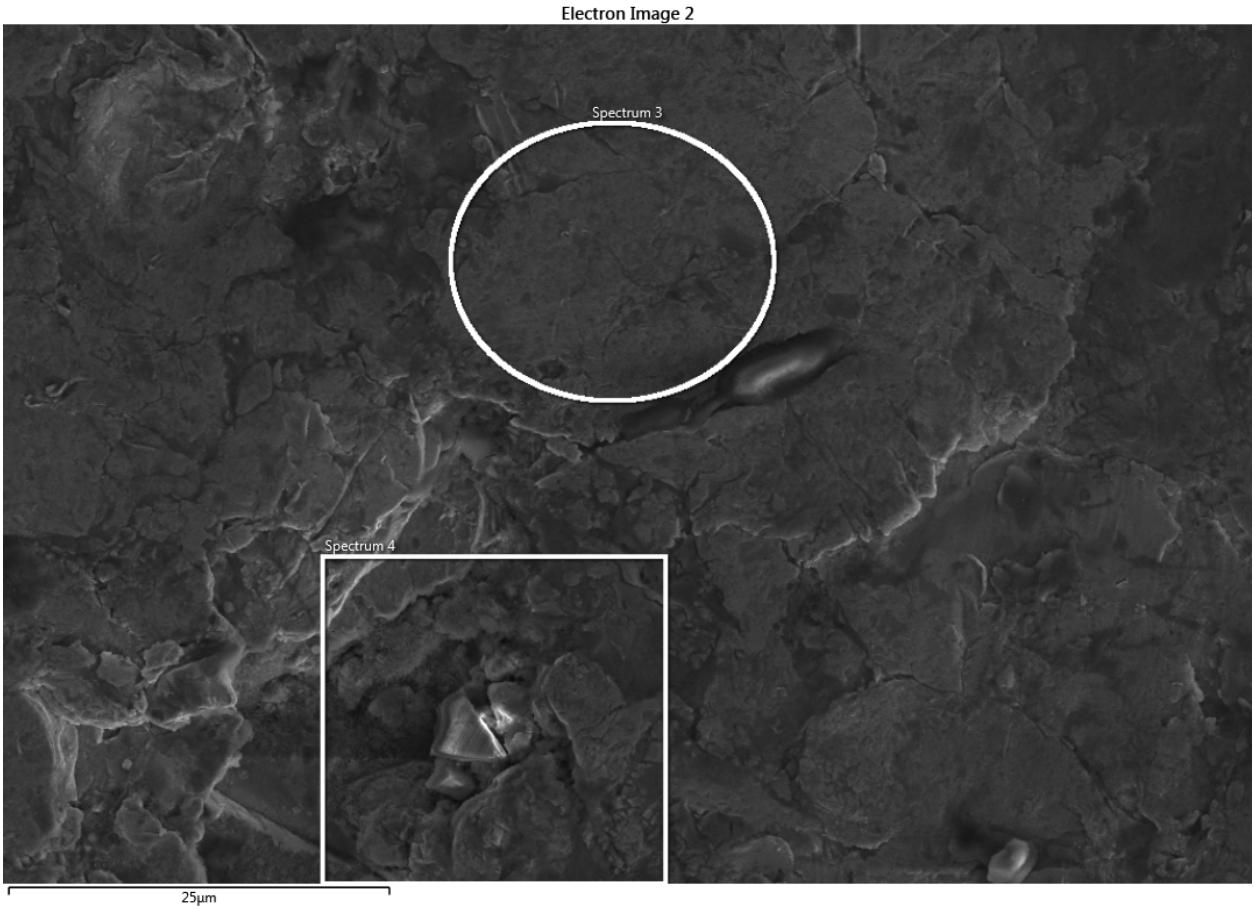

Figure 3.14: Micrography of IN718. The regions marked as Spectrum 3 and Spectrum 4 correspond to spectra shown in Fig. 3.15

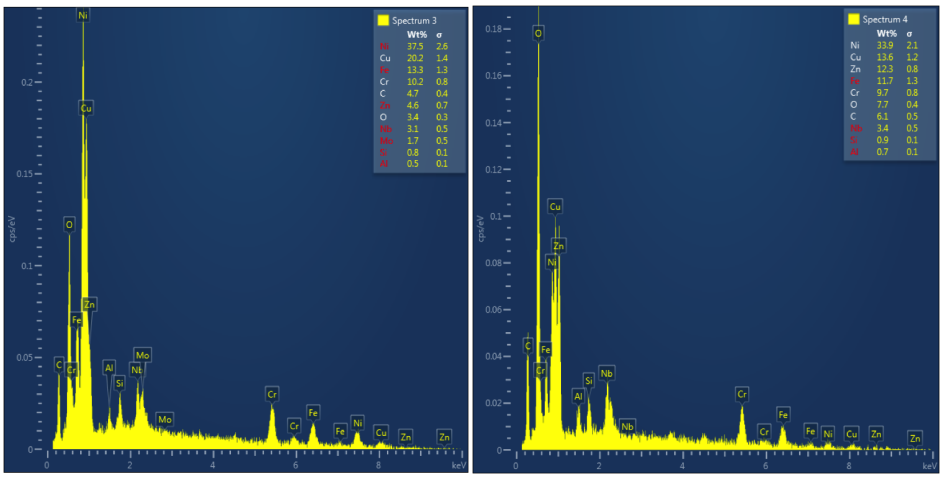

Figure 3.15: X-ray back-scatter spectrum of regions 3 and 4 shown in Fig. 3.14.

Chapter 4

Conclusions

In our DOE Phase I SBIR we have examined the impact that AM can have on plasma diagnostic **cost** by taking 15 separate diagnostics through an engineering design using Conventional Manufacturing (CM) techniques to determine costs of components and labor costs associated with getting the diagnostic to work as intended. With that information in hand, we set about optimizing the design to exploit the benefits of AM. The impact on cost is found to be in several areas. First, the cost of materials falls because AM parts can be manufactured without waste, and engineered to use less material than CM. Next, the cost of fabrication falls for AM parts relative to CM since the fabrication process can lead to the combination of multiple components as highly complex monoliths, which can be manufactured less expensively than separate unit components. We find that complexity, for example adding cooling channels on plasma-facing components, comes at no additional cost. Costs associated with assembly are lower for AM because many components can be combined and printed as monoliths, thereby mitigating the need for alignment or calibration. Finally, the cost of engineering is impacted by exploiting AM design tools that allow standard components to be customized through web-interfaces. We find that concept design costs can also be impacted by scripting interfaces for the online engineering design tools.

Chapter 5

Recommendations

Our recommendations fall in to the cost categories as described in this proposal.

5.1 Reduce Concept Design costs by scripting physics

All of the decisions that need to be made in order to obtain a measurement in an experiment can be scripted into a logic tree, whose output forms the input to the engineering design, and a synthetic response function for the measurement. A logic tree ought to be designed with a user friendly interface. A well planned and scripted design process is recommended to reduce design costs.

5.2 Reduce Engineering Design costs by exploiting scripting tools that allow for easy customization

Taking the design point data from the scripted concept design, existing diagnostic designs can be customized using either online scripting design tools or proprietary ones (such as Solidworks). Each diagnostic should first be optimized for AM then scripted to be readily customized. Scripted engineering designs can drastically reduce design costs and should be considered.

5.3 Reduce Fabrication costs by optimizing design for AM

The primary driver of cost for CM is complexity, while the primary driver of cost for AM is volume. Diagnostics parts with many complex features usually are cheaper to produce with AM. Additionally, parts which were previously considered prohibitively expensive with CM may be printed economically with AM. Materials selection for the diagnostic components can depend on operating environment, so the customer must be able to select these in the concept design stage (e.g. inconel for neutron/high power loading environments, plastics for other). Further, the optimization of the design for high complexity and miniaturization using state of the art design tools (such as Zemax, ANSYS and Solidworks) should occur in order to minimize costs. Combining diagnostics into packages using the monolithic structures ought to further reduce costs.

5.4 Reduce labor costs in assembly and testing

Printing diagnostics as monolithic structures where possible reduces both assembly and testing costs. We recommend utilizing design techniques which will minimize these labor costs.

5.5 Qualify components in a test facility

Diagnostics produced using AM need to be qualified in test facilities. Materials qualification is currently underway at ORNL, Penn State, NIST and many others [15]. Massive effort is needed to qualify new materials for use in fusion environment, which will be impacted by materials testing.

5.6 Continue testing of components in-situ

A necessary aspect of all prototyping is testing the functionality of the components in their intended environment.

5.7 Continue metal outgassing research and testing

In collaboration with UMBC, we plan to continue to investigate how the components outgas at various conditions compared to traditionally processed parts. We plan on investigating post processing techniques in metal-printed parts such as shot peening and coating with a refractory metal such as titanium nitride, in order to mitigate the surface defects and to decrease outgassing rates. Shot peening is a cold working process in which small spheres bombard the surface of the metal inducing plastic deformation. This process generates residual compressive stresses which increase the hardness of the material, improves fatigue resistance and decreases the thermal conductivity of the material due to its dependence on grain size [1-2]. The residual stresses also provide retardation or prevention of crack initiation and propagation [3-5]. However, shot peening may also increase the surface roughness of the material. A study conducted on titanium alloy for total joint replacement found that electro-polishing the part after shot peening increased the fatigue limit by 30% compared to a 10% increase after grit blasting [5]. Coating the sample with titanium nitride after shot peening can reduce outgassing by acting as a diffusion barrier. It has been reported that coating a 304L stainless steel vacuum chamber with titanium nitride yielded an outgassing rate of $6.44(\pm 0.05) \times 10^{-13}$ $[Torr\ L/s\ cm]$ with an initial bake of 90 $^{\circ}C$ and after a final bake of 250 $^{\circ}C$ the chamber reached $2(\pm 20) \times 10^{-16}$ $[Torr\ L/s\ cm]$, while an uncoated chamber baked at 250 $^{\circ}C$ reached an outgassing rate of $3.560(\pm 0.05) \times 10^{-12}$ $[Torr\ L/s\ cm]$ [6].

[1] L. Tan, X. Ren, K. Sridharan, and T. Allen, âĂIJEffect of shot-peening on the oxidation of alloy 800H exposed to supercritical water and cyclic oxidation,âĂİ Corrosion Science, vol. 50, no. 7, pp. 2040âĂŞ2046, 2008.

[2] F. Guo, N. Trannoy and J. Lu, "Analysis of thermal properties by scanning thermal microscopy in nanocrystallized iron surface induced by ultrasonic shot peening", Materials Science and Engineering: A, vol. 369, no. 1-2, pp. 36-42, 2004.

[3] O. Unal, "Novel type shot Peening applications on railway axle steel," Journal of Mineral, Metal and Material Engineering, vol. 2, Jun. 2016.

[4] J. da S. Peltz, L. V. R. Beltrami, S. R. Kunst, C. Brandolt, and C. de F. Malfatti, "Effect of the shot Peening process on the corrosion and oxidation resistance of AISI430 stainless steel," Materials Research, vol. 18, no. 3, pp. 538âĂŞ545, Jun. 2015.

[5] M. Long and H. J. Rack, "Titanium alloys in total joint replacementâĂŤa materials science perspective," Biomaterials, vol. 19, no. 18, pp. 1621âĂŞ1639, Sep. 1998

[6] M. A. A. Mamun, A. A. Elmustafa, M. L. Stutzman, P. A. Adderley, and M. Poelker, "Effect of heat treatments and coatings on the outgassing rate of stainless steel chambers," Journal of Vacuum Science Technology A: Vacuum, Surfaces, and Films, vol. 32, no. 2, p. 021604, Mar. 2014.

Bibliography

[1] http://www.iter.org/

[2] S. Zinkle Challenges in Developing Materials for Fusion Technology Past, Present and Future AND TOFEy Nashville 2012 http://fire.pppl.gov/TOFE_2012_materials_Zinkle.pdf

[3] I. A. Hutchinson, Principles of Plasma Diagnostics, Cambridge University Press; 2 edition (July 14, 2005)

[4] M. Walsh, et al Overview of High Priority ITER Diagnostic Systems IAEA Fusion Energy Conference 2010 Proc. 2010 http://www-pub.iaea.org/mtcd/meetings/PDFplus/2010/cn180/cn180_papers/itr_p1-07.pdf

[5] Measurement Science Roadmap for Metal-based Additive Manufactrure Prepared by Energetics Incorporated May 2013 http://www.nist.gov/el/isd/upload/NISTAdd_Mfg_Report_FINAL-2.pdf

[6] NIST Dec. 2012 Roadmapping Workshop http://events.energetics.com/NIST-AdditiveMfgWorkshop/downloads.html

[7] The Economist, The Printed World: Three- dimensional printing from digital designs, 10 February 2011. www.economist.com/ node/18114221

[8] Hales and Gooch 'Managing Engineering Design' Springer 2nd Ed 2004

[9] E.J.Strait et al., Chapter 2: Magnetic diagnostics, Fusion Science and Technology 53(2) (2008), 304

[10] E. J. Strait Magnetic diagnostic system of the DIII-D tokamak Rev. Sci. Instrum. 77, 023502 (2006)

[11] R. Pitts et. al. A Retarding Field Energy Analyser for the JET Plasma Boundary EFDAJETPR(03)30 http://www.iop.org/Jet/fulltext/EFDP03030.pdf

[12] T. N. Carlstrom et al Real-time, vibration-compensated CO2 interferometer operation on the DIII-D tokamak Rev. Sci. Instrum. 08/1988

[13] http://arxiv.org/pdf/1406.4817v1.pdf

[14] http://www.woodruffscientific.com/ShapeJS-Example

[15] Jennifer Bryant Report of the Breakout Group NIST AM Qualification and Certification http://events.energetics.com/NIST-AdditiveMfgWorkshop/pdfs/AM_ReportOut_QualCert.pdf

[16] https://github.com/AbFab3D/AbFab3D/

[17] H. McLean, A. Ahmed, D. Buchenauer, D. Den Hartog, C. Domier, D. Hill, C. Holcomb, E. Hooper, E. Morse, M. Nagata, Y. Roh, B. Stallard, R. D. Wood, S. Woodruff, G. Wurden, Z. Wang, and G. Wurden, "Plasma diagnostics for the sustained spheromak physics experiment," Review of Scientific Instruments, vol. 72, no. 1, pp. 556-561, 2001.

[18] S. Howard, R. D. Horton, D. Hwang, R. Evans, and S. Brockington, "Calibration of magnetic probes in the vicinity of a conducting well," Review of Scientific Instruments, vol. 79, no. 2, pp. 023503-023503-10, 2008.

[19] P. V. Savrukhin and E. A. Shestakov, "Movable magnetic probe system in the t-10 tokamak," Review of Scientific Instruments, vol. 83, no. 1, pp. 013505-013505-5, 2012.

[20] E. J. Strait, "Frequency response of metal-clad inductive magnetic field probes," Review of Scientific Instruments, vol. 67, no. 7, pp. 2538-2540, 1996.

[21] C. Romero-Talamas, P. Bellan, and S. Hsu, "Multielement magnetic probe using commercial chip inductors," Review of Scientific Instruments, vol. 75, no. 8, pp. 2664-2667, 2004.

[22] G. Labik, T. Brown, D. Johnson, N. Pomphrey, B. Stratton, M. Viola, M. Zarnstorff, M. Duco, J. Edwards, M. Cole, and E. Lazarus, "National compact stellarator experiment vacuum vessel external flux loops design and installation," in Fusion Engineering, 2007. SOFE 2007. 2007 IEEE 22nd Symposium on, 2007, pp. 1-3.

[23] A. Elahi and M. Ghoranneviss, "A modified flux loop for the determination of plasma position in irt1 tokamak," Plasma Science, IEEE Transactions on, vol. 38, no. 11, pp. 3163-3167, 2010.

[24] M. Hole, L. C. Appel, and R. Martin, "A high resolution mirnov array for the mega ampere spherical tokamak," Review of Scientific Instruments , vol. 80, no. 12, pp. 123507-123507-10, 2009.

[25] E. Fredrickson, R. Colchin, K. McGuire, W. Morris, and N. Sauthoff, "Tftr mirnov loop system," Review of Scientific Instruments, vol. 57, no. 8, pp. 2084-2086, 1986.

[26] D. Brower, Y. Jiang, W. X. Ding, S. D. Terry, N. E. Lanier, J. Anderson, C. Forest, and D. Holly, "Multichannel far-infrared polarimeter-interferometer system on the mst reversed field pinch," Review of Scientific Instruments, vol. 72, no. 1, pp. 1077-1080, 2001.

[27] C. T. Holcomb, T. Jarboe, A. Mattick, D. Hill, H. Mclean, R. D. Wood, V. Cellamare, R. Bulmer, and E. Hooper, "Nonperturbing field profile measurements of a sustained spheromak," Review of Scientific Instruments, vol. 72, no. 1, pp. 1054-1058, 2001.

[28] D. Buchenauer, W. L. Hsu, J. Smith, and D. Hill, "Langmuir probe array for the diii-d divertor," Review of Scientific Instruments, vol. 61, no. 10, pp. 2873-2875, 1990.

[29] D. A. Taussig, J. G. Watkins, and R. Boivin, "Improved langmuir probe array for DIII-D," in Fusion Engineering, 2007. SOFE 2007. 2007 IEEE 22nd Symposium on 2007, pp. 1-4.

[30] V. Sokolov and A. Sen, "Ion energy analyzer for measurement of ion turbulent transport," Review of Scientific Instruments, vol. 83, no. 10, pp. 103503-103503-4, 2012.

[31] R. Stenzel, R. Williams, R. Aguero, K. Kitazaki, A. Ling, T. McDonald, and J. Spitzer, "Novel directional ion energy analyzer," Review of Scientific Instruments, vol. 53, no. 7, pp. 1027-1031, 1982.

[32] M. J. McCarrick, R. Ellis, M. Koepke, and R. Majeski, "Perpendicular ion energy analyzer for hot-ion plasmas," Review of Scientific Instruments, vol. 56, no. 7, pp. 1463-1464, 1985.

[33] D. Kumar and P. M. Bellan, "Heterodyne interferometer with unequal path lengths," Review of Scientific Instruments, vol. 77, no. 8, pp. 083503-083503-6, 2006.

[34] W. Yongqian, Z. Yudong, and W. Fan, "Design of far-infrared interferometer at 10.6 mum," in Photonics and Optoelectronics, 2009. SOPO 2009. Symposium on, 2009, pp. 1-4.

[35] Y. Kawano, A. Nagashima, T. Hatae, and S. Gunji, "Dual CO2 laser interferometer with a wavelength combination of 10.6 and 9.27 mum for electron density measurement on large tokamaks," Review of Scientific Instruments, vol. 67, no. 4, pp. 1520-1528, 1996.

[36] Y. P. Zhang, Y. Liu, J. W. Yang, X. Y. Song, M. Liao, X. Li, G. Yuan, Q. Yang, X. Duan, and C. H. Pan, "A new soft x-ray pulse height analysis array in the hl-2a tokamak," Review of Scientific Instruments, vol. 80, no. 12, pp. 126104-126104-3, 2009.

[37] P. Beiersdorfer, M. Bitter, M. May, and L. Roquemore, "High-resolution soft x-ray spectrometer for the NSTX tokamak," Review of Scientific Instruments, vol. 74, no. 3, pp. 1974-1976, 2003.

[38] B. Joye, P. Marmillod, and S. Nowak, "Multichannel bolometer for radiation measurements on the TCA tokamak," Review of Scientific Instruments, vol. 57, no. 10, pp. 2449-2454, 1986.

[39] A. Murari, K. F. Mast, L. DAmbra, P. T. Lang, L. Marrelli, P. Martin, and A. Romagnolo, "Multichord calibrated bolometer array for the RFX experiment," Review of Scientific Instruments, vol. 66, no. 1, pp. 665-667, 1995.

[40] R. Barnsley, I. Coffey, R. Lucock, and M. F. Stamp, "Jet beamline with integrated x-ray, vuv, and visible spectrometers, for burning plasma experiments," Review of Scientific Instruments, vol. 74, no. 3, pp. 1969-1973, 2003.

[41] I. H. Coffey and R. Barnsley, "First tritium operation of iter-prototype vuv spectroscopy on jet," Review of Scientific Instruments, vol. 75, no. 10, pp. 3737-3739, 2004.

[42] A. Graf, S. Howard, R. Horton, D. Hwang, M. May, P. Beiersdorfer, and J. Terry, "Visible spectrometer at the compact toroid injection experiment and the alcator c-mod tokamak for doppler width and shift measurements," Review of Scientific Instruments, vol. 77, no. 10, pp. 10F125-10F125-3, 2006.

[43] J. D. King, H. McLean, R. D. Wood, C. Romero-Talamas, J. Moller, and E. Morse, "An ion doppler spectrometer instrument for ion temperature and flow measurements on sspx," Review of Scientific Instruments, vol. 79, no. 10, pp. 10F535-10F535-4, 2008.

[44] D. J. Den Hartog and R. Fonck, "A fast spectroscopic diagnostic for the measurement of plasma impurity ion dynamics," Review of Scientific Instruments, vol. 65, no. 10, pp. 3238-3242, 1994.

[45] T. N. Carlstrom, G. L. Campbell, J. DeBoo, R. Evanko, J. Evans, C. M. Greenfield, J. Haskovec, C. L. Hsieh, E. McKee, R. T. Snider, R. Stockdale, P. Trost, and M. Thomas, "Design and operation of the multipulse thomson scattering diagnostic on DIII-D (invited)," Review of Scientific Instruments, vol. 63, no. 10, pp. 4901-4906, 1992.

[46] K. Narihara, I. Yamada, H. Hayashi, and K. Yamauchi, "Design and performance of the thomson scattering diagnostic on lhd," Review of Scientific Instruments, vol. 72, no. 1, pp. 1122-1125, 2001.

[47] H. McLean, J. Moller, and D. Hill, "Use of fast scopes to enable Thomson Scattering measurement in presence of fluctuating plasma light," Review of Scientific Instruments, vol. 75, no. 10, pp. 3887-3890, 2004.

[48] R. Boivin, M. Koltonyuk, C. P. Munson, and R. Mayo, "Time-of-flight neutral particle analyzer for alcator c-mod," Review of Scientific Instruments, vol. 68, no. 1, pp. 982-985, 1997.

[49] E. Mezonlin, S. Roberson, C. Raynor, R. Appartaim, I. Johnson, J.A., V. Afanasyev, S. S. Kozlovsky, J. M. Moller, D. Hill, E. Hooper, H. S. McLean, and R. D. Wood, "Neutral particle analyzer measurements on the sspx spheromak," Review of Scientific Instruments, vol. 78, no. 5, pp. 053504-053504-7, 2007.

[50] D. Darrow, H. Herrmann, D. Johnson, R. Marsala, R. W. Palladino, S. Zweben, and M. Tuszewski, "Measurement of loss of dt fusion products using scintillator detectors in TFTR (invited)," Review of Scientific Instruments, vol. 66, no. 1, pp. 476-482, 1995.

CDR BIBLIOGRAPHY

All or Multiple CDRs

[51] Dolan, Thomas James. Fusion research. 1982.

Magnetics

[52] Tumanski, Slawomir. "Induction coil sensorsâĂŤA review." Measurement Science and Technology 18.3 (2007): R31.

[53] Kovac, D., Ocilka, M., Vansac, M. (2012). Calculating of Inductance of Spiral Coil Using Comsol Multiphysics. Electromechanical and energy systems, modeling and optimization methods, 89-90.

Electrostatics

[54] Chen, F. F. (2003, June). Langmuir probe diagnostics. In IEEE-ICOPS Meeting, Jeju, Korea.

Refractive Index

[55] Bamford, D. J., Cummings, E. A., Panasenko, D., Fenner, D. B., Hensley, J. M., Boivin, R. L., ... Van Zeeland, M. A. (2013). CO2 laser-based dispersion interferometer utilizing orientation-patterned gallium arsenide for plasma density measurements. Review of Scientific Instruments, 84(9), 093502.

[56] Van Zeeland, M. A., Boivin, R. L., Brower, D. L., Carlstrom, T. N., Chavez, J. A., Ding, W. X., ... Watts, C. (2013). Conceptual design of the tangentially viewing combined interferometer-polarimeter for ITER density measurements. Review of Scientific Instruments, 84(4), 043501.

[57] Kumar, D. (2009). Experimental investigations of magnetohydrodynamic plasma jets. California Institute of Technology.

Scattering

[58] Donne, A. J. H., Barth, C. J. (2006). Laser-aided plasma diagnostics. Fusion Science and Technology, 49(2T), 375-386.

[59] Selden, A. C. (1980). Simple analytic form of the relativistic Thomson scattering spectrum. Physics Letters A, 79(5), 405-406.

[60] Matoba, T., Itagaki, T., Yamauchi, T., Funahashi, A. (1979). Analytical approximations in the theory of relativistic Thomson scattering for high temperature fusion plasma. Japanese Journal of Applied Physics, 18(6), 1127.

[61] Kawano, Y., Kondoh, T., Hatae, T. (2006). Diagnostics of relativistic runaway electrons in a tokamak plasma based on laser inverse Compton scattering. Plasma Phys. Control. Fusion 48, 12B (2006), 30I, P4.138.

[62] Y. Kawano et al., Proc. Plasma Science Symposium 2005 / The 22nd Symposium on Plasma Processing, 26-28 January 2005, Will Aichi, Nagoya, Japan (2005) 93-94.

[63] Chouffani, K., Wells, D., Harmon, F., Jones, J., Lancaster, G. (2002). Laser-Compton scattering from a 20MeV electron beam. Nuclear Instruments and Methods in Physics Research Section A: Accelerators, Spectrometers, Detectors and Associated Equipment, 495(2), 95-106.

[64] Chouffani, K., Wells, D., Harmon, F., Lancaster, G., Jones, J. (2003). Laser-Compton Scattering as a Potential Bright X-Ray Source.

[65] Uesaka, M. (2003). Femtosecond beam science. Imperial College Press.

[66] Leemans, W. P., Schoenlein, R. W., Volfbeyn, P., Chin, A. H., Glover, T. E., Balling, P., ... Shank, C. V. (1997). Interaction of relativistic electrons with ultrashort laser pulses: Generation of femtosecond x-rays and microprobing of electron beams. Quantum Electronics, IEEE Journal of, 33(11), 1925-1934.

Spectroscopy

[67] Stutman, D., Finkenthal, M., Suliman, G., Tritz, K., Delgado-Aparicio, L., Kaita, R., ... May, M. J. (2005). Spectroscopic imaging diagnostics for burning plasma experiments. Review of scientific instruments, 76(2), 023505.

[68] Chernyshev, F. V., Afanasyev, V. I., Dech, A. V., Kick, M., Kislyakov, A. I., Kozlovskii, S. S., ... Petrov, S. Y. (2004). A compact neutral-particle analyzer for plasma diagnostics. Instruments and Experimental techniques, 47(2), 214-220.

[69] Tang, V., Liptac, J., Parker, R. R., Bonoli, P. T., Fiore, C. L., Granetz, R. S., ... Petrasso, R. D. (2006). Compact multichannel neutral particle analyzer for measurement of energetic charge-exchanged neutrals in Alcator C-Mod. Review of scientific instruments, 77(8), 083501.

Appendix A

Engineering Design Points

A.1 Magnetic arrays

A.2 HeNe Interferometer

A.3 Microwave interferometer

A.4 Langmuir probes

A.5 Retarding grid energy analyzers

A.6 Rogowski shunt current monintors

A.7 Rogowski probes

A.8 Fiber-based interferometer

A.9 2-color interferometer

Woodruff Scientific Inc
4000 Aurora Ave N,
Suites 5 & 6, Seattle, WA 98103
(206) 905 9477 8am to 5pm Pacific
sales@woodruffscientific.com
http://www.woodruffscientific.com

Model number(s): M1-B-Array
Descriptive name: Array of B-dot coils two directions on plastic form

Miniature insert-able PLA probe form with boron nitride shroud and thin-walled ss boundary.

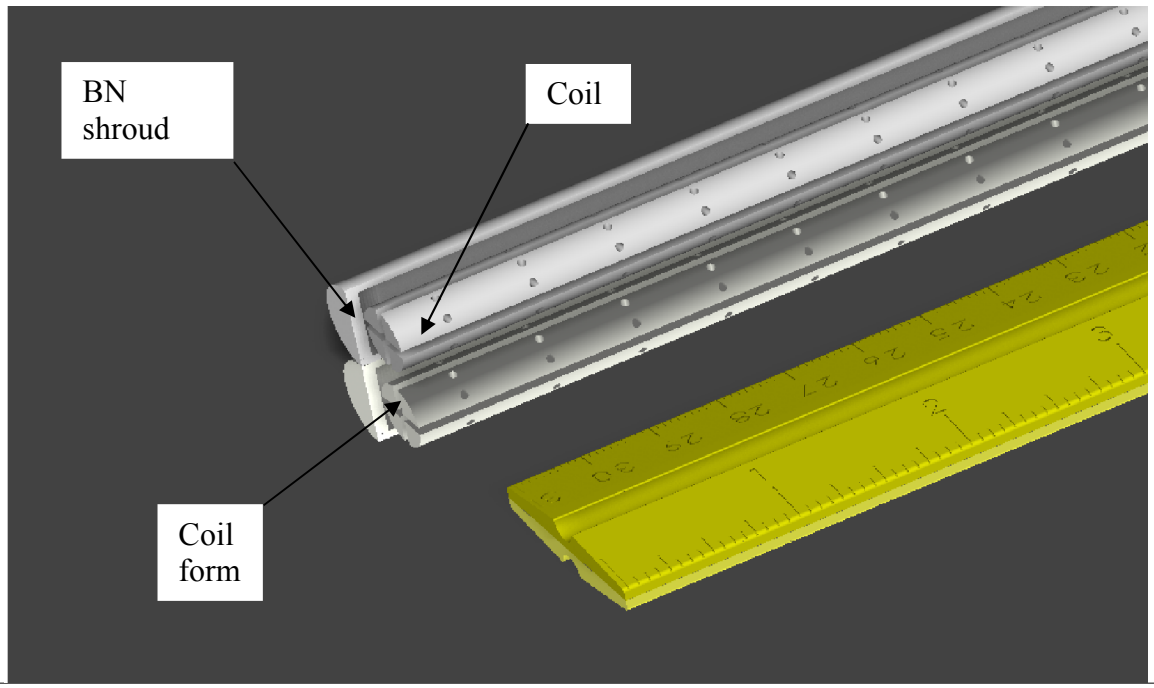

Features:

- Measure components of magnetic field for correlation analysis
- Single piece construction
- Slotted for windings in two directions (or three axis)
- Wound with low errors (custom tolerance)
- Options for wire (Cu is standard)
- Options for form material (inc 3d printed)
- Harnessing lengths custom
- Custom sizing/configurations available

Woodruff Scientific Inc
4000 Aurora Ave N,
Suites 5 & 6, Seattle, WA 98103
(206) 905 9477 8am to 5pm Pacific
sales@woodruffscientific.com
http://www.woodruffscientific.com

Model number(s): M1-B-Array
Descriptive name: Array of B-dot coils two directions on plastic form

Engineering Drawing

Notes:

1. Mounting holes are sized as a clearance fit for a 1/4-20 screw
2. For higher power operation in steady state, attach coils to suitable heat sink
3. Electrical connections to the coil are made with 1/4” lugs, soldered to coil winding

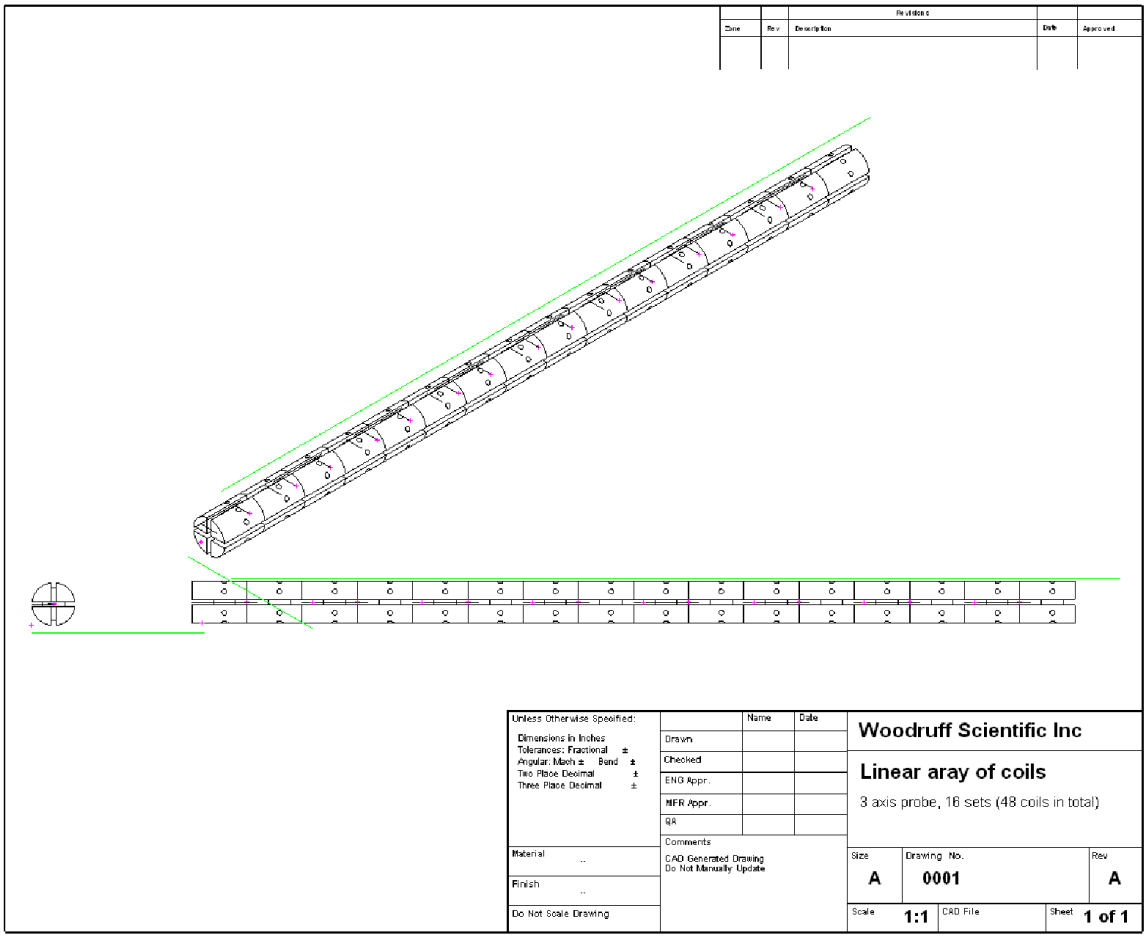

Woodruff Scientific Inc
4000 Aurora Ave N,
Suites 5 & 6, Seattle, WA 98103
(206) 905 9477 8am to 5pm Pacific
sales@woodruffscientific.com
http://www.woodruffscientific.com

Model number(s): M1-B-Array
Descriptive name: Array of B-dot coils two directions on plastic form

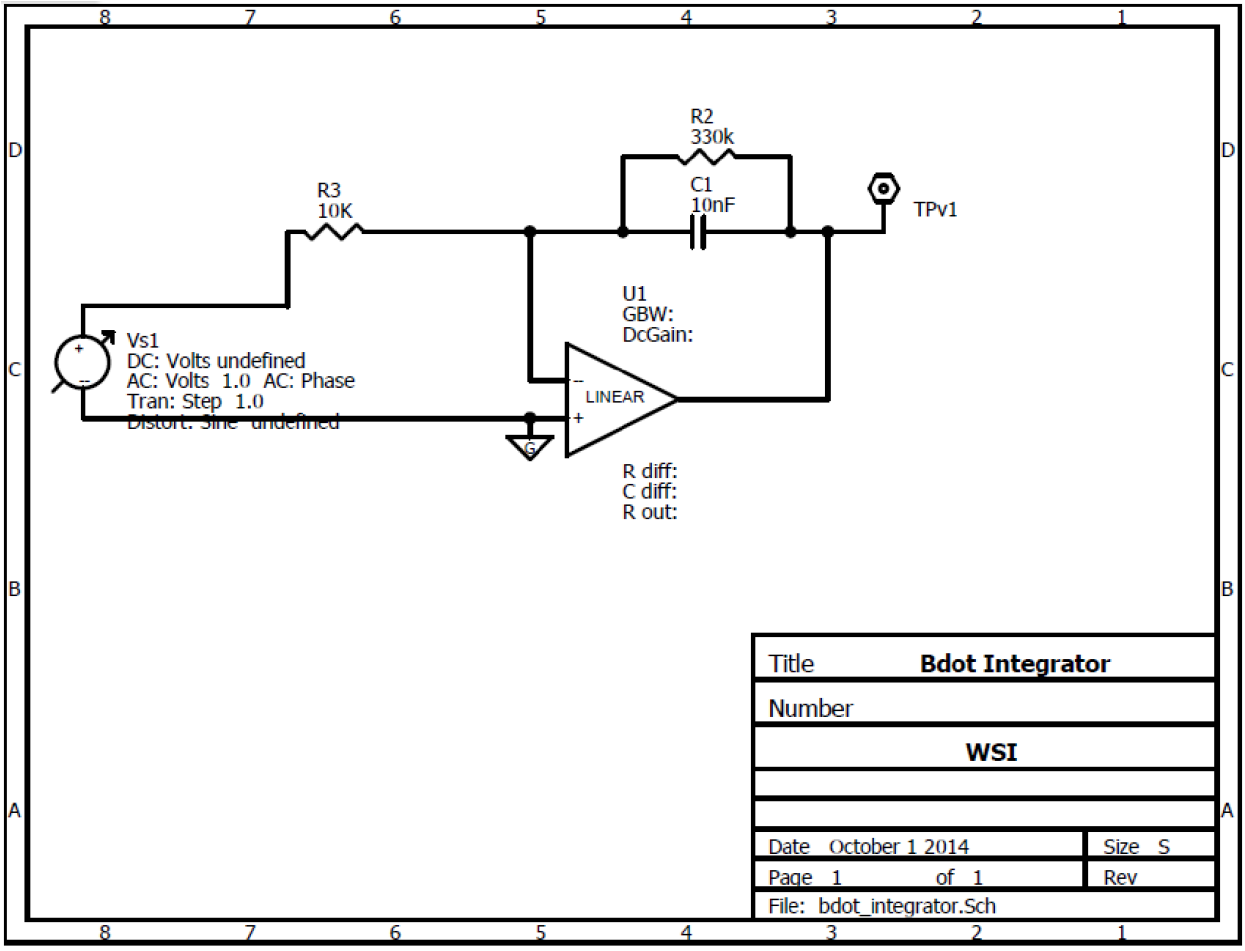

Circuit – Integrator

Woodruff Scientific Inc
4000 Aurora Ave N,
Suites 5 & 6, Seattle, WA 98103
(206) 905 9477 8am to 5pm Pacific
sales@woodruffscientific.com
http://www.woodruffscientific.com

Model number(s): M1-B-Array
Descriptive name: Array of B-dot coils two directions on plastic form

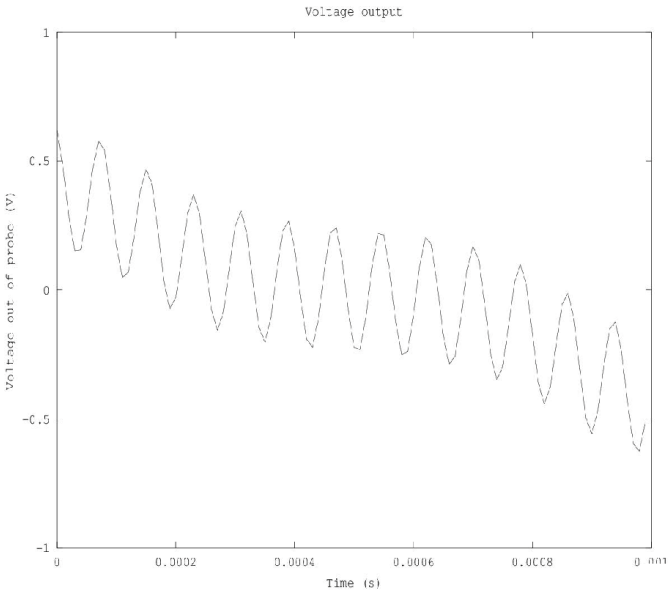

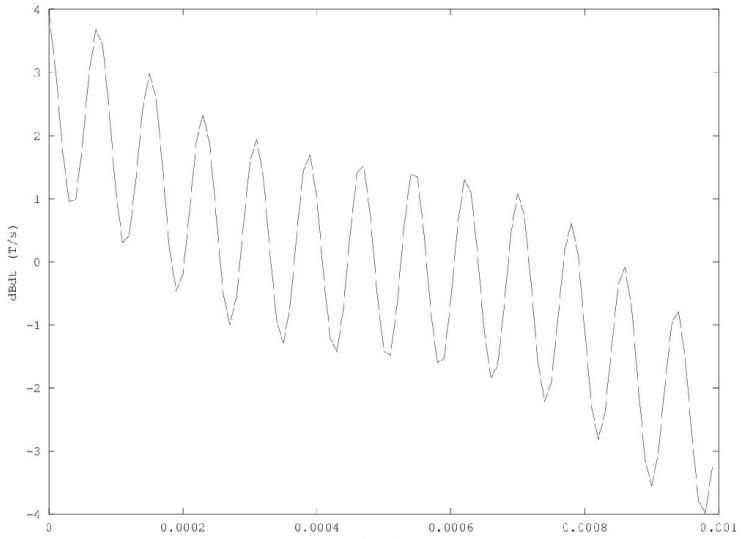

In order to reconstruct the time varying magnetic field, coil voltage signals are first multiplied by the turns-area factor, then integrated. Shown in the plots are example waveforms that could be obtained from experiment. Bottom right is the reconstructed time-history of magnetic field strength.

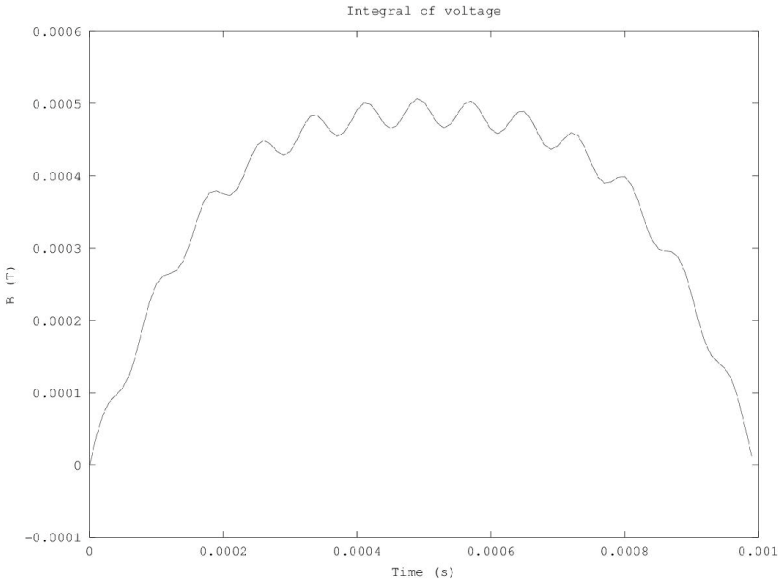

Woodruff Scientific Inc
4000 Aurora Ave N,
Suites 5 & 6, Seattle, WA 98103
(206) 905 9477 8am to 5pm Pacific
sales@woodruffscientific.com
http://www.woodruffscientific.com

Model number(s): R1-HeNe
Descriptive name: HeNe Unequal Path Length Interferometer

Features:

- Measures line-integrated plasma density
- Unequal path length for cost-effective and compact design
- Heterodyne configuration
- Vibration isolation table available at extra cost
- Custom configurations available

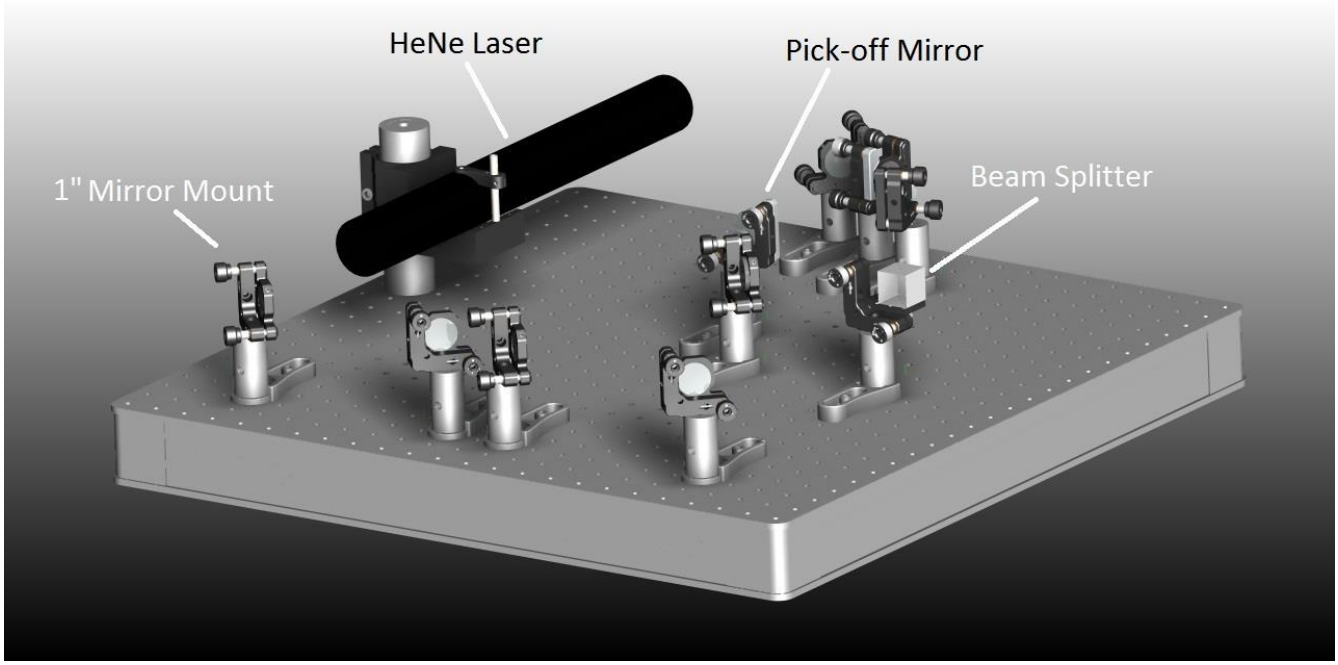

Woodruff Scientific Inc
4000 Aurora Ave N,
Suites 5 & 6, Seattle, WA 98103
(206) 905 9477 8am to 5pm Pacific
sales@woodruffscientific.com
http://www.woodruffscientific.com

Model number(s): R1-HeNe
Descriptive name: HeNe Unequal Path Length Interferometer

Operational ratings:

Electron Line Density: $\geq 10^{21}$ / m^2

Options:

Laser:	5mW standard Higher powers available
AOM:	80 MHz standard
Feedthroughs:	2-3/4” ConFlat mounts standard
Controls:	National Instruments DAQ and controls available Contact us for more information on interfacing with your experiment

Signal Output:

Quadrature mixer/splitter outputs sin and cos of phase difference. Example software for calculating line-integrated density available.

Woodruff Scientific Inc
4000 Aurora Ave N,
Suites 5 & 6, Seattle, WA 98103
(206) 905 9477 8am to 5pm Pacific
sales@woodruffscientific.com
http://www.woodruffscientific.com

Model number(s): R1-HeNe
Descriptive name: HeNe Unequal Path Length Interferometer

Schematics:

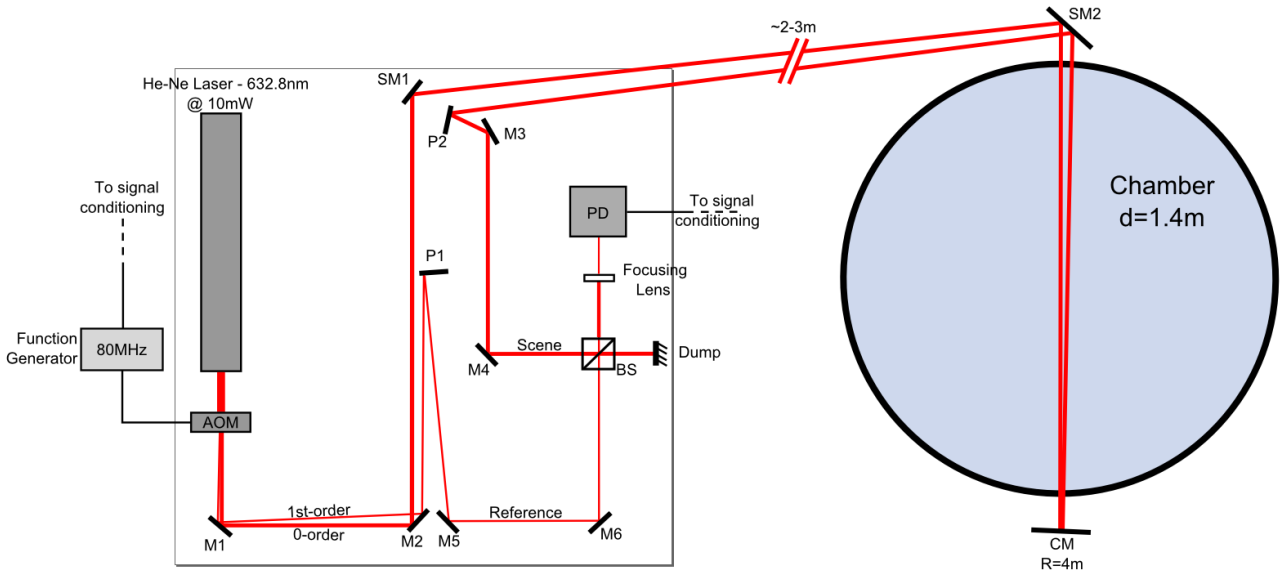

Layout Schematic

Woodruff Scientific Inc
4000 Aurora Ave N,
Suites 5 & 6, Seattle, WA 98103
(206) 905 9477 8am to 5pm Pacific
sales@woodruffscientific.com
http://www.woodruffscientific.com

Model number(s): R1-HeNe
Descriptive name: HeNe Unequal Path Length Interferometer

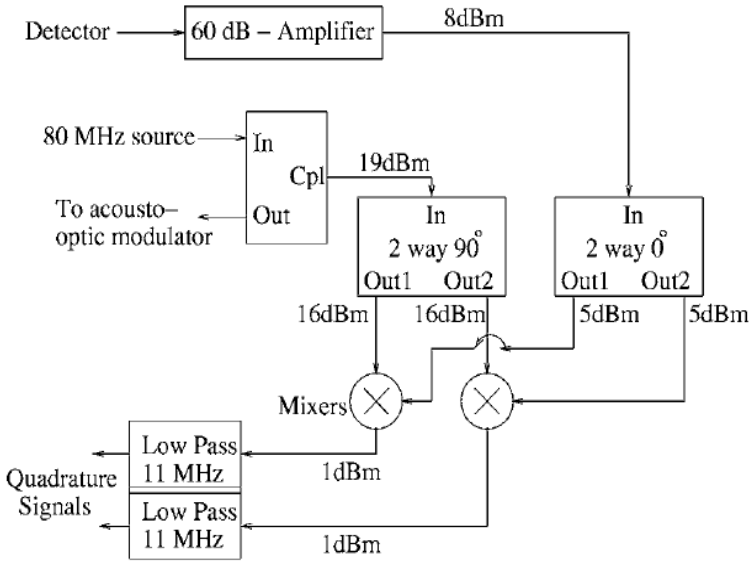

RF Circuit Schematic

Woodruff Scientific Inc
4000 Aurora Ave N,
Suites 5 & 6, Seattle, WA 98103
(206) 905 9477 8am to 5pm Pacific
sales@woodruffscientific.com
http://www.woodruffscientific.com

Model number(s): R1-HeNe
Descriptive name: HeNe Unequal Path Length Interferometer

Example Data:

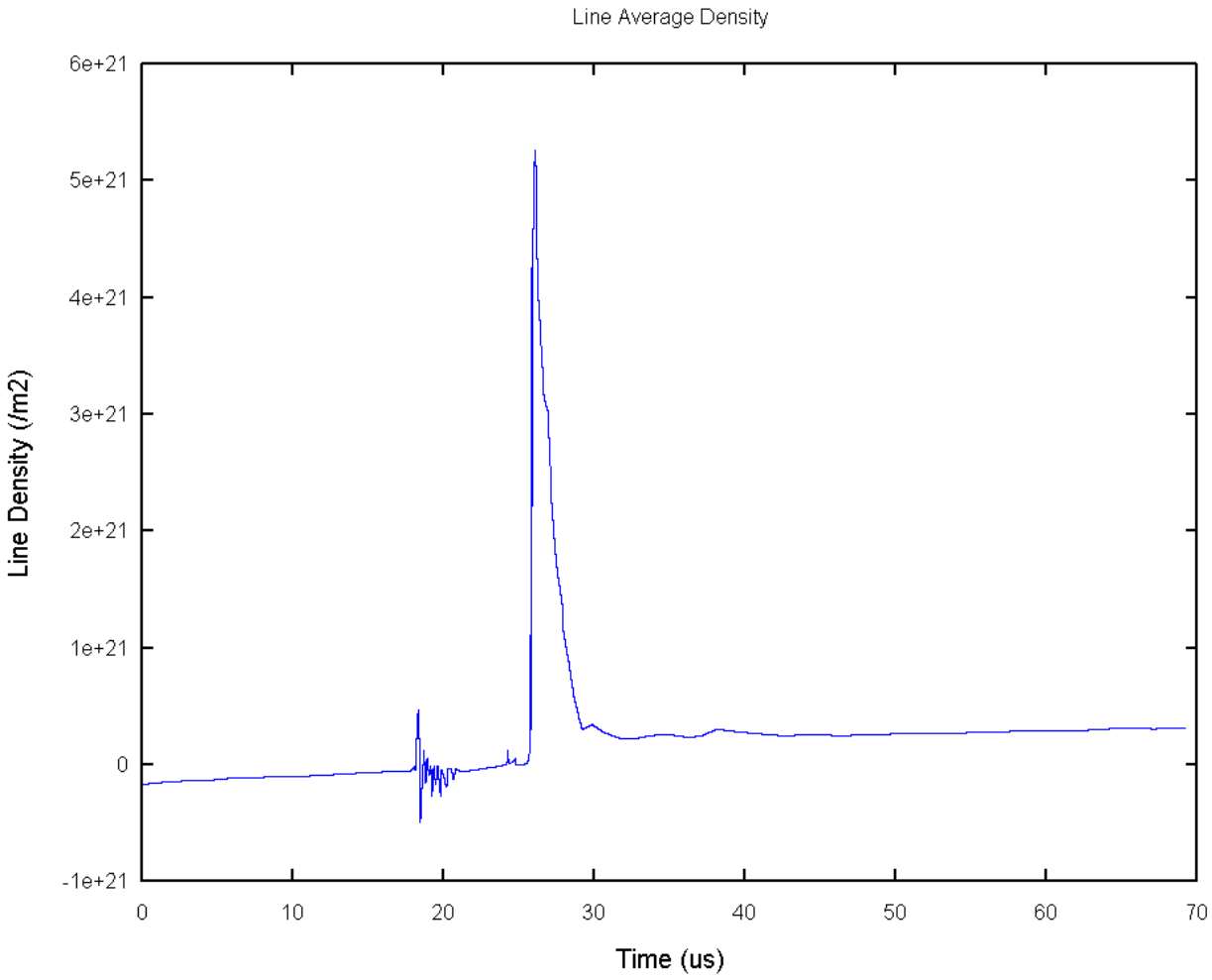

Line Density interpretation (simulated signal)

WOODRUFF • SCIENTIFIC

Woodruff Scientific Inc
4000 Aurora Ave N,
Suites 5 & 6, Seattle, WA 98103
(206) 905 9477 8am to 5pm Pacific
sales@woodruffscientific.com
http://www.woodruffscientific.com

Model number(s): E1-RFA-U / E1-RFA-B / E1-RFA-A
Descriptive name: Retarding Field Analyzer – Unidirectional / Bidirectional / Axial

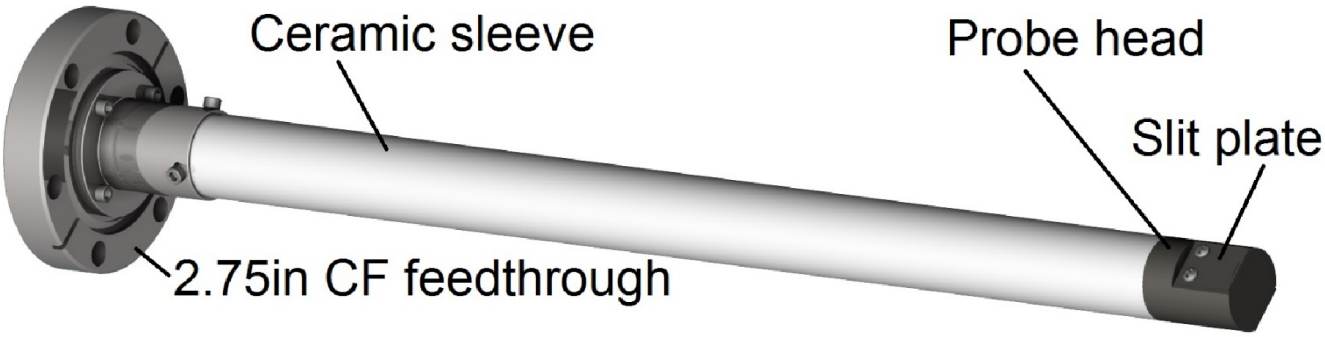

Features:
- Measures ion and electron energy distributions in accessible plasma region
- Unidirectional, bidirectional (shown), and axial (see last page) options available
- Custom sizing and materials based on Debye length and heat flux
- Wedge slit and 2-grid design provides low perturbation sampling and includes secondary electron suppression
- Fast, swept electronics for time-resolved measurement during a single shot
- Mounts to many standard vacuum electrical feedthrough
- Can be angled to align with magnetic field
- Design for ultra-high vacuum (UHV) compatibility
- Can be used on a reciprocating drive

Operational ratings:
Debye length (λ_D): ≥ 16 μm
Heat flux: ≤ 10 MW/m^2

Options:
- Orientations: Unidirectional / Bidirectional / Axial
  Unidirectional and bidirectional orientations allow for better alignment with the magnetic field in toroidal plasmas; axial orientation allows measurement perpendicular to the magnetic field and may be better suited for non-toroidal plasmas
- Electronics: Static / Swept
  Static electronics provide a high temporal resolution measurement of the ion current during an experimental shot; swept electronics provide a high energy resolution measurement of the entire energy distribution during a single shot

Woodruff Scientific Inc
4000 Aurora Ave N,
Suites 5 & 6, Seattle, WA 98103
(206) 905 9477 8am to 5pm Pacific
sales@woodruffscientific.com
http://www.woodruffscientific.com

Model number(s): E1-RFA-U / E1-RFA-B / E1-RFA-A
Descriptive name: Retarding Field Analyzer – Unidirectional / Bidirectional / Axial

Engineering drawing:

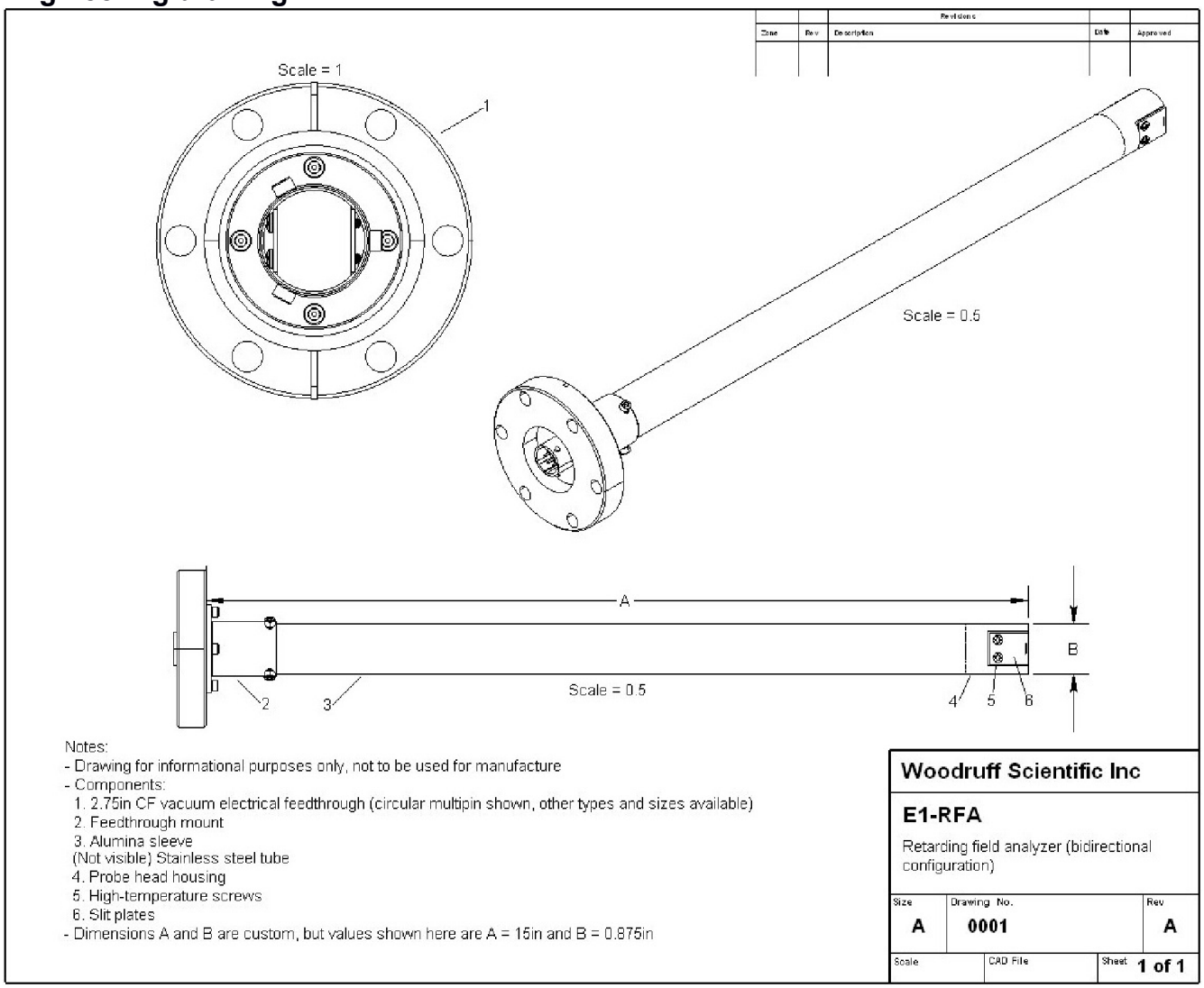

Woodruff Scientific Inc
4000 Aurora Ave N,
Suites 5 & 6, Seattle, WA 98103
(206) 905 9477 8am to 5pm Pacific
sales@woodruffscientific.com
http://www.woodruffscientific.com

Model number(s): E1-RFA-U / E1-RFA-B / E1-RFA-A
Descriptive name: Retarding Field Analyzer – Unidirectional / Bidirectional / Axial

Electronics schematic:

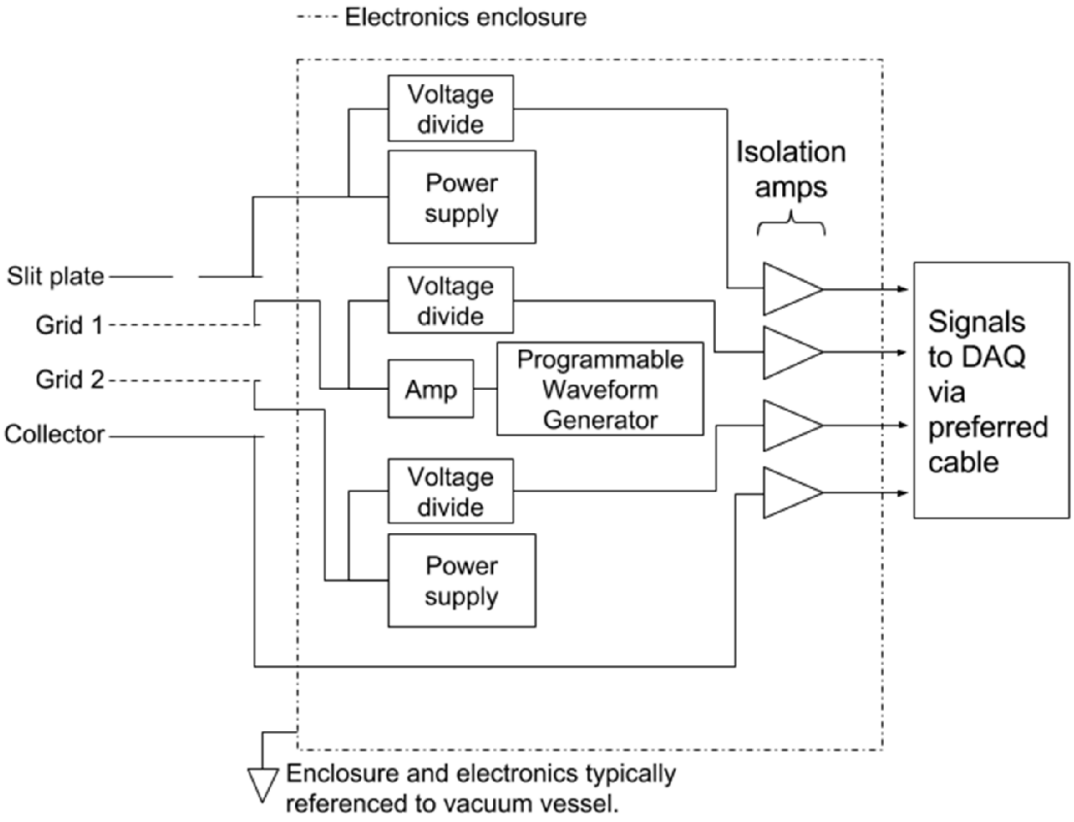

The electronics schematic is shown above for the unidirectional and axial variations; the bidirectional electronics include additional collector and slit plate circuits. The sweep frequency and grid/slit plate potentials are remotely controlled. Potential divides on the grid/slit plate circuits and isolation amplifiers (circuit shown on right) on all circuits ensure that the data acquisition system is protected.

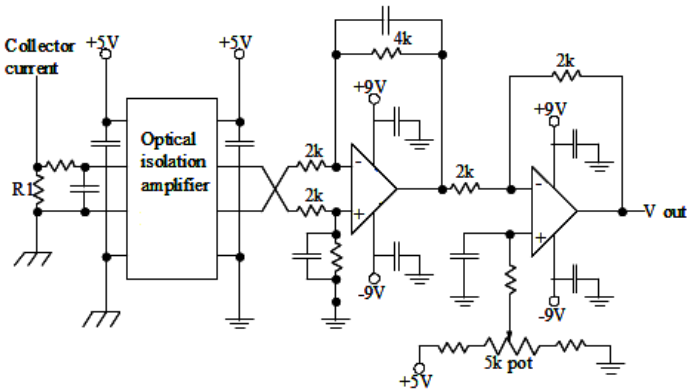

WOODRUFF • SCIENTIFIC

Woodruff Scientific Inc
4000 Aurora Ave N,
Suites 5 & 6, Seattle, WA 98103
(206) 905 9477 8am to 5pm Pacific
sales@woodruffscientific.com
http://www.woodruffscientific.com

Model number(s): E1-RFA-U / E1-RFA-B / E1-RFA-A
Descriptive name: Retarding Field Analyzer – Unidirectional / Bidirectional / Axial

Example post-processing:

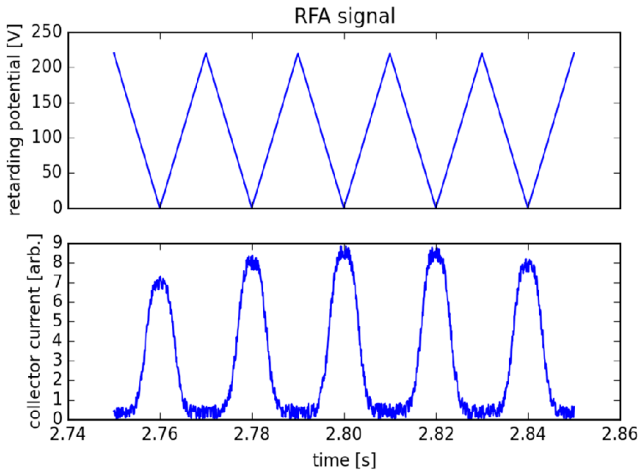

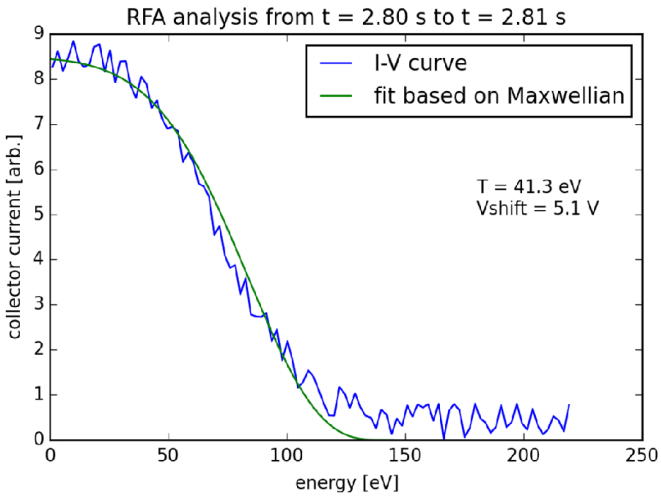

Post-processing of RFA data can be integrated with the experiment monitoring software to provide real-time results, like those shown above. On the left is an example of an RFA signal for a given experimental shot, showing both the retarding potential and collector current. On the right is the signal from one half-period of the retarding potential waveform, with a fit based on a Maxwellian distribution that provides the ion temperature and energy shift. The RFA post-processing software allows the user to select multiple time intervals during which to calculate the energy distribution.

Customization:
In addition to the options listed previously, the RFA is highly customizable. For example, the axial orientation shown on the right includes an aperture with multiple entrances for high-flux applications and can be designed to mount on any vacuum electrical feedthrough.

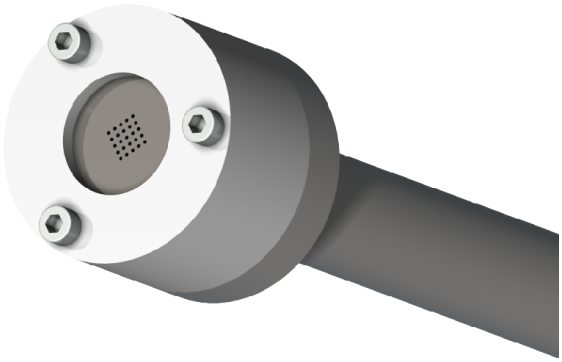

WOODRUFF • SCIENTIFIC

Woodruff Scientific Inc
4000 Aurora Ave N,
Suites 5 & 6, Seattle, WA 98103
(206) 905 9477 8am to 5pm Pacific
sales@woodruffscientific.com
http://www.woodruffscientific.com

Model number(s): M1-R-C
Descriptive name: Rogowski Coil

Features:

- Measures the current passing through the coil
- Designed for ultra-high vacuum (UHV) compatibility
- Custom coil diameter and casing material
- Can be mounted behind wall tiles (right), around central column, diverter posts, and other locations
- Electrostatically shielded by thin-walled metal case for low capacitive noise and choked for common-mode isolation
- Includes custom integrator circuit
- Includes full calibration and transfer function characterization
- Can be mounted on a probe and inserted into plasma for current profile measurement (see M1-R-P spec sheet)

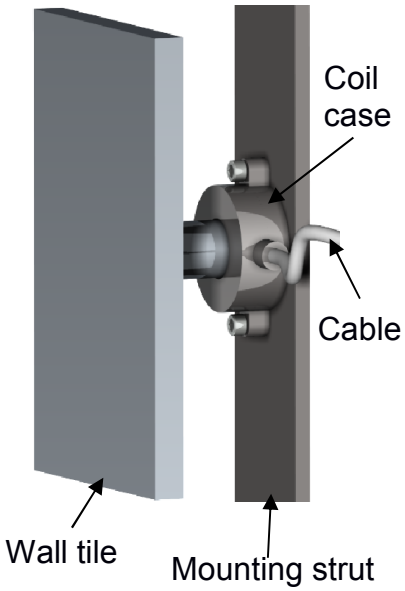

Operational ratings:

Max. current	: 50 kA
Max. frequency	: 1 MHz
Bandwidth	: 3 MHz
Min. major radius	: 1 cm (pictured above)

Options and customization:

Coil diameter:	determines the spatial resolution or designed to fit around post
Casing material:	stainless steel (standard, shown), molybdenum for high heat applications, or boron nitride if electrical isolation from mount is required
Mounting interface:	can be customized to mount in many configurations
Split or slip-on coil:	split coils can me mounted around posts already in place
Full or partial coil:	an array of partial coils may be used to reconstruct plasma location or linked together to surround the entire cross-section of the plasma

Woodruff Scientific Inc
4000 Aurora Ave N,
Suites 5 & 6, Seattle, WA 98103
(206) 905 9477 8am to 5pm Pacific
sales@woodruffscientific.com
http://www.woodruffscientific.com

Model number(s): M1-R-C
Descriptive name: Rogowski Coil

Engineering drawing of probe configuration:

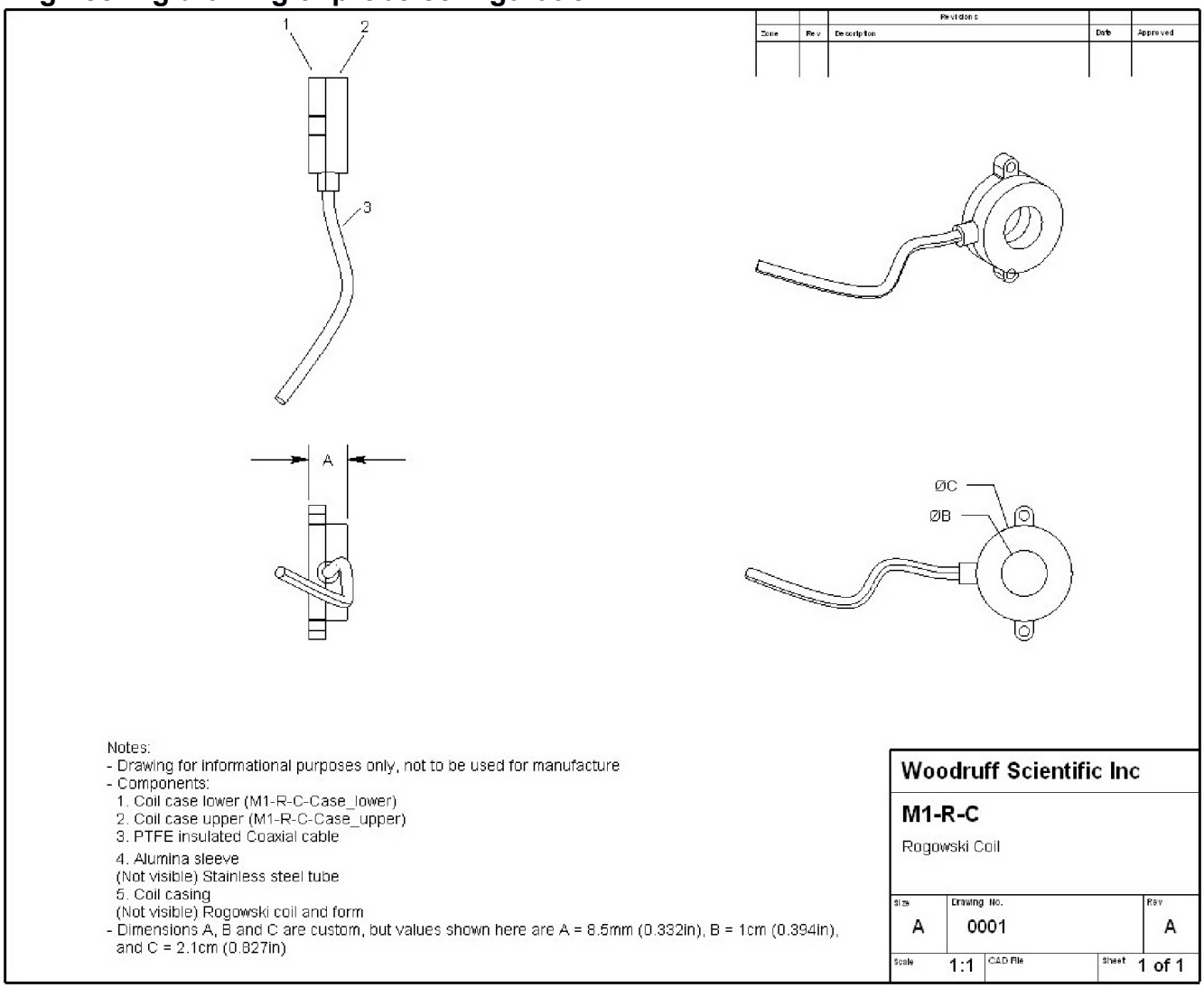

Woodruff Scientific Inc
4000 Aurora Ave N,
Suites 5 & 6, Seattle, WA 98103
(206) 905 9477 8am to 5pm Pacific
sales@woodruffscientific.com
http://www.woodruffscientific.com

Model number(s): M1-R-C
Descriptive name: Rogowski Coil

Signal integrator circuit:

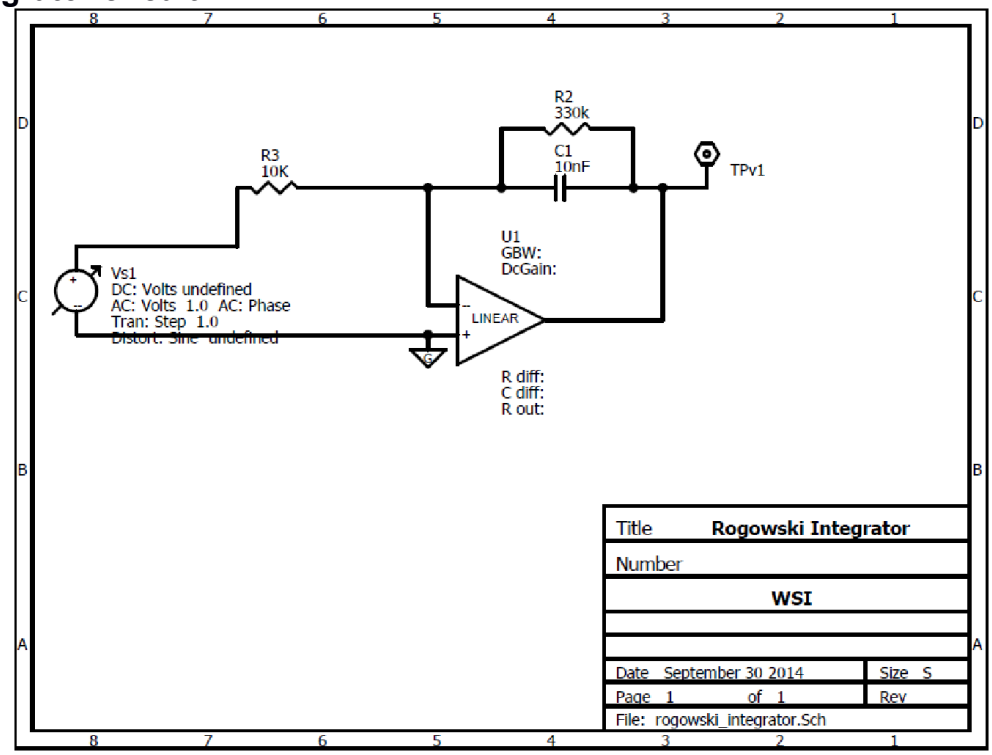

Connection diagram:

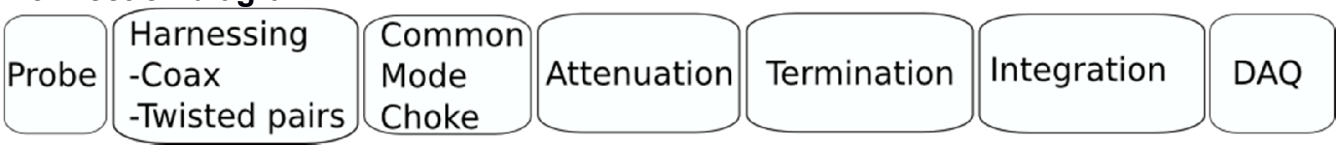

Woodruff Scientific Inc
4000 Aurora Ave N,
Suites 5 & 6, Seattle, WA 98103
(206) 905 9477 8am to 5pm Pacific
sales@woodruffscientific.com
http://www.woodruffscientific.com

Model number(s): M1-R-C
Descriptive name: Rogowski Coil

Data analysis:
Recovering the current from a Rogowski coil measurement (potential trace at right) involves multiplying the Fourier transform of the signal (shown at bottom left) with the response function of the device (shown at bottom right). This response function is determined during calibration and provided with the device. Taking the inverse Fourier transform of the result provides the measured current (shown at right).

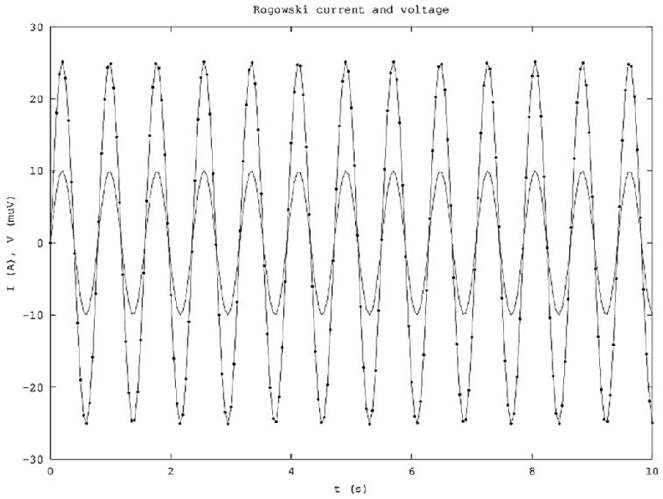

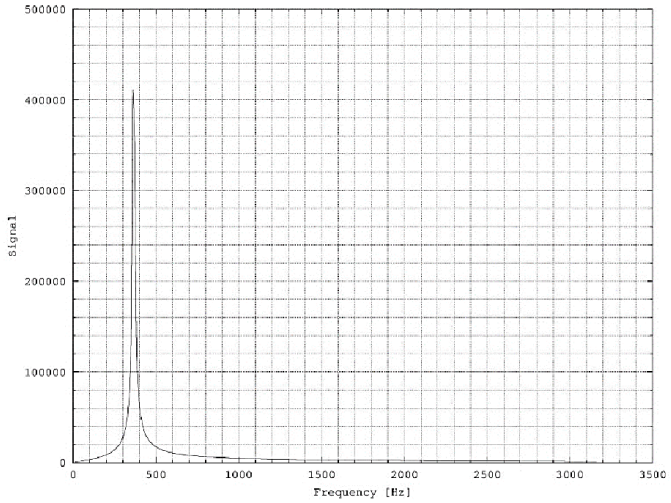

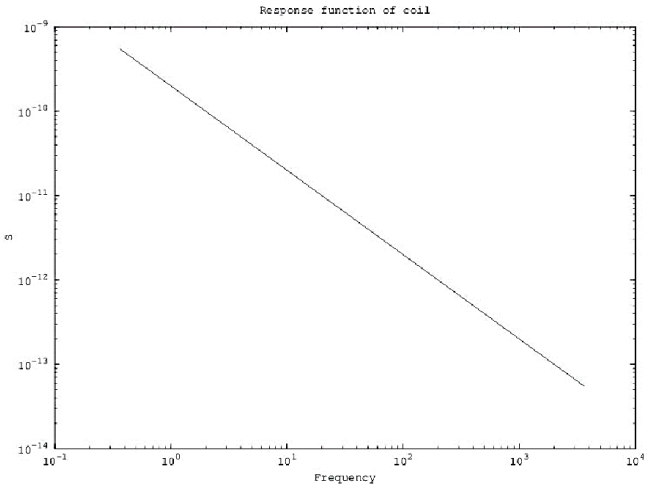

WOODRUFF • SCIENTIFIC

Woodruff Scientific Inc
4000 Aurora Ave N,
Suites 5 & 6, Seattle, WA 98103
(206) 905 9477 8am to 5pm Pacific
sales@woodruffscientific.com
http://www.woodruffscientific.com

Model number(s): M1-R-P
Descriptive name: Rogowski Coil Probe

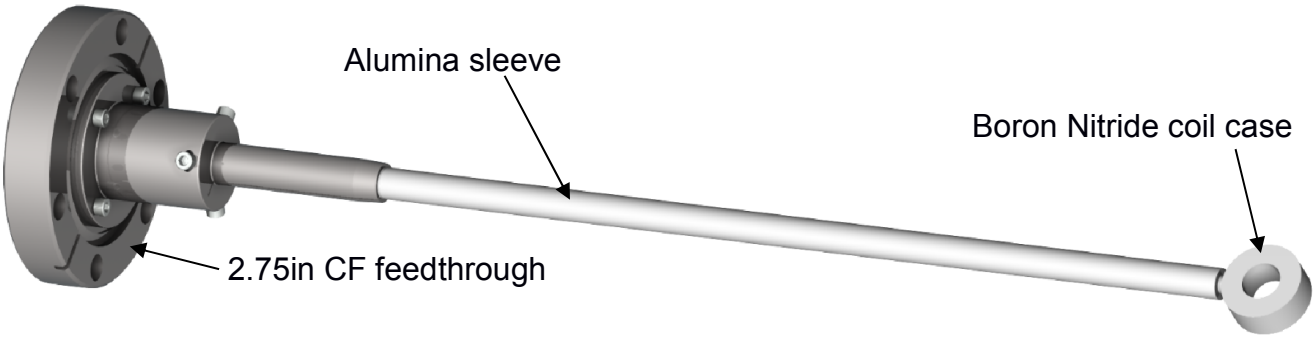

Features:

- Measures the current passing through the coil
- Designed to be inserted into the plasma
- Designed for ultra-high vacuum (UHV) compatibility
- Custom coil diameter and probe arm length
- Mounts to many vacuum electrical feedthroughs
- Can be mounted on reciprocating drive for current profile measurement
- Electrostatically shielded for low capacitive noise and choked for common-mode isolation
- Includes custom integrator circuit
- Includes full calibration and transfer function characterization
- Probe head can be mounted behind wall tiles, around central column, diverter posts, and other locations (see M1-R-C spec sheet)

Operational ratings:

Max. current	: 50 kA
Max. heat flux	: 500 W/cm^2
Max. frequency	: 1 MHz
Bandwidth	: 3 MHz
Min. major radius	: 1 cm (pictured above)

Options and customization:

Coil diameter:	determines the spatial resolution and collected current
Probe arm length:	determines point (or range) of plasma profile to be measured
Mounting interface:	various flange sizes and types (CF, KF, etc.) or custom drive mount
Full or partial coil:	an array of partial coils may be used to reconstruct plasma location

Woodruff Scientific Inc
4000 Aurora Ave N,
Suites 5 & 6, Seattle, WA 98103
(206) 905 9477 8am to 5pm Pacific
sales@woodruffscientific.com
http://www.woodruffscientific.com

Model number(s): M1-R-P
Descriptive name: Rogowski Coil Probe

Engineering drawing of probe configuration:

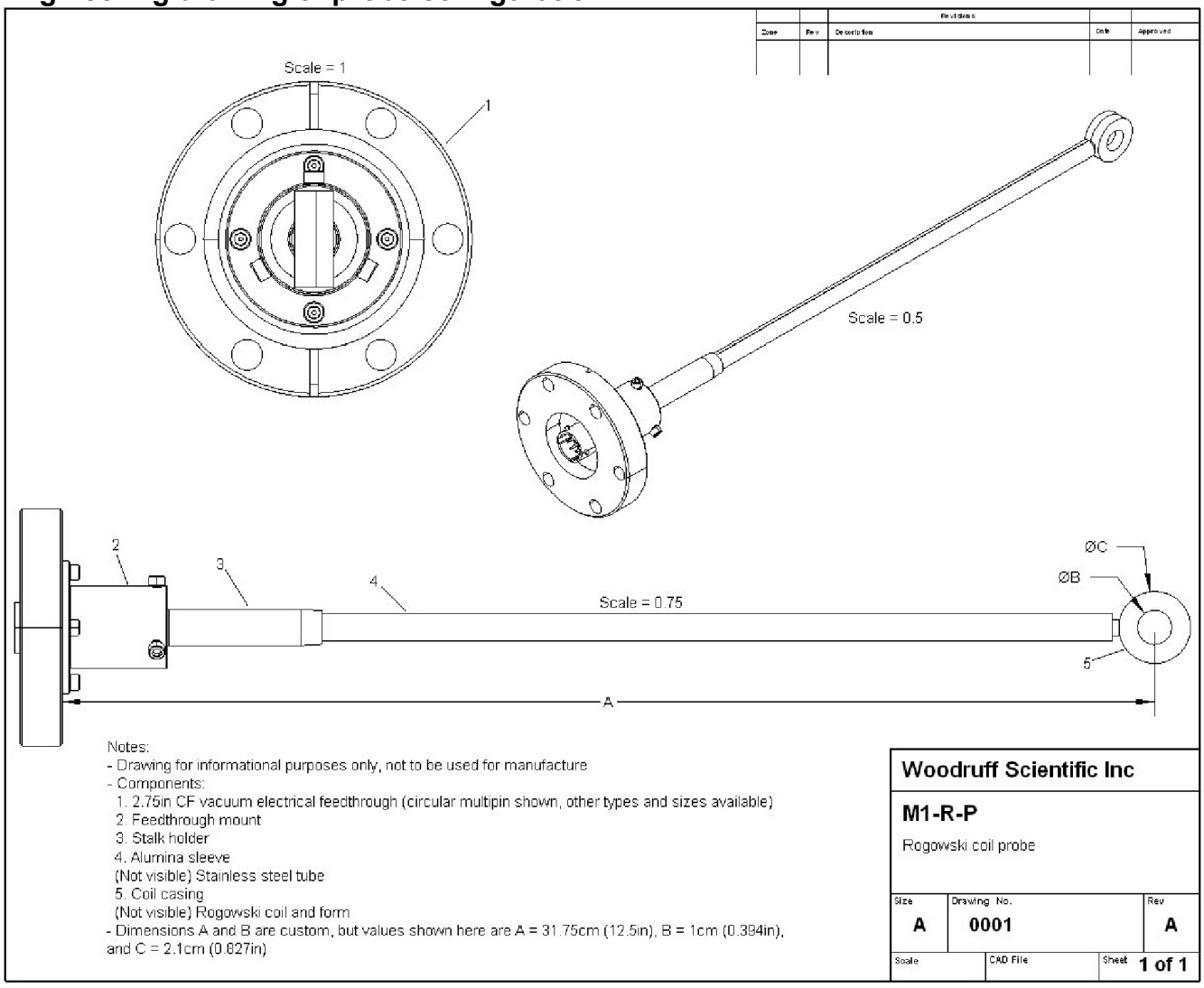

Woodruff Scientific Inc
4000 Aurora Ave N,
Suites 5 & 6, Seattle, WA 98103
(206) 905 9477 8am to 5pm Pacific
sales@woodruffscientific.com
http://www.woodruffscientific.com

Model number(s): M1-R-P
Descriptive name: Rogowski Coil Probe

Signal integrator circuit:

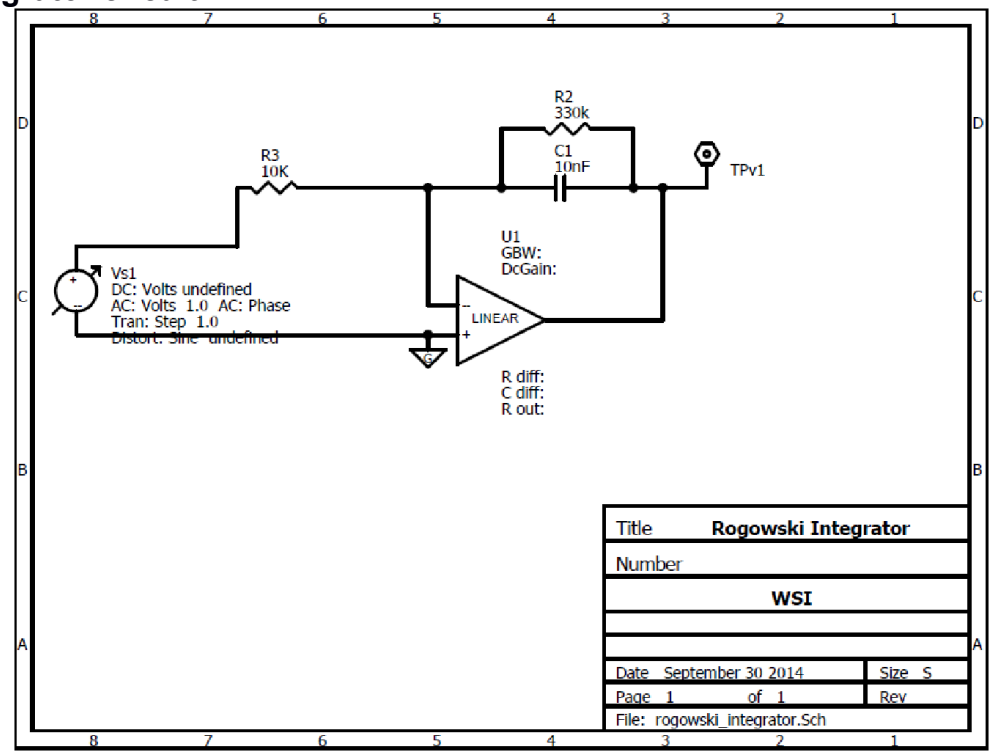

Connection diagram:

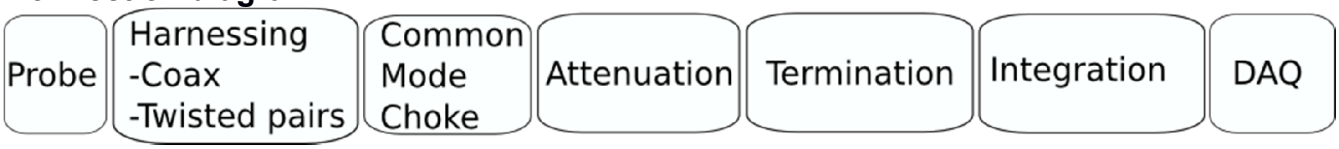

Woodruff Scientific Inc
4000 Aurora Ave N,
Suites 5 & 6, Seattle, WA 98103
(206) 905 9477 8am to 5pm Pacific
sales@woodruffscientific.com
http://www.woodruffscientific.com

Model number(s): M1-R-P
Descriptive name: Rogowski Coil Probe

Data analysis:
Recovering the current from a Rogowski coil measurement (potential trace at right) involves multiplying the Fourier transform of the signal (shown at bottom left) with the response function of the device (shown at bottom right). This response function is determined during calibration and provided with the device. Taking the inverse Fourier transform of the result provides the measured current (shown at right).

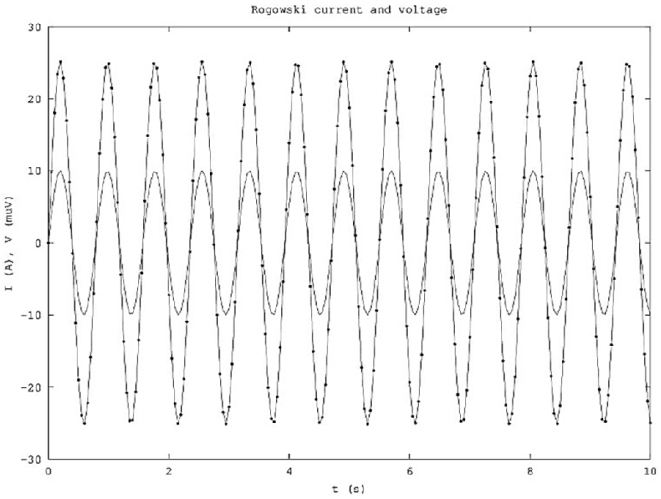

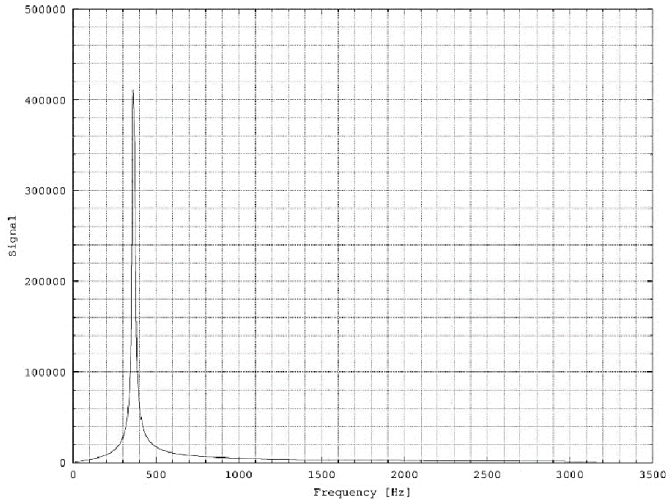

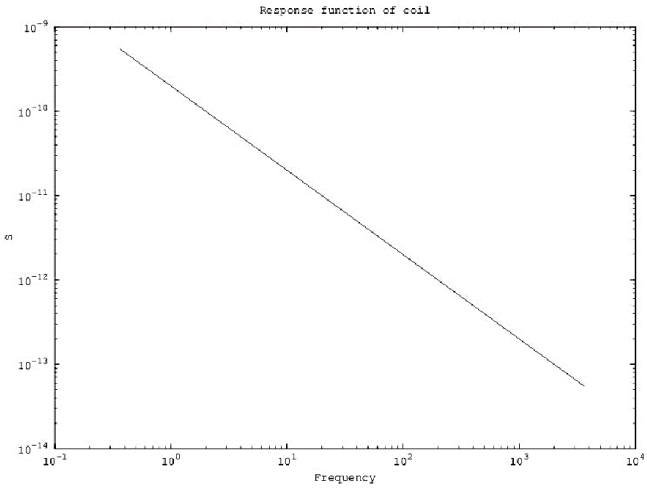

Woodruff Scientific, Inc.
4000 Aurora Ave N, Suites 5 & 6,
Seattle, WA 98103
(206) 905 9477 8am to 5pm Pacific
sales@woodruffscientific.com
http://www.woodruffscientific.com

Model number(s): R1-F-2C
Descriptive name: Fiber-Coupled, 2-color Interferometer

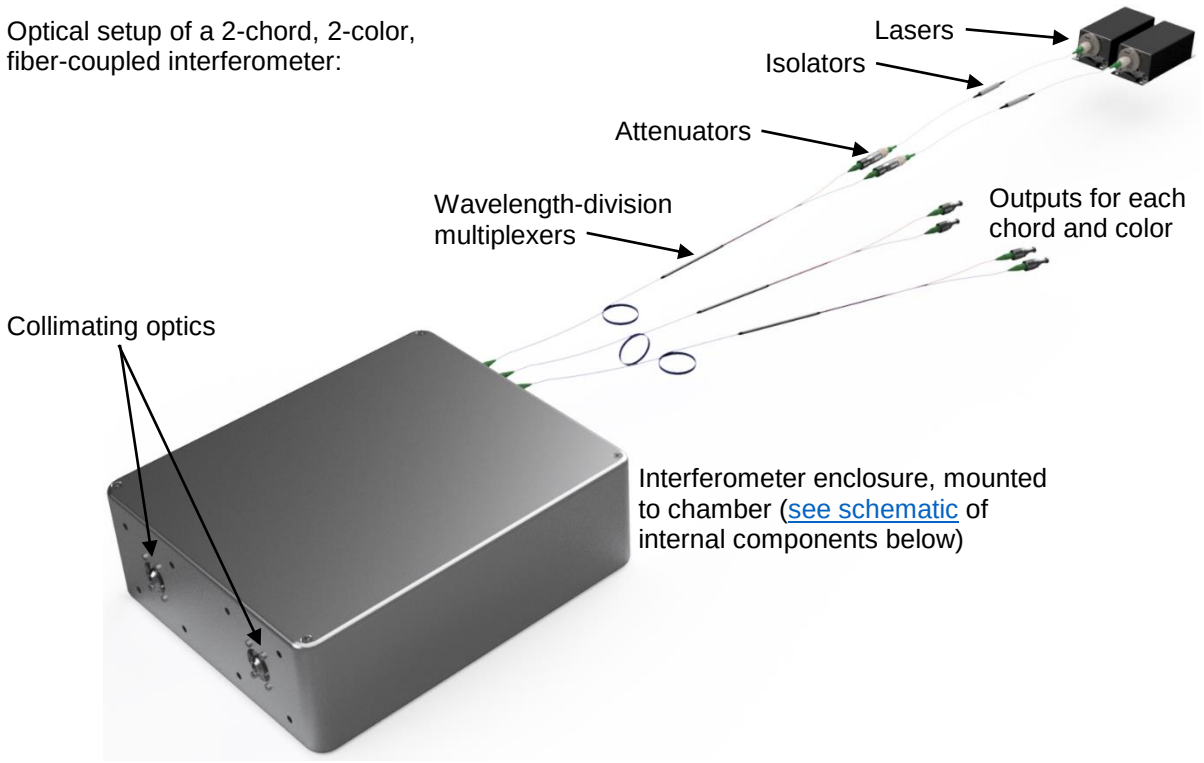

Features:

- Measures chord-averaged electron density using two laser wavelengths for vibration compensation
- Fiber-based design allows line of sight to be changed without realignment of optics
- High-frequency laser provides high temporal resolution
- Heterodyne configuration for extended unambiguous measurement range
- Extendable to multiple chords
- Custom mounting to vacuum chamber
- Laser sources in 1.31 μm and 1.55 μm wavelengths
- Uses FC/APC fiber optic connections for high quality beam launching
- Includes simple alignment system using fiber-coupled HeNe laser “seen beam”
- Class 3B lasers are housed in an interlocked enclosure with output attenuated to safe level

Woodruff Scientific, Inc.
4000 Aurora Ave N, Suites 5 & 6,
Seattle, WA 98103
(206) 905 9477 8am to 5pm Pacific
sales@woodruffscientific.com
http://www.woodruffscientific.com

Model number(s): R1-F-2C
Descriptive name: Fiber-Coupled, 2-color Interferometer

Operational ratings:

Electron density (n_e):	$< 5 \times 10^{26}$ m^{-3}
Density resolution* ($\delta \langle n_e L \rangle$):	3×10^{19} m^{-2}
Temporal resolution** ($d\langle n_e L \rangle/dt$):	1×10^{30} $m^{-2}s^{-1}$

** corresponding to 1.0° phase resolution; actual resolution may vary with application*

*** depending on data acquisition*

Options:

Number of chords
Having multiple chords allows for the spatial reconstruction of the electron density profile or analysis of plasma propagation, but increases the cost and complexity of the system.

WSI also offers a single-color, fiber-coupled interferometer, as well as standard HeNe, CO_2, and microwave interferometers. See the website for more information.

Contact WSI for pricing, operational ratings specific to your application, and more information on which options may be appropriate for you. Please provide any information you may have about your application's density, size, and timescale, as well as any preferences.

Woodruff Scientific, Inc.
4000 Aurora Ave N, Suites 5 & 6,
Seattle, WA 98103
(206) 905 9477 8am to 5pm Pacific
sales@woodruffscientific.com
http://www.woodruffscientific.com

Model number(s): R1-F-2C
Descriptive name: Fiber-Coupled, 2-color Interferometer

Schematic (1-chord option shown):

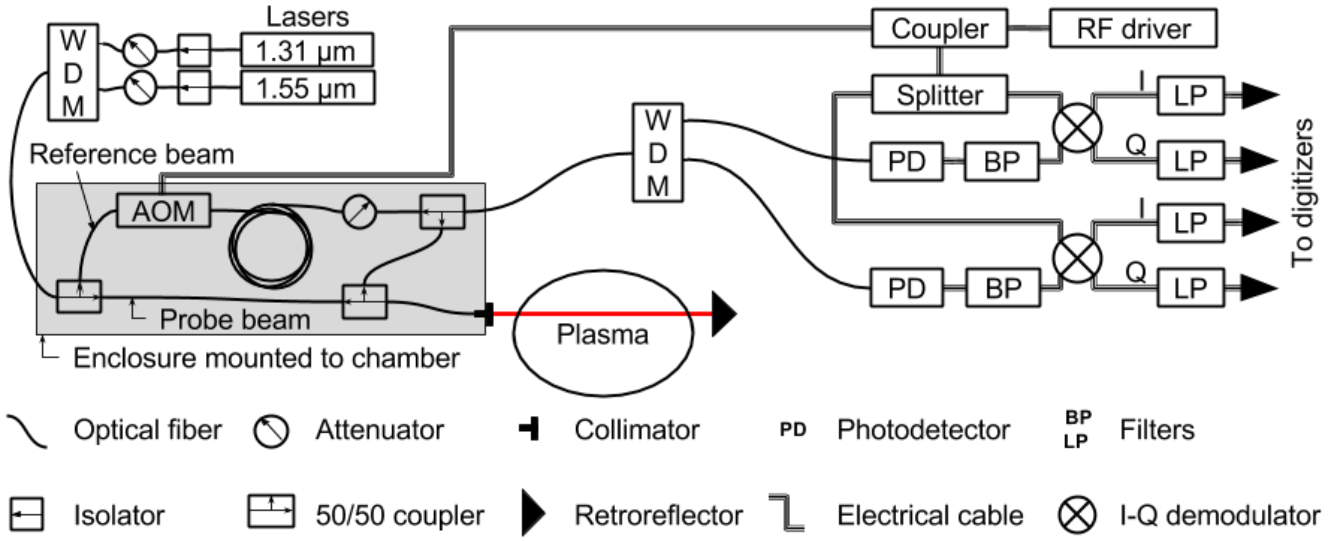

Shown above are the optical (left) and electrical (right) schematics for a 1-chord R1-F-2C interferometer. The fiber-coupled lasers are sent through isolators and attenuators to a wavelength-division multiplexer (WDM), which combines the two beams. The combined beam is then routed to an enclosure mounted to the vacuum chamber. The beam is divided by a 50/50 coupler into the probe and reference beams.

The reference beam is frequency shifted by an acousto-optic modulator (AOM), then send through a fiber delay and an attenuator. The probe beam goes backwards through another coupler, through a collimator and the plasma, is reflected, crosses the plasma again, and reenters the enclosure via the collimator. When the probe beam goes forwards through the coupler, half is sent back toward the lasers and is stopped by the isolators. The other half is sent to another coupler, where it is recombined with the reference beam.

The recombined beam is split into the two colors by another WDM. The two colors are separately converted to an electrical signal, filtered, and mixed with the RF driver signal. The I and Q for each color are output to coaxial cables for connection to the experiment DAQ system.

Woodruff Scientific, Inc.
4000 Aurora Ave N, Suites 5 & 6,
Seattle, WA 98103
(206) 905 9477 8am to 5pm Pacific
sales@woodruffscientific.com
http://www.woodruffscientific.com

Model number(s): R1-F-2C
Descriptive name: Fiber-Coupled, 2-color Interferometer

Example data:

At right is example data from an interferometer. The I and Q signals represent the cosine and sine of the phase shift, respectively. These values are used to unambiguously compute the phase shift for each color, $\Delta\varphi_i$. Both colors experience a phase shift due to the plasma and acoustic vibration, but the shorter wavelength is more sensitive to the vibration. Subtracting a portion of the shorter wavelength's phase shift from that of the longer wavelength allows the phase shift caused only by the plasma to be determined, as shown below. The line-integrated electron density, $\overline{n_e L}$, is calculated from the plasma-induced phase shift, and is shown in the bottom of the plot.

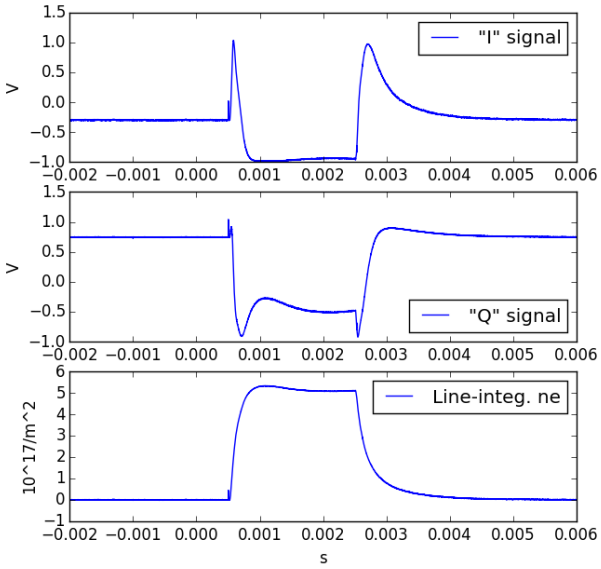

$$\Delta\varphi_i = \Delta\varphi_{plasma} + \Delta\varphi_{vibration} = k\lambda_i\overline{n_e L} + \frac{2\pi}{\lambda_i}\Delta L, \qquad k \equiv \frac{e^2}{2c^s m_e \varepsilon_0}$$

$$\Delta\varphi_{plasma} = \Delta\varphi_1 - \frac{\lambda_2}{\lambda_1}\Delta\varphi_2, \qquad \lambda_1 > \lambda_2$$

$$\overline{n_e L} = \frac{\lambda_1}{k(\lambda_1^2 - \lambda_2^2)}\left[\Delta\varphi_1 - \frac{\lambda_2}{\lambda_1}\Delta\varphi_2\right]$$

where, e is the electron charge, c is the speed of light, m_e is the electron mass, and ε_0 is the vacuum permittivity.

Woodruff Scientific, Inc.
4000 Aurora Ave N, Suites 5 & 6,
Seattle, WA 98103
(206) 905 9477 8am to 5pm Pacific
sales@woodruffscientific.com
http://www.woodruffscientific.com

Model number(s): R1-F-2C
Descriptive name: Fiber-Coupled, 2-color Interferometer

Engineering drawing:

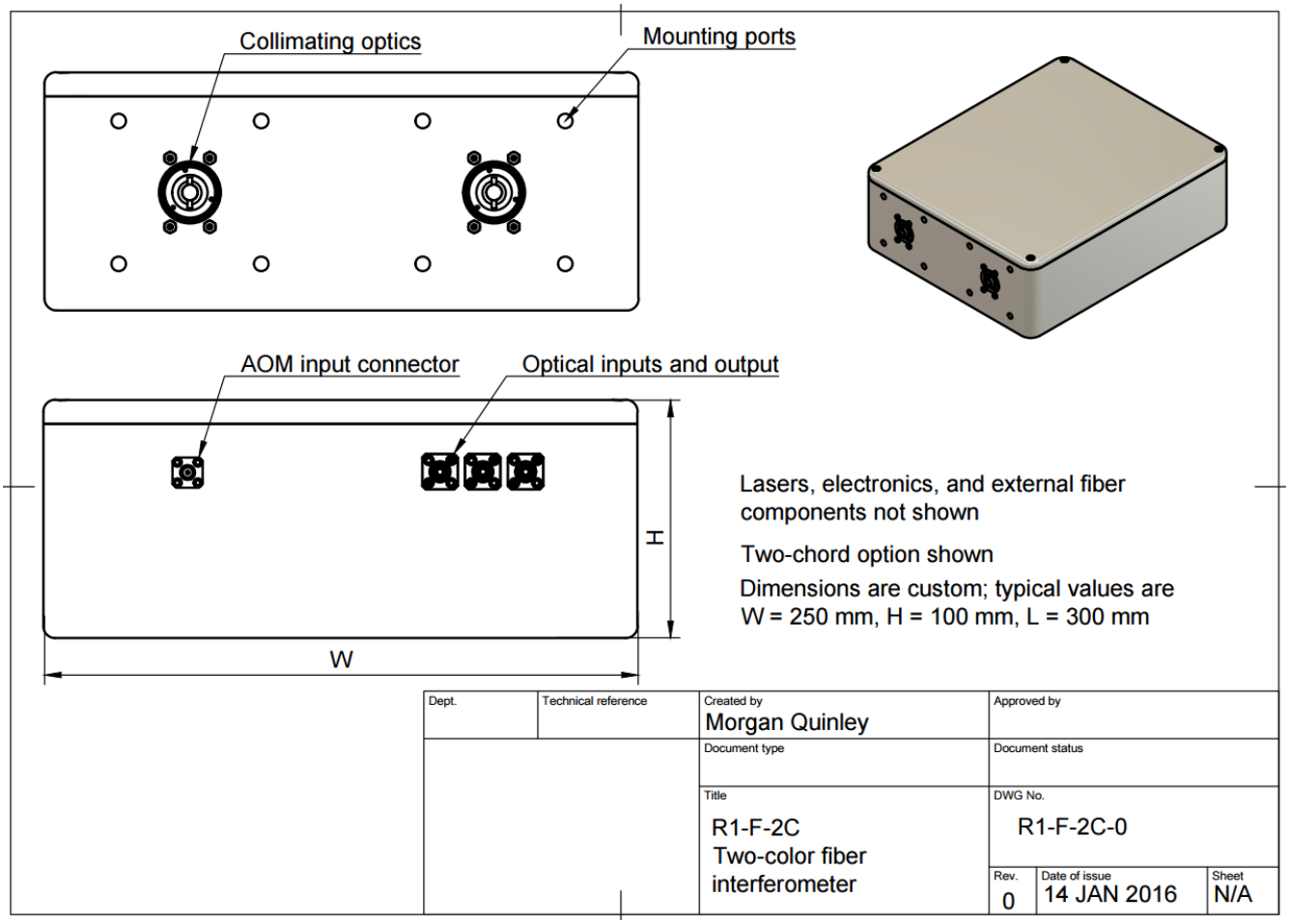

Appendix B

Test prints for outgas testing

B.1 Titanium Ti64

B.2 Inconel IN718

B.3 Stainless PH1

B.4 Aluminum AL5I10


Titanium Ti64
WOODRUFF • SCIENTIFIC

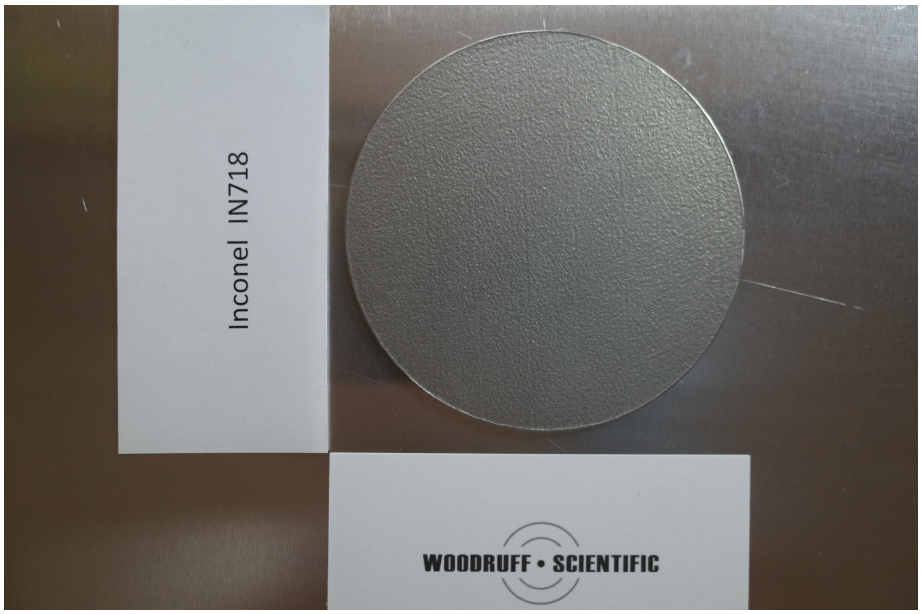
Inconel IN718
WOODRUFF • SCIENTIFIC

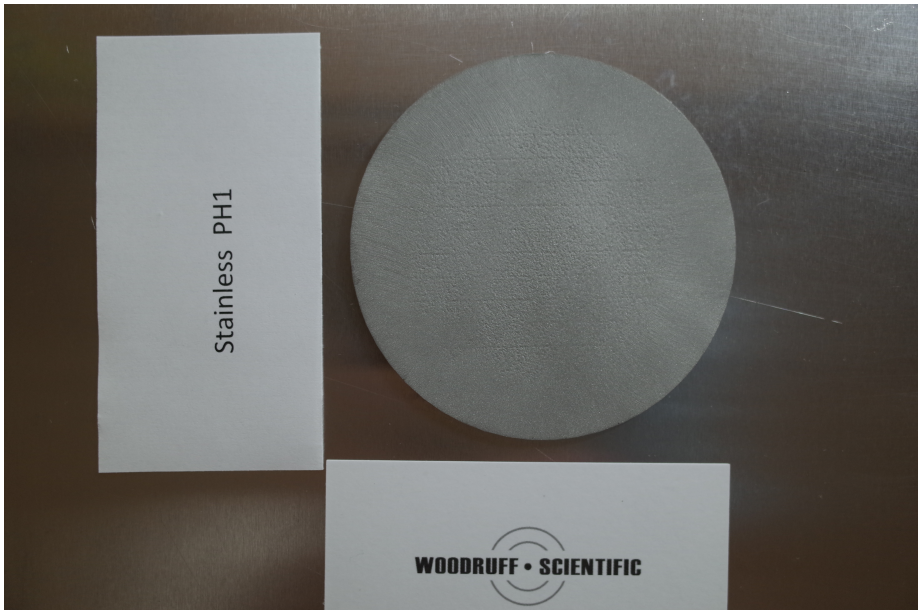
Stainless PH1
WOODRUFF • SCIENTIFIC

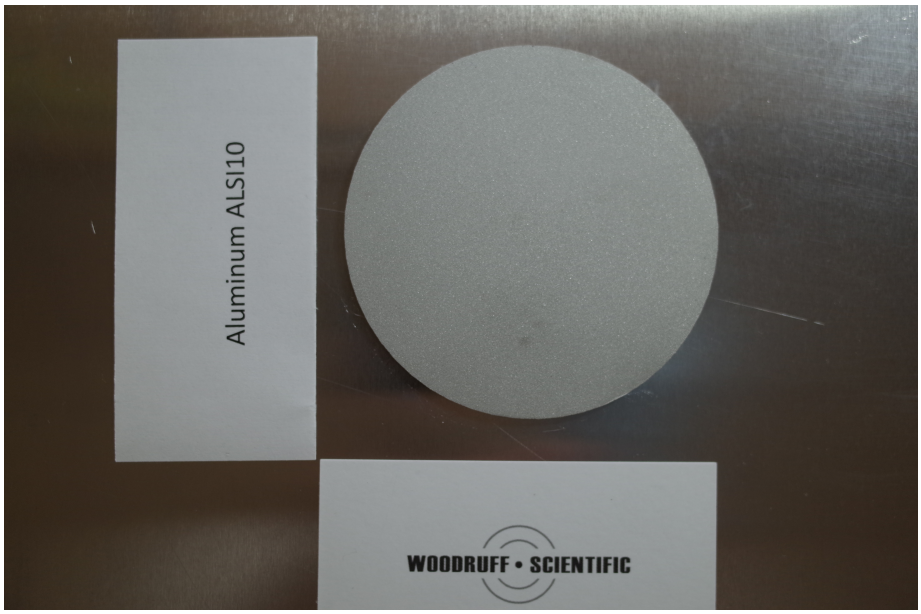
Aluminum ALSI10
WOODRUFF • SCIENTIFIC

Appendix C

Costing analysis

C.1 Magnetic arrays

C.2 HeNe Interferometer

C.3 Microwave interferometer

C.4 Langmuir probes

C.5 Retarding grid energy analyzers

C.6 Rogowski shunt current monintors

C.7 Rogowski probes

C.8 Fiber-based interferometer

C.9 2-color interferometer

HeNe Interferometer

Components	#	Cost per	CM Cost 1	Cost 2	Cost 10
Kumar thesis					
Mirror mounts, posts, misc mechanical hardware	30	200	6000	12000	60000
Table with vibration isolation	1	5000	5000	10000	50000
NI 6133	1	3200	3200	6400	32000
AO Isolator	1	2800	2800	5600	28000
Acoustic optic cell	1	2300	2300	4600	23000
Misc RF components	1	2000	2000	4000	20000
4mW linearly polarized HeNe Laser 25cm cavity length	1	1290	1290	2580	12900
2 axis rotation mount for AO modulator	1	1000	1000	2000	10000
Power supplies	2	500	1000	2000	10000
Beam expander	1	950	950	1900	9500
Half wave plate	2	425	850	1700	8500
Fringe counting electronics	1	600	600	1200	6000
Flat mirrors	5	80	400	800	4000
Detector Mercury Cadmium Telluride Detectors	1	300	300	600	3000
BS	1	200	200	400	2000
Sapphire windows	2	80	160	320	1600
Spherical mirror (4m)	1	100	100	200	1000
Iris	1	100	100	200	1000
SUBTOTAL			28050	56100	280500
CONTINGENCY			5610	11220	56100
TOTAL MATERIALS			**33660**	**67320**	**336600**

LABOR COSTS	Time	Cost/hour	CM Cost	Cost 2	Cost 10
0. CDR	8	180	1440	1440	1440
1. Engineering Design	8	180	1440	1440	1440
2. Procurement	8	100	800	1600	8000
3. Fabrication					
--Component layout in side lab	40	120	4800	9600	48000
--Alignment of all components	40	120	4800	9600	48000
--Calibration of the detectors	40	120	4800	9600	48000
--Testng with movement	40	120	4800	9600	48000
--Installation onto the main experiment	40	120	4800	9600	48000
--Fab fringe-counting circuit	8	120	960	1920	9600
--Testing of the circuit	12	120	1440	2880	14400
--Software development for phase counting	40	120	4800	4800	4800
--Routing cables to DAQ	4	120	480	960	4800
TOTAL LABOR			**35360**	**63040**	**284480**
TOTAL			**69020**	**130360**	**621080**

CO2 Interferometer

Carlstrom et al 1988	#	Cost per	Cost	Cost 2	Cost 10
Table 4x6 with vibration isolation	1	5000	5000	10000	50000
Acoustic optic cell	2	2300	4600	9200	46000
NI 6133	1	3200	3200	6400	32000
AO Isolator	1	2800	2800	5600	28000
CO2 Laser	1	2000	2000	4000	20000
CO2 shutter	1	1400	1400	2800	14000
Flat mirors	15	80	1200	2400	12000
2mW HeNe	1	1150	1150	2300	11500
Mirror mounts	20	40	800	1600	8000
Corner cubes (1.5cm)	2	360	720	1440	7200
Fringe detector electronics	1	600	600	1200	6000
Magnetic shields for laser and detector	3	200	600	1200	6000
BaF2 windows	2	250	500	1000	5000
In-vessel corner-cube and protection	1	500	500	1000	5000
ZnSe beam splitter	1	420	420	840	4200
10-in flocal ZnSe lens	1	400	400	800	4000
HgCdTe photoresistor	1	300	300	600	3000
Ge flat mirror	1	250	250	500	2500
Concave mirrors (R=6m)	2	100	200	400	2000
Fiber optics	1	80	80	160	800
f=25cm Lens	1	50	50	100	500
1in focal length lens	1	50	50	100	500
Subtotal			26820	53640	268200
Contingency			5364	10728	53640
TOTAL MATERIALS			**32184**	**64368**	**321840**

LABOR COSTS	Time	Cost/hour	Cost	Cost 2	Cost 10
0. CDR	8	180	1440	1440	1440
1. Engineering Design	8	180	1440	1440	1440
2. Procurement	8	100	800	1600	8000

3. Fabrication					
--Component layout	40	120	4800	9600	96000
--Alignment	40	120	4800	9600	96000
--Calibration	40	120	4800	9600	96000
--Testng	40	120	4800	9600	96000
--installation	40	120	4800	9600	96000
--Fab PCB	8	120	960	1920	19200
--Testing	12	120	1440	2880	28800
--Software dev	40	120	4800	9600	96000
--Routing cables to DAQ	4	120	480	960	9600
TOTAL LABOR			**35360**	**67840**	**644480**
TOTAL LABOR AND MATERIALS			**67544**	**132208**	**966320**

CO2 polarimeter

Akiyama	**#**	**Cost per**	**Cost 1**	**Cost 2**	**Cost 10**
CO2 Laser – GN-802-GES	1	2500	2500	5000	25000
AOM AGD-406B1	1	1500	1500	3000	15000
Oscillator DFE-400C4J	1		0	0	0
IR photovoltaic detectors PDI series	1	200	200	400	2000
Mounts for photovoltaic detectors	1	50	50	100	500
Beam expander BECZ-10.6-C1.9:10-03-FFA	1	800	800	1600	8000
Polarizer LP01, LPo2	1	300	300	600	3000
Lock in amp SR 830 Stanford Research System	1	5000	5000	10000	50000
EG&G Princeton Applied Research Lock-in amp 5302	1	4000	4000	8000	40000
7265 EG&G Signal Recovery	1	5000	5000	10000	50000
Beam expander x3 magnification 2.5m	1	800	800	1600	8000
Mirrors flat	22	80	1760	3520	17600
HeNe laser	3	1290	3870	7740	38700
Beam splitters	5	260	1300	2600	13000
Table 1600x1100	1	5000	5000	10000	50000
Table 1000x700	1	2500	2500	5000	25000
Power meter for CO2 laser	1	1200	1200	2400	12000
Spectrum analyzer for CO2 laser	1	1500	1500	3000	15000
Gold coated retro-reflectors	1	120	120	240	1200
ZnSe window	2	250	500	1000	5000
SUBTOTAL			35400	70800	354000
CONTINGENCY			7080	14160	70800
TOTAL			**42480**	**84960**	**424800**

LABOR COSTS	**Time**	**Cost/hour**	**Cost**	**Cost 2**	**Cost 10**
0. CDR	8	180	1440	1440	1440
1. Engineering Design	8	180	1440	1440	1440
2. Procurement	8	100	800	1600	8000
3. Fabrication					
--Component layout	40	120	4800	9600	48000
--Alignment	40	120	4800	9600	48000
--Calibration	40	120	4800	9600	48000
--Testng	40	120	4800	9600	48000
--installation	40	120	4800	9600	48000
--Fab PCB	8	120	960	1920	9600
--Testing	12	120	1440	2880	14400
--Software dev	40	120	4800	9600	48000
--routing cables to DAQ	4	120	480	960	4800
TOTAL LABOR			**35360**	**67840**	**327680**
TOTAL PARTS AND LABOR			**77840**	**152800**	**752480**

mmWave Interferometer
Willis

Components	**#**	**Cost per**	**Cost**	**Cost 2**	**Cost 10**
YIG Oscillator	2	400	800	1600	8000
Function gnerator sweeping linear 4-8Ghz	1	5000	5000	10000	50000
Log Periodic Antenna	1	2000	2000	4000	20000
Mixer	2	200	400	800	4000
Receiving antenna	1	2000	2000	4000	20000
High pass filter > 4Ghz	1	300	300	600	3000
Low pass filter < 8Ghz	1	300	300	600	3000
Isolator for YIG Oscillator	2	400	800	1600	8000
Isolator for mixer	1	400	400	800	4000
NI 6133	1	3200	3200	6400	32000
Electronics	1	600	600	1200	6000
Misc hardware:			0	0	0
T-junctions	2	10	20	40	200
90 degrees	6	30	180	360	1800
RF enclosure (Al box	1	600	600	1200	6000
Surface mount connections	10	20	200	400	2000

SMA cables	10	13	130	260	1300
			0	0	0
Ermak			0	0	0
131 Ghz Oscillator			0	0	0
133 GHz Oscillator			0	0	0
Mixer	6		0	0	0
			0	0	0
			0	0	0
			0	0	0
			0	0	0
Phase gain evaluation board (AD8302)	2	292	584	1168	5840
SUBTOTAL			17514	35028	175140
CONTINGENCY		20.00%	3502.8	7005.6	35028
TOTAL MATERIALS			**21016.8**	**42033.6**	**210168**

LABOR COSTS	**Time**	**Cost/hour**	**Cost**	**Cost 2**	**Cost 10**
0. CDR	8	180	1440	1440	1440
1. Engineering Design	8	180	1440	1440	1440
2. Procurement	8	100	800	1600	8000
3. Fabrication			0	0	0
--Component layout	40	120	4800	9600	48000
--Alignment	40	120	4800	9600	48000
--Calibration	40	120	4800	9600	48000
--Testng	40	120	4800	9600	48000
--installation	40	120	4800	9600	48000
--Fab PCB	8	120	960	1920	9600
--Testing	12	120	1440	2880	14400
--Software dev	40	120	4800	9600	48000
--routing cables to DAQ	4	120	480	960	4800
TOTAL LABOR			**35360**	**67840**	**327680**
TOTAL PARTS AND LABOR			**56376.8**	**109873.6**	**537848**

mmWave Reflectometer

	#	**Cost per**	**Cost 1**	**Cost 2**	**Cost10**
Transmitter power source	1		0	0	0
mmw mixer	2		0	0	0
rf mixer	2	70	140	280	1400
Protection Switch	1		0	0	0
MMW source	1		0	0	0
Crystal Oscillator	1		0	0	0
Amps	5		0	0	0
I & Q Detector	1		0	0	0
Antenna	2	200	400	800	4000
Bandpass Filter	2		0	0	0
Enclosure	1		0	0	0
SUBTOTAL			**540**	**1080**	**5400**
CONTINGENCY		20.00%	108	216	1080
TOTAL MATERIALS			**648**	**1296**	**6480**

LABOR COSTS	**Time**	**Cost/hour**	**Cost**	**Cost 2**	**Cost 10**
0. CDR	8	180	1440	2880	14400
1. Engineering Design	8	180	1440	2880	14400
2. Procurement	8	100	800	1600	8000
3. Fabrication					
--Component layout	40	120	4800	9600	48000
--Alignment	40	120	4800	9600	48000
--Calibration	40	120	4800	9600	48000
--Testng	40	120	4800	9600	48000
--installation	40	120	4800	9600	48000
--Fab PCB	8	120	960	1920	9600
--Testing	12	120	1440	2880	14400
--Software dev	40	120	4800	9600	48000
--routing cables to DAQ	4	120	480	960	4800
TOTAL LABOR			**35360**	**70720**	**353600**
TOTAL LABOR AND MATERIALS			**36008**	**72016**	**360080**

Mechanical					AM design principles:	
Optical						
Electronics						
Conductor						
Insulator						
B-dot probes	Example:	Strait, E.	http://scitation.aip.org/content/aip/journal/rsi/77/2/10.1063/1.2166493	CM		
	MATERIALS	**#**	**Cost per**	**Cost 1**	**Cost 2**	**Cost 10**
	Alumina rods	1	50	50	100	400
	MgO-insulated coax	1	200	200	400	1600
	SS sheath on coax	1	200	200	400	1600
	Inconel substrate	1	300	300	600	2400
	Integrating Circuit	1	1000	1000	2000	8000
	Plastic rods			0	0	0
	Wire	1	200	200	400	1600
	TOTAL MATERIALS			**1950**	**3900**	**15600**
	LABOR	**Time**	**Cost/hour**	**Cost 1**	**Cost 2**	**Cost 10**
	0. CDR	8	180	1440	1440	1440
	1. Engineering Design	8	180	1440	1440	1440
	2. Procurement	2	100	200	200	200
	3. Fabrication					
	--CNC mill	8	120	960	1440	7200
	--Wind turns	8	120	960	1920	9600
	--Install shroud	8	120	960	1920	9600
	--Mechanical	8	120	960	1440	7200
	--Calibration	8	120	960	1440	7200
	--harnessing	4	120	480	960	4800
	--UHV (bake/sonic/glow)	8	120	960	960	4800
	--installation	8	120	960	1920	9600
	--routing cables to DAQ	4	120	480	720	3600
	TOTAL LABOR			**10760**	**15800**	**66680**
	TOTAL			**12710**	**19700**	**82280**
Spiral pancake coils	Example	Ocilka	http://mechatronika.polsl.pl/owd/pdf2012/471.pdf			
	Components	**#**	**Cost per**	**Cost**	**Cost 2**	**Cost 10**
	Copper wire	1	50	50	100	400
	Inconel substrate	1	30	30	60	240
	Insulation	1	30	30	60	240
	TOTAL MATERIALS			**110**	**220**	**880**
	Fabrication/ea	**Time**	**Cost/hour**	**Cost 1**	**Cost 2**	**Cost 10**
	0. CDR	4	180	720	720	720
	1. Engineering Design	4	180	720	720	720
	2. Procurement	1	100	100	100	100
	3. Fabrication			0		
	--CNC mill	0	120	0	0	0
	--Wind turns	8	120	960	1920	9600
	--Install shroud	1	120	120	240	1200
	--Mechanical	1	120	120	240	1200
	--harnessing	2	120	240	480	2400
	--HV	2	120	240	240	1200
	--installation	8	120	960	1920	9600
	--routing cables to DAQ	4	120	480	720	3600
	TOTAL LABOR			**4660**	**7300**	**30340**
	TOTAL			**4770**	**7520**	**31220**
Linear arrays	Talamas	http://scitation.aip.org/content/aip/journal/pop/13/2/10.1063/1.2140682				
	MATERIALS	**#**	**Cost per**	**Cost**	**Cost 2**	**Cost 10**
	Forms	1	50	50	100	400
	MgO-insulated coax	0		200	400	1600
	SS sheath	1		50	100	400
	Inconel substrate	1	300	300	600	2400

Mechanical					AM design principles:	
Optical						
Electronics						
Conductor						
Insulator						
	Integrating Circuit	1		1000	2000	8000
	Heat shield			200	400	1600
	Wire			200	400	1600
	TOTAL MATERIALS			**2000**	**600**	**2400**
	LABOR	**Time**	**Cost/hour**	**Cost 1**	**Cost 2**	**Cost 10**
	0. CDR	80	180	14400	14400	14400
	1. Engineering Design	80	180	14400	14400	14400
	2. Procurement	15	100	1500	1500	1500
	3. Fabrication			0		
	--CNC mill	8	120	960	1440	7200
	--Wind turns	8	120	960	1920	9600
	--Install shroud	8	120	960	1920	9600
	--Mechanical	8	120	960	1920	9600
	--harnessing	4	120	480	960	4800
	--HV	8	120	960	960	4800
	--installation	8	120	960	1920	9600
	--routing cables to DAQ	4	120	480	720	3600
	TOTAL LABOR			**37020**	**42060**	**89100**
	TOTAL			**39020**	**42660**	**91500**
Rogowskis	Examples:	Hutchinson				
		Strait, E.		CM		
	MATERIALS COSTS	**#**	**Cost per**	**Cost 1**	**Cost 2**	**Cost 10**
	0.01” enameled wire	100	2	200	400	1600
	teflon core	1	20	20	40	160
	Coaxial cable with sheath and	1	20	20	40	160
	Integrating circuit	1	1000	1000	2000	8000
	Case	1	50	50	100	400
	Plastic case	0	50	0	0	0
	Metal case	1	50	50	100	400
	TOTAL			**1340**	**2680**	**10720**
	LABOR COSTS	**Time**	**Cost/hour**	**Cost 1**	**Cost 2**	**Cost 10**
	0. CDR	8	180	1440	1440	1440
	1. Engineering Design	8	180	1440	1440	1440
	2. Procurement	2	100	200	200	200
	3. Fabrication					
	--CNC mill	8	120	960	1440	7200
	--Wind turns	8	120	960	1920	9600
	--Install shroud	8	120	960	1920	9600
	--Mechanical	8	120	960	1920	9600
	--harnessing	4	120	480	960	4800
	--HV	8	120	960	960	4800
	--installation	8	120	960	1920	9600
	--routing cables to DAQ	4	120	480	720	3600
	TOTAL Labor			**9800**	**14840**	**61880**
	TOTAL			**11140**	**17520**	**72600**
Rogowskis for banks	Pearson					
				CM		
	MATERIALS COSTS	**#**	**Cost per**	**Cost 1**	**Cost 2**	**Cost 10**
	0.01” enameled wire	100	2	200	400	1600
	teflon core	1	20	20	40	160
	Coaxial cable with sheath and	1	20	20	40	160
	Integrating circuit	1	200	200	400	1600
				0	0	0
	Case	1	50	50	100	400
	Plastic	1	50	50	100	400
	Metal	0	50	0	0	0
	TOTAL			**540**	**1080**	**4320**

Mechanical					AM design principles:	
Optical						
Electronics						
Conductor						
Insulator						
	LABOR COSTS	**Time**	**Cost/hour**	**Cost 1**	**Cost 2**	**Cost 10**
	0. CDR	8	180	1440	1440	1440
	1. Engineering Design	8	180	1440	1440	1440
	2. Procurement	2	100	200	200	200
	3. Fabrication					
	--CNC mill	8	120	960	1440	7200
	--Wind turns	8	120	960	1920	9600
	--Install shroud	8	120	960	1920	9600
	--Mechanical	8	120	960	1920	9600
	--harnessing	4	120	480	960	4800
	--HV	8	120	960	960	4800
	--installation	8	120	960	1920	9600
	--routing cables to DAQ	4	120	480	720	3600
	TOTAL Labor			**9800**	**14840**	**61880**
	TOTAL			**10340**	**15920**	**66200**
Insitu calibration jig	Woodruff			**CM**		
	MATERIALS COSTS	**#**	**Cost per**	**Cost 1**	**Cost 2**	**Cost 10**
	0.01” enameled wire	100	2	200	400	1600
	teflon core	1		20	40	160
	Coaxial cable with sheath and	1		19	38	152
	Integrating circuit	1		500	1000	4000
					0	0
	Case	1	50	50	100	400
	Plastic	1	50		0	0
	Metal	1	50		0	0
	TOTAL			**789**	**1578**	**6312**
	LABOR COSTS	**Time**	**Cost/hour**	**Cost 1**	**Cost 2**	**Cost 10**
	0. CDR	8	180	1440	1440	1440
	1. Engineering Design	8	180	1440	1440	1440
	2. Procurement	2	100	200	200	200
	3. Fabrication					
	--CNC mill	8	120	960	1440	7200
	--Wind turns	8	120	960	1920	9600
	--Install shroud	8	120	960	1920	9600
	--Mechanical	8	120	960	1920	9600
	--harnessing	4	120	480	960	4800
	--HV	8	120	960	960	4800
	--installation	8	120	960	1920	9600
	--routing cables to DAQ	4	120	480	720	3600
	TOTAL Labor			**9800**	**14840**	**61880**
	TOTAL			**10589**	**16418**	**68192**
Calibration jigs	Woodruff			**CM**		
	MATERIALS COSTS	**#**	**Cost per**	**Cost 1**	**Cost 2**	**Cost 10**
	0.01” enameled wire	100	2	200	400	1600
	teflon core	1		20	40	160
	Coaxial cable with sheath and	1		19	38	152
	Integrating circuit	1		500	1000	4000
					0	0
	Case	1	50	50	100	400
	Plastic	1	50		0	0
	Metal	1	50		0	0
	TOTAL			**789**	**1578**	**6312**
	LABOR COSTS	**Time**	**Cost/hour**	**Cost 1**	**Cost 2**	**Cost 10**
	0. CDR	8	180	1440	1440	1440
	1. Engineering Design	8	180	1440	1440	1440

Mechanical					AM design principles:	
Optical						
Electronics						
Conductor						
Insulator						
	2. Procurement	2	100	200	200	200
	3. Fabrication					
	--CNC mill	8	120	960	1440	7200
	--Wind turns	8	120	960	1920	9600
	--Install shroud	8	120	960	1920	9600
	--Mechanical	8	120	960	1920	9600
	--harnessing	4	120	480	960	4800
	--HV	8	120	960	960	4800
	--installation	8	120	960	1920	9600
	--routing cables to DAQ	4	120	480	720	3600
	TOTAL Labor			**9800**	**14840**	**61880**
	TOTAL			**10589**	**16418**	**68192**
Insertable rogowskis	Martin	http://iopscience.iop.org/0741-3335/3		**CM**		
	MATERIALS COSTS	**#**	**Cost per**	**Cost 1**	**Cost 2**	**Cost 10**
	0.01” enameled wire	100	2	200	400	1600
	teflon core	1		20	40	160
	Coaxial cable with sheath and	1		19	38	152
	Integrating circuit	1		500	1000	4000
					0	0
	Case	1	50	50	100	400
	Plastic	1	50		0	0
	Metal	1	50		0	0
	TOTAL			**789**	**1578**	**6312**
	LABOR COSTS	**Time**	**Cost/hour**	**Cost 1**	**Cost 2**	**Cost 10**
	0. CDR	8	180	1440	1440	1440
	1. Engineering Design	8	180	1440	1440	1440
	2. Procurement	2	100	200	200	200
	3. Fabrication					
	--CNC mill	8	120	960	1440	7200
	--Wind turns	8	120	960	1920	9600
	--Install shroud	8	120	960	1920	9600
	--Mechanical	8	120	960	1920	9600
	--harnessing	4	120	480	960	4800
	--HV	8	120	960	960	4800
	--installation	8	120	960	1920	9600
	--routing cables to DAQ	4	120	480	720	3600
	TOTAL Labor			**9800**	**14840**	**61880**
	TOTAL			**10589**	**16418**	**68192**
Flux loops	Hutchinson			**CM**		
	MATERIALS	**#**	**Cost per**	**Cost 1**	**Cost 2**	**Cost 10**
	Alumina rods	0	50	200	400	1600
	MgO-insulated coax	1		20	40	160
	SS sheath on coax	1		19	38	152
	Inconel substrate	1	300	500	1000	4000
	Integrating Circuit	1			0	0
	Plastic rods	0	200	50	100	400
	Feedthrough	1	200		0	0
	High-Temperature Conductive	1	200		0	0
	TOTAL MATERIALS			**789**	**1578**	**6312**
	LABOR	**Time (hours)**	**Cost/hour**	**Cost 1**	**Cost 2**	**Cost 10**
	0. CDR	2	180	360	360	360
	1. Engineering Design	2	180	360	360	360
	2. Procurement	2	100	200	200	200
	3. Fabrication					
	--CNC mill	0	120	0	0	0
	--Wind turns	0	120	0	0	0

Mechanical					AM design principles:	
Optical						
Electronics						
Conductor						
Insulator						
	--Install shroud	8	120	960	1920	9600
	--Mechanical	2	120	240	480	2400
	--harnessing to feedthru	4	120	480	960	4800
	--HV (bake / sonic bath)	8	120	960	960	4800
	--installation	8	120	960	1920	9600
	--routing cables to DAQ	4	120	480	720	3600
	TOTAL LABOR			**5000**	**7880**	**35720**
	TOTAL			**5789**	**9458**	**42032**

Mechanical					
Optical					
Electronics					
Conductor					
Insulator					
Electrostatic	**Reference**	**Link**			
Voltage monitors (HV, voltage dividers)	Pearson	http://www.pearsonelectronics.com/products/capacitive			
Langmuir probe – static	Boedo	eb.b.ebscohost.com.offcampus.lib.washington.edu/ehc			
	Francs Chen	http://www.seas.ucla.edu/~ffchen/Publs/Chen210R.pdf			
	Components	**#**	**Cost per**	**Cost 1**	**Cost 1**
Single tip	Mounting flange	1	1000	1000	1000
	Mount	1	100	100	100
	Probe body insulator	1	50	50	50
	Reference electrode	1	5	5	5
	Complex tip electrode	1	5	5	100
	Tip electrode	1	5	5	5
	Ceramic insulator #2	1	30	30	30
	Compensation electrode	1	5	5	5
	RF blocking inductors	1	50	50	50
	HV source	1	500	1000	1000
	Oscilloscope	1	500	700	700
	TOTAL			**2950**	**3045**
Two tips	Mounting flange	1	1000	1000	0
	Mount	1	100	100	0
	Probe body	1	50	50	100
	Reference electrode	1	5	5	0
	Ceramic insulator	1	30	30	100
	Compensation electrode	1	5	5	0
	RF blocking inductors	1	50	50	300
	TOTAL			**1240**	**500**
Triple probe	Mounting flange	1	1000	1000	0
	Mount	1	100	100	0
	Probe body	1	50	50	100
	Reference electrode	1	5	5	0
	Ceramic insulator	1	30	30	100
	Compensation electrode	1	5	5	0
	RF blocking inductors	1	50	50	300
	TOTAL			**1240**	**500**
Quadruple probe	Mounting flange	1	1000	1000	0
	Mount	1	100	100	0
	Probe body	1	50	50	100
	Reference electrode	1	5	5	0
	Ceramic insulator	1	30	30	100
	Compensation electrode	1	5	5	0
	RF blocking inductors	1	50	50	300
	TOTAL			**1240**	**500**

Mechanical					
Optical					
Electronics					
Conductor					
Insulator					
	LABOR COSTS	**Time**	**Cost/hour**	**Cost 1**	Cost 1
	0. CDR	8	180	1440	1440
	1. Engineering Design	8	180	1440	1440
	2. Procurement	2	100	200	200
	3. Fabrication			0	
	--Weld adapter to flange	4	120	480	0
	--Make electrical connections to feedthrc	4	120	480	120
	--cut tubes to length, and clean	4	120	480	120
	--assemble tubes with cores	4	120	480	0
	--polish and clean	4	120	480	0
	--print up circuit	1	120	120	0
	--install components in circuit	4	120	480	960
	--test circuit	4	180	720	0
	--calibrate	8	180	1440	480
	TOTAL LABOR			**8240**	**4280**
	TOTAL			**9480**	**4280**
Langmuir probe – reciprocating	J. G. Bak	http://epsppd.epfl.ch/Sofia/pdf/P2_204.pdf			
	Grigull			CM	AM
	Components	**#**	**Cost per**	**Cost 1**	**Cost 1**
	Tip	1	100	100	0
	Ceramic insulator	2	50	100	0
	Pipe	1	120	120	100
	Copper Connector	1	30	30	0
	Plug		20	0	100
	Plug spring	1	15	15	0
	Target deform spring	1	15	15	300
				0	
	Actuator (pneumatic drive)	1	900	900	
	TOTAL PARTS			**1280**	**500**
	LABOR COSTS	Time	Cost/hour	Cost 1	Cost 1
	0. CDR	8	180	1440	0
	1. Engineering Design	8	180	1440	0
	2. Procurement	2	100	200	0
	3. Fabrication				
	--Weld adapter to flange	4	120	480	
	--Make electrical connections to feedthrc	4	120	480	
	--cut tubes to length, and clean	4	120	480	
	--assemble tubes with cores	4	120	480	
	--polish and clean	4	120	480	
	--print up circuit	1	120	120	0
	--install components in circuit	4	120	480	960
	--test circuit	4	180	720	
	--calibrate	8	180	1440	480

Mechanical					
Optical					
Electronics					
Conductor					
Insulator					
	TOTAL labor			**8240**	**960**
	TOTAL			**9520**	**960**
Retarding Grid Energy Analyzers	Pitts	http://www.iop.org/Jet/fulltex		CM	AM
	MATERIALS COSTS	**#**	**Cost per**	**Cost 1**	**Cost 1**
	Mounting flange	1	50	50	0
	Mount	1	100	100	0
	Probe body	1	50	50	100
	Reference electrode	1	5	5	0
	Ceramic insulator	1	30	30	100
	Compensation electrode	1	5	5	0
	Grids	3	100	300	300
	RF blocking inductors	1	50	50	
	TOTAL			**590**	**500**
	LABOR COSTS	**Time**	**Cost/hour**	**Cost**	Cost
	0. CDR	80	180	14400	0
	1. Engineering Design	80	180	14400	0
	2. Procurement	15	100	1500	0
	3. Fabrication			0	
	--CNC mill	8	120	960	
	--Wind turns	8	120	960	
	--Install shroud	8	120	960	
	--Mechanical	8	120	960	
	--harnessing	4	120	480	
	--HV	8	120	960	0
	--installation	8	120	960	960
	--routing cables to DAQ	4	120	480	480
	TOTAL LABOR			**37020**	**1440**
	TOTAL				**1940**

Mechanical						
Optical						
Electronics						
	Components	**#**	**Cost per**	**Cost**	**Cost 2**	**Cost 10**
Laser Compton Scattering	*per Chouffani*					
	Nd:Yag Laser - 100MW 7ns, 1064nm,	1	25000	25000	50000	250000
	Broadband Mirror	2	100	200	400	2000
	CCD camera	2	500	1000	2000	10000
	ND:YAG mirror	2	300	600	1200	6000
	Iris	1	400	400	800	4000
	Beam expander (9mm to 45mm)	1	1000	1000	2000	10000
	Optical bench	1	5000	5000	10000	50000
	Lens (5m focal length (to center of inte	1	400	400	800	4000
	Iris #2	2	400	800	1600	8000
	PMT	1	1200	1200	2400	12000
	Kapton Window (detector)	1	300	300	600	3000
	Flourescent screens	2	200	400	800	4000
	Quadrupoles (Triplet)	1	400	400	800	4000
	OTER ladder	0		0	0	0
	Steerer cameras	2	300	600	1200	6000
	Gate valve	1	600	600	1200	6000
	Scintillator	1	10000	10000	20000	100000
	Adjustable lead slits	1	500	500	1000	5000
	SI(Li) X-ray detector	1	400	400	800	4000
	Telescope	1	500	500	1000	5000
	HeNe laser (for alignment)	2	1300	2600	5200	26000
	SS Foil (in front of detector)	1	100	100	200	1000
	SUBTOTAL			**52000**	**104000**	**520000**
	CONTINGENCY			**10400**	**20800**	**104000**
	TOTAL MATERIALS COSTS			**62400**	**124800**	**624000**
	LABOR COSTS	**Time**	**Cost/hour**	**Cost**	**Cost 2**	**Cost 10**
	0. CDR	8	180	1440	1440	1440
	1. Engineering Design	8	180	1440	1440	1440
	2. Procurement	12	100	1200	2400	12000
	3. Fabrication					
	--Component layout	40	120	4800	9600	48000
	--Alignment	40	120	4800	9600	48000
	--Calibration	40	120	4800	9600	48000
	--Testng	40	120	4800	9600	48000
	--installation	40	120	4800	9600	48000
	--Fab Circuits	8	120	960	1920	9600
	--Testing	12	120	1440	2880	14400
	--Software dev	40	120	4800	9600	48000
	--routing cables to DAQ	4	120	480	960	4800
	TOTAL LABOR			**35760**	**71520**	**357600**
	Total costs			**87760**	**175520**	**877600**
YAG Thomson Scattering	*Per Mclean (SSPX)*	**#**	**Cost per**	**Cost**	**Cost 2**	**Cost 10**
	ND:YAG lasers 2J, multipulse	1	90000	90000	180000	900000
	Single pulse YAG	0	60000	0	0	0
	Optical bench breadboard	1	5000	5000	10000	50000
	Avalanche Photodiode power supplies	1	20000	20000	40000	200000
	Mirrors Nd:YAG	10	130	1300	2600	13000

Mechanical						
Optical						
Electronics						
	Components	**#**	**Cost per**	**Cost**	**Cost 2**	**Cost 10**
	Collection optics	1	20000	20000	40000	200000
	Focal lens	1	60	60	120	480
	Mirrors turning mounts	2	400	800	1600	6400
	Mirrors: high performance coated	2	150	300	600	2400
	Optical mounts translation	5	400	2000	4000	16000
	Polychromators	10	15000	150000	300000	1500000
	Muli pulse scopes	15	6000	90000	180000	900000
	Calibration equipment	1	20000	20000	40000	200000
	Beam tubes	2	3000	6000	12000	60000
	Beam duimp	1	500	500	1000	4000
	Fiber bundle (including heads)	1	30000	30000	60000	240000
	Polychromators	1	30000	30000	60000	240000
	Temperature control for polyChromato	1	10000	10000	20000	80000
	baffles	10	600	6000	12000	60000
	TV camera to monitor alignment	1	600	600	1200	6000
	Optical fibers, mounts and lenses	10	700	7000	14000	70000
	HeNe for alignment	1	1300	1300	2600	13000
	Avalanche photodiodes	10	40	400	800	4000
	Enclosure	2	700	1400	2800	11200
	Structure (Al boxbeams)	2	500	1000	2000	8000
	Al sheet	0	600	0	0	0
	Misc hardware	50	10	500	1000	4000
	Collection optics mount	1	1000	1000	2000	8000
	Baffles	2	100	200	400	1600
	Inv vacuo alignment target & insterter	1	1000	1000	2000	8000
	SUBTOTAL			**496360**	**992720**	**4806080**
	CONTINGENCY			**99272**	**198544**	**961216**
	TOTAL MATERIALS COSTS			**595632**	**1191264**	**5767296**
	LABOR COSTS FOR 1st year OPS	**Time**	**Cost/hour**	**Cost**	**Cost 2**	**Cost 10**
	0. CDR	120	180	21600	23760	43200
	1. Engineering Design	320	180	57600	115200	576000
	2. Procurement	80	100	8000	16000	80000
	3. Fabrication					
	--Fabricate structure	160	100	16000	32000	160000
	--Component layout	20	180	3600	7200	36000
	--Testing laser output (off shelf)	20	180	3600	7200	36000
	--Testing laser output (legacy)	80	0	0	0	0
	--Testng of components	40	180	7200	14400	72000
	--Installation	80	180	14400	28800	144000
	--Alignment & focusing	40	120	4800	9600	48000
	--Infrastructure (trays / interlocks, etc)	40	120	4800	9600	48000
	--Integrated system testing (shots)	80	120	9600	19200	96000
	--Software dev	40	120	4800	9600	48000
	--Routing cables to DAQ	8	120	960	1920	9600
	TOTAL LABOR			**156960**	**313920**	**1569600**
	Total costs			**653320**	**1306640**	**6375680**
Ruby Thomson Scattering	*Per Golingo*	**#**	**Cost per**	**Cost**	**Cost 2**	**Cost 10**

Mechanical						
Optical						
Electronics						
	Components	**#**	**Cost per**	**Cost**	**Cost 2**	**Cost 10**
Check cost	Ruby laser 7J 40ns pulse width	1	2500	2500	5000	20000
	HeNe for alignment	1	1300	1300	2600	10400
	Focal lens	1	60	60	120	480
	Mirrors turning mounts	2	400	800	1600	6400
	Mirrors: high performance coated	2	150	300	600	2400
	Optical mounts translation	5	400	2000	4000	16000
	Breadboards	2	400	800	1600	6400
Check cost	Brewster window	2	200	400	800	3200
	Brewster flange & mount for window	2	4000	8000	12000	24000
	Iris in brewster tube/beam collimator			0	0	0
	Bloom for focal lens	1	50	50	100	500
	Collection optics	4	100	400	800	3200
	AR Blooms for collection optics	4	800	3200	3200	3200
	Beam dump	1	500	500	1000	4000
	Viewing dump					
5um feature, 40um fiber diameter	Fiber heads	1	20000	20000	40000	160000
High thru-put fused silica	Fibers					
	Spectrometer/polychromator	1	30000	30000	60000	240000
	imaging visible grating spectrometer					
Usually used for Halpha	PMT	10	1300	13000	26000	104000
	PMT array on exit plane	1		0	0	0
	Digitizers (Techtronic scopes)	4	2000	8000	16000	64000
In a poster	Energy monitor (laser output)	1	400	400	800	3200
	Enclosure	2	700	1400	2800	11200
	Structure (Al boxbeams)	10	500	5000	10000	40000
	Al sheet	2	600	1200	2400	9600
	Misc hardware	50	10	500	1000	4000
	Collection optics mount	1	1000	1000	2000	8000
	Baffles	2	100	200	400	1600
	Inv vacuo alignment target & insterter	1	1000	1000	2000	8000
	SUBTOTAL			**102010**	**196820**	**753780**
	CONTINGENCY			**20402**	**39364**	**150756**
	TOTAL MATERIALS COSTS			**122412**	**236184**	**904536**
	LABOR COSTS FOR 1st year OPS	**Time**	**Cost/hour**	**Cost**	**Cost 2**	**Cost 10**
	0. CDR	40	180	7200	7920	14400
	1. Engineering Design	160	180	28800	57600	288000
	2. Procurement	40	100	4000	8000	40000
	3. Fabrication					
	--Fabricate structure	160	100	16000	32000	160000
	--Component layout	20	180	3600	7200	36000
Consultant / laser rep	--Testing laser output (off shelf)	20	0	0	0	0
	--Testing laser output (legacy)	80	180	14400	28800	144000
	--Testng of components	40	180	7200	14400	72000
two man job	--Installation	80	180	14400	28800	144000
	--Alignment & focusing	40	120	4800	9600	48000
	--Infrastructure (trays / interlocks, etc)	40	120	4800	9600	48000
	--Integrated system testing (shots)	80	120	9600	19200	96000
	--Software dev	40	120	4800	9600	48000
	--Routing cables to DAQ	8	120	960	1920	9600

Mechanical						
Optical						
Electronics						
	Components	#	Cost per	Cost	Cost 2	Cost 10
	TOTAL LABOR			120560	241120	1205600
	Total costs			222570	437940	1959380

Appendix D

Publications and reports

D.1 UMBC presentation overview - Woodruff

D.2 American Physical Society 2015 - Sieck

D.3 Vibration isolator - Smith

D.4 Phase II, Y1 Progress report - Woodruff

D.5 Outgas testing of 3D-printed components - Rivera

D.6 Optimization of optical dumps - Chun

D.7 FESAC white paper on 3D-printed components - Romero-Talamas

D.8 Technology of Fusion Energy abstract - Quinley

D.9 High Temperature Plasma Diagnostics poster - Quinley

D.10 American Physical Society 2016 - Quinley

D.11 American Physical Society 2016 - Stuber

D.12 Review of Scientific Instruments draft - Quinley

D.13 A new vision of plasma facing components - Nygren

D.14 Additive manufacturing and monolithic interferometry - Case

Additive manufacture of plasma diagnostics

S.Woodruff[1], J. E. Stuber[1], S. Diesburg[1], B. Utela[1], D. Lemmon[1], N.K.Hicks[2], C.A.Romero-Talamás[3]

[1]Woodruff Scientific Inc, 4000 Aurora Ave N, Seattle WA 98103

[2]University of Alaska Anchorage, 3211 Providence Dr, Anchorage, AK 99058

[3]University of Maryland Baltimore County, 1000 Hilltop Circle, Engineering 222 Baltimore, Maryland 21250

University of Maryland Baltimore County
March 13th 2015
Work supported under DOE subcontract number DE-SC0011858

Table of contents

Grand challenge for materials: fusion energy environment

- In the next few years, ITER will come online [1]
- Collaboration between US, China, EU, Japan, Russia, India, South Korea
- Plasma will be 10M degrees Celsius
- How to interface plasma to room temperature world?

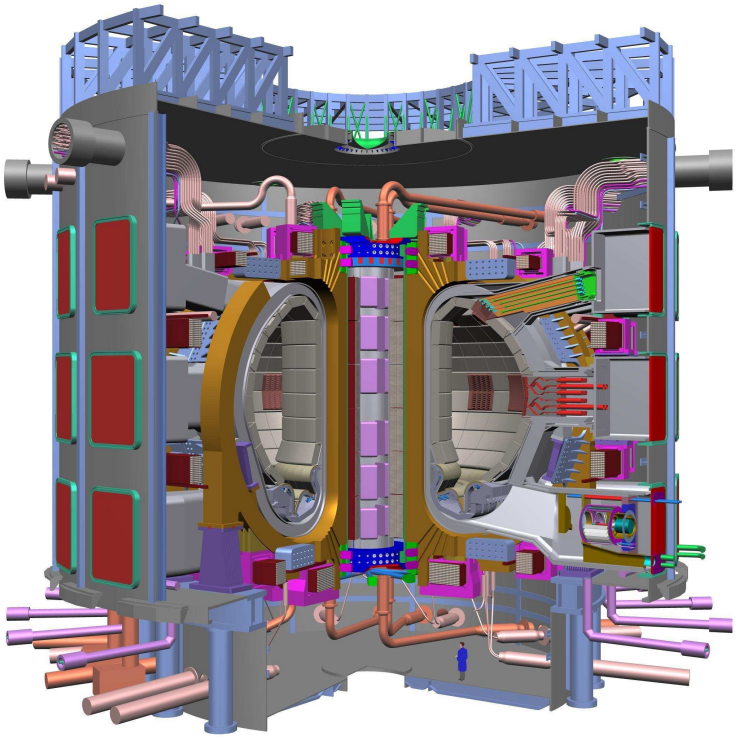

ITER currently under construction in Cadarace, France. ITER began as a Reagan-Gorbachov initiative in 1985, DT ops now planned for 2027

Fusion environment places stringent demands on materials

Materials must [2]:

- withstand high power loads (5MW/m^2 to 50MW/m^2)and neutron bombardment (200dpa)
- min rad waste, be safe and economic
- not out-gas in vacuum (i.e. UHV compatible)
- have low atomic mass number (low Z) so as not to produce radiation losses

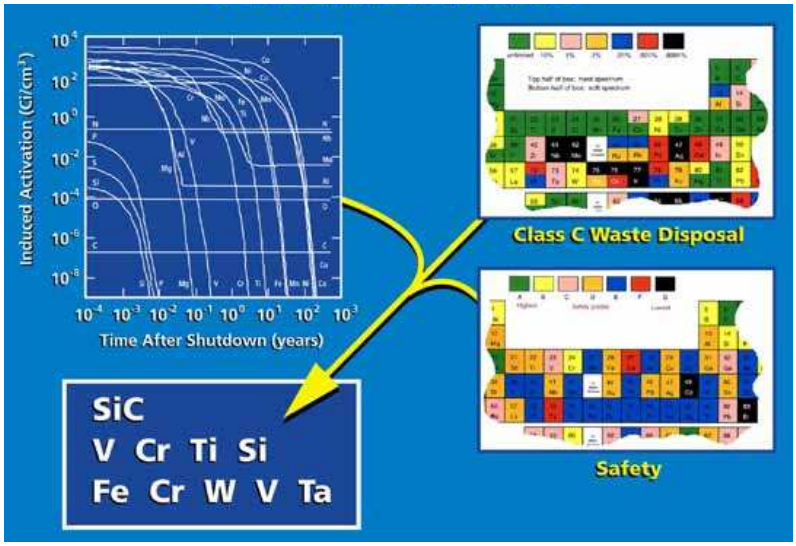

Ideal materials must be safe, must minimize rad waste (and be suitable for recycling), and must be economically competitive (high thermal efficiency, acceptable lifetime, reliable)

Diagnostic components are located close to fusing plasma

- Diagnostics are sensors that measure all important plasma parameters [3]
- Electrostatic probes designed to enter plasma
- Magnetics are usually protected beneath shielding
- Optical diagnostics usually have endoscopes to protect components, but exposed 1st mirrors
- RF diagnostics have horns or antennae close to plasma

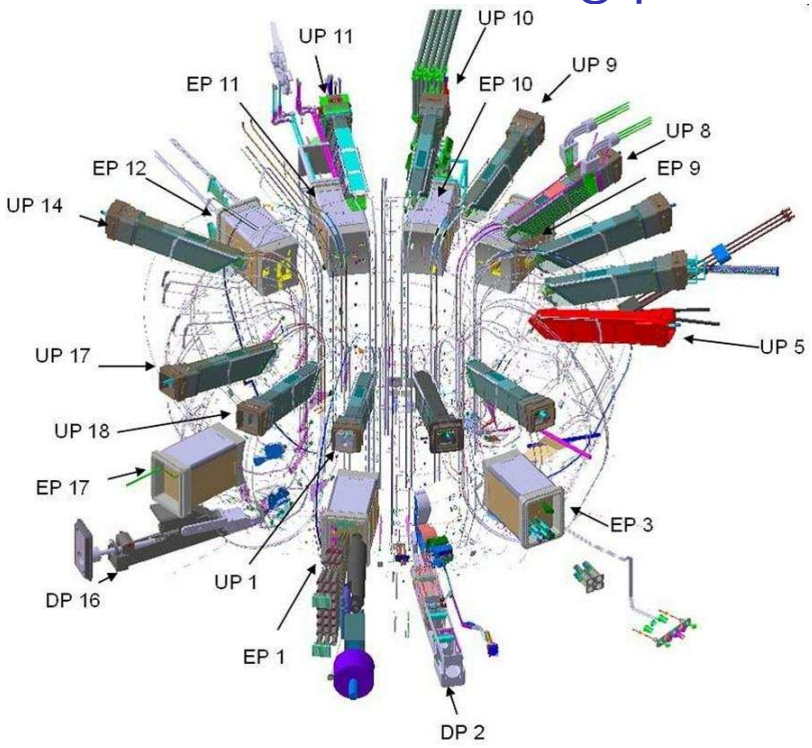

About 50 individual measurement systems will help to control, evaluate and optimize plasma performance in ITER and to further understanding of plasma [4]. These include lasers, X-rays, neutron cameras, impurity monitors, particle spectrometres, radiation bolometers, pressure and gas analysis, and optical fibres.

Some characteristcs of plasma diagnostics

- Highly customized, i.e. no mass-produced diagnostics
- Highly complex systems requiring cooling and integration with other systems
- Many components readily 'printable' if far from neutron environment
- Component requirements constantly evolving (endless prototyping) due to evolving scientific requirements

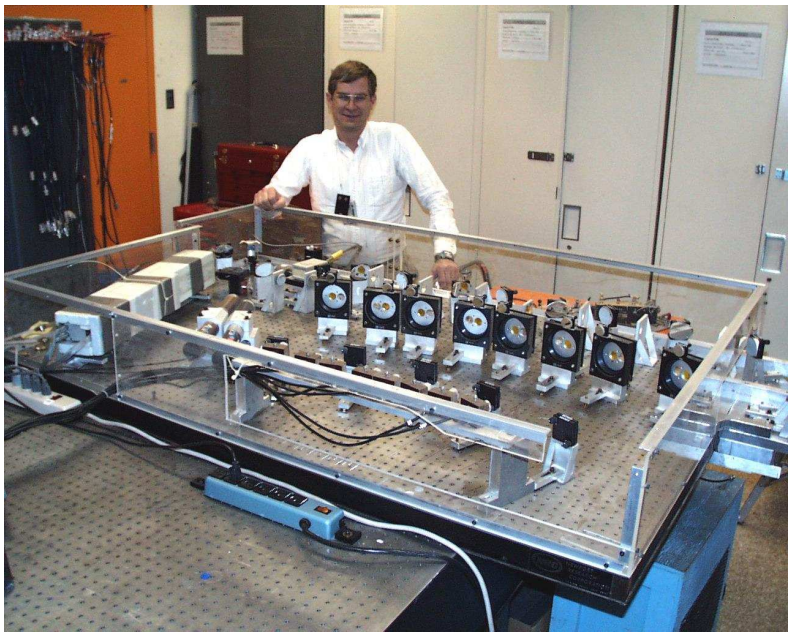

An interferometer with 8 chords (with dashing example of plasma physicist, to give sense of scale). On the optical bench (floating on vibration isolation legs) are over 150 separate components - lasers, mirrors, beam splitters, detectors, etc. Benches don't usually see neutrons. Only some parts can be AM'd today, but tomorrow?

Additive Manufacturing (AM) is ideally suited for plasma diagnostics

- Initially for rapid prototyping (since 1980's) but now fully functional components can be printed
- Diverse set of methods patented (though some patents now expiring)
- US recognizes potential of this disruptive tech and is preparing (e.g. [5])

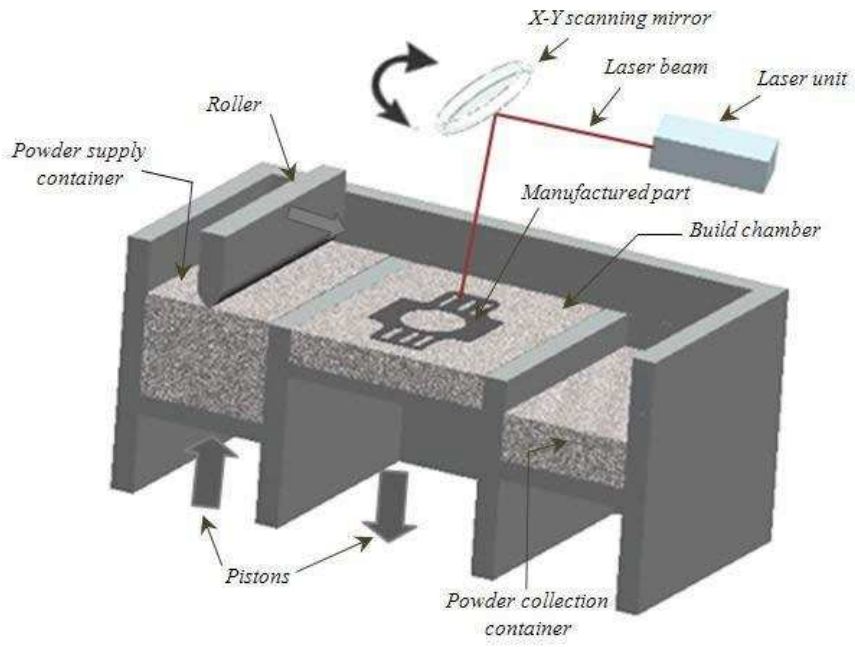

Method shown here is laser sintering of powder (metals, plastics, ceramics) in which the bed covered with a fine layer (few microns) of material, and a high power laser is scanned over the surface, melting it to the layer below. The bed is lowered, a fresh layer of power is rolled across and process is repeated.

Benefits of AM over Conventional Manufacturing (CM)

- Ideally suited to rapid prototyping and functional models [6]
- Low/no waste, low energy, predictable machine time
- No extra cost for complexity
- Reduced assembly - printed parts can be functional
- Cost of printing will fall rapidly in coming years as technology is adopted and printing becomes faster and more accurate.

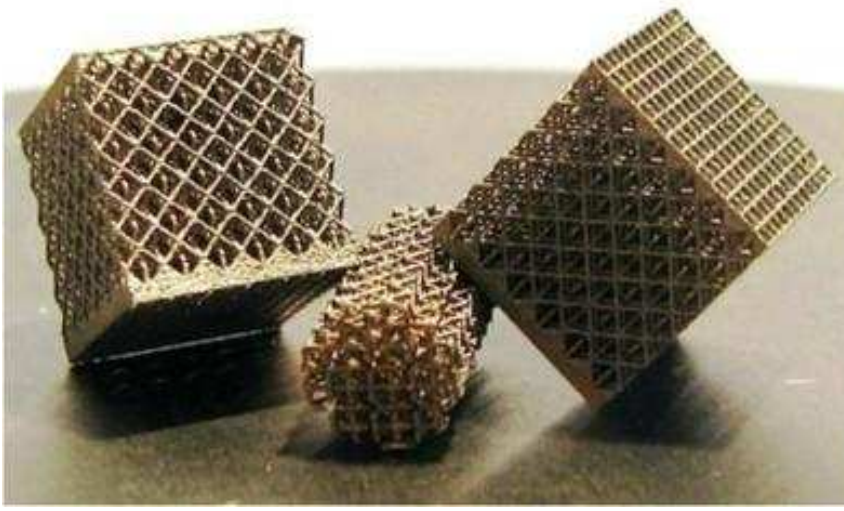

Complex alumina components, with lattice structure to reduce total volume of materials. Simlar components can be printed in metals, and plastics.

To compare costs, we did CDR, CM EDR and AM EDR for 15 diagnostics

Standard design review process [8]

- Pre-existing designs taken through EDR (so we'd know how to build them), then optimize the design for AM
- Two step design process: 1) obtain original functionality of components; 2) optimize full assembly for AM
- Where it was helpful to understand costs further, we printed prototypes

Diagnostics that we costed

Diagnostic	Example PI	Example Device
Magnetic field coil	Strait [9] [10]	DIII-D (GA)
Magnetic coil array	Strait	DIII-D (GA)
Rogowski coil	Strait	DIII-D (GA)
Calibration jig	Lambert	(KCL)
Langmuir probe		JET (CCFE)
RFEA	Pitts [11]	JET (CCFE)
HeNe interferometer	Kumar	BSE (Caltech)
CO2 interferometer	Carlstrom [12]	DIII-D (GA)
CO2 polarimeter	Akiyama	LHD (NIFS)
Microwave reflectometer	Willis	LDX (Columbia)
Thomson Scattering (Yag)	McLean	SSPX (LLNL)
Thomson Scattering (Ruby)	Golingo	ZAP (UW)
Inverse Compton	Wurden	DIII-D (LANL/GA)
Visible Spectrometer		
Bolometer	Wurden	TFTR (PPPL)
Scintillators	Mishnayot	

We developed a cost model (based on our usual quoting methods)

- Costing model considers materials and labor expenses
- Contingency and GA on materials
- Direct and indirect labor costs included
- Production scaled up from 1 OFF to 10 OFF
- Cost model (time and materials only):

$$C_{Total} = [(C_{CDR} + C_{EDR} + C_{PDR} + C_{Fab} + C_{Test}) * f_{Labor} + C_{Materials} * f_{Cont} + C_{Ship}] * f_{G\&A}(1)$$

Is $C_{Total\,AM} << C_{Total\,CM}$? (AM = Additive Manufacture, CM = Conventional Manufacture)

Costs of Materials, C_{Mat}

- Building objects up layer by layer, instead of cutting away material can reduce material needs and costs by up to 90%. [7]
- Parts can be made hollow or latticed to reduce amount of material
- C_{Mat} impacted up to 99% across all components

Material	UHV / HV / LV	Method
1. Metals		
Stainless steel	UHV	DMLS
Tungsten	UHV	DMLS
OFHC Copper	UHV	SLS
Titanium	UHV	DMLS
Aluminum	UHV	DMLS
Aluminum bronze	UHV	DMLS
Nickel-plated brass	HV	DMLS
Indium	HV	DMLS
Molybdenum	UHV	DMLS
Gold	UHV	DMLS
Niobium	UHV	DMLS
Cusiltin	UHV	DMLS
Inconel	UHV	DMLS
Glidcop	UHV	DMLS
2. Ceramics		
Macor	UHV	?
Boron nitride	UHV	?
Alumina	UHV	Extrusion
Borosilicate glass	HV	?
Quartz	HV	?
3. Plastics		
Kapton	HV	?
PEEK	HV	SLM
Vespel polyimide	HV	?
Delrin	V	?

Table: Materials in fusion environment

Costs of Fabrication, C_{Fab}

- Costs of printing are compared with CNC mill, lathe, drill press, etc
- AM is less expensive for complex parts
- AM also allows pre-assembly and monolithic parts that impact assembly costs
- AM allows fab of parts that are impossible to engineer with CM
- Energy efficient process reduces costs
- C_{Fab} reduced by up to 90%

Alumina Langmuir probe head with cooling channels and WSI logo - less expensive than without!

C_{Fab} example: Magnetic coils

- DIIID initial case (Strait)
- Multi material assy replaced with 2 step AM piece
- Modular design of AM coil allows varous magnetic coil configurations
- C_{Fab} impacted by up to 90% in components and full assy

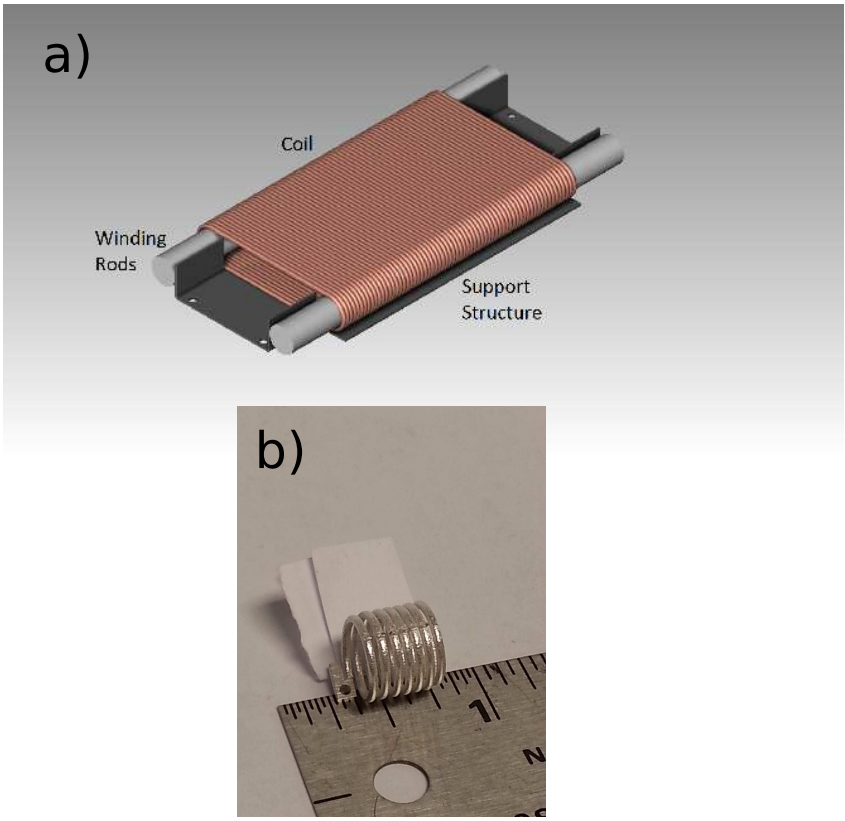

a) Strait design; b) our monolithic printing of modular magnetic coil in silver

C_{Fab} example: Laser-based diagnostics

- Most optomechanical components can be printed in plastic
- Baffles, beam dumps, lens array holders all doable
- Lenses - not yet, but soon
- Monolithic designs being printed (alignment built in)
- C_{Fab} impacted by up to 99% in some components, but only 20% in full assy

a) Interferometer mirror mounts: $190 store bought vs $2.86 printed (raw materials); b) mount installed in interferometer

C_{Fab} example: Radiation/bolometer

- Based on LANL IR camera target, placed close to plasma
- Monolithic design replaces CM
- Complex cooling channels do not add cost
- C_{Fab} impacted by up to 80% in some components, but only 10% in full assy (IR camera still expensive)

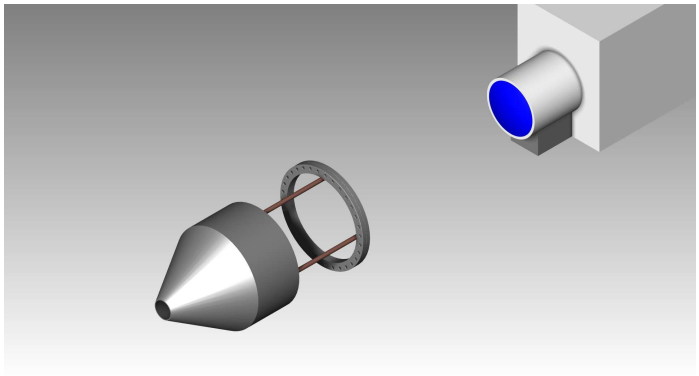

IR camera head for bolometer

Costs of Engineering Design, C_{EDR}

- AM tools now exist for scripting engineering design
- Small variations in commonly used parts can be scripted
- Monolithic designs can be taken straight from physics model
- C_{EDR} impacted by 100% in most cases

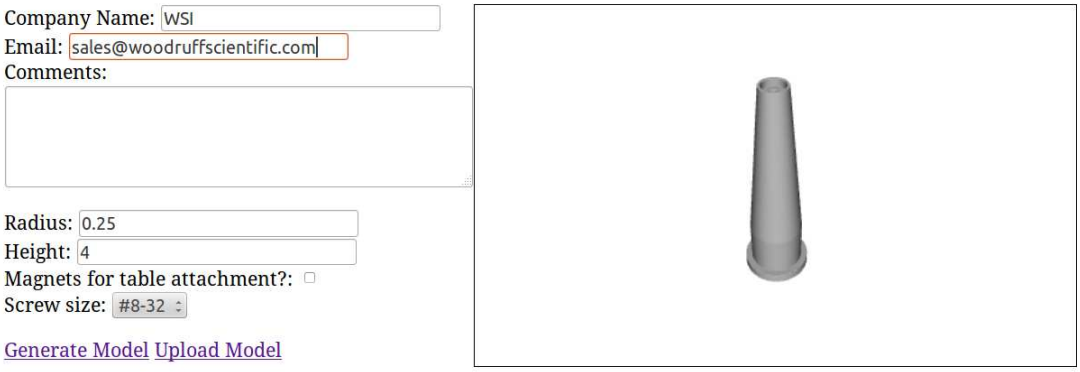

Scripted example of a mirror post: input is only length or width. Other examples we developed included mirror mounts and helmholtz calibration coils. [14]

Costs of Testing, C_{Test}

- For AM the balance is struck between monolithic designs and sufficient degrees of freedom (dof) to tune assy (e.g. alignment of optical components)
- Optimization of these costs occurs by specifying narrow tolerances
- C_{Test} impacted by up to 100% for magnetics, 50-60% for optical diagnostics (by eliminating many dof)

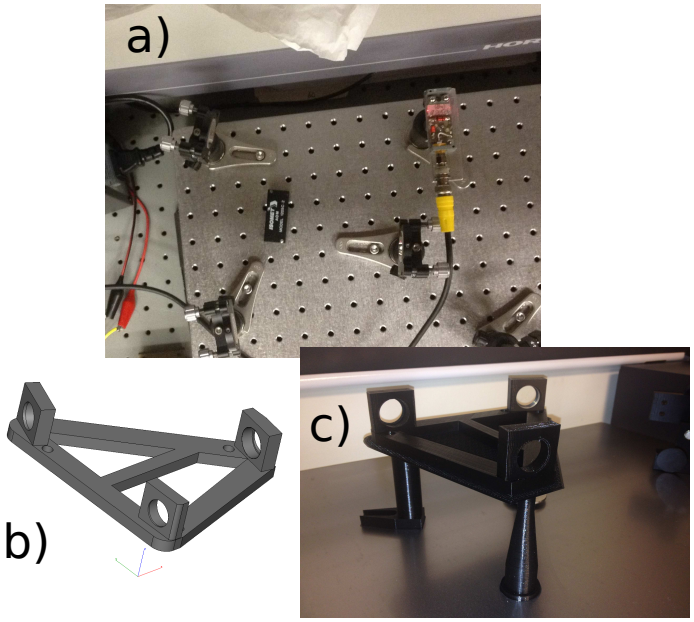

a) original interferometer components; b) pre-aligned monolithic mirror mounts; c) printed monolithic assy

Costs of Concept Design, C_{CDR}

- Experienced physicist examines measurement and maps out best approach
- For all conventional diagnostics, this process can be scripted.
- Web-based form can be used to constrain online scripted EDR
- C_{CDR} can be zero after first iteration.

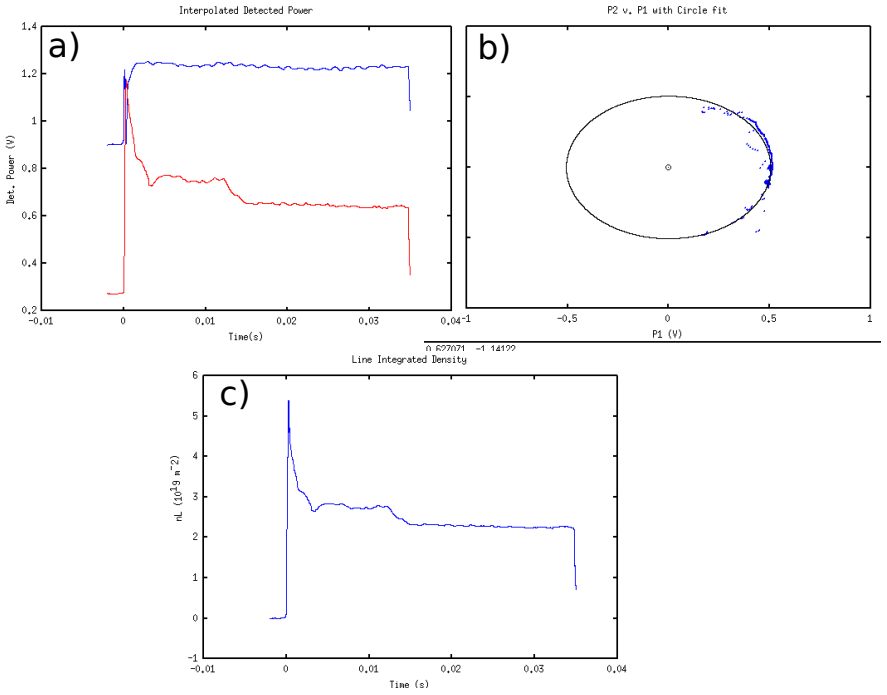

a) data from two separate detectors; b) fitting of data in phase plot;

c) reconstruction of plasma density.

Costing summary AM relative to CM

Diagnostic	C_{Total}	C_{CDR}	C_{EDR}	C_{PDR}	C_{Fab}	C_{Test}	C_{Mat}
Magnetic field coil	0.06	0	0	0.1	0.1	0.1	0.1
Magnetic coil array	0.062	0	0	0.1	0.1	0.1	0.1
Rogowski coil	0.062	0	0	0.1	0.1	0.1	0.1
Calibration jig	0.14	0	0	0.1	0.5	0.1	0.1
Langmuir probe	0.35	0	0	0.1	0.5	1	0.9
RFEA	0.35	0	0	0.1	0.5	1	0.9
HeNe interferometer	0.71	0	0	0.1	0.9	0.2	0.9
CO2 interferometer	0.72	0	0.2	0.1	0.9	0.2	0.9
CO2 polarimeter	0.72	0	0.2	0.1	0.9	0.2	0.9
mm interferometer	0.73	0	0.2	0.1	0.9	0.2	0.9
Thomson Scattering	0.85	0.1	0.9	1	0.9	0.2	0.95
Inverse Compton	0.92	1	1	1	0.9	1	0.9
Spectrometer	0.49	0	0.1	0.1	1	1	0.95
Bolometer	0.59	0	0	1	0.7	1	0.95
Scintillator	0.33	0	0	0.1	0.1	1	0.9

Preparation for Phase II proposal

- Testing of vacuum components in UMBC test facility (PI: Romero-Talamás)
- Installation and testing of components at UW
- Garner interest from ITER and W7X (and other) diagnostics groups

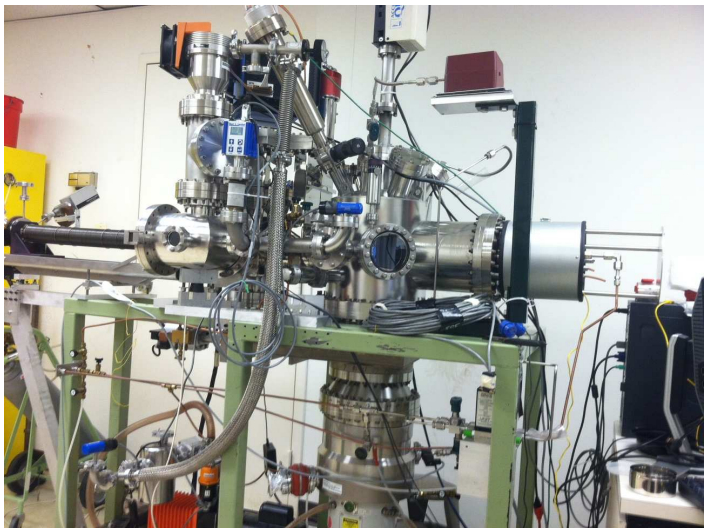

UMBC test facility: flexible configuration for surface testing, mas spectrometry and out-gas testing

State of the art: selective laser melting

- SLM might be path forwards for fusion - can print right materials (Inconel, Glicop, steels, etc)
- Highly accurate (few microns), and potentially multi-material
- Many techniques already compatible with UHV (e.g. ebeam melting), performed in vacuum or inert gas

UHV metal printing and materials qualification

- Currently underway at ORNL, Penn State, NIST and many others [15]
- Massive effort to qualify new materials for use in fusion environment
- Currently no standards (e.g. SS316) for 'digital materials'

Summary

- AM is now a technology that can significantly impact the cost of diagnostic design and faburication for fusion systems TODAY, despte stringent materials requirements in fusion
- In the near future AM will lead to more significant cost savings

- **Phase II of this work will seek to design and build complete diagnostic subcomponents for use in fusion environment, and push development of materials qualification.**

Bibliography


http://www.iter.org/


S. Zinkle Challenges in Developing Materials for Fusion Technology Past, Present and Future AND TOFEy Nashville 2012 http://fire.pppl.gov/TOFE_2012_materials_Zinkle.pdf


I. A. Hutchinson, Principles of Plasma Diagnostics, Cambridge University Press; 2 edition (July 14, 2005)


M. Walsh, et al Overview of High Priority ITER Diagnostic Systems IAEA Fusion Energy Conference 2010 Proc. 2010 http://www-pub.iaea.org/mtcd/meetings/PDFplus/2010/cn180/cn180_papers/itr_p1-07.pdf


Measurement Science Roadmap for Metal-based Additive Manufactrure Prepared by Energetics Incorporated May 2013 http://www.nist.gov/el/isd/upload/NISTAdd_Mfg_Report_FINAL-2.pdf


NIST Dec. 2012 Roadmapping Workshop http://events.energetics.com/NIST-AdditiveMfgWorkshop/downloads.html


The Economist, The Printed World: Three- dimensional printing from digital designs, 10 February 2011. www.economist.com/ node/18114221


Hales and Gooch 'Managing Engineering Design' Springer 2nd Ed 2004


E.J.Strait et al., Chapter 2: Magnetic diagnostics, Fusion Science and Technology 53(2) (2008), 304


E. J. Strait Magnetic diagnostic system of the DIII-D tokamak Rev. Sci. Instrum. 77, 023502 (2006)


R. Pitts et al A Retarding Field Energy Analyser for the JET Plasma Boundary EFDAJETPR(03)30 http://www.iop.org/Jet/fulltext/EFDP03030.pdf


T. N. Carlstrom et al Realtime, vibrationcompensated CO2 interferometer operation on the DIIID tokamak Rev. Sci. Instrum. 08/1988


http://arxiv.org/pdf/1406.4817v1.pdf

Additive manufacture of plasma diagnostics

P.E. Sieck[1], S.Woodruff[1], J. E. Stuber[1], S. Diesburg[1], B. Utela[1], D. Lemmon[1], M. J. Quinley[1], P. A. Melnik[1], A. Card[2], S. You,[2], C.A.Romero-Talamás[3], W. Rivera[3]

[1]Woodruff Scientific Inc, 4000 Aurora Ave N, Seattle, WA 98103 [2]University of Washington Department of Aeronautics and Astronautics, Box 352250, Seattle, WA 98185 [3]University of Maryland Baltimore County, 1000 Hilltop Circle, Engineering 222, Baltimore, MD 21250

American Physical Society Division of Plasma Physics, November 20th 2015

Work supported under DOE subcontract number DE-SC0011858

Abstract

Additive manufacturing (AM, or 3D printing) is now becoming sufficiently accurate with a large range of materials for use in printing sensors needed universally in fusion energy research. Decreasing production cost and significantly lowering design time of energy subsystems would realize significant cost reduction for standard diagnostics commonly obtained through research grants. There is now a well-established set of plasma diagnostics, but these are expensive since they are often highly complex and require customization, sometimes pace the project. Additive manufacturing is developing rapidly, including open source designs. Basic components can be printed for (in some cases) less than 1/100th costs of conventional manufacturing. We have examined the impact that AM can have on plasma diagnostic cost by taking 15 separate diagnostics through an engineering design using Conventional Manufacturing (CM) techniques to determine costs of components and labor costs associated with getting the diagnostic to work as intended. With that information in hand, we set about optimizing the design to exploit the benefits of AM.

Grand challenge for materials: fusion energy environment

- In the next few years, ITER will come online [1]
- Collaboration between US, China, EU, Japan, Russia, India, South Korea
- Plasma will be 10M degrees Celsius
- How to interface plasma to room temperature world?

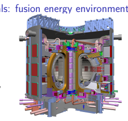

ITER currently under construction in Cadarache, France. ITER began as a Reagan-Gorbachov initiative in 1985, DT ops now planned for 2027

Fusion environment places stringent demands on materials

Materials must [2]:

- withstand high power loads ($5MW/m^2$ to $50MW/m^2$)and neutron bombardment (200dpa)
- min rad waste, be safe and economic
- not out-gas in vacuum (i.e. UHV compatible)
- have low atomic mass number (low Z) so as not to produce radiation losses

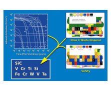

Ideal materials must be safe, must minimize rad waste (and be suitable for recycling), and must be economically competitive (high thermal efficiency, acceptable lifetime, reliable)

Diagnostic components are located close to fusing plasma

- Diagnostics are sensors that measure all important plasma parameters [3]
- Electrostatic probes designed to enter plasma
- Magnetics are usually protected beneath shielding
- Optical diagnostics usually have endoscopes to protect components, but exposed 1st mirrors
- RF diagnostics have horns or antennae close to plasma

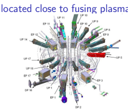

About 50 individual measurement systems will help to control, evaluate and optimize plasma performance in ITER and to further understanding of plasma [4]. These include lasers, X-rays, neutron cameras, impurity monitors, particle spectrometers, radiation bolometers, pressure and gas analysis, and optical fibers.

Some characteristcs of plasma diagnostics

- Highly customized, i.e. no mass-produced diagnostics
- Highly complex systems requiring cooling and integration with other systems
- Many components readily 'printable' if far from neutron environment
- Component requirements constantly evolving (endless prototyping) due to evolving scientific requirements

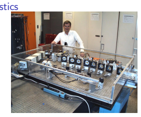

An interferometer with 8 chords (with dashing example of plasma physicist, to give sense of scale). On the optical bench (floating on vibration isolation legs) are over 150 separate components - lasers, mirrors, beam splitters, detectors, etc. Benches don't usually see neutrons. Only some parts can be AM'd today, but tomorrow?

Additive Manufacturing (AM) is ideally suited for plasma diagnostics

- Initially for rapid prototyping (since 1980's) but now fully functional components can be printed
- Diverse set of methods patented (though some patents now expiring)
- US recognizes potential of this disruptive tech and is preparing (e.g. [5])

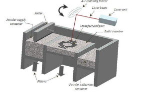

Method shown here is laser sintering of powder (metals, plastics, ceramics) in which the bed covered with a fine layer (few microns) of material, and a high power laser is scanned over the surface, melting it to the layer below. The bed is lowered, a fresh layer of power is rolled across and process is repeated.

Benefits of AM over Conventional Manufacturing (CM)

- Ideally suited to rapid prototyping and functional models [6]
- Low/no waste, low energy, predictable machine time
- No extra cost for complexity
- Reduced assembly - printed parts can be functional
- Cost of printing will fall rapidly in coming years as technology is adopted and printing becomes faster and more accurate.

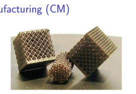

Complex alumina components, with lattice structure to reduce total volume of materials. Simlar components can be printed in metals, and plastics.

To compare costs, we did CDR, CM EDR and AM EDR for 15 diagnostics

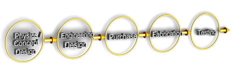

Standard design review process [8]

- Pre-existing designs taken through EDR (so we'd know how to build them), then optimize the design for AM
- Two step design process: 1) obtain original functionality of components; 2) optimize full assembly for AM
- Where it was helpful to understand costs further, we printed prototypes

Diagnostics that we costed

Diagnostic	Example PI	Example Device
Magnetic field coil	Strait [9] [10]	DIII-D (GA)
Magnetic coil array	Strait	DIII-D (GA)
Rogowski coil	Strait	DIII-D (GA)
Calibration jig	Lambert	(KCL)
Langmuir probe		JET (CCFE)
RFEA	Pitts [11]	JET (CCFE)
HeNe interferometer	Kumar	BSE (Caltech)
CO2 interferometer	Carlstrom [12]	DIII-D (GA)
CO2 polarimeter	Akiyama	LHD (NIFS)
Microwave reflectometer	Willis	LDX (Columbia)
Thomson Scattering (Yag)	McLean	SSPX (LLNL)
Thomson Scattering (Ruby)	Golingo	ZAP (UW)
Inverse Compton	Wurden	DIII-D (LANL/GA)
Visible Spectrometer		
Bolometer	Wurden	TFTR (PPPL)
Scintillators	Mishnayot	

We developed a cost model (based on our usual quoting methods)

- Costing model considers materials and labor expenses
- Contingency and G&A on materials
- Direct and indirect labor costs included
- Production scaled up from 1 OFF to 10 OFF
- Cost model (time and materials only):

$$C_{Total} = [(C_{CDR} + C_{EDR} + C_{PDR} + C_{Fab} + C_{Test}) * f_{Labor} + C_{Materials} * f_{Cont} + C_{Ship}] * f_{G\&A} \quad (1)$$

Is $C_{TotalAM} << C_{TotalCM}$? (AM = Additive Manufacture, CM = Conventional Manufacture)

Costs of Materials, C_{Mat}

- Building objects up layer by layer, instead of cutting away material can reduce material needs and costs by up to 90%. [7]
- Parts can be made hollow or latticed to reduce amount of material
- C_{Mat} impacted up to 99% across all components

Material	UHV / HV / LV	Method
1. Metals		
Stainless steel	UHV	DMLS
Tungsten	UHV	DMLS
OFHC Copper	UHV	SLS
Titanium	UHV	DMLS
Aluminum	UHV	DMLS
Aluminum bronze	UHV	DMLS
Nickel-plated brass	HV	DMLS
Indium	HV	DMLS
Molybdenum	UHV	DMLS
Gold	UHV	DMLS
Niobium	UHV	DMLS
Cusiltin	UHV	DMLS
Inconel	UHV	DMLS
Glidcop	UHV	DMLS
2. Ceramics		
Macor	UHV	?
Boron nitride	UHV	?
Alumina	UHV	Extrusion
Borosilicate glass	HV	?
Quartz	HV	?
3. Plastics		
Kapton	HV	?
PEEK	HV	SLM
Vespel polyimide	HV	?
Delrin	V	?

Table: Materials in fusion environment

Costs of Fabrication, C_{Fab}

- Costs of printing are compared with CNC mill, lathe, drill press, etc
- AM is less expensive for complex parts
- AM also allows pre-assembly and monolithic parts that impact assembly costs
- AM allows fab of parts that are impossible to engineer with CM
- Energy efficient process reduces costs
- C_{Fab} reduced by up to 90%

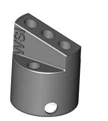

Alumina Langmuir probe head with cooling channels and WSI logo - less expensive than without!

C_{Fab} example: Laser-based diagnostics

- Most optomechanical components can be printed in plastic
- Baffles, beam dumps, lens array holders all doable
- Lenses - not yet, but soon
- Monolithic designs being printed (alignment built-in)
- C_{Fab} impacted by up to 99% in some components, but only 20% in full assy

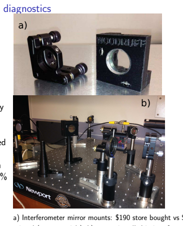

a) Interferometer mirror mounts: $190 store bought vs $2.86 printed (raw materials); b) mount installed in interferometer

C_{Fab} example: Radiation/bolometer

- Based on LANL IR camera target, placed close to plasma
- Monolithic design replaces CM
- Complex cooling channels do not add cost
- C_{Fab} impacted by up to 80% in some components, but only 10% in full assy (IR camera still expensive)

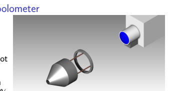

IR camera head for bolometer

Costs of Engineering Design, C_{EDR}

- AM tools now exist for scripting engineering design
- Small variations in commonly used parts can be scripted
- Monolithic designs can be taken straight from physics model
- C_{EDR} impacted by 100% in most cases

Costs of Testing, C_{Test}

- For AM the balance is struck between monolithic designs and sufficient degrees of freedom (DOF) to tune assembly (e.g. alignment of optical components)
- Optimization of these costs occurs by specifying narrow tolerances
- C_{Test} impacted by up to 100% for magnetics, 50-60% for optical diagnostics (by eliminating many DOF)

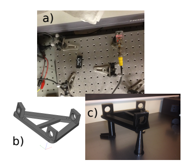

a) original interferometer components; b) pre-aligned monolithic mirror mounts; c) printed monolithic assy

Costs of Concept Design, C_{CDR}

- Experienced physicist examines measurement and maps out best approach
- For all conventional diagnostics, this process can be scripted.
- Web-based form can be used to constrain online scripted EDR
- C_{CDR} can be zero after first iteration.

Costing summary AM relative to CM

Diagnostic	C_{Total}	C_{CDR}	C_{EDR}	C_{PDR}	C_{Fab}	C_{Test}	C_{Mat}
Magnetic field coil	0.06	0	0	0.1	0.1	0.1	0.1
Magnetic coil array	0.062	0	0	0.1	0.1	0.1	0.1
Rogowski coil	0.062	0	0	0.1	0.1	0.1	0.1
Calibration jig	0.14	0	0	0.1	0.5	0.1	0.1
Langmuir probe	0.35	0	0	0.1	0.5	1	0.9
RFEA	0.35	0	0	0.1	0.5	1	0.9
HeNe interferometer	0.71	0	0	0.1	0.9	0.2	0.9
CO2 interferometer	0.72	0	0.2	0.1	0.9	0.2	0.9
CO2 polarimeter	0.72	0	0.2	0.1	0.9	0.2	0.9
mm interferometer	0.73	0	0.2	0.1	0.9	0.2	0.9
Thomson Scattering	0.85	0.1	0.9	1	0.9	0.2	0.95
Inverse Compton	0.92	1	1	1	0.9	1	0.9
Spectrometer	0.49	0	0.1	0.1	1	1	0.95
Bolometer	0.59	0	0	1	0.7	1	0.95
Scintillator	0.33	0	0	0.1	0.1	1	0.9

Component Testing

- Testing of vacuum components in UMBC test facility (PI: Romero-Talamás)
- Installation and testing of components at UW
- Garner interest from ITER and W7X (and other) diagnostics groups

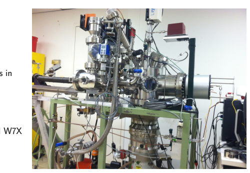

UMBC test facility: flexible configuration for surface testing, mass spectrometry and out-gas testing

State of the art: Selective Laser Melting (SLM)

- SLM might be path forwards for fusion - can print right materials (Inconel, Glidcop, steels, etc)
- Highly accurate (few microns), and potentially multi-material
- Many techniques already compatible with UHV (e.g. ebeam melting), performed in vacuum or inert gas

UHV metal printing and materials qualification

- Currently underway at ORNL, Penn State, NIST and many others [15]
- Massive effort to qualify new materials for use in fusion environment
- Currently no standards (e.g. SS316) for 'digital materials'

Summary

- AM is now a technology that can significantly impact the cost of diagnostic design and fabrication for fusion systems TODAY, despite stringent materials requirements in fusion
- In the near future AM will lead to more significant cost savings
- **We are currently in the design stage on producing complete diagnostic subcomponents for use in fusion environments. In parallel, we are pushing qualification of materials for these applications.**

Bibliography

[1] http://www.iter.org/
[2] S. Zinkle Challenges in Developing Materials for Fusion Technology Past, Present and Future AND TOFEy Nashville 2012 http://fire.pppl.gov/TOFE_2012_materials_Zinkle.pdf
[3] I. A. Hutchinson, Principles of Plasma Diagnostics, Cambridge University Press; 2 edition (July 14, 2005)
[4] M. Walsh, et al Overview of High Priority ITER Diagnostic Systems IAEA Fusion Energy Conference 2010 Proc. 2010 http://www-pub.iaea.org/mtcd/meetings/PDFplus/2010/cn180/cn180_papers/itr_p1-07.pdf
[5] Measurement Science Roadmap for Metal-based Additive Manufactrure Prepared by Energetics Incorporated May 2013 http://www.nist.gov/el/isd/upload/NISTAdd_Mfg_Report_FINAL-2.pdf
[6] NIST Dec. 2012 Roadmapping Workshop http://events.energetics.com/NIST-AdditiveMfgWorkshop/downloads.html
[7] The Economist, The Printed World: Three- dimensional printing from digital designs, 10 February 2011. www.economist.com/node/18114221
[8] Hales and Gooch 'Managing Engineering Design' Springer 2nd Ed 2004
[9] E.J.Strait et al., Chapter 2: Magnetic diagnostics, Fusion Science and Technology 53(2) (2008), 304
[10] E. J. Strait Magnetic diagnostic system of the DIII-D tokamak Rev. Sci. Instrum. 77, 023502 (2006)
[11] R. Pitts et al A Retarding Field Energy Analyser for the JET Plasma Boundary EFDAJETPR(03)30 http://www.iop.org/Jet/fulltext/EFDP03030.pdf
[12] T. N. Carlstrom et al Realtime, vibrationcompensated CO2 interferometer operation on the DIIID tokamak Rev. Sci. Instrum. 08/1988
[13] http://arxiv.org/pdf/1406.4817v1.pdf
[14] http://www.woodruffscientific.com/ShapeJS-Example
[15] Jennifer Bryant, Report of the Breakout Group, NIST AM Qualification and Certification http://events.energetics.com/NIST-AdditiveMfgWorkshop/pdfs/AM_ReportOut_QualCert.pdf

Vibration Isolator Design and Testing: Additive Manufacturing for Affordability

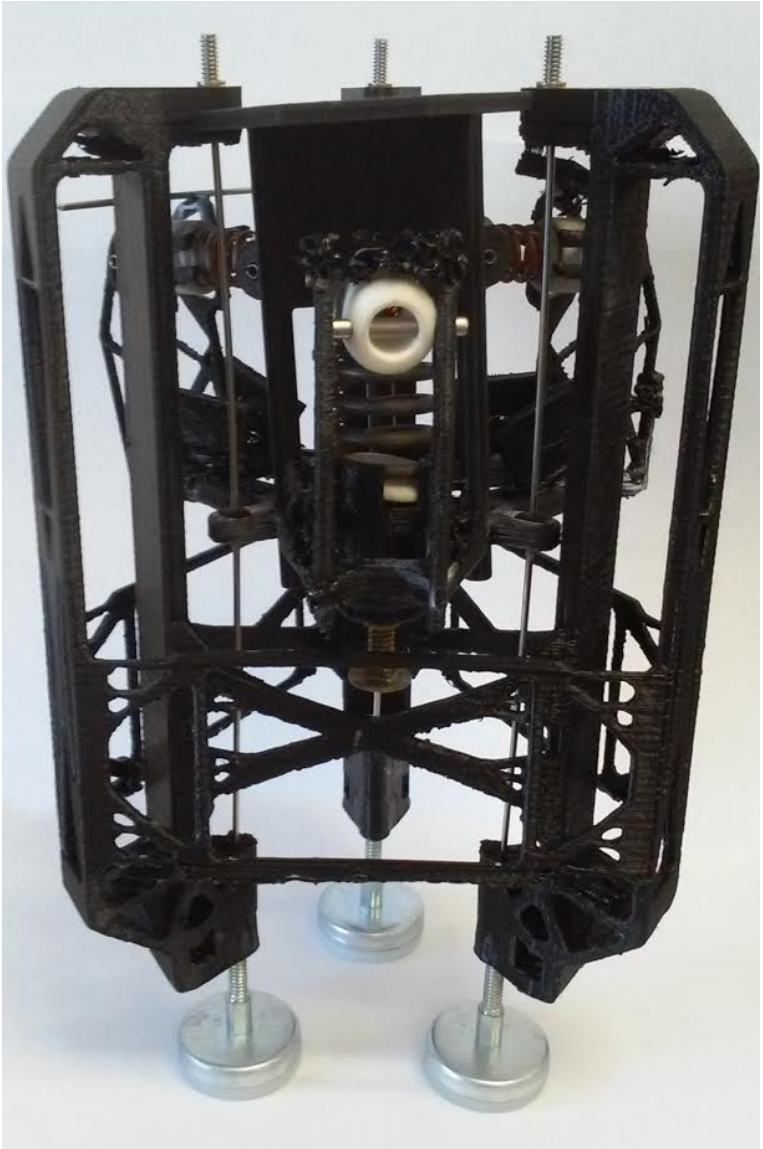

Trevor Smith
Woodruff Scientific, Inc.
April 4, 2017

Abstract

Vibration isolation is the task of filtering mechanical disturbances at a boundary. This can be achieved with a spectrum of techniques that typically require technical calibration and installation either by the provider or the end user. In this attempt to create a vibration isolation system that saves price while allowing extended flexibility, additive manufacturing in the form of PLA extrusion was used. By taking advantage of simple design parameters, finite element analysis and iterative design, a prototype was produced for testing. Experimental data showed that the optimized design worked as intended, proving that there is viability for additive manufacturing as a method for production of more affordable, customizable and accurate vibration isolation systems.

1. Introduction

Vibration isolation is a staple of the modern research facility. Without the capacity to guarantee that recorded data contains little amounts of noise, results may be inconsistent or unreadable all together. Many solutions to the issue of unpredictable cyclical noise are available from science supply and engineering service companies. These include active air springs, micro actuated cancellation motion motors, passive springs, and rubber pads.

These products tend to form two classes: the inaccurate and the expensive. The commonplace isolators (e.g. passive springs, rubber pads) have typically high natural frequencies, limited noise quieting, and are used as basic deterrence from large resonance stresses. Often times, the lower level isolator products do nothing to prevent vibration transmission. The technically advanced isolators (e.g. active air springs, micro actuated cancellation motion motors) are carefully designed and calibrated to possess relatively low natural frequencies to ensure that high frequency disturbances transmit a lower amplitude displacement to the payload. These can be found as tabletop workstations for the price of several thousand US Dollars or as entire tables for the price of tens of thousands of US Dollars.

Challenged with making vibration isolation more approachable for all research institutions, additive manufacturing (AM) may prove to be a powerful tool. It provides the capacity for rapid prototyping, flexibility to end user specifications, and, of most interest to this project, unconventional design for manufacturability.

In part due to the California Space Grant Consortium (CaSGC), Woodruff Scientific Inc. (WSI) was funded to design and test an AM minded vibration isolation system.

2. Nomenclature

Symbol	Variable
E	Elastic Modulus
F_{si}	Horizontal Spring Force
F_{sv}	Vertical Spring Force
G	Beam Restoring Force
I	Second Moment of Area of Beam Cross Section
k_i	Horizontal Spring Constant
k_v	Vertical Spring Constant
L	Compressed Horizontal Spring Length
L_0	Unsprung Horizontal Spring Length
P	Prestressing Load
W	Payload Weight
x	Beam Displacement
y	Spring Displacement
Z	Length of Beam

3. Theory

For each degree of freedom that requires isolation, a system must be introduced between the location of disturbance and the payload. For optimal isolation, each of these systems must first be designed with

frequency response transfer function that minimizes the cutoff frequency. Then, the designs can be altered to lower the impulse response gain toward zero (or negative infinite deciBels). For the sake of this project, the three cartesian translational degrees of freedom were designed for. Two systems were created: one for the direction of gravity and one for the two remaining directions.

The system for the gravitywise isolation takes form as a set of perpendicular, precompressed springs. As seen in Figures 1 and 2, the central spring provides the supporting force to counter the payload weight. While in the neutral state, the other springs cancel out to not have an effect on the payload. When displaced, the horizontal components of the springs will cancel and the vertical springs will add together in the direction of the displacement.

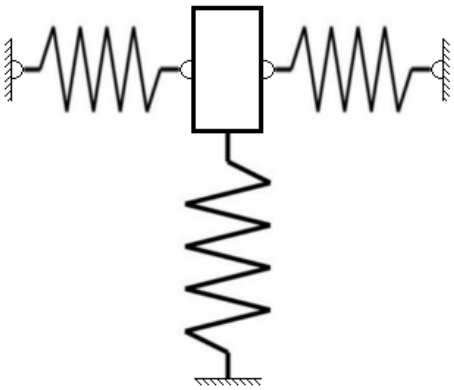

Figure 1: Neutral State Gravitywise Isolator

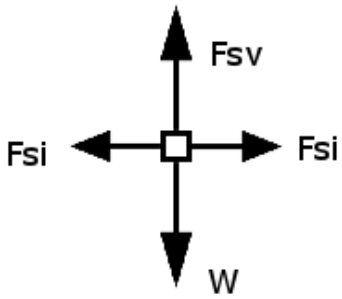

Figure 2: Neutral State Gravitywise Isolator
Free Body Diagram

By evaluating the proposed isolator in a displaced configuration, as seen in Figures 3 and 4, a driving system equation can be derived with simple rules of mechanics. The equation for a system containing three horizontal springs is found to be:

$$\Sigma F_y = 3 * k_i * (L_0 - \sqrt{L^2 + y^2}\ ) * y * \frac{1}{\sqrt{L^2+y^2}} - k_v * y$$

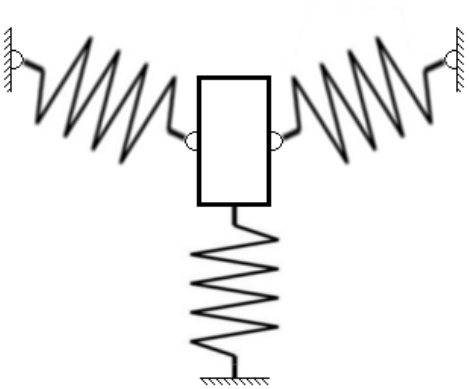

Figure 3: Displaced Gravitywise Isolator

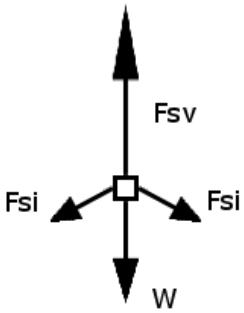

Figure 4: Displaced Gravitywise Isolator
Free Body Diagram

Evaluating the instantaneous change of force as the system approaches the neutral state provides the following relationship for the horizontal spring constant:

$$k_i = k_y * \frac{1}{3*(L_0/L-1)}$$

This relationship ensures that displacements near the neutral state will result in very low, nearly zero amounts of force transmitted.

The system for the isolation of the remaining directions is a set of prestressed beam columns. Each beam is modeled with fixed-fixed boundary condition; the neutral position is shown in Figure 5. When acted on by a displacing motion, the beam will deform to accommodate; this is shown in Figure 6. One boundary condition remains fixed while the other will translate while maintaining a perpendicular attachment. This is referred to as guided. When the beam deforms, it provides a restoring force to attempt to return it to its neutral state. This gives the system the elasticity which can be manipulated to isolate the system from vibrations.

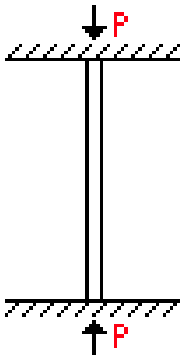

Figure 5: Fixed-fixed boundary condition model of beams

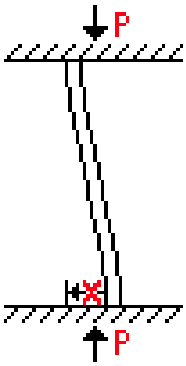

Figure 6: Guided-fixed boundary condition model of beams with displacement

To manipulate this model, each beam is dissected in the center and evaluated as cantilevered. When a displacement acts on the system, a restoring force will act on the interior crosssectional face of the beam where the dissection was taken; this is shown in Figure 7.

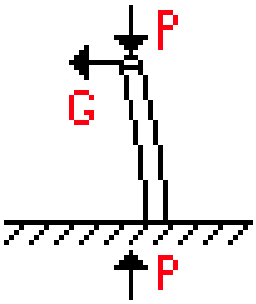

Figure 7: Dissected beam reaction to displacement

The deflection of a cantilever beam from a study of solid mechanics can be derived as a function of various conditions. From Roark's Formulas for Stress and Strain 7e, a guided-fixed preloaded beam acted on by a force perpendicular to the beam at the guided end will deform according to:

$$x = \frac{G\sqrt{EI}}{P\sqrt{P}} * (2 * tan\frac{Z\sqrt{P}}{2\sqrt{EI}} - \frac{Z\sqrt{P}}{\sqrt{EI}})$$

With corresponding stiffness:

$$k = \frac{P\sqrt{P}}{\sqrt{EI}*(2*tan\frac{Z\sqrt{P}}{2\sqrt{EI}} - \frac{Z\sqrt{P}}{\sqrt{EI}})}$$

To achieve the goal of no transmission of force to the payload, this requires the restoring force to be zero and, as a direct result, the stiffness of the beam to be zero. This will occur when the tangent term goes to an unbounded infinity at $\pi/2$. Applying this results in a required pretensioning force of:

$$P = \pi^2 EI/Z^2$$

This happens to be the critical buckling load for a beam in this boundary condition. From an intuitional perspective, this is sensible. The beam is loaded to a point where its neutral state is in a buckled position. The beam is in a metastable vertical position until acted on. It will then buckle without any force resisting this movement.

To compensate for possible changes in payload weight, an upper beam was added to the design; this is seen in Figure 8. Any change in the weight will load the lower beam and unload the upper beam of the same magnitude of force. This will result in a negative stiffness of the lower beam and a positive stiffness of the lower beam of the same magnitude. Overall, these will cancel to still provide the zero stiffness desired for isolation.

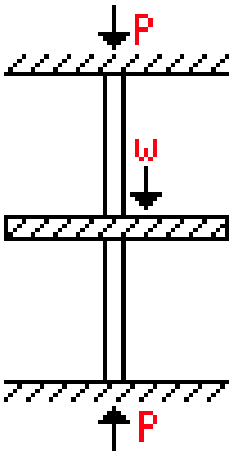

Figure 8: Modified beam-style isolator accommodating for changes in payload weight

The final significant design point to affect the frequency response of the vibration isolation is the geometry of the supports that maintain the alignment of the springs and beam for optimum isolation. The natural frequency of the support structure is dependent on the location and conjoining of the mass. If the natural frequency is prevalent enough, the isolation will be ruined by the amplification of displacement through the support structure. To ensure that the natural frequency of the system as an assembled whole will only depend on the springs and the beams, the optimum design is one that maximizes the relevant stiffnesses. With maximum stiffness, the springs and beams can also be ensured to remain aligned while exposed to cyclical displacement.

Since AM is quoted on volumetric basis for most materials, to achieve an economical design, a minimization of material was made a design point. For the first rendition of the vibration isolator, a Python based program named ToPy was used. This program optimizes minimum compliances for a set amount of volume. This will maximize stiffnesses since compliance is the inverse property of stiffness. ToPy is based on the common 99 and 88 line MatLab topology optimization algorithms and provides strictly cubic meshes of objects that define void to solid ratio of each differential element.

An example of the topology optimization process on the uprights holding the beams can be seen in Figure 9. An assembled system optimization can be seen in Figure A.1. Two dimensional models were optimized for the best resolution. These results were cross checked with their lower resolution three dimensional counterparts, finite element analysis of displacement and common sense.

Figure 9: Beam Uprights
Left: Before Topology Optimization
Right: After Topology Optimization

4. Experiment Setup

To test the efficiency of the vibration isolator prototype, a forced vibration test was performed and recorded. Two piezoelectric accelerometers were each mounted to a separate plated through hole breadboard and used as the data capture hardware. A photo of the accelerometers can be seen in Figure 10.

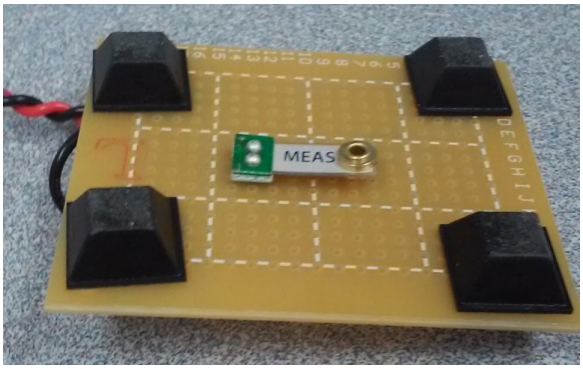

Figure 10: Accelerometers for vibration response testing

The voltage from the accelerometers were discretely digitized through an onboard soundcard in a desktop computer. This data was then sparsed through a python script and printed out in comma separated value format. The script also printed a graph of the data to screen to verify that the accelerometers were producing a reading as expected.

Using this setup, seven datasets were recorded for analysis. Two control tests were recorded: once at the beginning of testing and once at the end. A photo of the control tests can be seen in Figure 11. Two tests of vibration isolation via a standard McMaster-Carr catalogue were recorded: once using one accelerometer and once using the other. A photo of the catalogue testing can be seen in Figure 12. Finally, three tests of vibration isolation via the AM prototype vibration isolator were recorded: twice with one accelerometer and once with the other. A photo of the experiment setup for vibration testing of the vibration isolator can be seen in Figure 13.

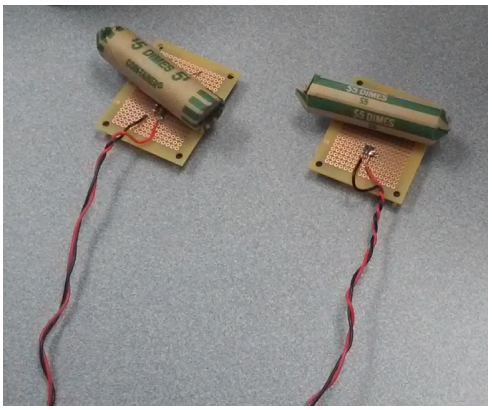

Figure 11: Control testing setup

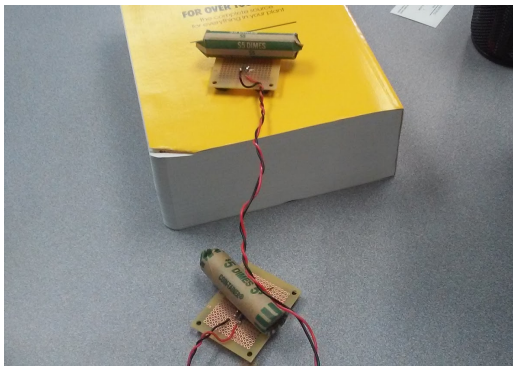

Figure 12: Catalogue testing setup

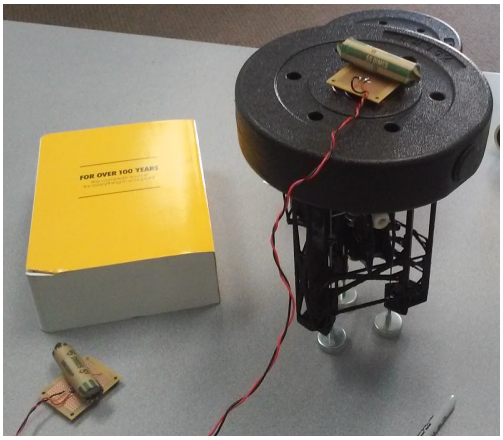

Figure 13: Vibration isolator testing setup

Each dataset recorded both accelerometers' response simultaneously. For the control data, both accelerometers were on the table. For the catalogue isolation data, one accelerometer was on the table and the other was on the catalogue. For the AM vibration isolator isolation data, one accelerometer was on the table and the other was on the isolator.

Post experiment, all data was stabilized for static recording noise. The data was then normalized using the control data. Comparing the magnitude of the recording from one accelerometer to the other, a coefficient was calculated that would equalized the difference in the accelerometers' readings due to differences in the hardware. The rest of the data was then normalized using this coefficient, stabilized for noise and compared.

5. Results

The normalizing coefficient was calculated as 0.41 by averaging the coefficients for the two control datasets.

The response for the first catalogue isolation test, seen in Figure 14, resulted in 155.86% average displacement transmission and 150.99% maximum displacement transmission.

The response for the second catalogue isolation test, seen in Figure A.2, resulted in 143.23% average displacement transmission and 346.31% maximum displacement transmission.

The response for the first isolator isolation test, seen in Figure 15, resulted in 0.4066% average displacement transmission and 3.5751% maximum displacement transmission.

The response for the second isolator isolation test, seen in Figure A.3, resulted in 2.7024% average displacement transmission and 22.182% maximum displacement transmission.

The response for the third isolator isolation test, seen in Figure A.4, resulted in 1.0744% average displacement transmission and 30.272% maximum displacement transmission.

A frequency spectrum decomposition showed that the vibrations being transmitted through the isolator were largely composed of an average frequency of $67\ Hz$.

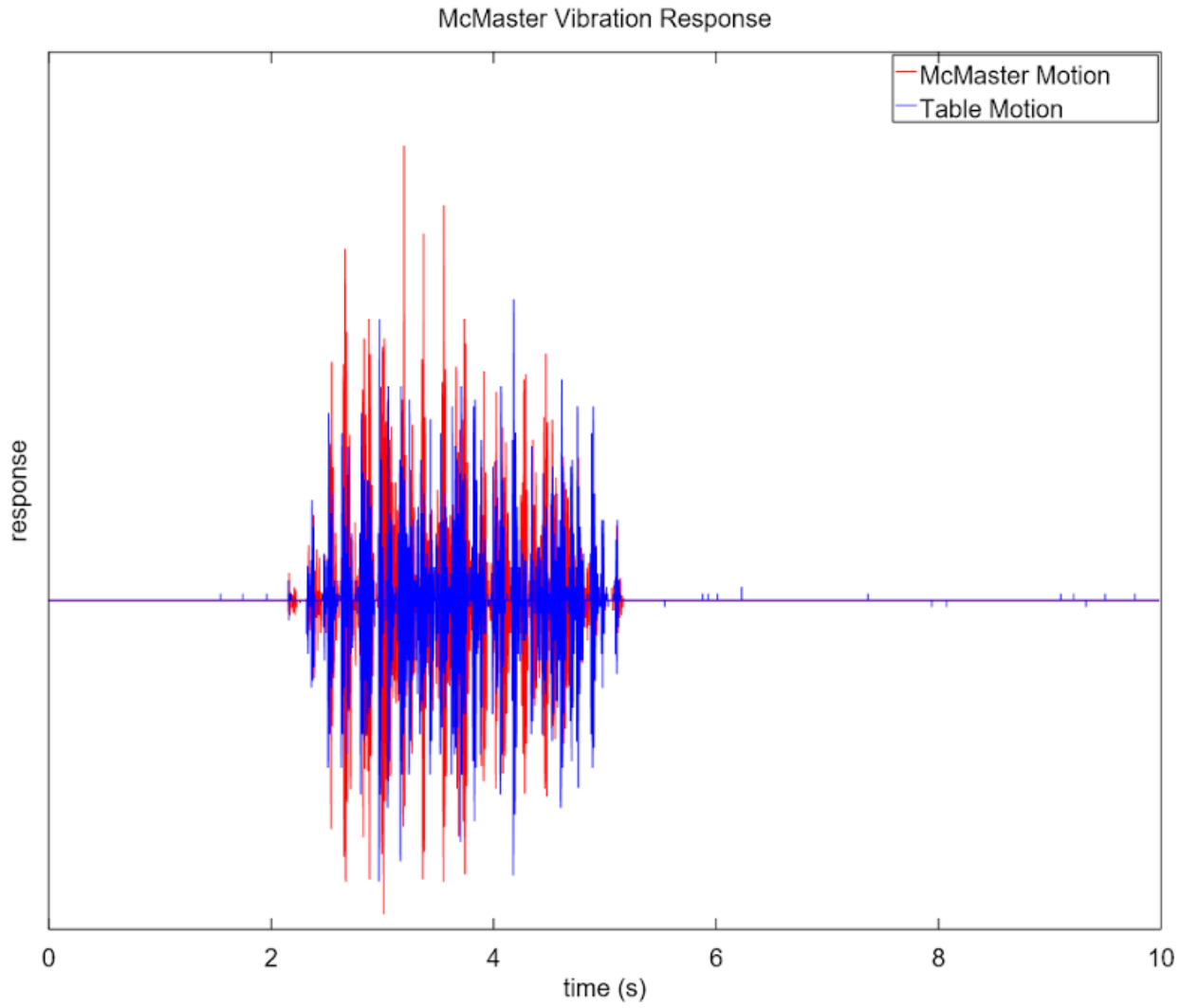

Figure 14: First catalogue isolation test

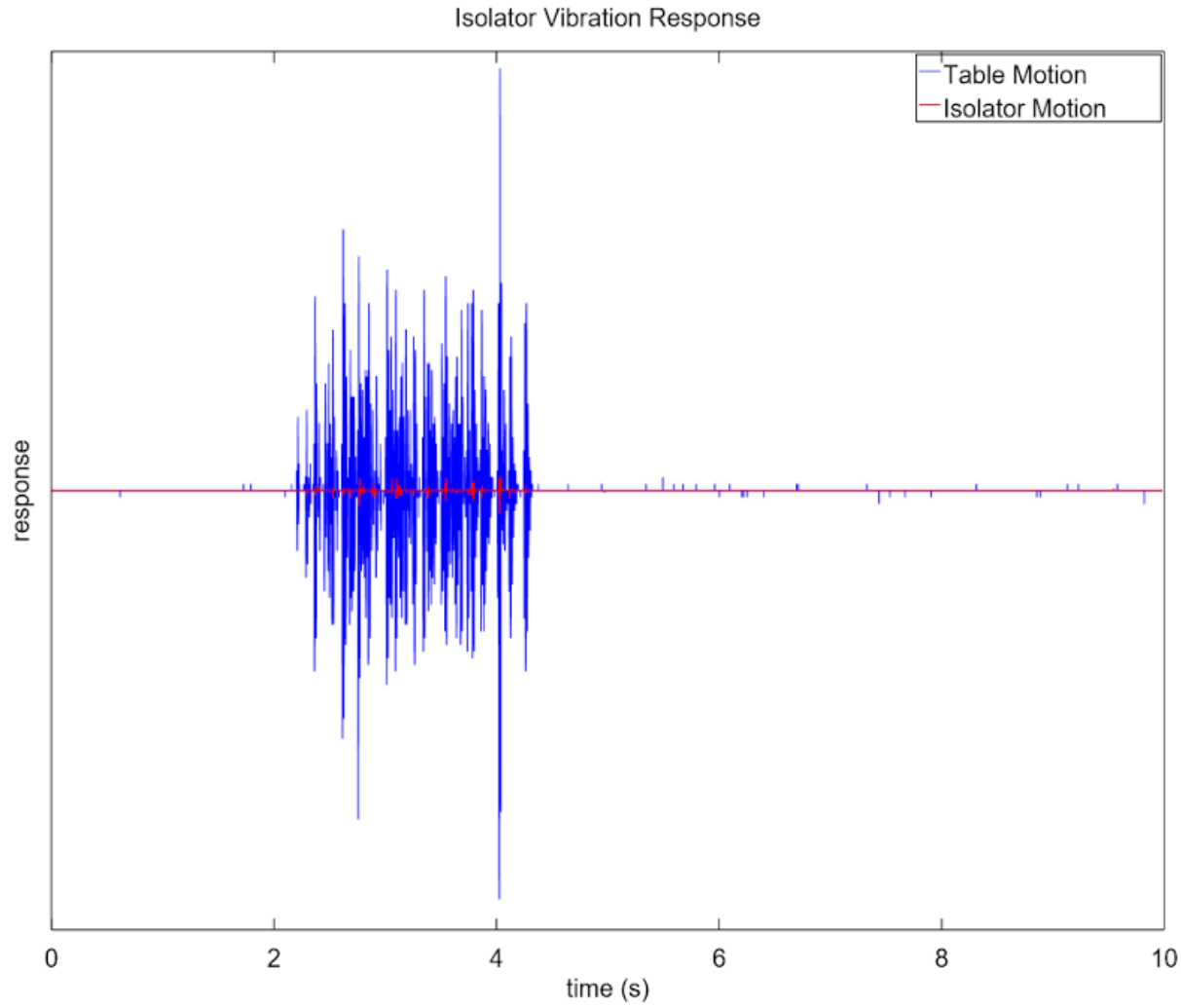

Figure 15: First isolator isolation test

6. Discussion

The data well represents the theory that was compiled into the design of the isolator. Most of the disturbances were attenuated to near negligible levels. The disturbances that did pass through the isolator appear to be made of relatively low frequencies. It should be noted that the $67\ Hz$ that the response of the isolator oscillated at is not necessarily the natural frequency. This is only the frequency of the response.

Most of the topology optimization worked well. This provided with large sums of mass saving which led to large savings in costs. The performance of the isolator does not appear to have suffered noticeably due to the mass loss.

The uprights that held the horizontal springs were the point of optimization failure. Due to the thin walls of the uprights and the large moment lever, these quickly fractured and required manually added struts. A picture of the failure point and repair can be seen in Figures 16 and 17. The topology analysis was ran on a two dimensional system and checked only for stiffness in those dimensions. Therefore, the weakness at the uprights was not identified until the testing.

Due to most of the isolator being extruded of polylactic acid (PLA), some signs of plastic creep due to cyclical use and constant prestress were evident. As a preliminary prototype, PLA worked to prove the viability of the concept. When moving forward to the next stage of design, a laser sintered metal would likely prove to be a wiser choice. There are many types of aluminum, steel and brass, among other metals, available from popular AM service providers.

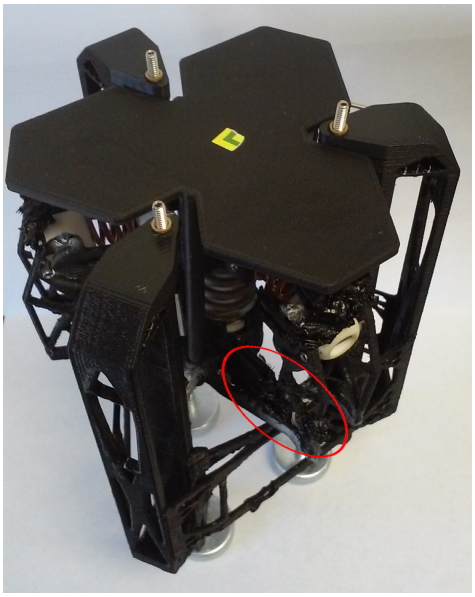

Figure 16: Location of failure point

Figure 17: Failure point close up

Another design strategy that would provide a more stable result is changing the constraints of the topology optimization. In ToPy, the script optimizes solely for minimum compliance. When the results are tested in standard FEA, the conclusion is that the provided geometry is stable; however, the

surface stresses due to bending may be greater than the maximum tensile strength. In this case, the part may fail despite the stiffness being maximized. Taking advantage of multiphysics computer aided engineering (CAE) optimization programs, problems could be defined that optimize for minimum compliance with both a volume fraction and a maximum surface stress defined as constraints.

7. Conclusions

As a proof of concept that an affordable, accurate vibration isolator can be produced, the prototype was successful. The data from the experiment, both numerical and physical, provided many new design points to launch a second rendition of an affordable vibration isolator using the same underlying physics.

A. Appendix

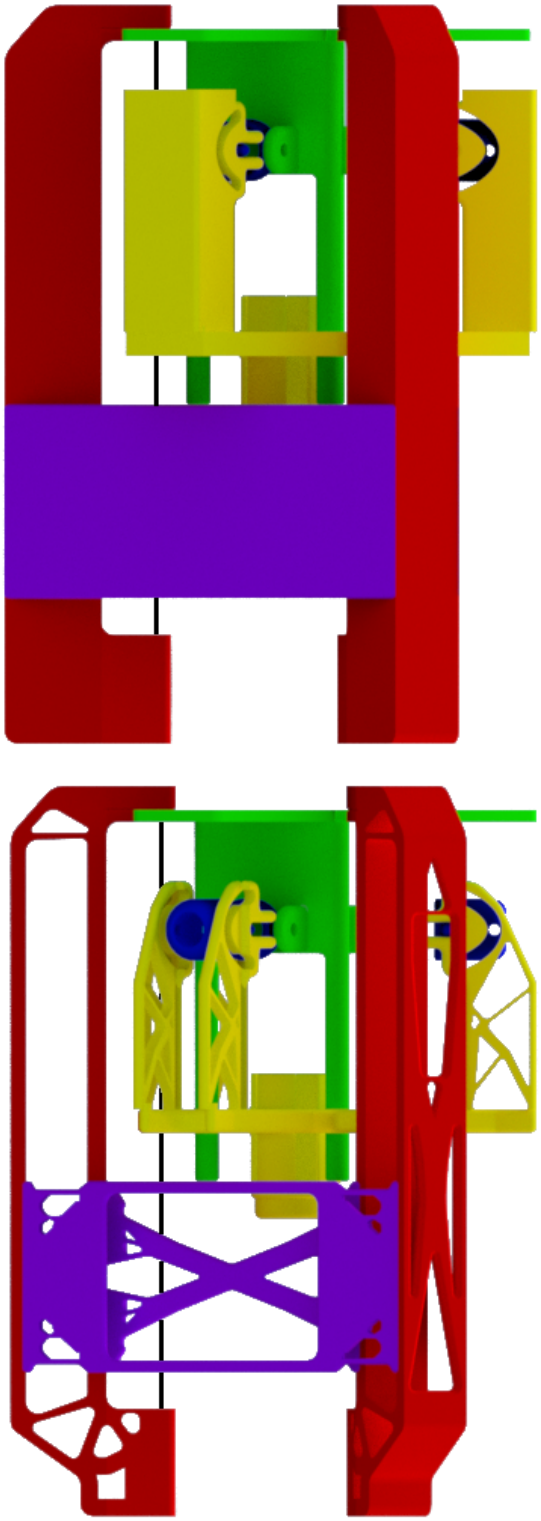

Figure A.1: Assembled Vibration Isolator
Top: Before Topology Optimization
Bottom: After Topology Optimization

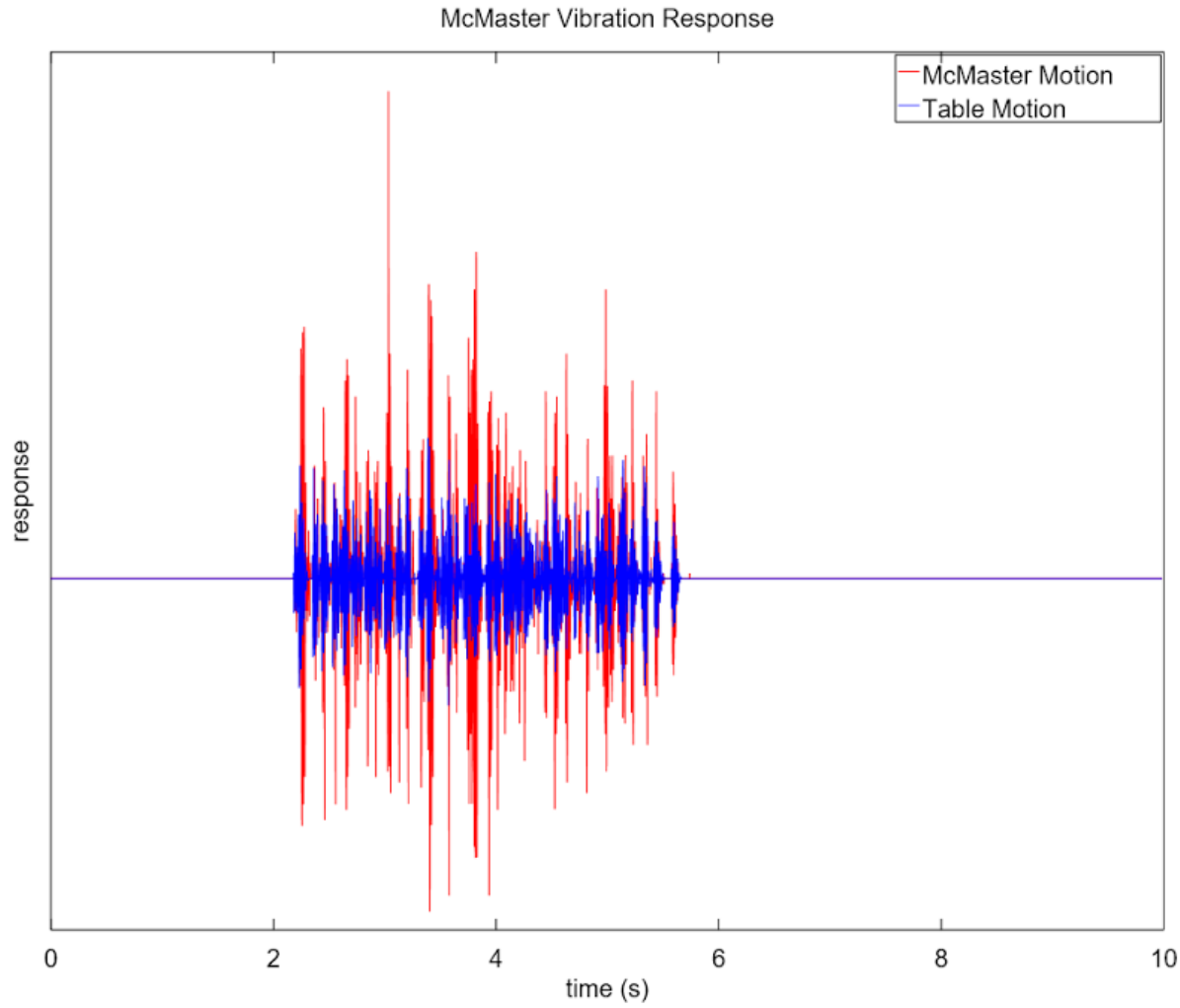

Figure A.2: Second catalogue isolation test

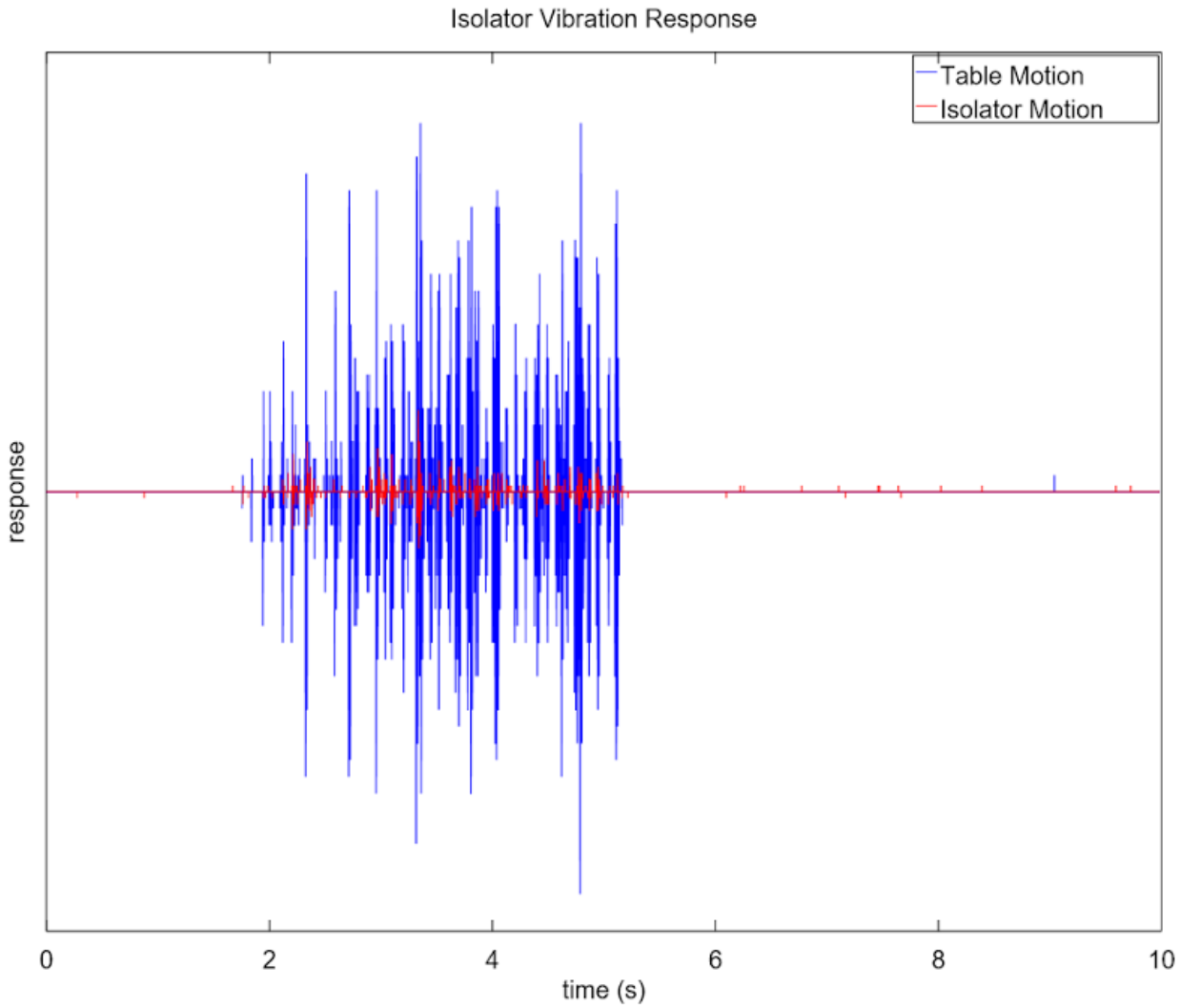

Figure A.3: Second isolator isolation test

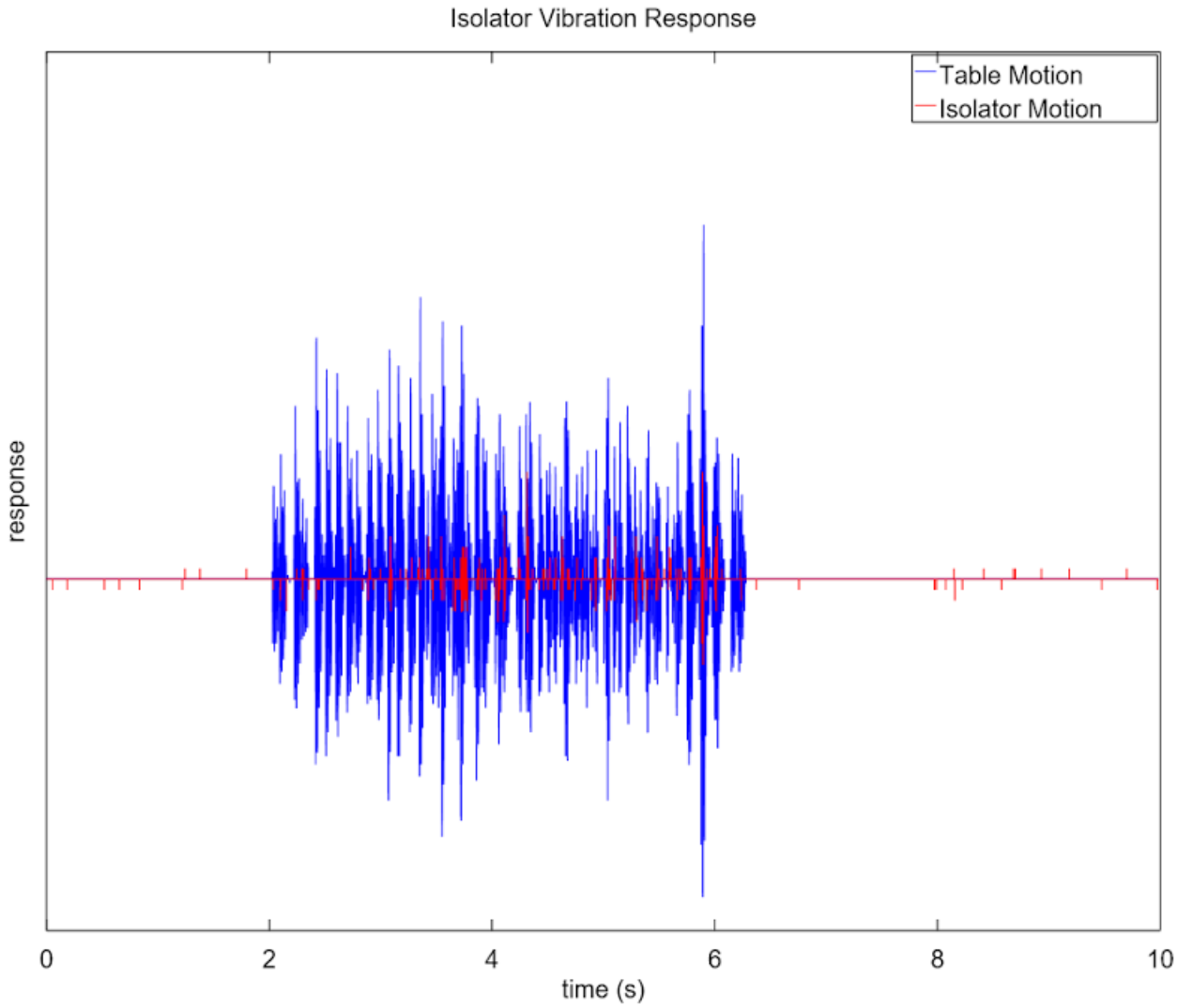

Figure A.4: Third isolator isolation test

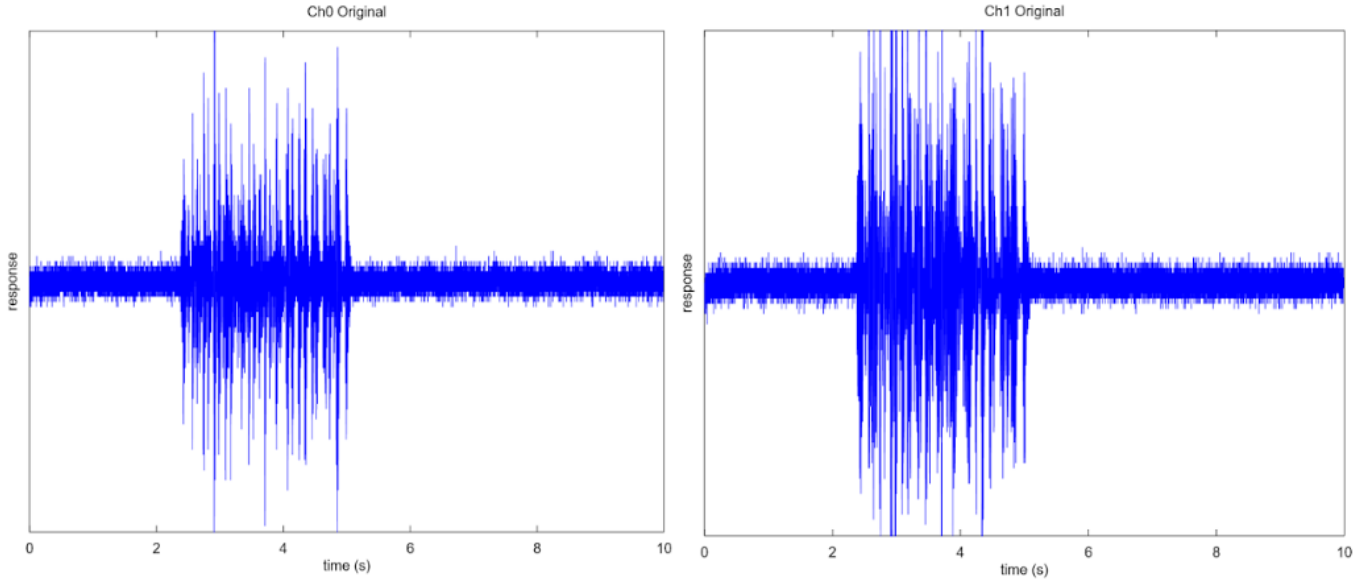

Figure A.5: Control test raw data

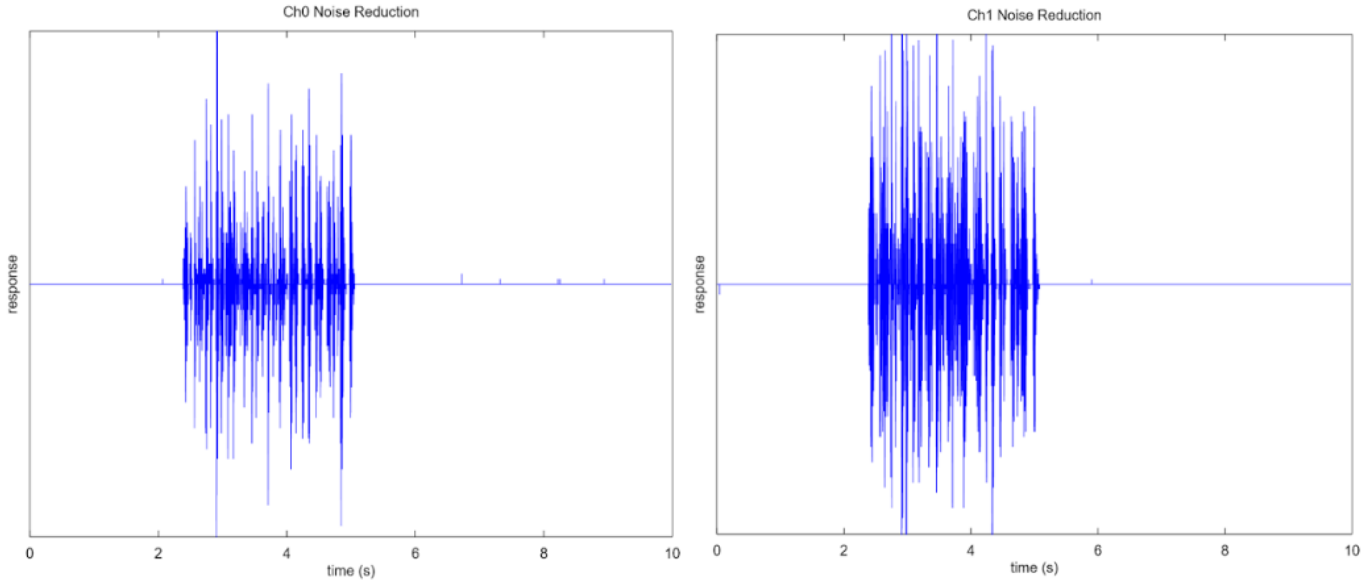

Figure A.6: Control test noise reduced data

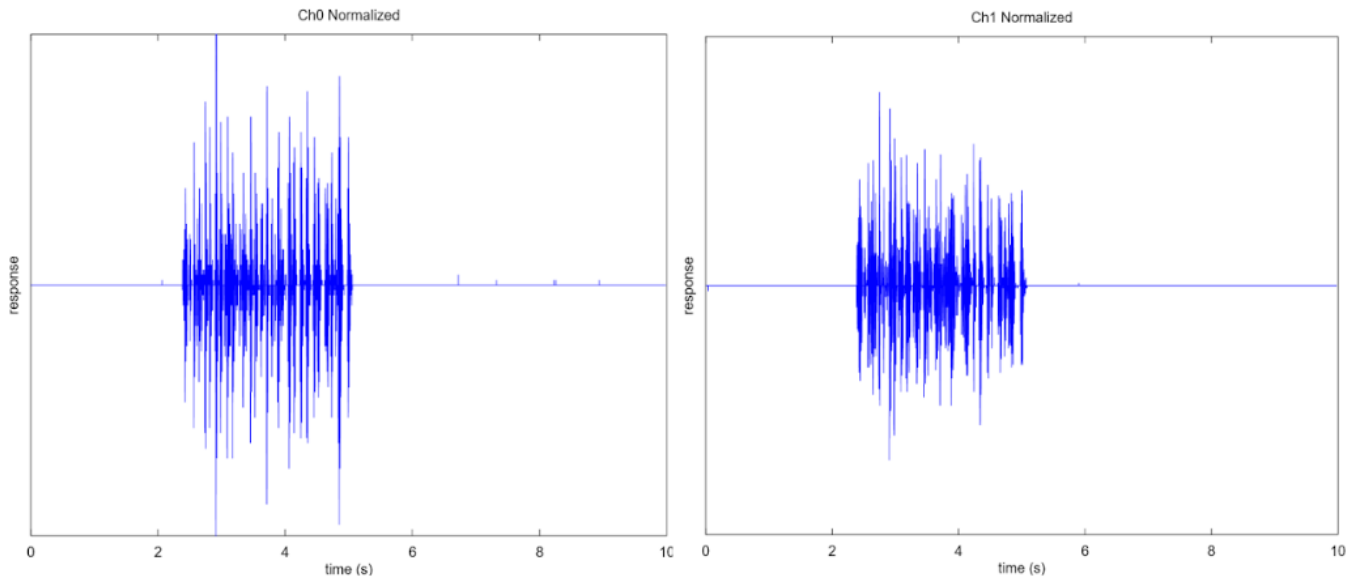

Figure A.7: Control test normalized data

References

[1] Mizuno, Takeshi; Toumiya, Takefumi & Masaya Takasaki, (2003). “Vibration isolation using negative stiffness.” JSME International Jounral, Series C, 46 (3), 807-812.

[2] Platus, David & Ferry, David, (2007). “Negative-stiffness vibration isolation improves reliability of nanoistrumentaion.” Laser Focus World, 43 (10), 107-109.

[3] Kilikevičius, Artūas; Jurevičius, Mindaugas & Michail Berba, (2011). “Impact of External excitations on the Dynamic properties of Negative-stiffness Vibration Isolation Table.” Journal of Vibroengineering, 13 (2), 352-357.

[4] Kashdan, Lia; Conner Seepersad, Carolyn; Haberman, Michael & Wilson, Preston, (2012). “Design, Fabrication, and Evaluation of Negative Stiffness Elements Using SLS.” Rapid Prototyping Journal, 18 (3), 194-200.

[5] Vijayan, Venkatraman & Karthekeya, Thangavelu, (2014). “Material Selection of Compliant Mechanism for Vibration Isolation.” Mechanics and Mechanical Engineering, 18 (2), 121-134.

[6] Hunter, William, (2009). “Predominantly solid-void three-dimensional topology optimisation using open source software.” (Unpublished master thesis). University of Stellenbosch, Matieland, Republic of South Africa.

COVER PAGE

Project Title: Additive Manufacture (3d. Printing) Of Plasma Diagnostic Components and Assemblies for Fusion Experiments	
Federal Award Identification Number: DE-SC0011858	
Agency Code: 8900	**Organization:** SBIR and STTR Programs Office
Recipient Award Identification Number: Not Provided	**Project Period:** 07/28/2015 - 07/27/2017
Reporting Period: 07/28/2015 - 07/27/2016	**Budget Period:** 07/28/2015 - 07/27/2016
Report Term: Once per Budget Period	**Submission Date and Time:** 05/17/2016 02:42 PM ET
Principal Investigator Information: Dr. Simon Woodruff 4000 Aurora Ave N, 6 6 Seattle, WA 98103 **Email:** simon@woodruffscientific.com **Contact:** (206) 697-9401	**Recipient Organization:** Woodruff Scientific, Inc. 4501 Shilshole Ave NW Seattle, WA 98107-4708 Country: USA **DUNS:** 613177240 **EIN:** 202797253
Submitting Official Information: Dr. Simon Woodruff 4000 Aurora Ave N, 6 6 Seattle, WA 98103 **Email:** simon@woodruffscientific.com **Contact:** (206) 697-9401	

ACCOMPLISHMENTS

1. What are the major goals of the project?

As stated in the approved application, our major goals of this project are to optimize the design points of ~15 plasma diagnostics for additive manufacture, and test some of those components in a world-class fusion facilities. There have been no changes in approach or methods outlined in the original proposal. Given a conventional physics point designs (i.e. published design points), we proposed to utilize state-of-the-art modeling for the development of the diagnostic designs through a usual Engineering Design Review that will be optimized for AM, and utilize online design tools that allow customization. The last stage will be to consider product categories that lead naturally to commercialization for entire range of diagnostics and also for any new AM techniques that we will need to develop. During the product design phase, we will seek to protect the IP by filing provisional patents on each design. To attain these goals, we proposed the following technical objectives:

Conceptual design
1. Downselect from existing Phase I diagnostic set (and sub-components) to set of 15 diagnostics that could most benefit from AM;
2. Complete analytical physics models (started in Phase I) for the responses of the diagnostic, considering operating environments and dynamic ranges of digitizers, allowing a point design for each diagnostic to be developed;
3. Optimize point designs to produce tolerances for Engineering design stage;
4. Downselect materials options according to intended operating environment;
5. Code physics concept design as a web-based form for customers to define their requirements, and to constrain online engineering design point, in order significantly reduce cost of Concept Design Review C_CDR.

Engineering design
1. Take design points for diagnostic set (produced in conceptual design stage) and complete full Engineering Design Reviews for Conventional Manufacture utilizing state-of-the-art design tools (e.g. Zemax for optical design, ANSYS for engineering modeling, Solidworks for CAD);
2. Optimize Engineering Design for Additive Manufacture, i.e. produce designs that minimize cost of materials (C_Mat), cost of fabrication (C_Fab), and cost of testing (C_Test);
3. Script the design point for use with online design tools (taking also input from online CDR) to allow customers to customize the design, seeking to significantly reduce costs of Engineering Design (C_EDR)
4. Consider separate cases of plasma-facing components that will be exposed to high neutron or heat fluxes (e.g. ITER optical dumps, per our design), from those that will be far from the plasma.
5. Consider modification of existing AM techniques to better satisfy technical specifications from leading fusion research devices (e.g. ITER).

Prototyping
1. Use state-of-the-art AM methods (e.g. e-beam or laser selective melting) to prototype diagnostic components to demonstrate feasibility;
2. Test plasma-facing components in UMBC vacuum quality test facility.
Product design
1. Examine in detail 15 separate case examples of diagnostics that can be packaged as products to be ordered online, including customization and multi-instrument packaging.

2. What was accomplished under these goals?

During the performance period, we have completed all of the conceptual design work (Objectives 1.1 through 1.5), some of the engineering design (Objectives 2.1 some of the AM design optimization (O2.2), 2.3 , and 2.4) and some of the prototyping (Objective 3.1) and materials testing (O3.2). We summarize the work in the following sections

1. Competed EDRs for most conventional plasma diagnostics

We have taken multiple diagnostics through a conventional Engineering Design process, which includes a) engineering schematics, b) circuit schematics; c) post-processing routines; d) variations; e) Bills of Materials and labor costs associated with diagnostic manufacture. These diagnostics included: Magnetic (Arrays, Single, Rogowskis); Electrostatic (langmuir, retarding grid energy analyser); Refractive index (Microwave interferometer, two color fiber-based interferometer, HeNe, CO2); Scattering (Thomson, Inverse Compton); and, Spectroscopy (Bolometer, line-based temperature measurement). All of the diagnostic design work is summarized as 'spec sheets' which have been made available on our

website.

2 Obtained tools for optimizing designs for AM and exercised those

The AM optimization process requires a comprehensive set of tools for modeling the diagnostics, starting with Physics modeling (such as Mathematica/Optica and Matlab), then implementation of the physics design point with CAD (such as Shark, ViaCAD and Fusion360), finally use of FEM codes for optimizing the thermal or mechanical aspects of the design (we have opted for COMSOL in this performance period). New tools for topology optimization such as ToPy (open-source Python implementation), allow us to optimize the CAD engineering design point for thermal and mechanical properties while reducing mass, or material costs.

Because complexity is not penalized when using AM, non-standard structures can be designed and utilized. Topology optimization (TO) is a computational approach which produces designs optimized for requirements with a limited amount of material. Designs can be optimized for minimum compliance, heat conduction, or other loads. The reduction in material used can lead to lighter and lower-cost designs. With CM, TO could only be used to guide design, as its output often results in unusual shapes difficult to manufacture. With AM, these limitations are removed and designs from TO can be directly printed (references from http://www.topopt.dtu.dk). The workflow proceeds by defining requirements (heat loading? Structural loading?) then to setup parameters for topology optimization problem. The topology optimization code is run that generates a rough mesh of the problem. The mesh then needs to be refined to be read back into a CAD package, which then requires further refinement before results are checked in FEM engineering program such as COMSOL, before finally being sent to a printer.

3 Started to look in detail at optimization of some diagnostics components for AM

Some design points were immediately accessible for optimization for AM. These included the Retarding Field Analyzer, a bolometer, some of the magnetic coil forms (Rogowski, single coils, arrays), and also an optical device: a HeNe interferometer. The RFA and interferometer are discussed further below.

The process for magnetic B-dot coil (or Rogowski coil) design now starts with an online script, with the customer first defining the expected magnitude of the measured quantity and digitizer dynamic range. These determine the minimum and maximum nA of the coil. The customer then defines the frequency response. What is the frequency (or range of frequencies) that need to be measured? This determines the required inductance, L, and resistance, R, of the coil. The vacuum environment is then defined. Is the probe intended to be used in air or vacuum? High vacuum (HV, 10^{-3} - 10^{-9} torr) or ultra-high vacuum (UHV, 10^{-9} - 10^{-12} torr)? This determines the materials that can be used for customer applications. The thermal environment is then defined. This information also places restrictions on the materials that can be used. Information about the mounting interface is then specified. Will the probe be mounted to a vacuum flange, a custom mounting structure on the chamber wall, or something else? Finally, size constraints are defined. With this information, information is then handed to an automated Python script to produce an engineering design point for the coil form, which can then be sent directly to a printer.

4 Metal components printed for out-gas testing at UMBC

We have obtained out-gas test results from OD3”x0.25” disks printed in inconel, steel, aluminum, titanium and alumina to fit test rig at UMBC. A paper publication summarizes some of these results. Outgas testing relative to cast pieces is expected to be performed during this summer as the chamber is updated.

5 Collaborating with C-Mod to test one diagnostic in situ

Dan Brunner (PhD, MIT) designed a state-of-the-art, conventionally-manufactured retarding field analyzer (RFA) for use on Alcator C-Mod, which has successfully taken measurements. But the probe is still limited to the last closed flux surface by the heat loading, in spite of being made of tungsten and molybdenum, and requires periodic replacement of the probe head. WSI has identified a company with the capability to additively manufacture fully-dense tungsten parts with high resolution. This AM process not only provides opportunities for complex geometry, but also for active cooling of plasma facing components. WSI has designed and is currently having printed three modified versions of the C-Mod RFA probe head: one with the same geometry but made entirely of a single tungsten piece (instead of tungsten and molybdenum); one with a geometrically complex cavity behind the plasma facing surface that will be filled with a 3D printed copper or silver heat sink; one with a cooling channel routed through the probe head just 0.5mm behind the plasma facing surface for active helium cooling. These three probe heads will be installed on C-Mod and used to diagnose the plasma prior to the experiment’s shutdown

6 NSTX-U magnetic diagnostic collaboration

The primary purpose of the proposed collaboration would be to replace an existing tile shunt or in-vessel magnetic diagnostic aiming also to increase fidelity in the measurement (either spatial or temporal resolution). Potentially the time and spatial resolution of the tile shunts could be impacted, depending on the design optimization of the existing for such purposes. (Currently, ~10x~20cm tiles,with 0.1 msec resolution shunts are used.)

7 In-situ testing discussion continues with other leading fusion facilities

We approached DIII-D in this context a few months ago and talked with Dave Humphreys about magnetics, although they have just installed a complete set of magnetic diagnostics. We also approached Tokamak Energy, Tri-Alpha and General Fusion for testing of components in-situ, although have not yet obtained permission, discussions are ongoing. ITER (Mike Walsh) expressed receptivity to AM components in ITER, although we have yet to pin down a specific concept, and the implementation may well be many years away, if ever.

8 Printing mechano-optical components in plastic is perfectly ‘good enough’

In short, the additive manufacturing has been an attempt to produce a monolithic version of the unequal path-length heterodyne interferometer that is assembled in Dr. You's research laboratory. The purpose of this diagnostic is to achieve a time-resolved electron density measurement. Certain elements of the diagnostic have already utilized AM. The ConFlat (CF) mounts are 3D printed, and are shown on slide 4 of the *Figures* PPT. The CAD model of the interferometer is parametrically modular, meaning that the individual components seen in the CAD model are constrained only to the common surface plane. For example, if the user was to move the mirror in the expansion cavity, all downstream mirrors would move and rotate in real time in order to maintain alignment. When completed, this will enable the most compact design possible, with the least amount of effort. STL files are exported to an optical design module for Mathematica called Optica which is used to simulate the laser and verify alignment of the model. An initial cost estimate has been made, and for a single-chord layout, the costs have been reduced on the order of 10%, with an estimation of 50% reduction in labor The reason for only a 50% reduction in labor is that it still requires a technician to align the compact design with the vacuum chamber. Furthermore, the two mirrors upstream from the beamsplitter need adjustable (i.e., off-the-shelf components) in order for a technician to account for deviances in chamber alignment. One possible solution would be to couple the scene beam to a single-mode optical fiber, and provide a CF mount that auto-aligns the fibers across the vacuum chamber. The downside to this is a 50% reduction in phase angle response to plasma density, as opposed to a double-pass mirrored system. However, the scene fiber that returns back to the monolithic interferometer would be aligned properly, corresponding 90% reduction in labor. Before larger steps with the unequal path-length interferometer can be taken, verification is required as to the feasibility of preserved laser alignment through 3D AM with a Michelson-type interferometer.

3. What opportunities for training and professional development has the project provided?

We have provided support for Alex Card (UW) and Will Riviera (UMBC) as RAs, both of whom have contributed significantly to this project. We have provided opportunities to summer interns (Chris Bowman, and new interns this year through space grant). We have hired Morgan Quinley, Dr. Paul Melnik and Dr. Paul Sieck and provided opportunities for all to gain experience with new tools and participate in the project management. All participants are gaining.experience with new tools (COMSOL, Shark, Fusion 360) and innovative design techniques (topology optimization, parametric design).

4. How have the results been disseminated to communities of interest?

Mostly we have shared information that we are generating at talks, symposia and meetings. At the APS meeting we presented a poster outlining the project motivation and cost analysis (Sieck), at the HTPD workshop there will be a poster focused on design optimization (Quinley), at the TOFE there will be a poster (Quinley/Woodruff) on costing and broader implications for fusion technology. One paper was published in Transactions on Plasma Science (Rivera) on out-gas characteristics of AM components. We have also visited a wide range of organizations including CCFE, MIT, PPPL, GA, and had discussions with those at ITER. We have also started a White Paper started on cost impacts of 3D printing technology for fusion.

5. What do you plan to do during the next reporting period to accomplish the goals?

We are into the AM section of the work now, so we are on track. There are a few conventional EDRs to be completed in the next month or so, but by end of year 1 we will be fully into the AM section of the work. We are starting to spin out the company that will do the AM process development with Ben Utela playing a lead role in this company development. We have had input from Dawnbreaker on the potential market outside of fusion, so will be looking to do work for local space companies next through the new organization.

PRODUCTS - DETAILS

PUBLICATIONS DETAIL

1. Conference Paper/Presentation: Optimization of the Design of Plasma Diagnostics and Fusion Components for Additive Manufacture	
Conference Name: Topical Meeting on the Technology of Fusion Energy	**Conference Location:** Philadelphia
Publication Status: Accepted	**Conference Date:** 08/22/2016
Author(s): M. J. Quinley, S.Woodruff, P. E. Sieck, P. A. Melnik, J. E. Stuber, S. Diesburg, B. Utela, C.A. Romero-Talamas, W. Rivera, A. Card, S. You	
Acknowledgement of DOE Support: Yes	

2. Conference Paper/Presentation: Standardized Design of Custom Plasma Diagnostics and Fusion Components	
Conference Name: High Temperature Plasma Diagnostics Workshop	**Conference Location:** Madison, Wisconsin
Publication Status: Accepted	**Conference Date:** 06/06/2016
Author(s): M. J. Quinley, P. E. Sieck, S. Woodruff, J.E. Stuber, P. A. Melnik, C. A. Romero-Talamas, W. Riviera, S. You, A. Card	
Acknowledgement of DOE Support: Yes	

3. Conference Paper/Presentation: Additive manufacture (3d printing) of plasma diagnostic components and assemblies for fusion experiment	
Conference Name: American Physical Society Division of Plasma Physics	**Conference Location:** Savannah, Georgia
Publication Status: Published	**Conference Date:** 11/16/2015
Author(s): P. E. Sieck, S. Woodruff, J.E. Stuber, C. A. Romero-Talamas, W. Riviera, S. You, A. Card	
Acknowledgement of DOE Support: Yes	

4. Journal Article: Vacuum Compatibility of 3D Printed Parts	
Journal: Trans. Plasma Science	
Publication Date: Not Provided	**Publication Status:** Accepted
Volume: Not Provided	**First Page Number or eLocation ID:** Not Provided
Issue: Not Provided	**Publication Location:** Not Provided

Author(s): W. F. Rivera, C. A. Romero-Talamas	
Publication Identifier Type: Not Provided	**Publication Identifier:** Not Provided
Acknowledgement of DOE Support: Yes	**Peer Reviewed:** Yes

INTELLECTUAL PROPERTIES DETAIL

There are no intellectual properties to report.

TECHNOLOGIES AND TECHNIQUES DETAIL

1. Description:

Many tools for optimizing a component for additive manufacture are now available. The first tier are the CAD packages that allow components to be designed with voids or inter-connecting pieces that otherwise cannot be manufactured by conventional means. The next tier are the "generative design" or topology optimization algorithms. These algorithms are still rudimentary but undergoing rapid development, most of them in university programs. Because complexity is not penalized when using AM, non-standard structures can be designed and utilized. Topology optimization (TO) is a computational approach which produces designs optimized for requirements with a limited amount of material. Designs can be optimized for minimum compliance, heat conduction, or other loads. The reduction in material used can lead to lighter and lower-cost designs. With CM, TO could only be used to guide design, as its output often results in unusual shapes difficult to manufacture. With AM, these limitations are removed and designs from TO can be directly printed. Our techniques exploit advances in topology optimization in a multi-step process: 1) define requirements (heat loading? Structural loading?); 2) setup parameters for topology optimization problem; 3) run topology optimization code; 4) clean up and export mesh data; 5) validate results in FEM engineering program; 6) send to printer.

OTHER PRODUCTS DETAIL

1. Other Products: Instruments or Equipment

Description: During the conventional engineering design phase, we have taken 15 separate diagnostics through a complete engineering design. The new product offerings from Woodruff Scientific therefore entail these diagnostics and custom variations, detailed in the web-pages: http://www.woodruffscientific.com/diagnostics. The diagnostics are as follows: magnetic field probes, Langmuir probes (insertable, reciprocating and high power-loading), Retarding Energy Analyzers, CO2, HeNe, Microwave, diode interferometers, CO2 and Microwave polarimeters, Ruby and YAG Profile Thomson Scattering, Inverse Compton Scattering, Bolometers, Spectrometers and scintillator-type neutron detectors.

PARTICIPANTS AND OTHER COLLABORATING ORGANIZATIONS

PARTICIPANTS DETAIL

1. Participant: Mr. Alexander Card		
Project Role: Graduate Student (Research Assistant)	**Person Months Worked**: 9	**Funding Support (if other than this award)**: Not Provided
Contribution to the Project: Alex is developing diagnostic capability for testing on the Mochi experiment, with a focus on a HeNe interferometer, but broadly examining optical design optimization for AM.		
International Collaboration: No		
International Travel: No		

2. Participant: Mr. Steven Diesburg		
Project Role: Consultant	**Person Months Worked**: 9	**Funding Support (if other than this award)**: Not Provided
Contribution to the Project: Steven obtained his MSc in Engineering with a focus on additive manufacturing processes. He is advising the company on best methods for AM optimization.		
International Collaboration: No		
International Travel: No		

3. Participant: Dr. Paul Melnik		
Project Role: Staff Scientist (doctoral level)	**Person Months Worked**: 6	**Funding Support (if other than this award)**: Not Provided
Contribution to the Project: Diagnostics scientist/engineer. Has developed Langmuir, Bolometer and contributed to design reviews for all other diagnostics.		
International Collaboration: No		
International Travel: No		

4. Participant: Mr. Morgan Quinley		

Project Role: Other: Diagnostics Engineer	**Person Months Worked**: 6	**Funding Support (if other than this award)**: Not Provided
Contribution to the Project: Mr Quinley has provided support for diagnostics development, including pushing on the development of a Retarding Grid Energy Analyzer that will be 3d printed in tungsten and tested on Alcator CMOD.		
International Collaboration: No		
International Travel: No		

5. Participant: Mr. William Rivera		
Project Role: Graduate Student (Research Assistant)	**Person Months Worked**: 9	**Funding Support (if other than this award)**: Not Provided
Contribution to the Project: Will has been working with Carlos Romero-Talamas to determine outgas characteristics of metal test components that have been 3D printed on laser-melting or ebeam melting beds. He is co-author of one publication in Trans. Plasma Science on the outgas testing.		
International Collaboration: No		
International Travel: No		

6. Participant: Prof. Carlos A. Romero-Talamas		
Project Role: Faculty	**Person Months Worked**: 9	**Funding Support (if other than this award)**: Not Provided
Contribution to the Project: Carlos is advisor to Will Riviera and is developing capabilities for testing of components that have been additively manufactured at UMBC.		
International Collaboration: No		
International Travel: No		

7. Participant: Dr. Paul E. Sieck		
Project Role: Co-Investigator	**Person Months Worked**: 9	**Funding Support (if other than this award)**: Not Provided
Contribution to the Project: Paul is contributing to the conventional design of diagnostic components.		
International Collaboration: No		

International Travel: No

8. Participant: Mr. James E. Stuber		
Project Role: Other: Diagnostics Engineer	**Person Months Worked**: 9	**Funding Support (if other than this award)**: Not Provided
Contribution to the Project: James is developing the scripting capability for rapid customization of diagnostics through web-based interfaces.		
International Collaboration: No		
International Travel: No		

9. Participant: Dr. Ben Utela		
Project Role: Consultant	**Person Months Worked**: 9	**Funding Support (if other than this award)**: Not Provided
Contribution to the Project: Ben has a PhD in Mechanical Engineering with a focus on Additive Manufacturing. He is aiding the company in developing the process for AM optimization.		
International Collaboration: No		
International Travel: No		

10. Participant: Dr. Simon Woodruff		
Project Role: Principal Investigator/Project Director	**Person Months Worked**: 9	**Funding Support (if other than this award)**: Not Provided
Contribution to the Project: Primarily focused on costing analysis of all AM components, although contributing to CDRs, EDRs and AM EDRs.		
International Collaboration: No		
International Travel: No		

11. Participant: Prof. Setthivoine You		
Project Role: Faculty	**Person Months Worked**: 9	**Funding Support (if other than this award)**: Not Provided

Contribution to the Project: Sett is coordinating the work at UW for testing of prototyping components in his lab using the Mochi experiment. He is advisor to Alexander Card.

International Collaboration: No

International Travel: No

PARTNERS DETAIL

There are no partners to report.

OTHER COLLABORATORS DETAIL

1. Description of the Contribution:
Daniel Brunner at MIT PSFC is working with us to install a 3-D printed tungsten reciprocating RFA head in CMOD.

We are in discussion with Jon Menard and Stefan Gerhardt about design and installation of 3D printed magnetic diagnostics in NSTX.

We have engaged with Mike Walsh at ITER, although have yet to establish a specific concept, discussion ongoing.

2. Description of the Contribution:
Michael Porton, Engineering Section Leader for JET, Culham Centre for Fusion Energy (CCFE), UK.

Michael leads a small team at JET to test structural components for use in UHV and high power loading environments that have been additively manufactured. He is working with a broad consortium under the AMAZE banner. He is also developing additively manufactured diagnostic components for use in JET. We are issuing mutual NDAs so that we can collaborate more closely on the AM implementations.

IMPACT

1. What is the impact on the development of the principal discipline(s) of the project?

If we are able to publish a series of papers on the technique in RSI and see these being cited often, then this will be a measure of the impact. Further, if we can see that our prototype tools are being used online, then this might also indicate impact. It is hard to measure the impact of the work without quantitative assessment. Certainly we have lead the discussion on 3D printing for plasma diagnostics within our local sub-field.

2. What is the impact on other disciplines?

The impact of printing metal components for high power loading and ultra-high vacuum systems will make an impact for space applications, particularly with the ability to optimize the design point for mass reduction. We are assessing this impact with the help from Dawnbreaker - the commercialization assistance program - whose representatives are compiling a report on the impact of UHV-UH power-loading 3D printed components, the results of which are just coming in. For example, Lockheed Martin is very interested in interacting with us on this topic and we will be following up with them in the near future.

3. What is the impact on the development of human resources?

We have offered two internships for the summer months on the Phase II work, performed mainly by science students already familiar with the physics modeling. The next internships will be based primarily for coding for the integrated modeling needed to generate the full engineering process (getting both proprietary and open source codes talking to each other) to output designs to a web portal. We have also provided a rolling internship to a physics student who is helping with the scripting of the concept designs, allowing customers to access the design parameters themselves.

4. What is the impact on physical, institutional, and information resources that form infrastructure?

N/A

5. What is the impact on technology transfer?

We have defined the process of integrated modeling for component design that we have established a new start-up company that we aim to spin out of Woodruff Scientific to license the modeling capability or sell instances for clients to use as web-based interfaces for their customers. The new company is called 'Woodruff 3D Inc', and is comprised of the consultants and others from WSI currently doing scripting for 3d printing.

6. What is the impact on society beyond science and technology?

We are interested in the application of the technology to other areas - for example as proof of concept, we developed a 3d printed prosthetic for a child (as part of the enable project http://enablingthefuture.org/). We have also printed robot parts in weekend activities for pre-schoolers, so that they can see how 3D printing works, and how computers are used to control robots. It is becoming easier to see how design optimization with 3D printing can impact society as a whole, particularly in the areas of highly customized solutions tailored to the individual (think healthcare).

7. Foreign Spending

Not Provided

CHANGES - PROBLEMS

1. Changes in approach and reasons for change
No significant changes in approach. We opted for lower cost software tools than we first thought, which allowed us to get the tools that fit the job best. We also found some open source tools. We hired Morgan Quinley and Dr. Paul Melnik (in addition to Paul S) which brought considerable expertise into the program, reducing Simon Woodruff's hours a little.
2. Actual or anticipated problems or delays and actions or plans to resolve them
No problems or delays encountered.
3. Changes that have a significant impact on expenditures
No changes that resulted in significant changes in expenditures.
4. Significant changes in use or care of human subjects, vertebrate animals, and/or biohazards
N/A
5. Change of primary performance site location from that originally proposed
N/A
6. Carryover Amount
Estimated carryover amount for the next budget period: $0.00

Vacuum Compatibility of 3-D-Printed Parts

William F. Rivera and Carlos A. Romero-Talamás

***Abstract*— We present the design and preliminary results of a mass spectrometry system to assess the vacuum compatibility of 3-D-printed parts. The setup consists of a sectional vacuum chamber with a residual gas analyzer, a radiation heater, windows, and an access port for quick sample exchange. The vacuum chamber is set up in such a way that the samples can be inserted and retrieved with minimal contamination to the vacuum system. We perform this by having two connected chambers with independent vacuum pumps, and using one for sample access at atmospheric pressure, and then transferring the sample to the main chamber once vacuum is equalized. The equipment will be used as part of the dusty plasma experiment at UMBC, since many of the plasma-facing parts are 3-D-printed.**

***Index Terms*— Dusty plasmas, mass spectroscopy, plasma diagnostics, throughput, vacuum technology.**

I. Introduction

ADDITIVE manufacturing (3-D printing) offers many advantages over traditional manufacturing techniques. One advantage that the 3-D printing offers over subtractive manufacturing is that it adds material to a platform and builds the desired geometry layer by layer, reducing the cost and time associated with the production of the prototypes [1].

The material that we are studying at UMBC is a material that is usually not considered for vacuum applications, because it outgasses under vacuum conditions, and the operational temperature of many plastics is ∼100 °C. This also makes the 3-D-printed plastic parts undesirable for plasma-facing components, because the creep temperature associated with the plastics is usually the minimum temperature required for baking [2].

In the dusty plasma experiment, the fixtures used in the vacuum chamber are made of 3-D printed ABS plus plastics. The 50 μm dust grains in this environment were levitated successfully using a combination of RF and dc discharges without any apparent effect from outgassing. This is the motivation to examine how the outgassing affects the vacuum chamber.

In order to test the plastic parts, two identical parts were made: one was electroplated with copper and nickel and the other was left in its original form. Then, both the parts were separately inserted into the test chamber to analyze outgassing from both the specimens.

Manuscript received August 1, 2015; revised October 22, 2015 and January 21, 2016; accepted March 1, 2016. Date of current version May 6, 2016. This work was supported in part by the Department of Mechanical Engineering, University of Maryland Baltimore County, in part by Woodruff Scientific, Inc., and in part by the National Science Foundation Louis Stokes Alliance for Minority Participation Bridge to the Doctorate Fellowship Program under Grant NSF-LSAMP-BD.

The authors are with the Department of Mechanical Engineering, University of Maryland–Baltimore County, Baltimore, MD 21250 USA (e-mail: wrivera1@umbc.edu; romero@umbc.edu).

Color versions of one or more of the figures in this paper are available online at http://ieeexplore.ieee.org.

Digital Object Identifier 10.1109/TPS.2016.2540924

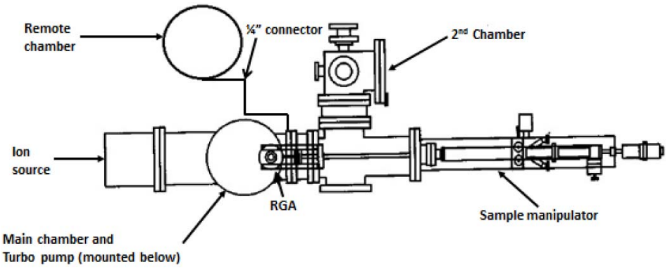

Fig. 1. Diagram of sectional vacuum system connected to the remote chamber by a 1/4-in connector, where the dusty plasma experiment is performed. Figure reproduced in part from [3].

Outgassing from each specimen is determined by analyzing the unique signal produced by the mass to charge ratio created by the ionization of molecules as they enter our spectrometer. Sometimes molecules dissociate in the spectrometer, creating several peaks in the spectrum, each molecule having a unique dissociation spectrum also called the cracking pattern. An example for the cracking pattern of water can be seen in Figs. 2 and 3 for the atomic mass units 18 (main peak), 17, 16, 2, and 1.

II. Apparatus

The total pressure in the vacuum chamber, shown in Fig. 1, was measured by two pressure gauges: an ion gauge that was located on the second chamber and a cold cathode gauge that was located on the main chamber. The partial pressures and the mass spectra were measured by the residual gas analyzer (RGA). The vacuum chamber was pumped down to the pressures ranging from $3.0 - 3.6 \times 10^{-6}$ [torr] by a turbomolecular pump at 80 [l/s] backed by a roughing pump. When samples were transported in or out of the system the main chamber was shut off by a gate valve to prevent the contamination of the whole chamber and to keep the humidity levels to a minimum.

A glass bell jar was used as the remote chamber and was pumped down to the pressures ranging from $1.5 - 50 \times 10^{-3}$ [torr] by a dry roughing pump. The dusty plasma experiments were performed with components that include 3-D printed ABS plus plastics fixtures. The remote chamber was connected to the main chamber via a 1/4 in fitting and a valve to regulate the flow rate.

III. Methods

A. Outgassing Experiment in Vacuum

Two samples were made from the ABS-plus plastic: one of the samples was electroplated with a base layer of copper and a top layer of nickel both the coatings have a thickness of 50 μm. Both the parts were cleaned by bathing them in ethanol and deionized water then blow drying the parts with helium. Before any parts were inserted in the

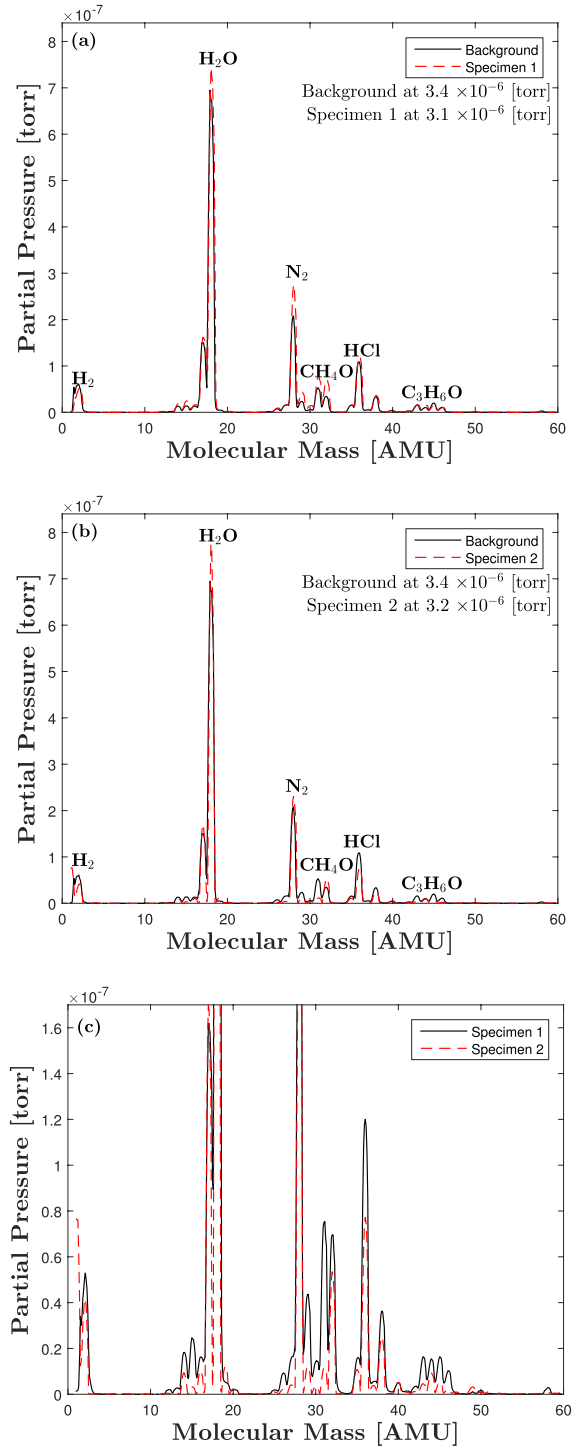

Fig. 2. Comparison mass spectra of (a) Background (no specimen in the vacuum chamber) with Specimen 1 (nonelectroplated part). (b) Background with Specimen 2 (electroplated part). (c) Specimen 1 with Specimen 2 plotted to 3×10^{-7} to show lower peaks.

vacuum chamber, a background of the empty chamber was taken in order to have a spectra to compare the outgassing of the parts. The spectra of the empty chamber was obtained after 48 h, when the pressure in the cold cathode gauge read 3.4×10^{-6} [torr]. Before repreasurizing the system the gate valve that separates the main chamber from the second chamber was closed in order to keep good vacuum conditions.

Once the second vacuum chamber equated to the atmospheric pressure, a door was opened, the part was inserted in the secondary chamber and pumped down again. The pressure in the secondary chamber was allowed to equate to the pressure in the main chamber. Once the pressures were equal, the gate valve was opened and it was pumped down for 48 h before taking the mass spectrum. This method was repeated for the second sample.

B. Argon Mass Spectrum From Remote Chamber

Dusty plasma experiments are performed in the remote chamber, where the pressure could be three orders of magnitude higher than in the main chamber. The size of the opening in the regulator valve was calculated to obtain the proper flow rate to the mass spectrometer [4].

Using ideal gas law for specific gas where pressure (P) times volume (V) equals mass (m) times the gas constant (R_A) times temperature in Kelvin (T). The following equation for gas density (n_A) was obtained, for the gas used in experiments (typically argon):

$$P = \rho R_A T$$
$$n_A = \frac{N_A}{M} P \tag{1}$$

ρ, N_A, and M is density, Avogadro's number, and molecular mass of argon, respectively. We first check that the flow is in the molecular regime by obtaining the Knudsen number (Kn) and verifying Kn > 1. The Knudsen number is defined as

$$\text{Kn} = \frac{\lambda}{d} \tag{2}$$

where λ is the mean free path and d is the pipe diameter. Using n_A to solve for λ, where d_0 is the molecular diameter [4]

$$\lambda = \frac{1}{2^{1/2} \pi d_0^2 n_A}. \tag{3}$$

The equation for the molecular regime throughput $Q = \upsilon/4A(P_1 - P_2)$ is used to obtain the area of the orifice (A) from the difference between the pressure of the remote chamber (P_1) and the main chamber (P_2), and average velocity (υ) for the gas

$$A = \frac{4Q}{\upsilon(P_1 - P_2)}. \tag{4}$$

IV. Results

A. Outgassing Experiment in Vacuum

Fig. 2 shows the mass spectrum of the chamber after 48 h of pumping to allow the pressure to get down to the low 10^{-6} [torr] range. The data were taken at room temperature and the vacuum chamber was not baked. The mass spectra of the empty chamber were compared with the chamber with the part inserted.

When the mass spectra of Specimen 1 was compared with the background [Fig. 2(a)], it was observed that the spectra was very similar, but had an increase in the peaks corresponding to water, nitrogen, methanol, and acetone. An increase in organics signals (molecules containing carbon) was also observed.

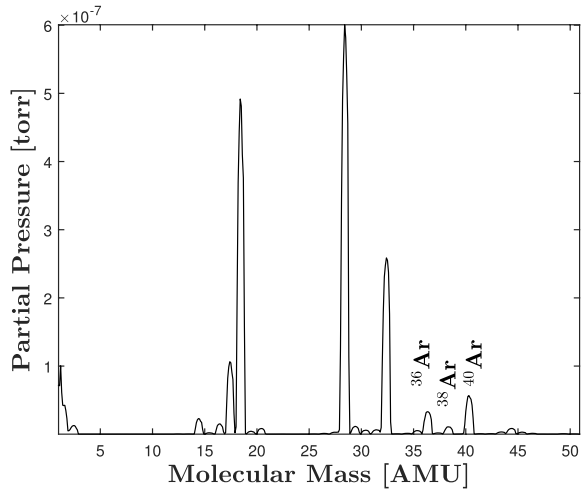

Fig. 3. Mass spectra of the main and remote chamber argon-cracking pattern visible.

From the cracking pattern corresponding to methanol and acetone, which gives an indication of outgassing from the 3-D printed part [5].

When comparing the mass spectrum of Specimen 2 [Fig. 2(b)] with the background we see a decrease in the cracking pattern of methanol and acetone. However, we see an increase in the cracking pattern of water and nitrogen. Organic peaks were also observed, but the peaks were not as intense as in Specimen 1 [Fig. 2(c)].

B. Argon Mass Spectrum From Remote Chamber

Fig. 3 shows the mass spectrum of the main chamber with gas flow from the remote chamber. The main chamber had been evacuated for six weeks and the remote chamber was flooded with argon gas. The signal of argon was observed, but the partial pressure is lower than the true value, because some argon is pumped out before it reaches the RGA. The values used to determine the size of the orifice are

$$P_1 = 10^{-3}\ [\text{torr}] \approx 1.33 \times 10^{-1}\ [\text{Pa}]$$
$$P_2 = 10^{-6}\ [\text{torr}] \approx 1.33 \times 10^{-4}\ [\text{Pa}]$$
$$Q = Q_{\max_{\text{Ar}}} = .3\left[\frac{\text{Pa} \times \text{m}^3}{\text{s}}\right]$$
$$v_{\text{Ar}} = 379\left[\frac{\text{m}}{\text{s}}\right].$$

Using (5) to solve for the area of the orifice yields $A = 23.8\ \text{mm}^2$. The diameter of a circular orifice is $d = 5.50\ \text{mm} \approx .22\ \text{in}$.

V. Conclusion

From the results of Specimen 1, it was observed that the nonelectroplated part had trapped the molecules of the solvents and outgassed them into the chamber. This is why the peaks of the solvent signal, such as methanol, are higher than that of the background. However, examining Specimen 2 signal, the solvents had decreased, but the amplitude of water had risen, concluding that water molecules are bonding to the surface of the electroplated part. It was expected that desorption of water molecules from the rough nickel surface was going to be difficult without any baking. From Fig. 2, we see that the electroplated part is superior to the nonelectroplated part, because it does not trap the solvents into the material but it does bond with water very well, which would make the electroplated parts adequate to use in low temperature plasma experiments, since the plasma sheath will assist in the desorption of the water molecules.

It was determined from the partial pressure of argon in Fig. 3 that the size of the orifice was not large enough to allow for higher signal to noise ratio of the argon signal. The intensity of the argon-cracking pattern was expected to be greater than the spectrum of the background, since a constant supply of argon is being inserted into the test chamber making it the most abundant gas in the chamber. Since the spectrum of the background is greater than the cracking pattern of argon, this implies that the flow of argon is choked so a larger orifice size is required to obtain the maximum flow from the low-pressure to the high-pressure side. We will address this with eliminating the 1/4 in swagelok valve, which has an unknown conductance, and replacing it with a two 3/4 in valve with a 1/4 in orifice for a higher conductance connection between the plasma chamber and the RGA chamber.

References

[1] Y. Zhai, D. A. Lados, and J. L. LaGoy, "Additive manufacturing: Making imagination the major limitation," *JOM-J. Minerals Met. Mater. Soc.*, vol. 66, no. 5, pp. 808–816, May 2014.

[2] A. R. Gans, M. M. Jobbins, D. Y. Lee, and S. A. Kandel, "Vacuum compatibility of silver and titanium parts made using three-dimensional printing," *J. Vac. Sci. Technol. A*, vol. 32, no. 2, p. 023201, 2014.

[3] J. V. Hryniewicz, Y. J. Chen, S. H. Hsu, C.-H. D. Lee, and G. A. Porkolab, "Ultrahigh vacuum chemically assisted ion beam etching system with a three grid ion source," *J. Vac. Sci. Technol. A*, vol. 15, no. 3, pp. 616–621, 1997.

[4] J. F. O'Hanlon, *A User's Guide to Vacuum Technology*. New York, NY, USA: Wiley, 2005.

[5] R. Schubert, *Partial Pressure Analyzers, Analysis, and Applications* (AVS Monograph Series). New York, NY, USA: AVS, 2000. [Online]. Available: https://books.google.com/books?id=kxvTtwAACAAJ

Authors' photographs and biographies not available at the time of publication.

Optical Beam Dump Optimization for Additive Manufacturing

K. Chun, J. Stuber, S. Woodruff

Woodruff Scientific Inc, 4000 Aurora Ave N, Seattle, WA 98103, USA

E-mail: katherine@woodruffscientific.com

March 2017

Abstract.

This paper explores the applications of additive manufacturing (3D printing) to optical beam dump design complexity with the goal of decreasing the ratio of light output. Traditional manufacturing limits the geometric complexity of beam dump designs. The additive manufacturing process of laser sintering is investigated with specific concern for outgassing and integrity of the part under vacuum. The cylinder-and-fin design originally decreased beam dump light output by 2 orders of magnitude. Modifications were made to the original design and tested for improvement in light capture. Incorporating ribbing along the cylinder's interior was found to decrease beam dump light output by an additional order of magnitude. Further optical dump analysis was executed for ribbed optical beam dumps with varying numbers of fins. Light output analysis was determined by methods of 3D modelling in Autodesk Fusion 360 and light ray tracing in ZEMAX.

Keywords: Beam Dump, Optical Dump, Additive Manufacturing

1. Introduction

A recent study on the ITER tokamak revealed that stray light from the metal walls of the machine interfered with the desired measurement of H-alpha and Be I emissions from the scrape-off layer [1]. Stray light interference would likely be present in any metal-walled fusion device that utilizes bolometers. Interference can be minimized by placing optical beam dumps within the reactor to absorb stray light near the measured emissions [2]. These optical beam dumps were previously limited by the practical considerations of traditional manufacturing techniques. However, additive manufacturing allows for more complex geometries. Laser sintering is a particularly effective additive manufacturing technique for metal, where laser energy melts metal powder and creates an object layer-by-layer [3]. This paper investigates the use of additive manufacturing for increased complexity of beam dump design in a low-outgas, laser sintered material [4]. Optical beam dump design was optimized for both incoming light rays simulating the laser absorption of a beam dump, and randomly-oriented incoming light rays simulating the ambient light of an optical dump.

2. Background

2.1. Stray Light in ITER

ITER's plasma-facing components produce significantly more stray light than generated diagnostic signals. Some major causes are the the high reflections of tungsten in the divertor and beryllium in the first wall, 85% and 80% respectively [2]. The tokamak surface materials' low emissivity essentially behaves as a mirror [5]. Reflection compensation was further deemed necessary for temperature measurement in the divertor [2]. One common absorption design is a stack of razor blades, where the light rays are split by the fine edge and bounce between two adjacent blade faces until it loses all intensity. Another common design is simply a dark-colored absorptive plate [6]. An alternate version is the optical beam dump shown in Figure 1, which is a cylinder with a single open side, a central cone to split the light rays, and parallel fins to "catch" the reflected rays. Optical beam dumps act as both optical dumps and beam dumps. Optical dumps absorb ambient light, modeled by randomly-directed light rays pointed towards the optical dump's entrance. Beam dumps absorb incoming laser light rays, modeled by parallel light rays entering the beam dump in a coaxial orientation. Both are used in plasma research and share a similar geometry. Simple optical dump designs have been tested for their absorption and reflection ratios, the highest of which decreased reflectance by nearly 2 orders of magnitude. [1]

In this study, both optical dump and beam dump applications were investigated. A common material of stainless steel was used to model the absorbance and reflection of the optical beam dumps, measured at 20% absorbance, 98% Gaussian specular reflection at 12 degrees FWHM and 2% Lambertian reflection [2]. Due to program limitations, an absorbance of

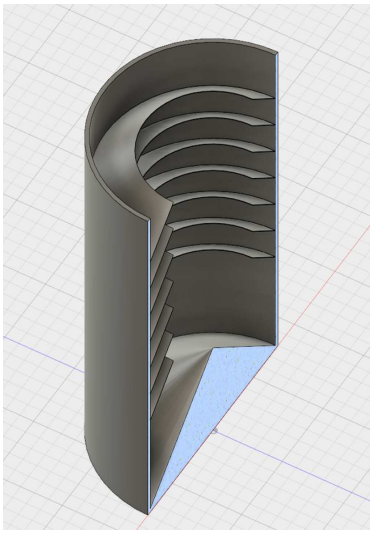

Figure 1. Original model prior to optimization for minimum emittance.

20% and a 12 degree FWHM Gaussian specular reflection was applied.

2.2. Laser Sintering Concerns

Laser sintering is an additive manufacturing technique where a laser heats the top layer of a bed of metal powder and melts the part together layer-by-layer. This process allows metals to be printed into complex geometries previously difficult to achieve by traditional manufacturing methods [7]. Outgassing under vacuum was a previous concern with 3D printing, especially with beam dumps on the plasma-facing side of the chamber. However, outgassing experiments confirmed the minimal outgassing experienced by a 3D printed part when placed in a vacuum chamber [7, 4]. This validates additive manufacturing as a technique for vacuum-bound parts, allowing the increased level of complexity in design to be applied to plasma research diagnostics.

3. Method

A standard beam dump design was scripted for varying interior fin placement and central cone height in Autodesk Fusion 360. Parameters investigated were fin distance, fin angle, initial fin height, and cone height. Fixed parameters were height, outer radius, aperture radius, and fin and wall thicknesses, since customized beam dumps for plasma diagnostic use typically have predetermined dimension specifications. A cross-sectional image of the original design parameters is displayed in Figure 2. Optimal design for both parallel and ambient light rays was determined for the previously stated parameters and used as the

base optical beam dump design. Further modifications were added in Autodesk Fusion 360: increased density of fins, ribbing between fins, short intermediate fins, secondary fins, cone fins, elongated fins, and an organic spiral [8]. All modification cross-sections are shown in Figure 3. These modified beam dumps were tested for parallel light ray absorption for simplicity, and the modified beam dumps which outperformed the base design were further tested for ambient incoming light.

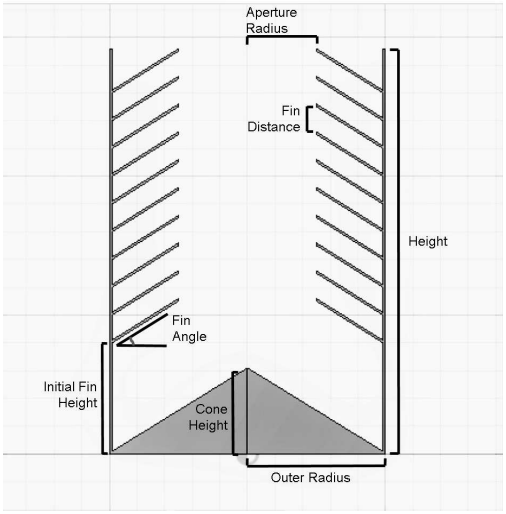

Figure 2. Cross-section of optimized beam dump parameters.

4. Tools

Autodesk Fusion 360 provides a comprehensive computer-aided design (CAD) suite with automated scripting capabilities. The python-based application program interface (API) allowed for variable parameter input into a single user-input graphical user interface (GUI), which generated variations of the base beam dump design. Modifications beyond the listed parameters were generated with standard CAD manipulation within Autodesk Fusion 360. Ribs were given triangular cross-sections, similar to fins in thickness, and rotated around the central axis of the cylinder.

ZEMAX is a light ray tracing program which allows the import of 3D CAD files, application of material properties, and calculation of light output. Beam dump designs were imported into ZEMAX via STL and given appropriately reflective/absorptive material properties. A Gaussian scattering pattern was also applied to the beam dump's surfaces, simulating materials typically used for first wall tiles. The 80% absorbance and 20 % reflectance of stainless steel was implemented, analyzing the least ideal material for maximum beam dump efficacy. Parallel light rays were directed into the beam dump to simulate laser light absorption, as shown in Figure 4. Randomly-oriented light rays were directed into the beam

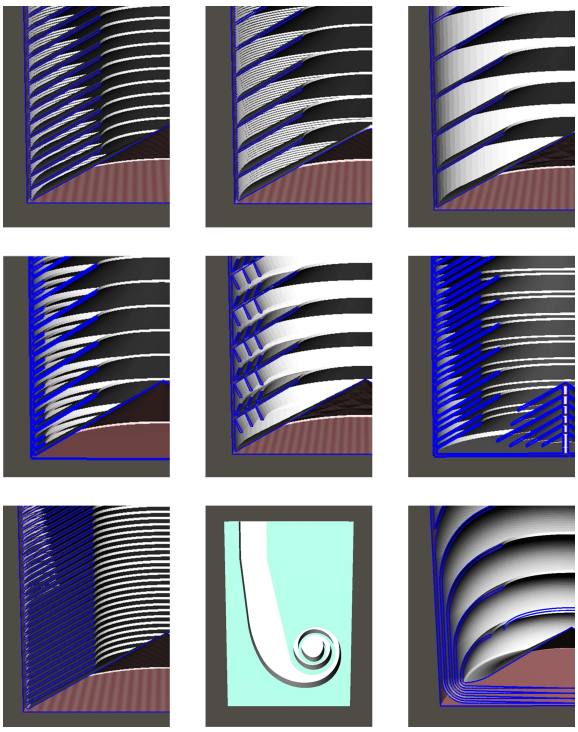

Figure 3. Variations on optimized classic beam dump design. Left to right, top to bottom: 28 fins with ribbed cylinder design, 14 fins with ribbed cylinder design, optimized classic beam dump, mid-length intermediate fin design, secondary fin design, conal fin design, 56 fins with ribbed cylinder design, organic spiral design, elongated fin design.

dump to simulate stray light absorption. The absorbance efficacy was measured by the number and intensity of light rays exiting the beam dump through the aperture.

5. Results

5.1. Standard Fin and Cone Optimization

The standard optical beam dump shown in Figure 1 has assigned parameters of height, outer radius, aperture radius, fin thickness, and wall thickness. Optimized parameters were cone height, fin angle, and fin distance. The initial cone heights investigated were limited by a height of 0cm and the point where the cone would intersect fins lower in the cylinder, returning an optimized cone height of 3cm. More fins returned a lower light emittance ratio, indicating that the number of fins should be maximized for an optimal beam dump. To save on runtime and complexity, nine fins were chosen for the standard optical beam dump used for further analysis. Fin angles between 10 degrees and 80 degrees were tested on the beam dump, returning an optimal fin angle parallel to the cone angle.

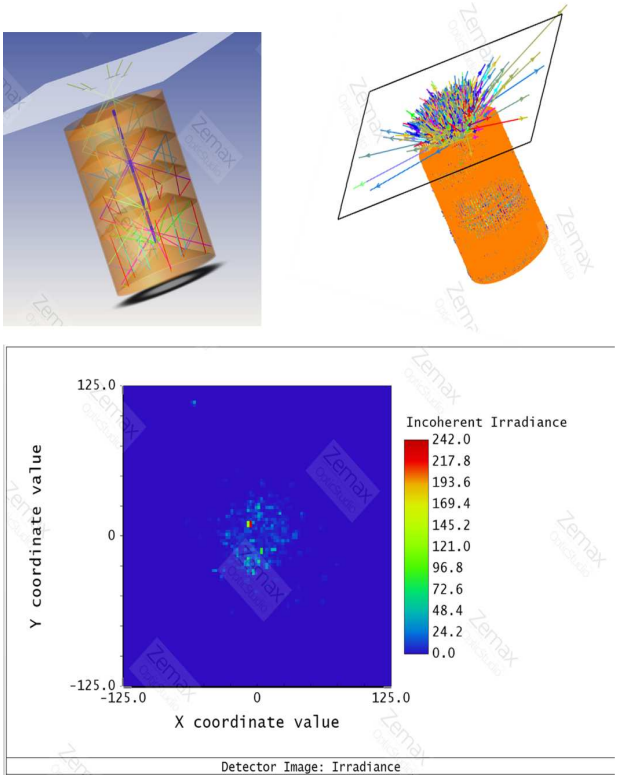

Figure 4. ZEMAX analysis applied to each optical beam dump iteration. Clockwise from top left: Light ray trace without scattering, light ray trace with scattering, emittance as captured by the screen above the optical beam dump's aperture.

Parameter	Assigned Size	Optimized Size
Height	15 cm	-
Outer Radius	5 cm	-
Aperture Radius	2.5 cm	-
Number of Fins	9	-
Fin Thickness	0.1 cm	-
Wall Thickness	0.1 cm	-
Cone Height	-	3cm
Fin Angle	-	Parallel to Cone
Fin Distance	-	Evenly Spaced

Table 1. Parameters for optimized optical beam dump.

5.2. Optical Beam Dump Modification Analysis

Each modification is shown in Figure 3, along with their light outputs in 5. The ribbed cylinders were the only modification to improve the optical beam dumps' light absorbance,

prompting further investigation into ambient absorption in Figure 6. The optimal beam dump for laser light absorption was the 28 fin ribbed cylinder, while the optimal optical dump for ambient light absorption was the 56 fin ribbed cylinder. There is a possible threshold for fin density in beam dumps, which was reached earlier for parallel light rays than in ribbed cylinder dumps.

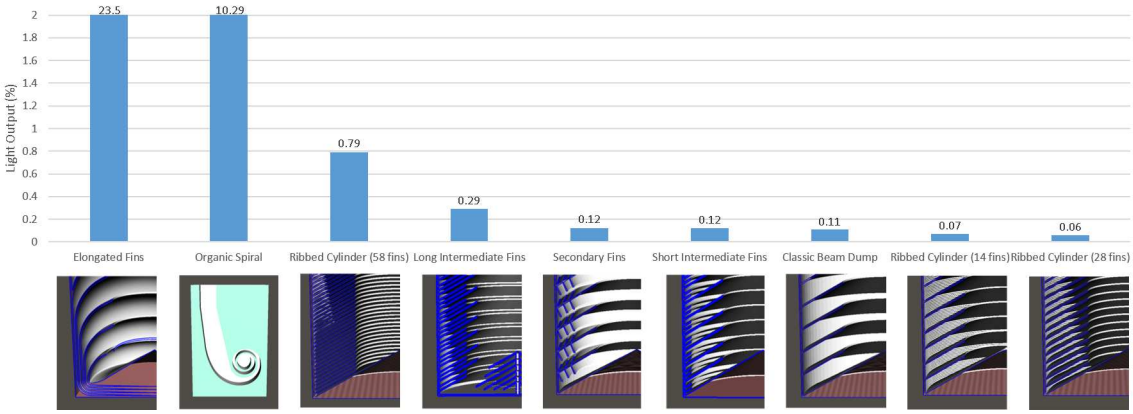

Figure 5. Emittance data for optical beam dump variations presented in Fig. 5.

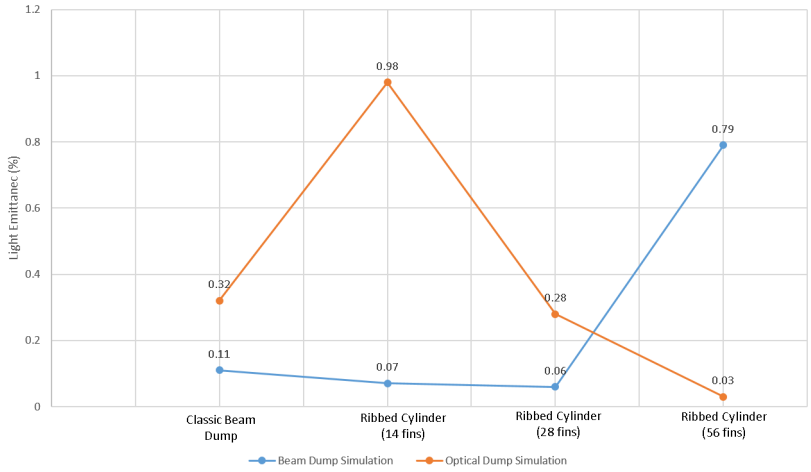

Figure 6. Emittance data for ribbed optical beam dump variations presented in Fig. 3.

6. Discussion

The primary mechanism for light absorption is the light ray's impact with the beam dump material, causing an incremental absorption of energy with each collision. In our experiment, the standard optical beam dump design reduced the light output by 2 orders of magnitude. This is likely due to the optimized optical beam dump's parallelism between the cone and

each fin. Parallelism between surfaces within the beam dump allows the cone to reflect a majority of the rays into the channels created by the fins, further increasing the optical beam dumps' light absorption. The light rays appeared to reflect off the central cone into a low-level fin channel, bounce between the parallel fin surfaces, reflect into a higher level fin channel, and repeat until exiting back out the top. Each collision with the beam dump's surface produced some scattering, further diffusing the intensity of each light ray. Higher fin density means a decrease in channel width and an increase in energy-absorbing reflections for each light ray. Ribbing appears to contribute to these light-dispersing effects via scattering, further reducing the light output by one order of magnitude. As a general trend, ribbing increases the diffusion rate of light rays per collision, creating the ability to increase light absorption without changing the absorptive properties of a material.

There was one discrepancy in the 56-fin ribbed cylinder beam dump which showed a higher light output than a majority of the modifications tested. This might be attributed to the density of fins reaching a threshold, which returned similar results as both intermediate fin versions. In the 56-fin ribbed cylinder case, the light rays appear to reflect off the inner face of the fins and redirect back into the open center of the optical beam dump. This suggests the extremely high density of fins acts more as a solid wall instead of a surface with fin-based cylindrical channels. The fin density threshold might also apply to the intermediate fin designs, where the intermediate fins were dense enough that they acted as a solid wall, creating shallower channels and providing for fewer reflections within each channel.

Beam dumps with rounded fin surfaces, such as the elongated fin and organic spiral models, were significantly worse at minimizing light output. This is likely due to the light ray's decreased ability to reflect between two parallel surfaces. Parallelism promotes reflections when the light ray both enters and exits the channel, whereas tapered channels promote more reflections only as the light ray enters the channel.

When tested as an optical dump, there appears to be a threshold where ribbing creates an equivalent light output ratio of a non-ribbed optical dump. In Figure 5, the 14-fin ribbed optical dump performed worse than the 9-fin classic optical dump. However, the 28-fin and 56-fin ribbed optical dumps show the expected decrease in light output as the number of fins increases.

7. Further work

Mathematica Optica would confirm the ZEMAX light ray analysis results on beam dump absorbance. STL import and light ray intput are currently implemented, shown in Figure 7. However, reflectance/absorption ratios, gaussian scatter patterns, and intensity-measuring setup issues are currently being resolved.

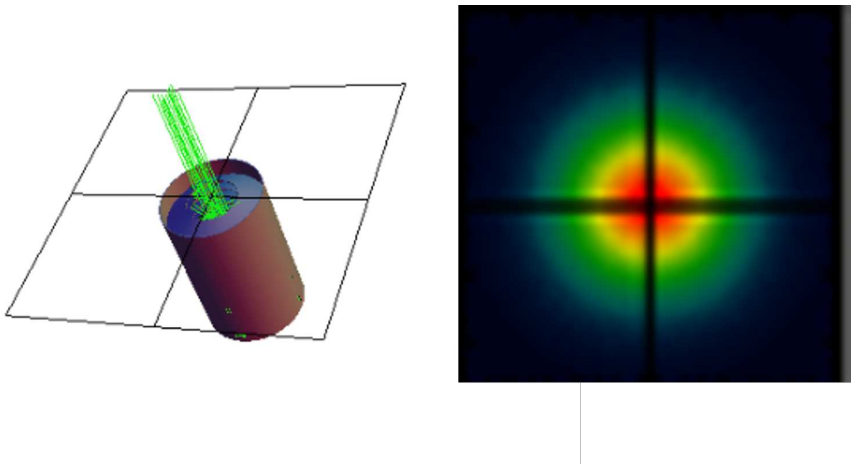

Figure 7. Sample Mathematica Optica ray tracing and emittance analysis.

The efficacy of ribbing indicates that surface quality is key in optical beam dump absorbance. The limit between surface roughness and defined ribbing would benefit from further investigation, since the study indicated that increased surface roughness increases light absorbance. The necessity of surface regularity (ribbing) versus irregularity (rough surface quality) could also be considered. The impact of large or small-grained irregularities in the surface is another topic of interest.

Further fin and cone modifications could be investigated for improvement of beam dump absorption. Different ribbing patterns might improve absorption within the cylinder, such as smaller triangular ribs, angled ribs, steeper ribs, etc. Smaller triangular ribs might imitate the tendency for more fins to decrease emitted light rays, providing more surfaces for the rays to continue depleting themselves within the dump. Angled ribs might imitate the efficacy of a parallel cone-fin structure, providing more parallel surfaces for the light rays to bounce between within the dump. Steeper ribs might imitate the beam dump itself, splitting more rays between the point of the rib and letting them bounce between the two ribbed surfaces to further increase absorbance. Organic dumps would also benefit from further investigation, since they might provide a minimal number of flat surfaces for the light rays to prematurely exit the optical beam dump.

A scripted pipeline for CAD design and light ray analysis is possible, through the ZEMAX API or Mathematica Optica. CAD design automation was successfully scripted in Autodesk Fusion 360 and Parametric Parts. Completion would require light ray analysis automation and integration with the CAD design.

8. Conclusions

Optical beam dumps for plasma diagnostic usage can be improved with a ribbed interior on the cylinder, maximum density of fins, and a central cone. The standard beam dump size assigned previously returned a light output percentage of 0.11% for beam dump light input and 0.32% for optical dump light input, both in the range of two orders of magnitude. A modified beam dump light output of 0.06% was returned with a 28 fin, ribbed cylinder design. An modified optical dump light output of 0.03% was achieved with a 56 fin, ribbed cylinder design. Both modified optical beam dump values are in the range of three orders of magnitude, yielding an improvement of one order of magnitude over previous designs. These modifications were previously deemed too expensive by traditional manufacturing methods due to their complicated geometric forms. Laser sintering has emerged as a low-cost, viable alternative with respect to these more complex parts.

9. Acknowledgements

Authors wish to acknowledge Donald Barnhardt for Mathematica Optica support. This work was performed under a subcontract of DOE SBIR.

10. Bibliography

[1] S. Kajita, E. Veshchev, S. Lisgo, R. Reichle, R. Barnsley, M. Walsh, A. Alekseev, A. Gorshkov, D. Vukolov, J. Stuber, and S. Woodruff, "Influence of stray light on visible spectroscopy for the scrape-off layer in iter," *Plasma Physics and Controlled Fusion*, vol. 55, no. 8, Aug. 2013.

[2] M.-H. Aumeunier, J.-M. Travere, T. Loarer, E. Gauthier, R. Reichle, D. Chabaud, and E. Humbert, "Simulation of the infrared views of the upper port vis/ir imaging system of iter," *IEEE Transactions on Plasma Science*, vol. 40.

[3] A. Simchi, "Direct laser sintering of metal powders: Mechanism, kinetics and microstructural features," *Materials Science and Engineering A*, vol. 428, July. 2006.

[4] W. S. Rivera and C. A. Romero-Talamas, "Vacuum compatibility of 3-d-printed parts," *IEEE Transactions on Plasma Science*, vol. 44, no. 5, pp. 874–876, May. 2016.

[5] P. Lotte, M.-H. Aumeunier, P. Devnyck, C. Fenzi, V. Martin, and J. M. Travere, "Wall reflection issues for optical diagnostics in fusion devices," *Review of Scientific Instruments*, vol. 81, no. 10, Oct. 2010.

[6] E. T. F. R, "Tokamak plasma diagnostics," *Nuclear Fusion*, vol. 18, no. 5, 1978.

[7] A. Gans, M. Jobbins, D. Lee, and S. Kandel, "Vacuum compatibility of silver and titanium parts made using three-dimensional printing," *Journal of Vacuum Science Technology A*, vol. 32, no. 2, Dec. 2013.

[8] W. B. H Yang Pang, Donald Harryman, "Beam dump for a very-high-intensity laserbeam," Patent US 8 047 663, 09 24, 2007.

Additive Manufacturing of Plasma Diagnostics: Opportunities and Challenges of a New Paradigm in Experimental Plasma Science

C. A. Romero-Talamás [1], W. F. Rivera [1], and S. Woodruff [2]

[1] University of Maryland, Baltimore County. 1000 Hilltop Circle, Baltimore, MD 21250

[2] Woodruff Scientific Inc., 4000 Aurora Ave N, Suite 6, Seattle, WA 98103 USA

Email: romero@umbc.edu

Abstract

Additive manufacturing (AM) holds the promise of being an enabling and cost-efficient technology for plasma diagnostics in high temperature plasma experiments. The technology is advanced to the prototype level, but questions of survivability of AM parts and effects on experiments remain, particularly on high temperature plasmas and the burning plasma regime. We present examples of AM parts that highlight the differences between conventionally manufactured parts and AM parts, and we discuss possible solutions to mitigate or eliminate such effects.

Additive Manufacuring Additive manufacturing (AM, also sometimes referred to as 3D-printing), is a manufacturing method in which parts are constructed by adding sections or layers of one or more materials. AM is now ubiquitous in industry, research laboratories, and even with hobbyists and home users. A variety of printing materials has been demonstrated and many are commercially available, such as plastics, elastomers, metals, and ceramics [1]. By far the most common materials for AM are plastics. However, for industrial applications AM with metals continue to gain ground not just for prototyping, but as an integral part of complex manufacturing processes [2]. Here, we are interested in applying AM to improve and reduce costs of plasma diagnostics.

Parts fabricated using AM are typically designed using computer aided design (CAD) programs. Although some CAD programs include modules that permit complex numerical analyses of mechanical and electrical designs using finite element methods (or some other numerical technique), there are basic CAD packages that are intuitive to learn and are in fact required in many engineering degree programs. Virtually all CAD programs allow for exporting design files in a language that the AM tool (3D-printer) can understand. The 3D design file is typically converted to a series of instructions for how the AM printer should build the part layer by layer. The accessibility of CAD packages, coupled with standardization of interface with 3D-printers, make the design and fabrication of parts using AM a new paradigm in manufacturing in and of itself. One example of this new design and fabrication paradigm is the addition of cooling channels to an AM part, which would be prohibitively expensive or not possible to manufacture with conventional manufacturing methods (machining, molding, stamping, etc.).

Application of AM to Plasma Diagnostics Diagnostics design, construction, installation, and operation, represent one of the largest costs in any plasma science experiment given the number of variables that need to be measured, and the complexity involved in measuring them (e.g Refs. [3, 4, 5]). Most diagnostics used in fusion-relevant experiments have been developed over many years, and thus the operating principles are usually well understood. However, most of these diagnostics are also usually custom-made for a particular experiment or even a particular location within an experiment (e.g. chamber port), making them expensive and time-consuming to design and build when using traditional methods.

We may divide plasma diagnostics in two categories: internal and external to the vacuum vessel. For both categories, AM represents a great opportunity not only to reduce manufacturing time and costs of plasma diagnostics, but also to innovate. For external components the performance requirements may vary, but wider choice of materials is available. For example, external optical mounts for a line-integrated density interferometer may be 3D-printed using plastics, ceramics, or metals, as long as the materials and shape satisfy dimensional accuracy and vibration specifications [6]. However, for components that are internal to the vacuum vessel and may even be plasma-facing, the requirements are necessarily more stringent. In this case the choice of materials is limited almost exclusively to metals and ceramics given the high temperatures from both heat conduction and radiation, and damage from particle impingement - including neutrons, for plasma-facing components. For this reason, we concentrate our attention below on AM plasma diagnostics that must be vacuum compatible.

Critical Variables and Objectives for AM For any diagnostic that will be placed inside a plasma vacuum chamber, whether it will be plasma-facing or not, outgassing is usually the highest concern for experimenters. Outgassing may interfere with plasma discharges often to the point of significantly lowering plasma temperature and may leave residual gas absorbed and adsorbed on other components even after the outgassing materials are removed from the experiment. In some cases, outgassing and surface features could lead to arcing, as is suspected in Fig. 1, where a comparison of a conventionally manufactured (CM) and AM retarding field analyzer probe heads are shown side by side. The AM probe was run in dwell mode in the edge of Alcator C-Mod, with a temperature of up to 30 eV (or higher right at the probe tip) and densities of $\sim 10^{18}\ m^{-3}$. Hot spots developed during a plasma shot, eventually bursting and spraying tungsten into the machine in enough quantities to cause a disruption. The AM probe head also seemed to heat up faster than the CM version. We speculate that there is lower heat

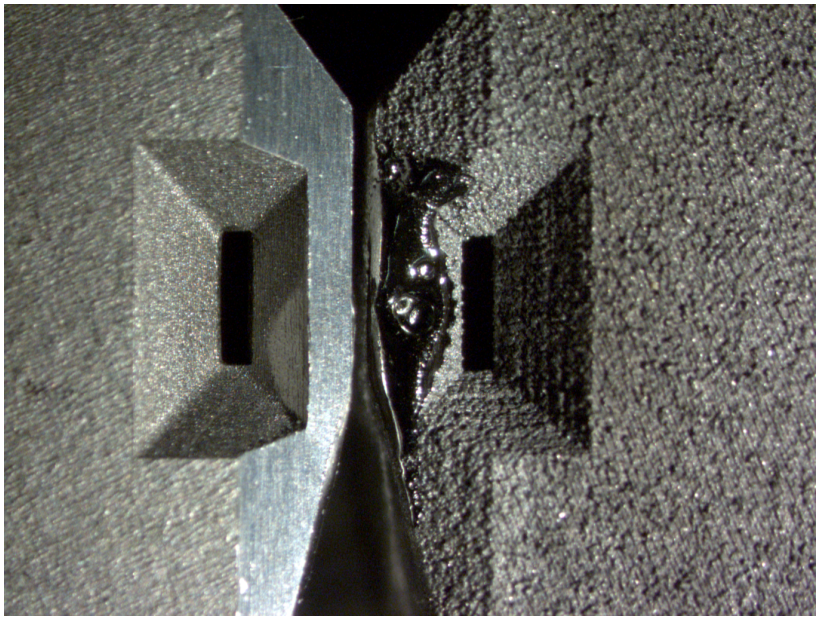

Figure 1: Left: Conventionally manufactured RFA probe head. Right: AM probe head showing signs of melting. Both heads are made of tungsten with a slit length approx. 1.5 mm. Image courtesy of Dan Brunner (Massachusetts Institute of Technology).

conductivity for this AM probe given the apparent surface roughness and lower material density than the CM part. Heat and electrical conductivity measurements for this and other test parts are ongoing and will be reported elsewhere.

Materials and Other Design Variables To date, there are only a few metals and refractory materials that are commercially available for AM. A selection of these is shown in Table 1. The design process typically takes place mostly in a CAD package, with the resulting electronic file being exported directly to the AM equipment. Such equipment is manufactured now in several countries around the world and by different manufacturers. There are also several types of printers, depending on the feed system (e.g. powder feed, wire feed, etc.) and the power source used (e.g. laser, electron beam) to clad the material. Commercial suppliers are typically reluctant or unable (in our experience at least) to disclose particulars of their process, or to vary parameters in order to test hypotheses on the AM process.

Risks and Uncertainties We have tested a some of these materials in laser-sintered AM samples at a purposely built chamber at UMBC, and compared their outgassing rates with similar CM materials published specifically for guidance in fusion applications [7]. We are also creating our own data base of CM materials outgassing to eliminate equipment differences with respect to previous reports. The equipment we use is similar to that reported in Ref. [8], except we now have added a specially designed heating plate to emulate the high temperature achieved in some plasma-facing components (but we do not have ion bombardment yet). What we are finding is that most of the AM parts outgass at a higher rate than the CM counterpart, but as expected, the differences virtually

Table 1: Selected alloys used in commercial AM processing (from Ref. [2]).

Titanium	**Aluminum**	**Tool steels**	**Super alloys**	**Stainless steel**	**Refractory**
Ti-6Al-4V	Al-Si-Mg	H13	IN625	316 and 316L	MoRe
ELI Ti	6061	Cermets	IN718	420	Ta-W
CP Ti			Stellite	347	CoCr
γ-TiAl				PH 17-4	Alumina

disappear after heating each part and letting it outgass for several days. In one case, however, an unheated Inconel IN718 part actually lowered the pressure (mostly by gettering water) after 20 hours at ultrahigh vacuum. The surface of our IN718 sample is much smoother than that shown in Fig. 1, but under higher magnification significant features appear that help us understand the material behavior in vacuum. Fig. 2 shows four levels of magnification taken with a scanning electron microscope (Nova NanoSEM 450 from FEI), where clumps and fissures of a few to tens of micrometers in length can be seen. X-ray spectra of that same surface taken at two different areas each of about $0.5\ mm^2$, but separated only by about $25\ \mu m$ (from the centroid of each area), show significant differences in element concentration, as shown in Table 2. This was probably caused by the intense heat gradients created by the cladding laser used for this part, and shows the variability inherent to AM and the need for better process control [9].

Table 2: Percentage by weight and standard deviation of surface composition using X-ray spectra at two different locations for the IN718 sample shown in Fig. 2.

Spectrum 1			**Spectrum 2**		
	Wt%	σ		Wt%	σ
Ni	37.5	2.6	Ni	33.9	2.1
Cu	20.2	1.4	Cu	13.6	1.2
Fe	13.3	1.3	Zn	12.3	0.8
Cr	10.2	0.8	Fe	11.7	1.3
C	4.7	0.4	Cr	9.7	0.8
Zn	4.6	0.7	O	7.7	0.4
O	3.4	0.3	C	6.1	0.5
Nb	3.1	0.5	Nb	3.4	0.5
Mo	1.7	0.5	Si	0.9	0.1
Si	0.8	0.1	Al	0.7	0.1
Al	0.5	0.1			

The technical readiness level (TRL) is high for AM plasma diagnostics: for parts external to the vacuum vessel TRL is 5 - 6, but may be lower for multicomponent diagnostics that are yet to be tested; for parts internal to the vacuum chamber TRL is 3 - 4. Although 3D-printers are constantly being improved for accuracy and control, post-processing of parts may still be required to reduce outgassing, reduce surface roughness (which in turn reduces adsorbed water and other gases), and plug cracks and voids at the surface of AM parts. Given that the composition of materials used in AM may differ from those used in CM, research is required on potentially beneficial post-processing surface treatment such as coatings and electropolishing. At the same time, care must be taken for the burning plasma regime, such that neutron activation of coatings and other AM materials will not overwhelm radiation safety limits. Research is also needed for operation of AM parts in high temperature plasmas during extended periods of time, under realistic conditions of ion energies and fluxes, and with 14.1 MeV neutrons for the burning plasma regime. Parts, materials, and fully assembled diagnostics will have to be qualified for burning plasmas in a similar way as conventionally manufactured diagnostics.

Advantages to Fusion Energy Science Additive manufacturing is becoming an enabler of more cost-efficient and innovative plasma diagnostics. It is certainly a technology that our community should continue to incorporate as part of the research portfolio towards the burning plasma experimental regime. Some estimates place the cost reduction from AM plasma diagnostics at least an order of magnitude lower than similar

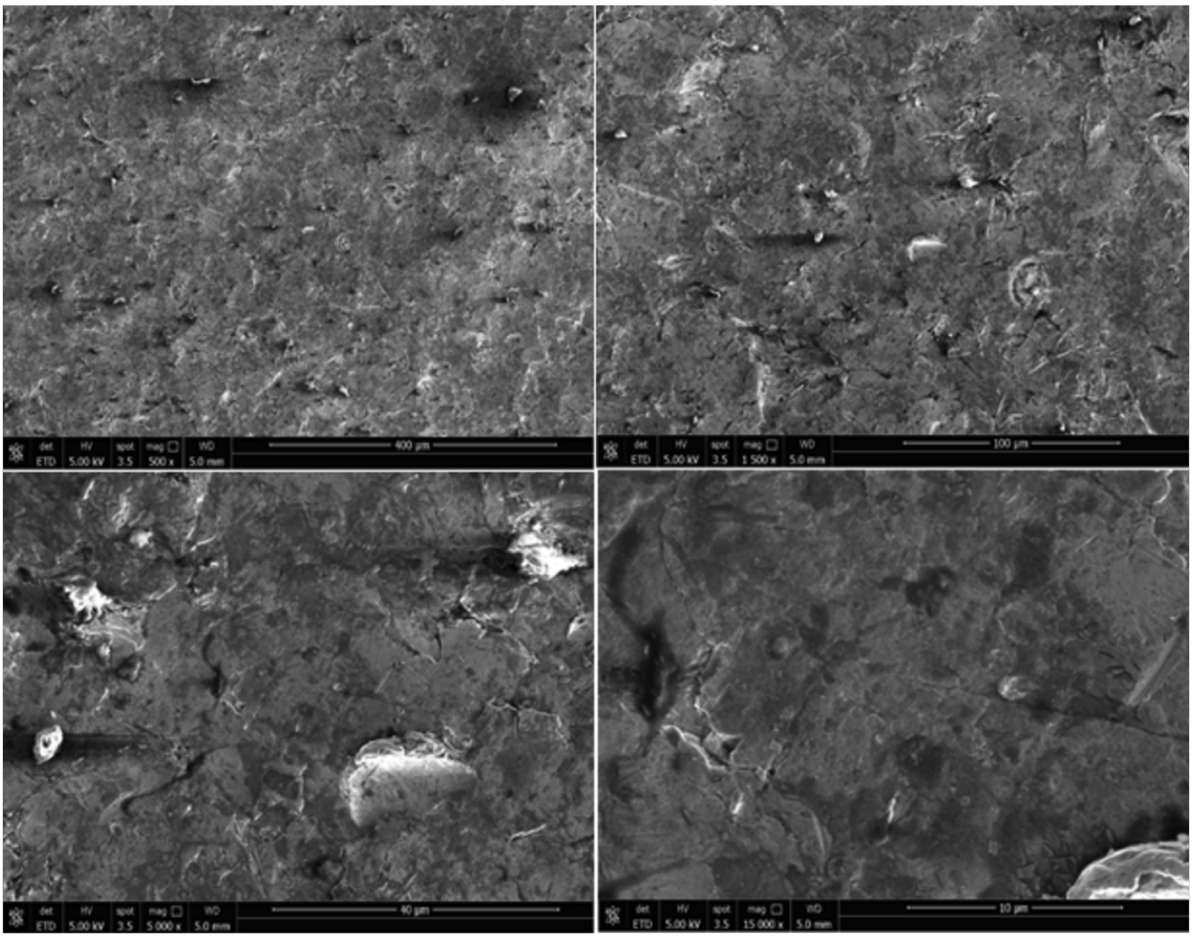

Figure 2: Scanning Electron Microscope images of IN718 specimen at UMBC. Magnifications, clockwise from top left: 500, 1500, 5000, 15000.

CM ones [6]. The biggest value comes from the potential to create components for plasma diagnostics that are not possible or cost-effective with CM methods.

References

[1] I. Gibson, D. Rosen, and B. Stocker. *Additive Manufacturing Technologies*. Springer, New York, 2015.

[2] W. E. Frazier. *J. Mater. Eng. Perform.*, 23:1917, 2014.

[3] N. C. Luhmann Jr. and W. A. Pebbles. *Rev. Sci. Instrum.*, 55:279, 1984.

[4] D. V. Orlinskij and G. Magyar. *Nucl. Fusion*, 28:611, 1988.

[5] H. S. McLean, A. Ahmed, D. Buchenauer, et al. *Rev. Sci. Instrum.*, 72:556, 2001.

[6] M. Quinley, D. Brunner, A. Card, C. A. Romero-Talamás, W. F. Rivera, M. Reinke, P. E. Sieck, J. Stuber, S. Woodruff, and P. A. Melnik. assemblies for fusion experiments. In *58th Annual Meeting of the APS Division of Plasma Physics*, San Jose, CA, November 2016.

[7] E. A. Moshey. A compilation of outgassing data in vacuum materials. Technical Report No. 82-001 Rev. A, PPPL, 15 Feb. 1982.

[8] W. F. Rivera and C. A. Romero-Talamás. *IEEE Trans. Plasma Sci.*, 44:874, 2016.

[9] C. Brown, J. Lubell, and R. Lipman. Additive manufacturing technical workshop summary report. Technical Note 1823, NIST, November 2013.

3D Printing & Scripted Design of Fusion Diagnostics

This work is supported by DOE Phase II SBIR Grant DE-SC0011858

M. Quinley[1], J. Stuber[1], S. Woodruff[1], P. Melnik[1], P. Sieck[1], A. Card[2], S. You[2], W. Rivera[3], C. Romero-Talamas[3]
[1]Woodruff Scientific, Inc.
[2]University of Washington
[3]University of Maryland, Baltimore County

Introduction

There is a well-established set of plasma diagnostics for fusion applications, but they can be expensive, difficult to fabricate, and require significant time to design. Woodruff Scientific, Inc. (**WSI**) has received a Phase II SBIR award from the DOE to investigate the potential of additive manufacturing (**AM**), or 3D printing, to impact this issue. AM relaxes or removes many of the constraints of conventional manufacture (**CM**), reducing the time and cost of both design and fabrication. Furthermore, AM allows for a significant increase in part complexity at little or no additional cost, potentially leading to improved diagnostic functionality.

WSI is currently:

- optimizing the design of several diagnostics for AM
- assessing the capability of state-of-the-art 3D printing processes for UHV-compatible, high-temperature metals and ceramics
- researching topology optimization and generative design algorithms
- developing scripted design processes that automatically generate semi-custom diagnostics from user input

Conventional Diagnostic Designs

Electrostatic probes

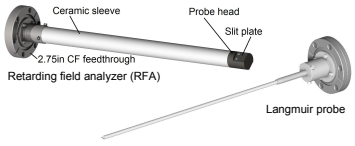

Interferometers

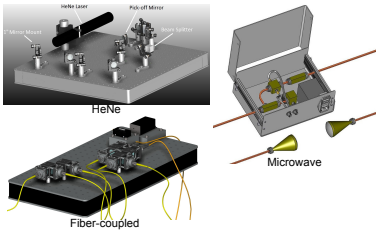

Magnetics

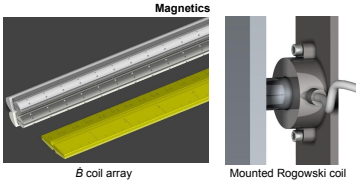

AM Optimization Methodology

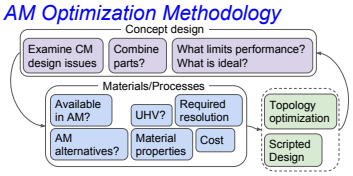

3D Printed RFAs for Alcator C-Mod

WSI is collaborating with Alcator C-Mod to test a set of AM tungsten (W) retarding field analyzer (RFA) probe heads, based on the state-of-the-art design by C-Mod researcher Dan Brunner and others[2]. The probe must reciprocate three times up to the LCFS during a shot, where it will encounter a heat flux of 0.4GW/m^2. Pictured below are the C-Mod RFA and the three AM RFA probe heads that are currently being printed.

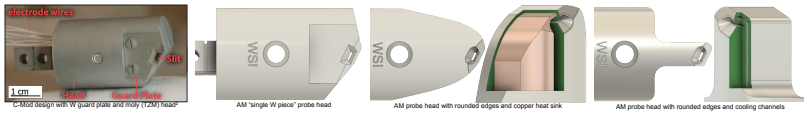

C-Mod design with W guard plate and moly (TZM) head

AM "single W piece" probe head

AM probe head with rounded edges and copper heat sink

AM probe head with rounded edges and cooling channels

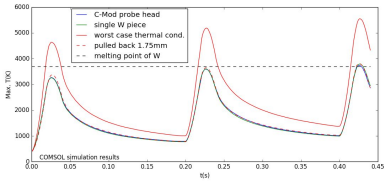

The thermal conductivity of AM tungsten may require the probe to be used a shallower depths.

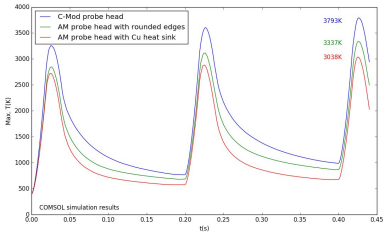

Rounding the sharp corners may provide a 450K reduction in peak temperature, and the Cu heat sink may reduce that by another 300K. This improvement would increase the lifetime of the probe, allow it to be inserted up to 0.85mm further into the plasma, or allow the reciprocation period to be reduced to collect more data, as shown to the right.

Topology Optimization

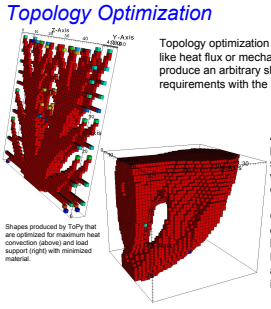

Shapes produced by ToPy that are optimized for maximum heat convection (above) and load support (right) with minimized material.

Topology optimization algorithms take inputs like heat flux or mechanical loads and produce an arbitrary shape that satisfies the requirements with the minimum material.

AM processes can print these arbitrary shapes at reduced weight and material cost.

Open source topology optimization packages like ToPy (written in Python) are readily available and improving rapidly.

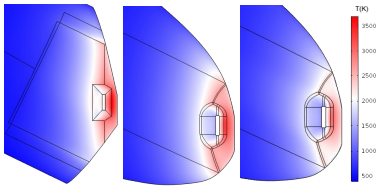

COMSOL simulation results showing the C-Mod RFA (left), RFA with rounded edges (center), and RFA with Cu heat sink (right) at peak temperature.

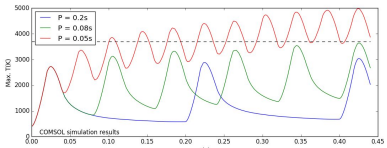

WSI and C-Mod intend to test the "single W piece" and heat sink probe heads before the planned shutdown of C-Mod in September. The probe head with cooling channels will not be tested on C-Mod, but will undergo helium flow testing to better assess its performance.

Scripted Design

Solid modeling and FEA tools are now providing access to their underlying APIs, which can be used to perform design tasks from scripts. These can be combined with web pages, open source design tools, and other scripts to allow for automated design of semi-custom diagnostics.

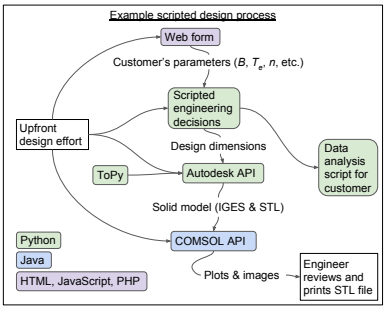

Pre-Aligned Monolithic Interferometer

Interferometers can take a long time and be very expensive to align.

WSI is exploring 3D printed, monolithic interferometers with the alignment built in. They just need to be aligned with the chamber.

Desktop printers are not accurate enough for this application, but laser sintering of plastic and metal is highly accurate and can produce parts with a wide range of stiffnesses.

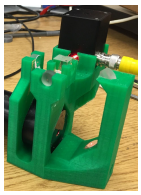

Outgassing of AM Metals for UHV

Preliminary results of outgas testing of AM aluminum (ALSI10), stainless steel (PH1), and Inconel (IN718) are shown below. Further testing is required for a statistical assessment and to compare the AM metals to their conventional counterparts tested in the same chamber, but this data suggests the AM metals perform comparably. Additional AM materials, including alumina, will also be tested.

AM metal	Outgas rate (Torr·L/cm^{2}s)	CM metal	Outgas rate (Torr·L/cm^{2}s)*
AlSi10	2.19x10^{-8}	Al-6061	2.5x10^{-9} (10h)
PH1	1.29x10^{-8}	SS 304	8x10^{-11} (44h)
IN718	-6.30x10^{-9} **	IN625	2x10^{-9} (20h)

*reached lower final pressure than control

Impact on Cost

Scripted design significantly reduces the cost of Concept (CDR), Engineering (EDR) and Product Design Reviews (PDR) for a diagnostic by automating the engineering labor.

AM reduces the cost of fabrication, testing, and materials in many cases by reducing the number of components and using less material.

This table shows estimates of the costs of AM devices relative to CM devices for a given cost category.

Diagnostic	C_{Total}	C_{CDR}	C_{EDR}	C_{PDR}	C_{Fab}	C_{Test}	C_{Mat}
Magnetic field coil	0.06	0	0	0.1	0.1	0.1	0.1
Magnetic coil array	0.062	0	0	0.1	0.1	0.1	0.1
Rogowski coil	0.062	0	0	0.1	0.1	0.1	0.1
Calibration jig	0.14	0	0	0.1	0.5	0.1	0.1
Langmuir probe	0.35	0	0	0.1	0.5	1	0.9
RFEA	0.35	0	0	0.1	0.5	1	0.9
HeNe interferometer	0.71	0	0	0.1	0.9	0.2	0.9
CO2 interferometer	0.72	0	0.2	0.1	0.9	0.2	0.9
CO2 polarimeter	0.72	0	0.2	0.1	0.9	0.2	0.9
mm interferometer	0.73	0	0.2	0.1	0.9	0.2	0.9
Thomson Scattering	0.85	0.1	0.9	1	0.9	0.2	0.95
Inverse Compton	0.92	1	1	1	0.9	1	0.9
Spectrometer	0.49	0	0.1	0.1	1	1	0.95
Bolometer	0.59	0	0	1	0.7	1	0.95
Scintillator	0.33	0	0	0.1	0.1	1	0.9

Conclusion

- Fusion diagnostics are often difficult and expensive to manufacture
- Additive manufacturing has progressed rapidly in the last decade, allowing high-resolution printing in materials applied in fusion
- There remain many aspects to be assessed (primarily properties of AM materials), but AM may have the potential to significantly affect diagnostic cost and performance right now

Future Work

In the second year of Phase II, WSI plans to:

- Test additively-manufactured RFA probe heads on Alcator C-Mod
- Test a laser-sintered, monolithic interferometer
- Assess the mechanical strength, outgassing and thermal properties of AM tungsten and other materials
- Further explore multi-material printing, including with tungsten
- Further explore topology optimization and generative design
- Optimize several additional diagnostics for AM
- Deploy a scripted process that designs and simulates several diagnostics from user input via a web form

References

[1]E. A. Mosney, "A compilation of outgassing data in vacuum materials" PPPL Technical Report No. 82-001 Rev. A, 15 Feb. 1982
[2]Brunner, LaBombard, Ochoukov, & Whyte. (2013). Scanning retarding field analyzer for plasma profile measurements in the boundary of the Alcator C-Mod tokamak. *Review of Scientific Instruments*, 84(3), Review of Scientific Instruments, 2013, Vol.84(3).

Additive Manufacture (3D Printing) of Plasma Diagnostic Components & Assemblies for Fusion Experiments

This work is supported by DOE Phase II SBIR Grant DE-SC0011858

M. Quinley[1], D. Brunner[2], A. Card[3], C. Romero-Talamás[4], W. Rivera[4], M. Reinke[5], P. Sieck[1], J. Stuber[1], S. Woodruff[1], P. Melnik[1],
[1]Woodruff Scientific, Inc., [2]MIT Plasma Science & Fusion Center, [3]University of Washington, [4]University of Maryland, Baltimore County, [5]Oak Ridge National Lab/Princeton Plasma Physics Lab

Motivation

There is a well-established set of plasma diagnostics for fusion applications, but they can be expensive, difficult to fabricate, and require significant time to design. Woodruff Scientific, Inc. (**WSI**) has received a Phase II SBIR award from the DOE to investigate the potential of additive manufacturing (**AM**), or 3D printing, to impact this issue. AM relaxes or removes many of the constraints of conventional manufacture (**CM**), reducing the time and cost of both design and fabrication. Furthermore, AM allows for a significant increase in part complexity at little or no additional cost, potentially leading to improved diagnostic functionality.

WSI is currently:

- optimizing the design of several diagnostics for AM
- assessing the capability of state-of-the-art 3D printing processes for UHV-compatible, high-temperature metals and ceramics
- developing a process for design optimization for AM, including the use of topology optimization and generative design algorithms

3D Printing of Metals & Ceramics

AM began with prototyping in plastics, but the technology is significantly matured. Many metals (stainless steel, aluminum, Inconel, titanium, and more) and even a few ceramics (alumina) can be printed with sufficient accuracy and performance for industrial applications.

These materials are printed by laser or e-beam sintering/melting:

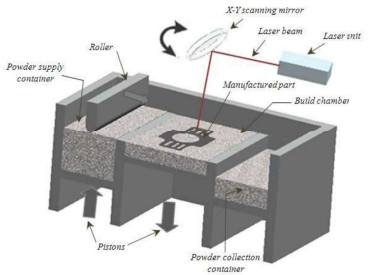

Properties of AM Materials for Fusion

Preliminary results of outgas testing of AM aluminum (ALSI10), stainless steel (PH1), and Inconel (IN718) are shown below. Further testing is required for a statistical assessment and to compare the AM metals to their conventional counterparts tested in the same chamber, but this data suggests the AM metals perform comparably. Additional AM materials, including alumina, will also be tested.

AM metal	Outgas rate (TorrL/cm²s)	CM metal	Outgas rate (TorrL/cm²s)[1]
AlSi10	2.19x10^{-8}	Al-6061	2.5x10^{-8} (10h)
PH1	1.29x10^{-8}	SS 304	8x10^{-11} (44h)
IN718	~6.30x10^{-9} **	IN625	2x10^{-9} (20h)

*reached lower final pressure than control

Further work includes additional outgas testing, as well as testing of SS316 for tensile strength, thermal conductivity, electrical resistivity, and many other properties. Upon completion of this testing, WSI will work with printers to implement process control.

AM Optimization Methodology

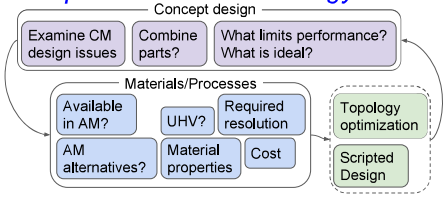

3D Printed RFAs for Alcator C-Mod

WSI has collaborated with Alcator C-Mod to test a set of AM tungsten (W) retarding field analyzer (RFA) probe heads, based on their state-of-the-art design[2].

Design

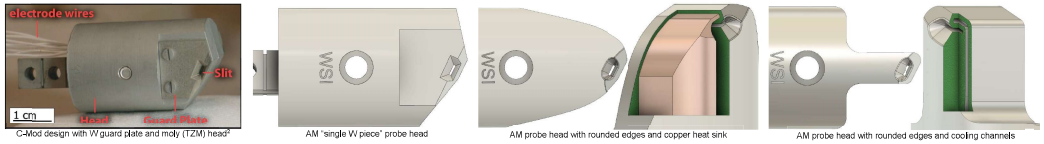

C-Mod design with W guard plate and moly (TZM) head[2] | AM "single W piece" probe head | AM probe head with rounded edges and copper heat sink | AM probe head with rounded edges and cooling channels

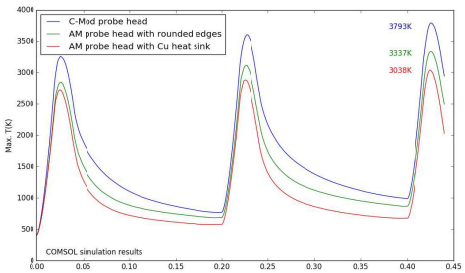

Rounding the sharp corners may provide a 450K reduction in peak temperature, and the Cu heat sink may reduce that by another 300K. Assuming AM W thermal conductivity can be improved to match CM.

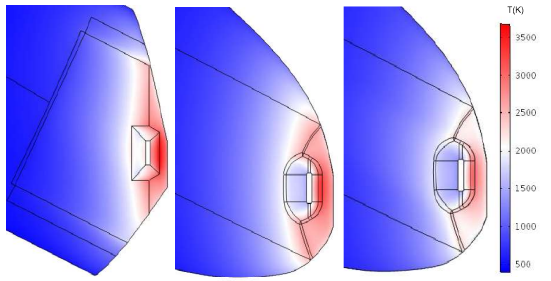

COMSOL simulation results showing the C-Mod RFA (left), RFA with rounded edges (center), and RFA with Cu heat sink (right) at peak temperature.

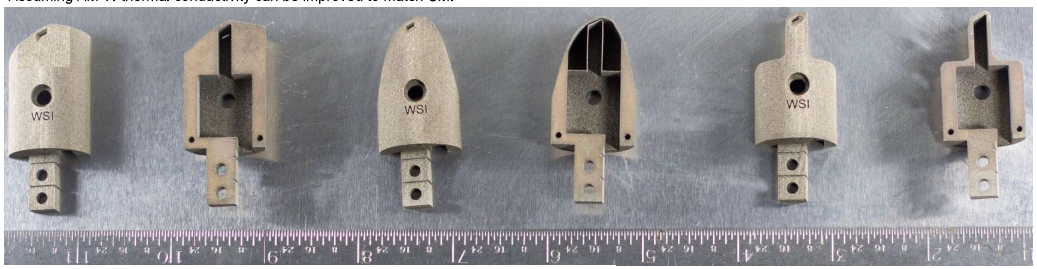

Results

The printed probe heads were evaluated on Alcator C-Mod, placing AM and CM probe head halves back-to-back and under the same plasma conditions, with results as follows:

- **Outgassing:** prior to plasma exposure, initial pumpdown slower than typical, with a lot of water present; during baking and operation it performed like conventional probe heads
- **Strength:** probe heads survived 100 scans on a bench-test reciprocating drive with ~50g acceleration with no visible cracking or damage
- **Use in C-Mod boundary layer:**
  - **Arcing:** rough surfaces arced to electrodes inside probe head when exposed to plasma; worsened throughout use as probe head heated up
  - **Melting:** after ~10 shots tip of probe head melted, spraying W into plasma and leading to disruption

Conclusions

- Laser-sintered tungsten not acceptable for PFCs at this time
  - Thermal conductivity is reduced (120-170 W/m-K) compared to W produced by conventional means (173 W/m-K)
  - Ultimate tensile strength, although marginally good enough for this application, is low (>35 Mpa) compared to that of conventional tungsten (941 MPa)
  - Melting allows trapped air to burst, spraying W into plasma
  - Surface roughness causes:
    - slow pumpdown due to significant water retention;
    - leads to electric field concentrations on floating PFCs, potentially causing arcing;
    - may negate effect of rounding sharp corners on PFCs
- Process improvements are required to meet standards for use in fusion environment
- Until then, materials with lower melting temp (easier to print) like moly and even SS316 may make better 3D printed PFCs

Next steps

- Attempt polishing to reduce arcing
- Destructive testing for tensile strength and thermal conductivity, SEM imaging
- Work with printer to improve process for this application

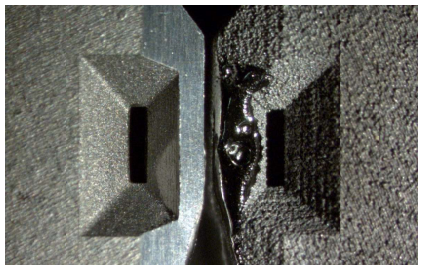

Comparison of CM guard plate (left) and AM probe head (right) after use in C-Mod, showing melting and roughness of AM part.

Monolithic 3D Michelson Interferometer

- Alignment of conventional interferometers is time consuming, and typically restricted to 2D
- WSI is exploring printed, monolithic interferometers that utilize compact 3D design
- Initial results show plastic printing methods (PLA extrusion, laser-sintering) are not accurate enough for HeNe lasers
- Integration of kinematic mounts upstream from recombination beamsplitter can account for this inaccuracy
- Laser-sintering of metals (e.g. aluminum alloys) offers increased print accuracy and stiffnesses
- Lasers with larger etendue might successfully interfere with looser print tolerances

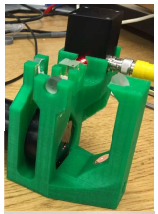

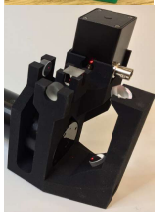

- Shown at right in green: desktop-printed compact Michelson interferometer, ~$10
- Shown at right in black: laser-sintered compact Michelson interferometer, ~$100
- This design printed in laser-sintered aluminum alloy would cost ~$1000

Bolometer Assembly for NSTX-U

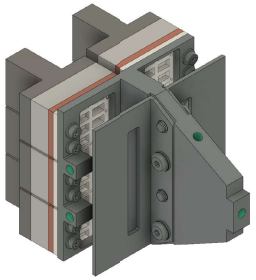

WSI is collaborating with NSTX-U diagnosticians to optimize a bolometer assembly for AM.

The CM design (left) has windows to limit the FOV.

The AM concept (below) includes a stair-step surface to reflect unwanted light and cooling channels to improve bolometer measurement.

This design will be iterated and printed in SS316 for evaluation.

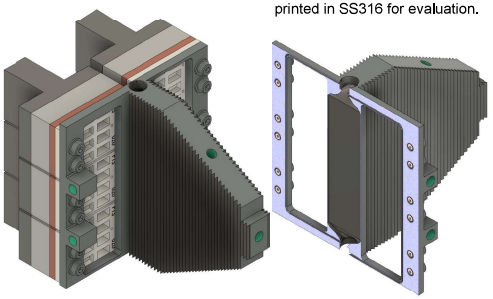

Future Work

- Follow-up testing of W RFA probe heads and W process development
- Evaluate performance of a laser-sintered, monolithic interferometer
- Evaluate an AM-optimized bolometer assembly printed in SS316 at NSTX-U
- Assess the mechanical strength, outgassing and thermal properties of AM tungsten, SS316 and other materials
- Further explore multi-material printing, including with tungsten
- Explore topology optimization and generative design
- Optimize several additional diagnostics for AM

References

[1]E. A. Mosher, "A compilation of outgassing data in vacuum materials" PPPL Technical Report No. 82-001 Rev. A. 15 Feb. 1982
[2]Brunner, LaBombard, Ochoukov, & Whyte, (2013). Scanning retarding field analyzer for plasma profile measurements in the boundary of the Alcator C-Mod tokamak. *Review of Scientific Instruments, 84*(3). Review of Scientific Instruments. 2013. Vol.84(3).

Optimized and Automated Design of Plasma Diagnostics for Additive Manufacture

J. E. Stuber[1], K. Chung[1], T. Smith[1], P. A. Melnik[1], P.E. Sieck[1], S.Woodruff[1], M. J. Quinley[1]

[1]Woodruff Scientific Inc, 4000 Aurora Ave N, Seattle, WA 98103

American Physical Society Division of Plasma Physics, November 2nd 2016

Work supported under DOE subcontract number DE-SC0011858

Abstract

Despite having mature designs, diagnostics are usually custom designed for each experiment. Most of these designs can be now be automated to reduce costs (engineering labor, and capital cost). We present results from scripted physics modeling and parametric engineering design for common optical and mechanical components found in many plasma diagnostics. We also outline the process for automated design optimization, employing scripts to communicate data from online forms through proprietary and open-source CAD and FE codes. The resulting design can be sent directly to a printer. As a demonstration of design automation, an optical beam dump is designed via an automated process and printed.

Diagnostics in fusion systems

- Diagnostics are sensors that measure all important plasma parameters [3]
- Electrostatic probes designed to enter plasma
- Magnetics are usually protected beneath shielding
- Optical diagnostics usually have endoscopes to protect components, but exposed 1st mirrors
- RF diagnostics have horns or antennae close to plasma

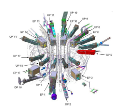

About 50 individual measurement systems will help to control, evaluate and optimize plasma performance in ITER and to further understanding of plasma [4]. These include lasers, X-rays, neutron cameras, impurity monitors, particle spectrometers, radiation bolometers, pressure and gas analysis, and optical fibers.

Additive Manufacturing (AM) is ideally suited for plasma diagnostics

- Initially for rapid prototyping (since 1980's) but now fully functional components can be printed
- Diverse set of methods patented (though some patents now expiring)
- US recognizes potential of this disruptive tech and is preparing (e.g. [5])
- Materials useful for plasma diagnostics such as metals, ceramics, and even lenses can be Additively Manufactured. These material's suitability for UHV and Plasma Facing is being evaluated.

Benefits of AM over Conventional Manufacturing (CM)

- Ideally suited to rapid prototyping and functional models [6]
- Low/no waste, low energy, predictable machine time
- No extra cost for complexity
- Reduced assembly - printed parts can be functional
- Cost of printing will fall rapidly in coming years as technology is adopted and printing becomes faster and more accurate.

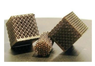

Complex alumina components, with lattice structure to reduce total volume of materials. Simlar components can be printed in metals, and plastics.

The Need for Automated Design in Fusion Diagnostics

- Labor cost of Design Engineers and Physicists is expensive
- Most diagnostics are designed from scratch despite being similar to existing
- By automating the bulk of the design work, costs can be reduced
- Turnaround time to diagnostics is reduced
- Customers can match their needs in a web browser (minutes vs days of back-and-forth)

Example Automated Design: Beam Dump

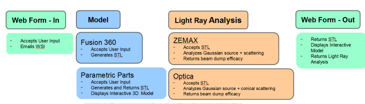

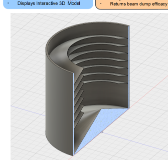

Cross section of a Beam Dump generated automatically using Fusion360's scripting abilities

Automated Design: CAD Model

CAD Programs like Fusion 360 or Parametric Parts can be scripted to generate CAD models automatically. Here the user inputs parameters–how many fins, depth, aperture, etc–and Fusion 360 produces a full CAD design.

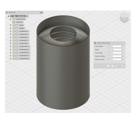

Automated Design: Physics Parameters

Engineering analysis of important physics parameters are commonly done using programs which can be scripted. Common programs in use at WSI include Octave, Matlab, Mathematica, Optica, Zemax, COMSOL. Each of these can be run automatically with Application Programming Interfaces (APIs). Other popular engineering programs also include similar abilities.

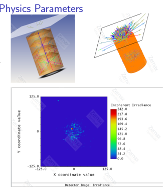

In our Beam Dump example, Zemax is used to simulate intensity leaving a beam dump. Here we see a 3 order of magnitude reduction in intensity. This script could be run automatically by receiving geometry parameters from the CAD model and utilizing Zemax's API.

Automated Design: Web Interface

Engineer or Customer can get a design suited for their application in minutes just by tweaking a few parameters. Compare to a long back-and-forth between customer, sales reps, and engineers, and then additional design labor costs.

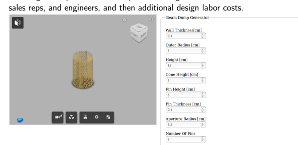

Online interface for generating a beam dump CAD model

Automated Design: 3D Print

Beam dump printed in plastic. Shapeways provides an API for ordering parts in a scripted manner.

Optimized Design

By integrating CAD scripting and analysis programs, design optimization can be performed very quickly. Variations of the inital beam dump design can be generated programmatically much quicker than having to draw each variation one at a time. These variations can then be fed into an analysis program automatically.

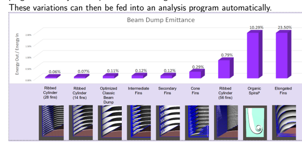

Beam Dump variations and their resultant emittance (lower is better), simulated in Zemax [12].

Topology Optimization of Vibration Isolator

Increased complexity does not increase the cost of AM, so we can reduce manufacturing costs by reducing volume. Topology Optimization is an approach that optimizes stiffness in a part while reducing volume. Using programs such as ToPy[13], we can reduce the volume and therefore the cost of Additively manufactured diagnostics.

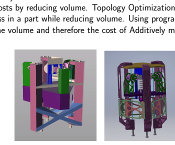

Vibration Isolator, and the same isolator with reduced volume using Topological Optimization

More Examples of Scriptable Diagnostics

Alumina Langmuir probe head with cooling channels

Printed Tungsten RFA Probe head, tested on Alcator C-Mod [14]

Scriptable Laser-based diagnostics

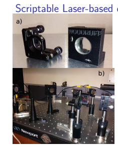

a) Interferometer mirror mounts: $190 store bought vs $2.86 printed (raw materials); b) mount installed in interferometer

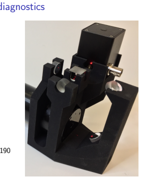

Additively Manufactured Monolithic Interferometer

Concept Design Approach for Automation and Optimization

- Experienced physicist examines measurement and maps out best approach
- Examine which commonly used parts can be scripted
- Examine which parts can be optimized in an automated manner
- Web-based form can be used to constrain online scripted EDR
- Cost of CDR can be close to zero after first iteration.

Further Work

- Integrate Analysis work directly into existing scripts
- Develop automated process for other diagnostics
- Continue reducing the need for interaction by a Design Engineer
- Allow a customer to input desired parameters in an online interface, order and receive and Additively Manufactured product

Summary

- AM is now a technology that can significantly impact the cost of diagnostic design and fabrication for fusion systems TODAY, despite stringent materials requirements in fusion
- The example case of a beam dump demonstrated that Automated Design is feasible
- In the near future Automated Design and AM will lead to more significant cost savings
- We are currently in the design stage on producing complete diagnostic subcomponents for use in fusion environments. In parallel, we are pushing qualification of materials for these applications.

Bibliography

[1] http://www.iter.org/

[2] S. Zinkle Challenges in Developing Materials for Fusion Technology Past, Present and Future AND TOFEy Nashville 2012 http://fire.pppl.gov/TOFE_2012_materials_Zinkle.pdf

[3] I. A. Hutchinson, Principles of Plasma Diagnostics, Cambridge University Press; 2 edition (July 14, 2005)

[4] M. Walsh, et al Overview of High Priority ITER Diagnostic Systems IAEA Fusion Energy Conference 2010 Proc. 2010 http://www-pub.iaea.org/mtcd/meetings/PDFplus/2010/cn180/cn180_papers/itr_p1-07.pdf

[5] Measurement Science Roadmap for Metal-based Additive Manufacture Prepared by Energetics Incorporated May 2013 http://www.nist.gov/el/isd/upload/NISTAdd_Mfg_Report_FINAL-2.pdf

[6] NIST Dec. 2012 Roadmapping Workshop http://events.energetics.com/NIST-AdditiveMfgWorkshop/downloads.html

[7] The Economist, The Printed World: Three- dimensional printing from digital designs, 10 February 2011. www.economist.com/node/18114221

[8] Hales and Gooch 'Managing Engineering Design' Springer 2nd Ed 2004

[9] R. Pitts et al A Retarding Field Energy Analyser for the JET Plasma Boundary EFDAJETPR(03)30 http://www.iop.org/Jet/fulltext/EFDP03030.pdf

[10] http://arxiv.org/pdf/1406.4817v1.pdf

[11] http://www.woodruffscientific.com/ShapeJS-Example

[12] K. Chun, et al Optical Beam Dump Optimization for Additive Manufacturing, Washington NASA Space Grant 2016

[13] https://github.com/williamhunter/topy

[14] M. Quinley, et al 3D Printing and Scripted Design of Fusion Diagnostics, HTPD 2016

[15] Jennifer Bryant, Report of the Breakout Group, NIST AM Qualification and Certification http://events.energetics.com/NIST-AdditiveMfgWorkshop/pdfs/AM_ReportOut_QualCert.pdf

3D Printed Pure Tungsten Plasma-Facing Components for Alcator C-Mod[a)]

M. Quinley,[1, b)] D. Brunner,[2] P. Melnik,[1] P. Sieck,[1] J. Stuber,[1] and S. Woodruff[1]
[1)] *Woodruff Scientific, Inc., Seattle, Washington*
[2)] *MIT Plasma Science & Fusion Center, Cambridge, Massachusetts*

(Dated: 9 March 2018)

Additive manufacturing (AM, or 3D printing) allows for the manufacture of highly complex structures. Materials of interest to the nuclear fusion community, including tungsten, can now be printed at high resolution (25 µm). Tungsten is a useful material as a plasma-facing component (PFC) because of its high melting temperature and reliance to sputter. In order to investigate the potential benefit of 3D printing for PFCs, the design of an Alcator C-Mod probe head was optimized and analyzed. AM allows for the use of complex internal cooling channels and geometry optimization to increase surface heat flux handling. To assess the technical readiness of one pure-tungsten printing process for PFCs, a reproduction of the original C-Mod probe using AM was built and evaluated at C-Mod. Results of both the design optimization and experimental evaluation are presented.

Keywords: 3D printing, additive manufacturing, plasma-facing components, retarding field analyzer

I. INTRODUCTION

There is a well-established set of plasma diagnostics for fusion applications[1], many of which would benefit from additive manufacturing (AM), or 3D printing. AM allows for the creation of complex 3D structures not possible with conventional manufacturing (CM) at no additional cost in design or manufacturing complexity over simpler structures. This can lead to improved diagnostic functionality. For these reasons, AM is likely to become the standard mode of manufacture of plasma-facing components (PFCs) in the future[2]. At this time, AM technology is sufficiently advanced that several commercial printers offer materials of interest to the fusion community (e.g. structural materials such as stainless steel type 316 and Inconel) and there is at least one provider of AM tungsten[3], an important material for PFCs due to its high thermal diffusivity, high melting temperature, and resistance to plasma erosion. Woodruff Scientific, Inc. (WSI) has received a Phase II SBIR award from the Department Of Energy to investigate the potential of additive manufacturing to impact plasma diagnostics.

In order to assess the readiness of AM tungsten for fusion PFCs and the potential benefits therein, the design of a conventional diagnostic PFC was optimized for this material, printed, and evaluated in Alcator C-Mod. The chosen PFC is the probe head of the Alcator C-Mod retarding field analyzer (RFA)[4]. This probe head was made with CM (primarily plunge EDM on a rolled tungsten plate) and is the state-of-the-art for probes for fusion plasmas, withstanding plasma temperatures $\sim 100\,\mathrm{eV}$, plasma densities $\sim 10^{20}\,\mathrm{m}^{-3}$, and surface heat flux up to $\sim 0.5\,\mathrm{GW\,m}^{-2}$. This paper aims to use AM to improve the thermal design of this probe head such that it can handle higher heat fluxes and be scanned deeper into the plasma for longer times. This process did not focus on reducing the cost of the probe head, but a comparison of the costs of the two methods is presented.

In general, active or passive cooling of PFCs stands to dramatically improve their performance and or lengthen their lifetime. In the case of the C-Mod RFA, cooling the tungsten guard plate could allow more reciprocations (and thus more data to be taken) prior to the onset of melting. The addition of cooling channels would be nearly impossible in CM tungsten, requiring very simple designs or the component to be machined in several pieces and welded together. Additive manufacturing enables the use of cooling channels,the complex geometry can be printed with no additional cost or additional manufacturing effort.

This paper presents the design of a plasma-facing component optimized for additive manufacture in tungsten along with the evaluation of the printed probe head in Alcator C-Mod. Section II presents an overview of the tungsten AM process. The optimized probe head designs are presented in Section III. Section IV discusses the impact of AM on the cost of these components. Section V presents the assessment of the material's technical readiness, including results of use on Alcator C-Mod.

II. ADDITIVE MANUFACTURING PROCESS

III. DESIGN OPTIMIZATION

Reciprocating probes on Alcator C-Mod are used in two ways: 1. plunged up to the last closed flux surface (LCFS) by a reciprocating drive or 2. a "dwell scan" at fixed depth for the entire plasma lifetime. It is reciprocated up to and sometimes a few millimeters inside the last closed flux surface, providing important information on the boundary plasma. Scans with the

[a)] This work is supported by DOE Phase II SBIR Grant DE-SC0011858.
[b)] Electronic mail: Morgan@WoodruffScientific.com.; www.WoodruffScientific.com.

TABLE I. Melting temperature and thermal conductivity (at room temperature) comparison of tungsten and molybdenum.

	$T_{\mathrm{melt},}$[K]	α[W m^{-1} K^{-1}]
tungsten	3695	173
molybdenum	2896	138

pneumatic probe system in[4] were at $1.4\,\mathrm{m\,s^{-1}}$ with a turn around acceleration of $600\,\mathrm{m\,s^{-2}}$. The reciprocation depth is set such that the tungsten plasma-facing surface (PFS) is near melting. The probe used in this paper were done with a new servomotor controlled system and were "dwelled" at a constant position in the far boundary plasma.

The original C-Mod RFA consisted of a 1.5 mm thick tungsten plasma facing surface and a TZM body (an alloy of molybdenum with zirconium and titanium to improve the thermal strength while maintaining the thermal properties of molybdenum). Tungsten has a better thermal performance (Table I) but is very difficult to machine using conventional techniques and it was infeasible to make the entire probe head out of it. Whereas TZM can be machined using conventional tooling and was thus used for the bulk of the complex probe head. Simulation of this probe head[4] indicated that the tungsten guard plate could survive scanning to peak surface heat fluxes of $\sim 0.4\,\mathrm{GW\,m^{-2}}$, with the tungsten approaching its melting point by the end of the third scan. In addition to its impressive thermal performance, the probe head is strong enough survive the turn around acceleration of $\sim 600\,\mathrm{m\,s^{-2}}$.

picture of Dan's probe head from his paper (you are going to need to request permission from RSI to reproduce this, I've placed a copy of the original in the images folder DFB)

The C-Mod probe head design has recently been optimized for additive manufacture. The original design was a compromise between thermal handling and the constraints of both wire- and plunge-EDM processes. The optimization first considered these compromised areas, almost exclusively at the tip of the probe where the bulk heating occurs. These areas were redesigned with the relaxed constraints of additive manufacturing. Following this optimization, cooling channels were added to the probe head. The optimizations were informed by performing thermal simulations in the commercial finite element code COMSOL, using similar conditions to the simulations for the conventional probe head. The goal of the design optimization was to reduce the peak temperature of the probe head for a given simulation, this allows it to either scan deeper into the plasma or dwell for longer times. No effort was made to strengthen the connection of the probe head to the probe arm. This process resulted in three AM-optimized probe head designs, described in detail in the following sections.

A. Single-Piece Probe Head

The first AM-optimized probe head design is referred to as the "single-piece probe head". This design is geometrically identical to the conventional probe head, except that the entire probe head is a single tungsten piece and there is a minor change to account for the inability to tap threads in tungsten. This addresses the compromise used in the original design, due to the difficulty of machining tungsten, of making the probe head in two pieces. (As shown in figure?) Additionally, it allows for a direct comparison in thermal, mechanical, and electrical performance to the CM probe head.

If the AM tungsten has the same thermal performance as CM, this new probe head unlikely to affect the ultimate scan depth since the 1.5 mm thick CM guard plate is effectively semi-infinite to the plasma heat flux on the timescale of a scan[4]. Direct comparison of the two by Alacator C-Mod was intended to allow an assessment of the readiness of the AM tungsten for this application (results reported in section **??**). However, this design may provide the advantage of allowing the plasma-facing surface to cool down more in between scans due to the removal of the thermal resistance between the guard plate and thermal sink of the body. Figure **??**, which shows the peak temperatures of the conventional probe head's PFC and the single-piece probe head, shows that this is not the case. Since C-Mod is highly magnetized and the heat flux at the LCFS falls off rapidly, a large amount of heat is deposited onto a very small area of the guard plate. This means that the heat has a large amount of relatively unexposed tungsten into which it can diffuse between scans; providing a larger reservoir of tungsten has little effect. (I don't understand this point. DFB)

CAD render of single piece probe head
picture of C-Mod RFA and single-piece peak temps versus time - did you use correct thermal resistance for C-Mod RFA? (I assumed perfect thermal contact DFB)

B. Probe Head with Heat Sink

CAD render and cutaway from APS poster
picture of C-Mod RFA, W heat sink and Cu heat sink peak temps vs time - heat sink does not help much during shot (100K), but between shots; rounded edges help
picture of surface heat contours side by side from APS poster - rounded edges help

C. Probe Head with Cooling Channels

CAD render and cutaway from APS poster
Has same rounded edges as heat sink probe head
The performance of this probe head was not simulated, as the ability to simulate fluid dynamics coupled with

convective heat transfer within the channel was not available at the time of design. Given its size, it is unlikely that the cooling channel could draw away the power deposited onto the tip of the probe head (?????????).

D. Printed Probe Heads

Figure **??** shows all of the printed pieces: the east- and west-facing probe head halves for each of the AM-optimized designs. Inspection of the pieces showed that

picture of all printed pieces next to one another

IV. IMPACT ON COST

The single piece design was printed for \$995 each[5] while the heat sink and cooling channels designs were printed for \$945 each. The purchase of the 6 probe head halves (3 total probes) included a \$535 setup fee. Including the setup fee, the average cost of a probe head was \$1050. It is not known what drives these costs. Additive manufacturing of metals is rarely done simply by sending a part file to the printing machine. Typically a manufacturing engineer analyzes the model to determine print orientation and parameters like laser scan speed, and may perform some post-processing after printing. This and other unknown costs may be covered entirely by the setup fee or may be covered partially by the part cost. The cooling channels and heat sink probe heads require 30% less material than the single piece probe head but cost only 5% less, suggesting that the part volume (i.e. cost of tungsten powder) is not a strong driver of cost.

The cost of the conventional probe head's guard plate and body were about \$225 and \$500, respectively, for a total cost of \$725 for a probe head half. These components were produced by electrical discharge machining (EDM) and CNC machining, respectively. In this case additive manufacture did not reduce the cost of the component, as the printed probe heads were 1.45 times the cost of the conventional probe heads. It is likely that this cost will decrease in the coming years as the technology develops and more tungsten printing providers enter the market. Other metals (e.g. stainless steel type 316 and aluminum) can currently be printed at similar resolution less expensively, with service offered by several commercial providers.

V. EVALUATION OF PRINTED TUNGSTEN

The single-piece, all-tungsten AM probe head was tested in C-Mod, directly comparing it the the CM tungsten plate on TZM probe head. Visual examination of the AM tungsten revealed it to have a much rougher surface than the EDM cut tungsten plate. Careful measurement of the critical dimensions showed them to meet design specifications.

Before being allowed in the C-Mod vacuum vessel, all potential PFCs must go through bake-out test. They are first placed in a room temperature vacuum chamber and pumped down to UHV while watching what out-gasses on a residual gas analyzer (RGA). The AM tungsten took longer to pump down than CM, out-gassing primarily water. Once pumped down, the PFC is baked for 1 h at 600 °C. Nothing of note occurred during the bake of the AM tungsten.

Due to meeting the critical dimensions, assembly of the AM half head with the internal component and the other CM half head was mostly straight forward. However, the clearance fit holes were not round enough and had to be rounded by hand with a diamond file. These holes are crucial for translating the force to the probe head through ceramic pins while maintaining electrical isolation of the probe head to ground. See Ref.[4] for more on this detail.

The manufacturer-reported strength, $\sim 30\,\mathrm{MPa}$ (compared to $\sim 1000\,\mathrm{MPa}$ for CM tungsten), was low enough to inspire caution in implementing it in C-Mod. Loss of a probe head into the vacuum chamber would result in ~ 1 of down time. The AM probe was bench-tested to 100 scans (equivalent to about one experimental day of scans) at full velocity ($1.4\,\mathrm{m\,s^{-1}}$) and acceleration ($600\,\mathrm{m\,s^{-2}}$). Detailed inspection of the probe head following these scans revealed no signs of cracking or damage. This qualified the probe for operation into the C-Mod vacuum vessel.

The AM/CM combined probe head was dwelled in the far boundary plasma in C-Mod for 10 shots (approximately 10 s total time in plasma). Each shot it was stepped in deeper than the previous shot. The last shot was operated at $\sim 30\,\mathrm{eV}$ and $\sim 1.5\times10^{18}\,\mathrm{m^{-3}}$ as measured with the slit plate (the tip was certainly at more intense conditions). This results in a surface heat flux of $\sim 3\,\mathrm{MW\,m^{-2}}$.

New probe heads typically take a few shots to condition up when inserted into C-Mod. This is characterized by intermittent arcing on plasma-facing electrodes and the arcing rate typically decreases with time. It is thought that this arcing is due to electron emission from heated oxides and that the oxides are eventually sputter-cleaned by the plasma exposure. However, the reduction in arc rate was non seen with the AM tungsten probe. The arc rate increased through the course of a shot and got worse with each shot. The arcing was noted on the CM slit plate and was assumed to be occurring to the uninstrumented AM probe head. It is thought that the rough AM surface facilitated local over-heating and electron emission, allowing for arcing between the probe head and slit plate. This arcing made the probe non-functional for measurements.

Spectroscopy indicated a source of melting tungsten $\sim 0.5\,\mathrm{s}$ into the last two shots, so the probe scans were stopped. This can be used to estimate the difference in effective thermal properties between this AM tungsten

and standard tungsten. Assuming constant material parameters and semi-infinite heat flux, the temperature rise is given as:

$$\Delta T = \frac{q}{\kappa}\sqrt{\frac{\pi\alpha}{4t}}. \quad (1)$$

Using the values for this case: $\Delta T = 3600\,\mathrm{K}$, $q = 3\,\mathrm{MW\,m^{-2}}$, and $t = 0.5\,\mathrm{s}$ we get $\frac{\sqrt{\alpha}}{\kappa} = 1.5\times10^{-3}\,\mathrm{Km^2/W/s^{1/2}}$. Comparing this to standard tungsten at room temperature with $\frac{\sqrt{\alpha}}{\kappa} = 4.7\times10^{-5}\,\mathrm{Km^2/W/s^{1/2}}$ we see that this AM is $\sim 30\times$ worse in thermal performance than CM.

Following the run, the probe head was removed and inspected. The CM tungsten guard plate showed no signs of thermal damage, consistent with operation at $3\,\mathrm{MW\,m^{-2}}$ for 1 s pulses. On the other hand, the AM tungsten was clearly damages. The tip was significantly melted and had small craters. The melting is likely due to poorer thermal diffusivity as a result of the microscopic structure of this AM tungsten. The craters were likely due to trapped pockets bursting under the melted surface.

VI. CONCLUSION

This work demonstrates that the relaxed constraints of additive manufacturing allow for significant improvement in the simulated thermal performance of a plasma-facing component. Geometries that cannot be produced conventionally can be used to reduce heat constrictions and provide a means of cooling. In the case of the Alcator C-Mod RFA probe head, these design changes reduced the peak temperature of the PFC by 20%, allowing for extended probe lifetime or additional data to be taken. Although it is unlikely that the addition of channels for active cooling would allow this probe head to be operated in steady state at the peak heat flux experienced by the conventional probe (performance not simulated), this feature would likely extend the allowable depth of steady state operation. On PFCs with looser spatial constraints it is likely that printed internal cooling channels would enable steady-state operation at higher heat flux than the conventional counterpart. Furthermore, AM is likely to allow improvements in other areas of PFC performance, for example magnetic field interaction and integration of sensors.

However, improvements in simulated PFC performance are practically achievable only if the tungsten produced by AM is comparable to that produced conventionally. In addition to the material specifications provided by the manufacture, evaluation by Alcator C-Mod ultimately demonstrated that this is not the case. Although the AM probe heads survived 100 scans on the reciprocating drive, the specified tensile strength of the AM tungsten is possibly 26 times lower than that of conventional tungsten. Ultimate tensile strength of AM tungsten may be highly anisotropic, causing the strength of a part to be dependent on print orientation, which may be accounted for during design. The ultimate issue with the use of AM tungsten for PFCs is the reduced thermal conductivity, possibly 44% lower than that of CM tungsten. This resulted in melting of the probe head during operation in moderate conditions, directly negating any improvements in thermal performance allowed for by design optimization. In addition, the rough and granular nature of the part caused several issues. It is possible that when the probe head melted, air trapped in internal voids cause bubbles of molten material to burst, spraying tungsten into the plasma and causing disruption. The rough surface also caused slow vacuum pumpdown due to significant water retention and produced electric field concentrations that led to arcing within the probe head. Finally, this roughness negates the thermal effect of rounding of sharp edges to some degree.

For these reasons, additively-manufactured tungsten components produced by this particular process are not acceptable for use as plasma-facing components in high-temperature plasmas at this time. Tungsten is a difficult material to laser sinter because of its high melting point and thermal conductivity. Significant improvements in printing processes for tungsten are required before its use in fusion applications. Until then, it is possible that other materials like molybdenum or even SS316 may be more appropriate for PFCs than tungsten in lower-temperature applications, as they have lower melting temperatures, are thus easier to print, and may be more comparable with their conventional counterparts.

[1] I. H. Hutchinson, *Principles of Plasma Diagnostics* (Cambridge University Press, The Edinburgh Building, Cambridge CB2 2RU, UK, 2002).

[2] R. E. Nygren, D. L. Youchison, B. D. Wirth, and L. L. Snead, "A new vision of plasma facing components," Fusion Engineering Design **109-111**, 192–200 (2016).

[3] Smit Röntgen, Veenpluis 6, 5684 PC Best, The Netherlands, see http://www.smitroentgen.com/en/pure-tungsten-parts/.

[4] D. Brunner, B. LaBombard, R. Ochoukov, and D. Whyte, "Scanning retarding field analyzer for plasma profile measurements in the boundary of the alcator c-mod tokamak," Review of Scientific Instruments **84** (2013).

[5] All dollar amounts are in USD.

Fusion Engineering and Design 109–111 (2016) 192–200

Contents lists available at ScienceDirect

Fusion Engineering and Design

journal homepage: www.elsevier.com/locate/fusengdes

A new vision of plasma facing components

Richard E. Nygren[a,*], Dennis L. Youchison[d], Brian D. Wirth[b], Lance L. Snead[c]

[a] Sandia National Laboratories[1], Albuquerque, NM, USA
[b] University of Tennessee, Knoxville, TN, USA
[c] Consultant
[d] Oak Ridge National Laboratory, Oak Ridge, TN, USA

HIGHLIGHTS

- New approach recommended to develop refractory fusion plasma facing components.
- Need to develop engineered materials architecture with nano-features.
- Need to develop PFCs with gas jet cooling with very fine scale for jet arrays.
- Emphasis on role of additive manufacturing as needed method for fabrication.

ARTICLE INFO

Article history:
Received 1 September 2015
Accepted 6 March 2016
Available online 18 April 2016

Keywords:
Plasma facing components
First wall
Divertor
Tungsten
Additive manufacturing

ABSTRACT

This paper advances a vision for plasma facing components (PFCs) that includes the following points. The solution for plasma facing materials likely consists of engineered structures in which the layer of plasma facing material (PFM) is integrated with an engineered structure that cools the PFM and may also transition with graded composition. The key to achieving this PFC architecture will likely lie in advanced manufacturing methods, e.g., additive manufacturing, that can produce layers with controlled porosity and features such as micro-fibers and/or nano-particles that can collect He and transmutation products, limit tritium retention, and do all this in a way that maintains adequate robustness for a satisfactory lifetime. This vision has significant implications for how we structure a development program.

1. Introduction

This paper advances a vision for plasma facing components (PFCs) motivated by our perceived need for a new approach to developing refractory plasma facing components for a fusion reactor. The high temperature coolant needed for efficient power extraction in a reactor drives the need for refractory materials. The ARIES Team's more recent DEMO studies [1,2] also have used refractory PFCs.

The EU power plant study of ~10 years ago [3] identified water cooling in one of four blanket systems of interest; and has now focused more aggressively on near term development of a water-cooled DEMO plus a second option for longer term development [4]. Also the US explored options for facilities for fusion nuclear science that includes D-T devices based on various confinement concepts and devices for testing PFCs [5–8], but effort in this area has decreased. And China had a strong program for developing a component test facility [9].

Several factors evolving in recent years point toward the need for a reactor PFC being an engineered structure. Among the issues of concern are:

a) mitigating brittleness in tungsten-based materials,
b) preempting deleterious effects from helium as the microstructure of tungsten-based materials evolve,
c) neutron-induced transmutations in tungsten and dimensional changes in graphite that lower their thermal conductivity and mechanical integrity, and
d) achieving higher efficiency heat transfer (to helium coolant), e.g., develop impinging jet arrays with much finer size than is currently used in fusion applications.

* Corresponding author. Present address: Sandia National Laboratories, PO Box 5800, Albuquerque, NM 87185, USA.
E-mail address: renygre@sandia.gov (R.E. Nygren).

[1] Sandia National Laboratories is a multi-program laboratory managed and operated by Sandia Corporation, a wholly owned subsidiary of Lockheed Martin Corporation, for the U.S. Department of Energy's National Nuclear Security Administration under contract DE-AC04-94AL85000.

http://dx.doi.org/10.1016/j.fusengdes.2016.03.031
0920-3796/

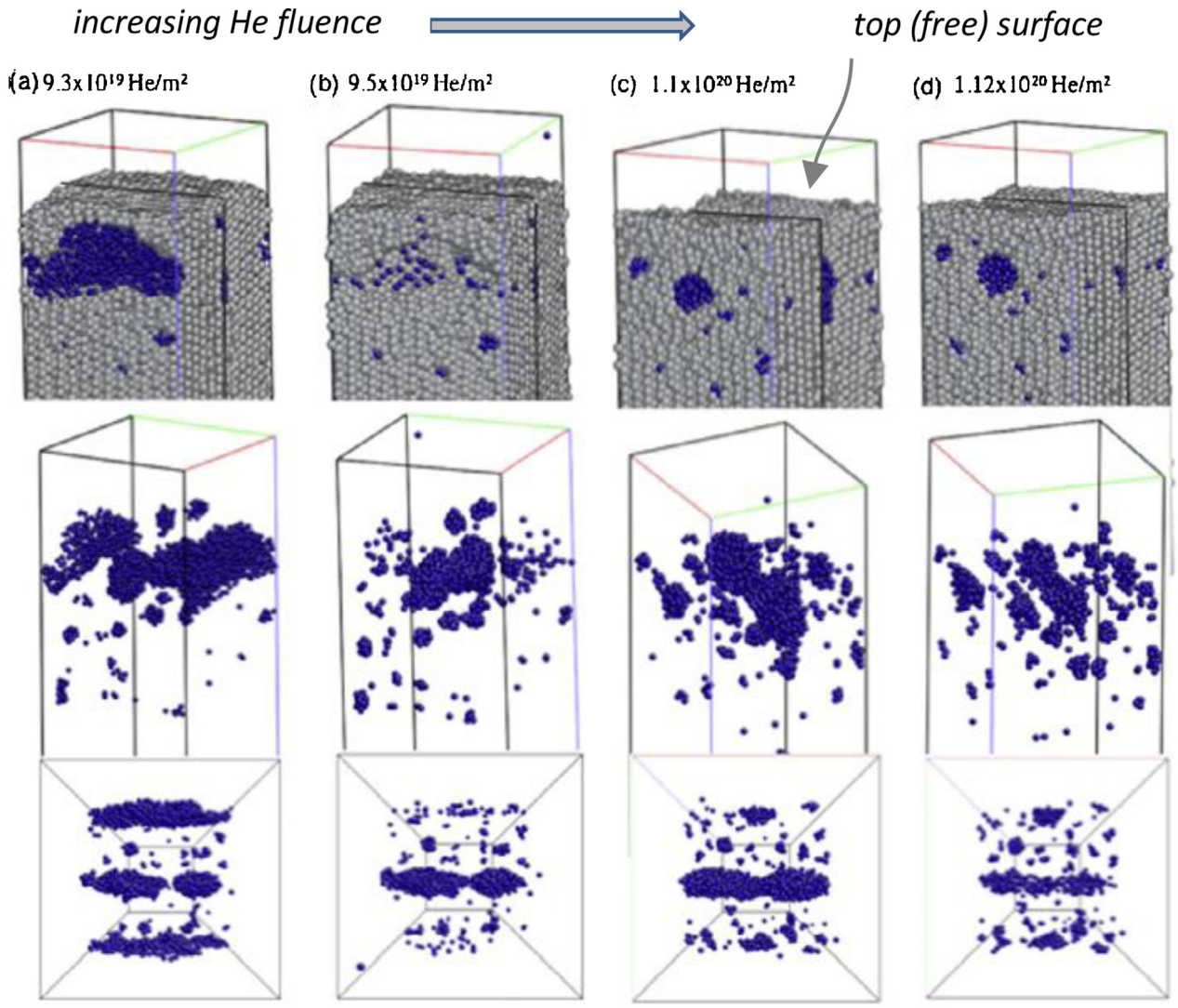

Fig. 1. Visualization of MD simulations of tungsten (light gray spheres) exposed to a 60 eV helium plasma implantation (blue or dark spheres are helium atoms), from Ref. [36] which gives a detailed explanation. (The web version of this article has a color figure.)

The first part of this paper expands upon the points above. The underlying theme is that the solutions for these issues will most likely come by developing materials and structures that have fine scale features such as nano-scale particles or small fibers as well as porosity in the PFM and fine scale coolant passages in the PFC substructure, and these structures may also require graded composition.

The underlying theme is the materials architecture and engineering structure that characterize these refractory PFCs. The second part of the paper discusses the directions in research and development that we believe are needed to make progress toward novel, engineered PFC solutions. Certainly progress is also necessary in confinement and power handling but these are not topics in this paper.

2. Plasma facing materials for a fusion reactor

Tungsten (W) or Carbon (C) are the leading choices for PFMs for FNSF and DEMO along with reduced activation ferritic steels (RAFS) for the first wall structure. With irradiation in a fusion neutron spectrum to 30 dpa, 10% of the W transmutes to Osmium. These transmutants, combined with the irradiation-induced defects produced, lead to significant tungsten embrittlement. Moreover the thermal conductivity, **k**, will drop by about half (based on irradiation data with Re) [10]. By 30 dpa, graphites begin to undergo significant dimensional changes with substantial swelling following the initial densification, along with a loss of mechanical integrity and decreases in thermal conductivity of as much as ~60%. Compared to nuclear graphite, the higher performance carbon fiber composites, which are typically considered for PFC applications will have significantly less lifetime, largely due to irradiation-induced dimensional instability [11]. With tungsten the threats of recrystallization and cracking are also concerns [12]. So the use of these materials in product forms in which they are currently available implies component lifetimes that would require replacement on a schedule that is unattractive for a commercial reactor.

The underlying constraints for this assertion about PFC lifetime are as follows and have been well summarized in the past [13–17].

1. The neutronics for tritium, specifically the fact that the flux of neutrons that transmute lithium to produce tritium decays rapidly with the radial distance beyond the first wall (FW), imposes a requirement that the FW in a breeding blanket are integral with the blanket structure rather than being a separately demountable structure.
2. Replacement of the FW requires removal of blanket modules and reinstallation of new modules.

3. Commercial fusion reactors will require a relatively high (>90%) plant availability.
4. The approaches to remote maintenance commonly adopted in design studies involve fairly cumbersome and time consuming procedures in which the first step is to warm the superconducting coils prior to the sector by sector removal of the blanket modules, each of which has piping that must be cut remotely and then rewelded. Certainly the procedures would be automated but even with well-established replacements this approach can be expected to take many months, and the need for robust PFCs with relatively long operating lifetimes in the range of 50–200 dpa has been cited in design studies [18–20], and world priorities are changing as in the EU emphasis and related choices for water-cooled PFCs in a near term DEMO [20].

Typically the larger design studies put forth approaches that include some optimism about the developments in technology but refrain from incorporating challenging technical leaps that as yet do not have a well-developed technical basis.

3. Cooling PFCs for a fusion reactor

An important objective in developing solid PFCs for an FNSF or DEMO is the capability for predictive modeling of efficient heat transfer and modeling of the combined stresses from high pressure gas cooling and thermal gradients. Our conception is that these PFCs will be cooled with helium (or CO_2) to be used with high efficiency power conversion systems. As noted earlier, cooling with an array of flow jets seems to be the best choice for efficient heat transfer at the cooled surface and has been the subject of development by EU and Russian collaborators [21] and others have also offered some simplifications of the designs that might be applied to cover a divertor and to integrated first walls [22].

An important step forward is to understand the engineering science of gas flow (CFD) at the flow conditions appropriate for fusion PFCs. Some early innovative approaches to flow used He in porous media with relatively short flow paths through porous media. However, the parametric approaches to model heat transfer were not successful for the conditions at high temperature, strong temperature gradients and high density. Subsequent Section 4.2 has more information on current approaches.

Thus there are opportunities for innovative technical advancements that may enable new approaches to PFCs and could radically affect how cooling is accomplished. One example is the development of junctions for superconducting magnets that would enable demountable toroidal field coils and the possibility that remote maintenance could be done with vertical access rather than by horizontal removal of sectors or sub-sectors. Such a development has a profound effect on what is possible for PFCs. The approach to materials and engineered structure in this paper is quite consistent with the novel design developed by MIT [8], which utilizes a unibody FW-blanket immersed in a liquid coolant and breeder.

4. PFC fabrication and advanced manufacturing

4.1. The PFM solution

The PFM, fabricated with an advanced manufacturing method, will likely have a graded composition and features such as fibers and nano-particles that can collect He and transmutation products in a way that maintains adequate robustness for a satisfactory lifetime. Recent laboratory experiments and computer modeling have clearly shown the significant effect of sub-surface helium bubble formation on surface modification of tungsten, as well as modifying the tritium trapping and permeation behavior.

Fig. 1 shows an example from molecular dynamics (MD) simulations by Wirth et al. [23]. This MD simulation shows progressive roughening of the free surface that begins with a flat (100) orientation and which is intersected by a Σ5 grain boundary.[2] The visualization shows helium gas bubble distributions beneath the surface as a function of increasing implanted helium dose (left to right). The top row, with both tungsten and helium atoms shown, shows substantial surface roughening on the surface around the boundary. The sub-surface helium bubble populations are more obvious in the second row of frames, which shows only helium atoms. The bottom row is a top–down perspective again with only the helium atoms shown.

The MD simulations indicate what is the likely precursor behavior for phenomena found in experiments with tungsten damaged by helium ions (or helium in combinations with other species). Pitted surfaces are observed below ~1000 K [24], whereas a "nanostructured," low-density "fuzz" or "coral" surface morphology is observed between approximately 1000 and 2000 K [25–27], while micron-sized holes, or pits, are observed to form above about 2000 K [28]. The nanostructured "fuzz" has also recently been observed in the divertor regions of a tokamak device operating with a helium plasma [29]. Such surface features could lead to changes in heat transfer, fuel (deuterium/tritium) retention, increased rates of erosion through both sputtering and dust formation, and embrittlement of the divertor, all of which can be detrimental to the plasma [30,31]. It is important to note that fuzz-like surface modification has not been observed for hydrogen-only plasma exposure, strongly indicating that helium implantation controls this phenomenon. Microstructural characterization [32,33] clearly implicates helium bubble formation as a key feature in this response of tungsten to low-energy plasma exposure involving helium. Such observations offer the possibility for a design approach for engineered PFCs in which diffusion paths on the order of hundreds of nanometers would be utilized to rapidly diffuse the implanted gas out of the PFC, or possibly to utilize interfaces to trap the helium and nucleate bubbles at such high density to limit the bubble growth below sizes required to substantially impact PFC performance.

4.2. The PFC solution

The term PFCs here includes divertors, specialized protection for RF launchers and the first wall (FW). As explained earlier, the FW must be integral with the blanket structure. This adds constraints for cooling the FW and blanket that differ from other PFCs. Another consequence of this integral structure is that a leak from a FW cooled by high pressure helium in the blanket would pressurize the blanket cavity.[3]

Youchison utilized CFD modeling from first principles for He flow with full fluid physics for an open-celled porous nuclear fuel and also applied this approach to fusion PFCs [34].

Motivation for a later study on jet flow came from earlier research on flow instabilities. Tests at Sandia of the thermal performance of refractory targets with He flow through porous media revealed unstable flow that had not been predicted in modeling [35]. The phenomenon occurred only at high heat loads and high He density and significant temperature gradients. The issue of concern was that the surface temperature increased on one channel as the cooling diminished and He flowed preferentially into the other channel. The threat is that runaway instabilities would produce melting and stress-induced cracking of armored plasma facing components under off-normal conditions, particularly in parallel

[2] Σ is a statistical measure equal to the reciprocal number of lattice atoms in coincidence across a grain boundary.

[3] This issue is not discussed further in this paper but has hug implications for safety, testing of blankets and provision for remote handling.

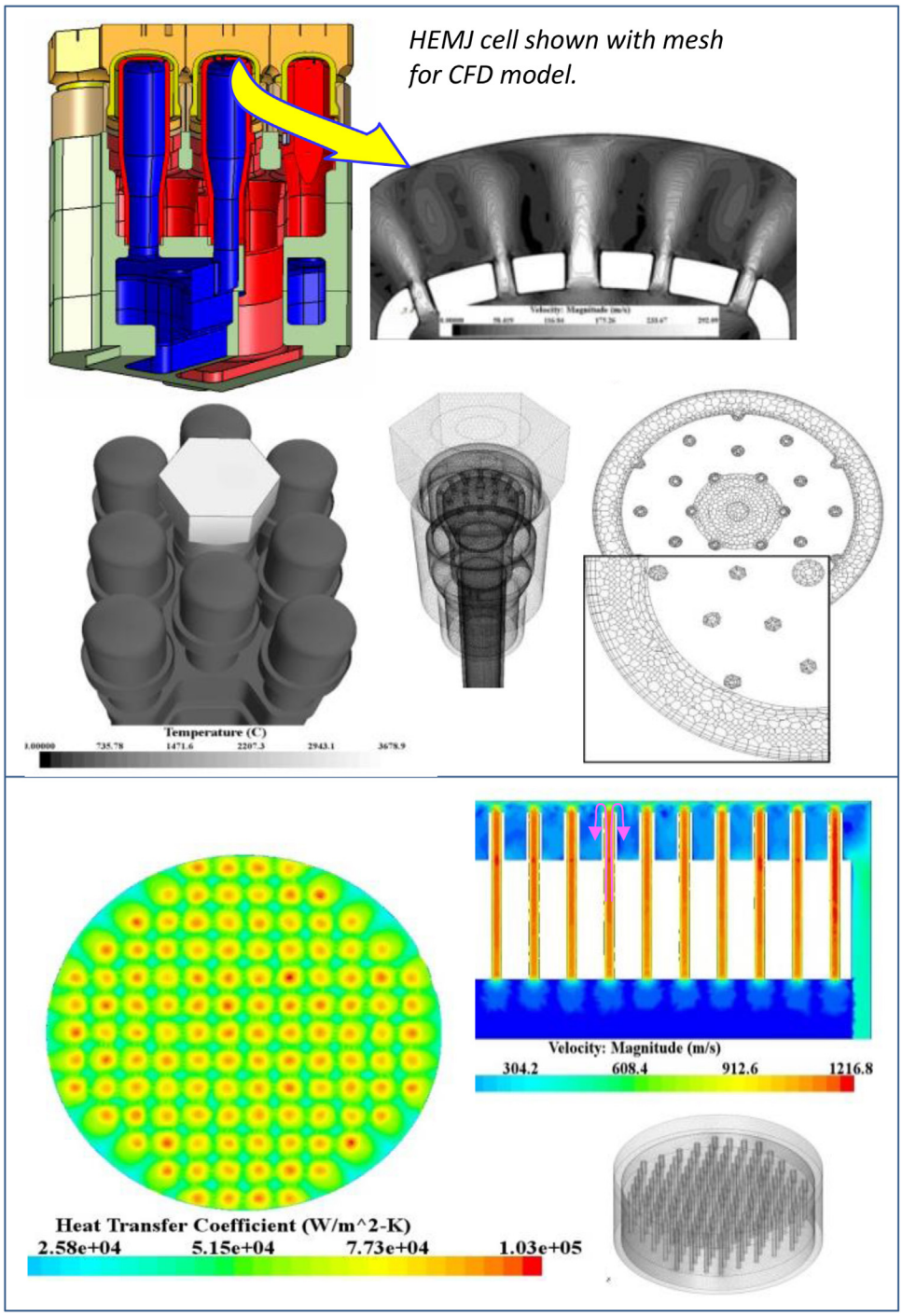

Fig. 2. HEMJ (figure with permission of Norijitra et al.) and results from Youchison's analyses comparing the variations in heat transfer coefficients for a coarse and fine array of flow jets, from Ref. [44].

channels or in porous media where bifurcation of the flow is possible.

Youchison then studied whether the flow instabilities seen in porous media would have similar deleterious effects on heat transfer in jet flow and used for this study what is currently the most developed refractory He-cooled divertor for DEMO, i.e., the HEMJ system started by Norajitra and others at the Karlsruhe Institute of Technology [21,36]. The HEMJ has had extensive R&D in materials, joining and fabrication as well as testing of the thermal performance of individual units and joined arrays in Russian facilities [37–41]. Fig. 2 shows the HEMJ along with results from several analyses. In addition to the work by Youchison noted here, researchers at the Georgia Institute of Technology performed CFD modeling and testing of a module with the configuration of the HEMJ [42,43].

In studying the He flow in the HEMJ, Youchison found jet flow less affected by flow instabilities and also showed that jet arrays on a finer scale provide more effective heat transfer [44]. He also succeeded in demonstrating in the modeling of the HEMJ the effect of the flow instabilities in jet flow. The high heat flux testing to date for the array with nine HEMJ cells has not revealed such flow instabilities; however the type of testing would not be likely to show

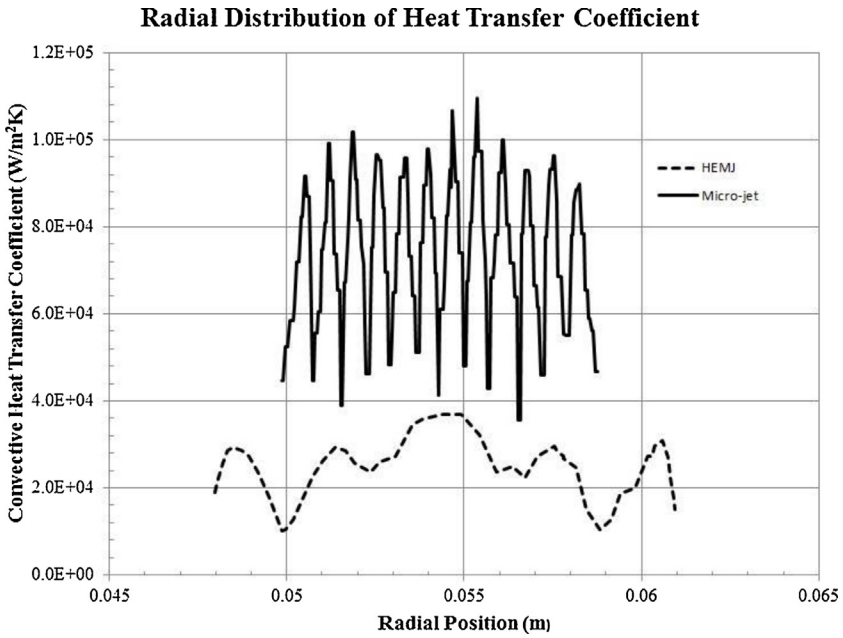

Fig. 3. Comparison of the global convective heat transfer coefficient of the fluid-cooled surface for the central 25 mm^2 region of the HEMJ cell and a micro-jet array with the heat load at the heat surface of 30 MW/m^2. Figure from Ref. [44].

this, e.g., uniform heat loads on all cells, and pressure measured only in the common manifolds.

A second objective in Youchison's studies was to explore the benefit of changing the scale of the jet array for the HEMJ. Youchison compared flow behavior and heat removal in an HEMJ cell, a similar area with much more dense micro-jet array and porous media under similar conditions. Fig. 3 from Ref. [44] compares the local heat transfer coefficients versus position for the HEMJ jet array and for an equivalent area with a denser array. To minimize the overlap of turbulence patterns between neighboring jets that can lead to areas where flow stagnates, the preferred structure for micro-jets is an array of nozzles.

An underlying premise here is that the refractory PFCs for a fusion reactor with solid walls will be engineered structures. These will have a materials architecture as noted previously and be He-cooled with high efficiency heat transfer and minimization of thermal stresses. Optimal heat removal will likely require features such as impinging jets in a fine array as noted previously. Realization of such PFCs requires advanced manufacturing methods, engineered materials and a new vision of the R&D path.

4.3. Advanced manufacturing of PFCs

Additive manufacturing (AM) comprises a number of techniques by which material is printed in 3-D directly from CAD models of a component. The process has many potential advantages for fusion components which include its wide flexibility and ability to form intricate parts (i.e. with micro-channels,) the ability to transition between materials perhaps minimizing the need for conventional joining, and the minimization of waste.

While this technology is relatively new and is in its infancy with regards to predicting the resulting structure-property relationships, it is now being applied to many high-value components. Most recently, General Electric made a step forward in announcing 3-D printed fuel nozzles for the Leap jet engine along with the recent ORNL demonstration of a Shelby Cobra with a frame made with AM. Currently a number of organizations are exploring turbine blade AM technology utilizing titanium aluminide powders.

The impressive progress in additive manufacturing provides a vision for future manufacturing of large parts, such as blanket modules or MIT's unibody blanket, and specifically the capability to generate engineering features on a small scale or to create a materials architecture that could be developed to mitigate the adverse effects from neutron and ion damage, transmutations, etc.

Current technology for micro-engineered mechanical systems (MEMS) such as lithography combined with advanced additive manufacturing can fabricate arrays with many hundreds of jets. Cooling high temperature refractories with helium will require strict control of oxygen and other impurities, so this is not an added requirement for manufacturing, and the use of 200 μm micro-jets is no more challenging than millimeter-size macro-jets, although clogging may be of more concern with the finer jets. Microelectronics and other applications have exploited micro-jet arrays. For example, micro-jet arrays in electronics are typically 100–500 μm in diameter with air cooling of copper or steel for actively cooled heatsinks for high power devices like Insulated Gate Bipolar Transistors (IGBTs) and Silicon-Controlled Rectifiers (SCRs) as well as other solid state switching devices like MOSFETS, JFETS and RF power transistors [45–48].

In the nearer term, we recommend that fusion programs invest in the development of PFCs (or probes, diagnostics, etc.) as a prudent approach for PFC development. Below are US examples to illustrate capabilities that additive manufacturing and other advanced manufacturing techniques.

Basic parameters are the size (area) and rate of deposition. Melting refractory materials such as tungsten will require high power. For fusion PFCs, the balance between printing speed, feature resolution and residual stresses that could promote cracking is an issue to be resolved in R&D. The literature has examples of very lightweight and strong (stiff) parts for aerospace, strongly blended compositions, complex bulk shapes such as engine blocks and integrated structures such as a robotic hand [49–51]. An example with appeal

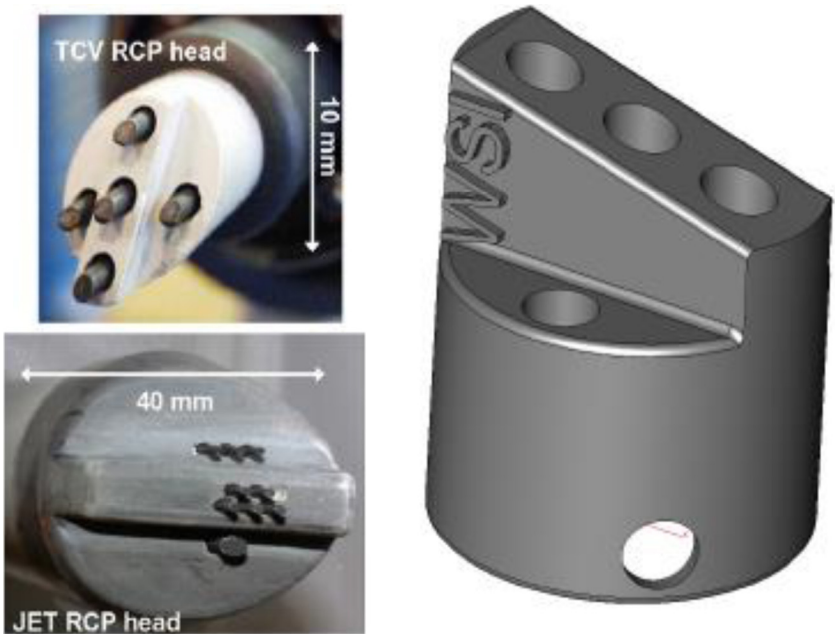

Fig. 4. Probe head made using AM; photo courtesy of Woodruff Scientific.

for enthusiasts of classic sports cars is a Shelby Cobra[4] built at the US Department of Energy's Manufacturing Demonstration Facility at ORNL using the Big Area Additive Manufacturing machine and displayed at the 2015 North American International Auto Show. ORNL is also strongly involved in magnetic fusion.

While AM has the potential for making large parts, e.g., fusion blanket modules, AM and other manufacturing processes also can produce smaller parts with the types of small scale features for cooling channels and materials architectures noted previously. Exploiting these techniques may be quite useful in the pathway for developing PFCs. Two examples of work related to fusion through proposals to DOE's Small Business Innovative Research program are given below.

The first is a small business, Woodruff Scientific. Under their initial grant from DOE, Woodruff designed prototypes of several fusion diagnostics [52], such as the probe head in Fig. 4, and compared estimated costs for conventional manufacturing with those for AM of parts for magnetic field coil diagnostics, a Rogowski coil, JET Langmuir probe, HeNe interferometer, CO2 interferometer, CO2 polarimeter, microwave reflectometer, Yag and ruby Thomson scattering systems, inverse Compton system, visible spectrometer, bolometer and scintillators. Their focus was the impact that AM can have on the costs of various plasma diagnostics with lower cost of materials due to (a) little to no waste, (b) less material in engineered systems, (c) reduced cost for assembly by combining subcomponents into a monolithic part often with no post-processing needed, and (d) precision in planning of fabrication. Other benefits are a flexible approach to complexity, e.g., cooling channels for PFCs, can be incorporated easily at little or cost and that needs for alignment or calibration can be reduced because the systems have fewer separate pieces. Other cost reductions relate to exploiting AM design tools that allow standard components to be customized through web-interfaces and scripting interfaces for online engineering design tools. In their follow-on (Phase II) effort, Woodruff will exploit advances in AM using novel materials, multi-materials, and easier tolerances required for manufacture, and continue their design effort on diagnostic systems and winnow the choices to items that will proceed to fabrication.

Another process lending itself to mass production is the so-called Spark Plasma Sintering (SPS) process. It is also referred to as Field Assisted Sintering Technology (FAST). The essence of this technique is that current is passed through the object being processed and the die in which it is held under stress. Process temperature is achieved through ohmic heating of the die and the part. For most materials SPS/FAST is identical to hot-pressing with the important difference there is no furnace to heat or cool allowing for a significant increase in throughput, and fast thermal cycles impede intermetallic formation. Also, the process lends itself to more precise microstructural control as a wider range of thermal history is achievable (more flexibility on heat-up and cool-down).

In spark sintering the pressure that the dies and containment can withstand limits the size of parts. In his facility at the Applied Research Lab (Penn State), Singh and co-workers have three Field Assisted Scintering Systems. The largest, shown in Fig. 5, is an industrial scale with a 340 ton press, pulsed currents to 10 kA and a temperature range from RT to 2400 °C and maximum part diameter of 340 mm. They can make parts larger than a DIII-D tile and have submitted a proposal for making PFCs [53].

For tungsten PFM's or engineered structures grading from tungsten to some underlying structure very high deposition energies are required requiring such techniques as Direct Metal Laser Sintering™ with high powered lasers. Recently, an electron beam ARCAM™ system was used to explore the melt kinetics of tungsten powers, whereby thin (~1.2 mm) powder layers were deposited and successively melted by rastered electron beam [54]. Similarly, a femtosecond laser was applied to iron and tungsten powders similarly demonstrating melt [55]. However, at this point no demonstration of a fully dense transition to steel has been made, with or without micro-channel cooling channels that should be achievable with commercial additive manufacturing systems.

[4] ORNL web news has information and a video of the production sequence of the Shelby Cobra on: http://web.ornl.gov/sci/manufacturing/media/news/detroit-show/

5. Discussion, conclusions and closing remarks

The basic premise supported in this paper is that PFCs for a fusion reactor will be engineered components with likely feature sizes that require advanced manufacturing methods. This view has several impacts.

5.1. PFM and PFC modeling and performance

First let us note an aspect of this approach that gives some additional freedom in the pathways forward but also brings a huge challenge. With this approach, we can separate the PFM layer from the engineered structure below it in our nearer term R&D. More specifically, the ability to design and produce structures layer by layer means that we can (a) tailor the architecture of the PFM layer(s) to be geared for performance that mitigates issues associated with ion implantation, formation of helium bubbles and tritium retention for the PFM Solution, and (b) separately design any necessary transition layers and, below those, a substructure with micro-features for cooling for the PFC Solution. While a concern for long term neutron damage still exists for the PFM, the solution for robustness of the PFM can be somewhat different than that for the substructure. For example, the basic requirement for the strength of the material may be drastically reduced. Nor is the radiation damage now a feature of a "bulk material" in a thick armor. A parallel logic applies to the engineered substructure of the PFC. The requirements, for example, those for strength and for resistance to tritium permeation, will likely differ from the PFM.

Close collaboration between modelers and experimenters is tremendously important. This means not just that modelers use experimental data, but that modeling is a tool both for identifying needs for data and for designing experiments, e.g., what can and should be measured. Testing then has the roles of scoping studies to identify issues empirically and iterative tests cycles that provide benchmark data for models. Recent examples of success in this coupled modeling and experiment inter-comparison by Wirth et al. [56], along with modeling developments as part of the Scientific Discovery through Advanced Computing (SciDAC) program provide examples of a paradigm shift in the coupling of modeling to experiments which we believe is now gaining maturity sufficient to utilize the multiscale models directly as part of the engineering design process of advanced PFCs.

Fig. 5. Industrial scale hot press used for Field Assisted Scintering at the Applied Research Lab at Penn State University.

While the decoupling of the PFM from the structure below it may simplify its path for development in the initial stages, the approach overall of an engineered structure for PFCs brings several complications. With the number of tools available in designing the architecture of the PFM (e.g., nano-porosity to promote the escape of helium and tritium, or nano-structures to confine helium that migrates to gain boundaries and gradients in composition), plus those for any transition layers and the interfacial connections to the engineered substructure, the number of possible variables for our engineered PFC is huge. This presents formidable challenges in obtaining appropriate data on radiation effects, developing any predictive capability to model performance, and converging on workable PFCs in a reasonable time and with reasonable cost.

The cooled substructure, although not subject to ion damage and the implantation of D, T and helium, nevertheless will suffer neutron damage, including transmutations, which affect thermal and mechanical properties as well as tritium permeation. Also, the CFD modeling of designs with small-scale cooling channels will require validation with testing to generate benchmark data.

The elements suggested here for a new vision of PFMs and PFCs are not yet accepted. We are recommending that fusion programs seriously explore the ideas put forth here and we suggest related near-term tasks.

5.2. Recommendations for near term work on PFMs

An important objective for PFMs is the capability for predictive modeling of performance and generation of data to benchmark the models. A corollary in this approach is the utility of surrogate materials in both modeling and testing that will advance the modeling even if these are not appropriate for end use in a PFC. To this end we suggest the tasks below.

- Use experts in materials and PSI and identify materials architectures and options for PFMs for DEMO or FNSF.
- Use materials experts and identify fabrication methods for FNSF and for DEMO.
- Identify materials (surrogates as needed) to validate models and for use testing in off-line facilities as well as exposures in confinement experiments, e.g., DIII-D, NSTX-U for the US and other devices.

5.3. Recommendations for near term work on PFCs

An important objective for PFCs is the capability for predictive modeling of efficient heat transfer and modeling of the combined stresses from high pressure gas cooling and thermal gradients. The near term goal is to investigate how much the advantages of a such a heat removal scheme, that can be fabricated only with advanced manufacturing techniques, can be realized within the requirements of (a) divertors, or protection such as poloidal limiters or guards for RF structures, and (b) first walls that have an integral structure with breeding blankets. The first step is to understand the engineering science in fluid flow (CFD) as applied to the complex array of interlaced coolant passages that are needed to place the flow jets close to the heat transfer surface while also providing an interlaced exhaust network. Again well-coordinated modeling and testing are needed, and surrogate materials in testing that will advance the fluid modeling are useful even if these are not appropriate for end use in a PFC. And we may be able to fabricate test targets more easily with spark sintering than with additive manufacturing. Suggested near-term tasks are:

- Design and refine the unit cell for a cooling structure with a microjet array and inlet and outlet channels and perform CFD modeling, and design a test with sufficient pressure and temperature gradients for appropriate fluid behavior but not necessarily high temperature.
- Identify development partners (e.g., SBIR companies in the US) and fabricate a module with one or more unit cells.
- Develop an initial test program with interested partners, perhaps as an international collaboration, and test the first microjet module.

5.4. Closing remarks

Plasma facing materials (PFMs) made of homogeneous C or W would have insufficient lifetimes in the extreme fusion environment to be useable for FNSF or DEMO. Extending the useful lifetime will require a suitable architecture that will likely include features like graded composition, nanostructures, and controlled porosity. An integrated PFC will also require transition layers to minimize stresses and small scale coolant passages. We in fusion need to revise our vision of PFMs and PFCs and extract new critical elements that enable us to identify appropriate research goals, investments in facilities and people, and appropriate decision points and metrics.

Let us be clear in closing that the vision and approach put forth in this paper comes from the authors and is not currently a part of the US fusion program as articulated by the Office of Fusion Energy Sciences (OFES, under the United States Department of Energy, Office of Science) nor is it endorsed by them. A white paper with this theme was presented at the FES Plasma Materials Interaction Workshop held in May 2015 that solicited input from the US fusion community for planning activities to be carried out by that office. A report on this workshop was posted in August 2015 on the US Burning Plasma Organization website listed below.

https://www.burningplasma.org/activities/?article=Plasma-Materials%20Interactions

References

[1] M.S. Tillack, X.R. Wang, S. Malang, F. Najmabadi, the ARIES Team, Fusion Sci. Technol. 64 (3) (2013) 427–434.
[2] A.R. Raffray, L. El-Guebaly, T. Ihli, S. Malang, X. Wang, the ARIES-CS Team, Engineering design and analysis of the ARIES-CS power plant, Fusion Sci. Technol. 54 (October (3)) (2008) 725–746.
[3] (a) D. Maisonnier, D. Campbell, I. Cook, et al., Power plant conceptual studies in Europe, Nucl. Fusion 47 (2007) 1524–1532;
D. Maisonnier et al., A Conceptual Study of Commercial Fusion Power Plants: Final Report of the European Fusion Power Plant Conceptual Study (PPCS),"EFDA report number EFDA(05)-27/4.10, 2005.
[4] G. Federici, R. Kemp, D. Ward, C. Bachmann, T. Franke, S. Gonzalez, C. Lowry, M. Gadomska, J. Harman, B. Meszaros, C. Morlock, Overview of EU DEMO design and R&D activities, Fusion Eng. Des. 89 (2014) 882–889.
[5] J. Menard, et al., Studies of ST-FNSF mission and performance dependence on device size, in: 1st IAEA DEMO Programme Workshop, Los Angeles, CA, 15–18 October, 2012.
[6] Y.K.M. Peng, et al., Fusion nuclear science facility (FNSF) before upgrade to component test facility (CTF), Fusion Sci. Technol. 60 (2011) 441.
[7] R.D. Stambaugh, V.S. Chan, A.M. Garofalo, M. Sawan, D.A. Humphreys, L.L. Lao, et al., Fusion nuclear science facility candidates, Fusion Sci. Technol. 59 (2011) 279–307.
[8] B.N. Sorbom, J. Ball, T.R. Palmer, F.J. Mangiarotti, J.M. Sierchio, P. Bonoli, et al., ARC: A compact, high-field, fusion nuclear science facility and demonstration power plant with demountable magnets, (2014) arXiv preprint arXiv:1409.3540.
[9] Y.T. Song, S.T. Wu, J.G. Li, B.N. Wan, Y.X. Wan, Peng Fu, Min You Ye, et al., Concept design of CFETR tokamak machine, IEEE Trans. Plasma Sci. 42 (3) (2014) 503–509.
[10] L.R. Greenwood, F.A. Garner, Transmutation of Mo, Re, W, Hf, and V in various irradiation test facilities and STARFIRE, J. Nucl. Mater. 212–215 (1994) 635–639.
[11] L.L. Snead, T.D. Burchell, Y. Katoh, Swelling of nuclear graphite and high quality carbon, J. Nucl. Mater. 381 (2008) 55–61.
[12] H. Greuner, H. Maier, M. Balden, Ch. Linsmeier, B. Böswirth, S. Lindig, P. Norajitra, S. Antusch, M. Rieth, Investigation of European tungsten materials exposed to high heat flux H/He neutral beams, J. Nucl. Mater. 442 (2013) S256–S260.
[13] M. Abdou, et al., Modeling, analysis and experiments for fusion nuclear technology, Fusion Eng. Des. 6 (2008) 3–64.
[14] M. Abdou, P. Gierszewski, M. Tillack, D. Sze, J. Bartlit, et al., Technical Issues and Requirements of Experiments and Facilities for Fusion Nuclear Technology, (FINESSE Phase I Report), Rep. PPG-909, UCLA-ENG-85-39, Univ. of California, Los Angeles, 1985.
[15] M. Abdou, P. Gierszewski, M. Tillack, M. Nakagawa, J. Reimann, et al., Technical issues and requirements of experiments and facilities for fusion nuclear technology, Nucl. Fusion 27 (4) (1987) 619–688.
[16] M. Abdou, The APEX TEAM, A. Ying, N. Morley, K. Gulec, S. Smolentsev, M. Kotschenreuther, S. Malang, et al., On the exploration of innovative concepts for fusion chamber technology, Fusion Eng. Des. 54 (2016) 181–247.
[17] L.M. Waganer, R.J. Peipert, Jr., X.R. Wang, S. Malang, ARIES Team, ARIES-CS maintenance system definition and analysis, Fusion Sci. Technol. 54 (3) (2008) 787–817.
[18] S.J. Zinkle, J.T. Busby, Structural materials for fission & fusion energy, Mater. Today 12 (11) (2009) 12–19.
[19] M. Rieth, J.L. Boutard, S.L. Dudarev, T. Ahlgren, S. Antusch, N. Baluc, et al., Review on the EFDA programme on tungsten materials technology and science, J. Nucl. Mater. 417 (2011) 463–467.
[20] D. Stork, P. Agostini, J.L. Boutard, D. Buckthorpe, E. Diegele, S.L. Dudarev, C. English, et al., Developing structural high-heat flux and plasma facing materials for a near-term DEMO fusion power plant: the EU assessment, J. Nucl. Mater. 455 (1) (2014) 277–291.
[21] P. Norajitra, et al., He-cooled divertor for DEMO: experimental verification of the conceptual modular design, Fusion Eng. Des. 81 (2006) 341–346.
[22] M.S. Tillack, A.R. Raffray, X.R. Wang, S. Malang, S. Abdel-Khalik, M. Yoda, D. Youchison, Recent US activities on advanced He-cooled W-alloy divertor concepts for fusion power plants, Fusion Eng. Des. 86 (2011) 71–98.
[23] B.D. Wirth, K.D. Hammond, S.I. Krashenninikov, D. Maroudas, Challenges and opportunities of modeling plasma-surface interactions in tungsten using high-performance computing, J. Nucl. Mater. 463 (2015) 30–38.
[24] H. Iwakiri, K. Yasunaga, K. Morishita, N. Yoshida, Microstructure evolution in tungsten during low-energy helium ion irradiation, J. Nucl. Mater. 283–287 (2000) 1134–1138.
[25] S. Takamura, N. Ohno, D. Nishijima, S. Kajita, Formation of nanostructured tungsten with arborescent shape due to helium plasma irradiation, Plasma Fusion Res. 1 (2006), 051.
[26] M.J. Baldwin, R.P. Doerner, Helium induced nanoscopic morphology on tungsten under fusion relevant plasma conditions, Nucl. Fusion 48 (2008), 035001.
[27] M.J. Baldwin, R.P. Doerner, D. Nishijima, K. Tokunaga, Y. Ueda, The effects of high fluence mixed-species (deuterium, helium, beryllium) plasma interactions with tungsten, J. Nucl. Mater. 390–391 (2009) 886–890.
[28] D. Nishijima, M.-Y. Ye, N. Ohno, S. Takamura, Formation mechanism of bubbles and holes on tungsten surface with low-energy and high-flux helium plasma irradiation in NAGDIS-II, J. Nucl. Mater. 329–333 (2004) 1029–1033.
[29] G.N. Wright, D. Brunner, M.J. Baldwin, R.P. Doerner, B. Lipschultz, J.L. Terry, D.G. Whyte, Tungsten nano-tendril growth in the Alcator C-Mod divertor, Nucl. Fusion 52 (2012) 042003.
[30] M.J. Baldwin, R.P. Doerner, W.R. Wampler, D. Nishijima, T. Lynch, M. Miyamoto, Effect of He on D retention in W exposed to low-energy, high-fluence (D, He, Ar) mixture plasmas, Nucl. Fusion 51 (2011) 103021.
[31] G. Federici, C.H. Skinner, J.N. Brooks, J.P. Coad, C. Grisolia, A.A. Haasz, A. Hassanein, V. Philipps, C.S. Pitcher, J. Roth, W.R. Wampler, Plasma-material interactions in current tokamaks and their implications for next step fusion reactors, Nucl. Fusion 41 (2001) 1967.
[32] S. Kajita, S. Takamura, N. Ohno, D. Nishijima, H. Iwakiri, N. Yoshida, ub-ms laser pulse irradiation on tungsten target damaged by exposure to helium plasma, Nucl. Fusion 47 (2007) 1358–1366.
[33] M. Miyamoto, D. Nishijima, M.J. Baldwin, R.P. Doerner, Y. Ueda, K. Yasunaga, N. Yoshida, K. Ono, Microscopic damage of tungsten exposed to deuterium–helium mixture plasma in PISCES and its impacts on retention property, J. Nucl. Mater. 415 (2011) S657–S660.
[34] D. Youchison, M. Ulrickson, J. Bullock, Predictions of critical heat flux in plasma facing components using computational fluid dynamics, Fusion Sci. Technol. 60 (1) (2011) 177–184.
[35] D.L. Youchison, Flow instabilities in a multi-channel, helium-cooled, porous metal divertor module, Fusion Eng. Des. 49–50 (2000) 407–415.
[36] M. Rieth, S.L. Dudarev, S.M. Gonzalez de Vicente, J. Aktaa, T. Ahlgren, S. Antusch, D.E.J. Armstrong, et al., Recent progress in research on tungsten materials for nuclear fusion applications in Europe, J. Nucl. Mater. 432 (2013) 482–500.
[37] S. Antusch, L. Commin, M. Mueller, V. Piotter, T. Weingaertner, Two component tungsten powder injection molding—an effective massproduction process, J. Nucl. Mater. 447 (2014) 314–317.
[38] P. Norajitra, A. Gervash, R. Giniyatulin, T. Hirai, G. Janeschitz, W. Krauss, V. Kuznetsov, et al., Helium-cooled divertor for DEMO: manufacture and high heat flux tests of tungsten-based mock-ups, J. Nucl. Mater. 386 (2009) 813–816.
[39] P. Norajitra, R. Giniyatulin, V. Kuznetsov, I.V. Mazul, G. Ritz, He-cooled divertor for DEMO: status of development and HHF tests, Fusion Eng. Des. 85 (10) (2010) 2251–2256.
[40] G. Ritz, T. Hirai, J. Linke, P. Norajitra, R. Giniyatulin, L. Singheiser, Post-examination of helium-cooled tungsten components exposed to DEMO specific cyclic thermal loads, Fusion Eng. Des. 84 (7) (2009) 1623–1627.

[41] S. Košmrlj, B. Koncar, Transient analysis of the divertor cooling finger subjected to high cyclic surface heatin, Proc. Int. Conf. Nuclear Energy for New Europe (2011) 12–15.
[42] M. Yoda, S.I. Abdel-Khalik, D.L. Sadowski, B.H. Mills, J.D. Rader, Experimental evaluation of the thermal hydraulics of helium-cooled divertors, Fusion Sci. Technol. 67 (2015) 142.
[43] B.H. Mills, B. Zhao, S.I. Abdel-Khalik, M. Yoda, An experimental study of the helium-cooled modular divertor with multiple jets at nearly prototypical conditions, Fusion Sci. Technol. 68 (3) (2015), in press.
[44] D.L. Youchison, Flow instabilities in non-uniformly heated helium jet arrays used for divertor PFCs, Fusion Sci. Technol. 68 (3) (2015).
[45] M.R. Overholt et al., Micro-Jet Arrays for Cooling of Electronic Equipment, 3rd Intl. Conf. on Microchannels and Minichannels, Toronto, Canada, June 13–15, Part B, 249–252, ASME, 2005.
[46] M.L. Griffith, et al., Understanding thermal behavior in the LENS process, Mater. Des. 20 (1999) 107–113.
[47] D.M. Keicher et al., Using the Laser Engineered Net Shaping (LENS) Process to Produce Complex Components from a CAD Solid Model, SPIE 2993 91, 1997.
[48] S.M. Gaytan, L.E. Murr, F. Medina, E. Martinez, M.I. Lopez, R.B. Wicker, Advanced metal powder based manufacturing of complex components by electron beam melting, Mater. Technol.: Adv. Perform. Mater. 24 (3) (2009) 180–190.
[49] The Economist, The Printed World: Three-dimensional Printing from Digital Designs, 10 February, 2011 www.economist.com/node/18114221.
[50] M. LaMonica, Additive Manufacturing, MIT Technology Review, 23 April 2013.
[51] NIST, Roadmapping Workshop, 2012 http://events.energetics.com/NISTAdditiveMfgWorkshop/downloads.html.
[52] S. Woodruff, J.E. Stuber, S. Diesburg, B. Utela, D. Lemmon, N.K. Hicks, C.A. Romero-Talamás, Additive manufacture of plasma diagnostics Work, 2015.
[53] A. Rape, S. Chanthapan, J. Singh, A. Kulkarni, Engineered chemistry of Cu-W composites sintered by field-Assisted sintering technology for heat sink applications, J. Mater. Sci. 46 (2011) 94–100.
[54] E.K. Ohriner, R. Dehoff, L.L. Snead, Electon-beam Additive Manufacturing of Tungsten Materials for Fusion, Fusion Reactor Materials Program. June 30, 2013. DOE/ER-0313/54, 2013, pp. 114–116.
[55] B. Nie, L. Yang, H. Huang, S. Bai, P. Wan, J. Liu, Femtosecond laser additive manufacturing of iron and tungsten parts, Appl. Phys. A: Mater. Sci. Process. (March) (2015), http://dx.doi.org/10.1007/s00339-015-9070-y.
[56] B.D. Wirth, X. Hu, A. Kohnert, D. Xu, Modeling defect cluster evolution in irradiated structural materials: Focus on comparing to high-resolution experimental characterization studies, J. Mater. Res. 30 (2015) 1440–1455.

D.15 Additive Manufacturing and Monolithic Interferometry - University of Washington Subcontract

D.15.1 Motivation of Concept

Additive manufacturing (AM) is a rapidly-evolving industry. It offers a manufacturing process by which material is added, typically layer-by-layer, to produce the final part. 3D printing is a common example of AM: two common types available at low cost are thermoplastic extrusion (PLA, ABS plastics) and laser sintering. 3D printers accept solid-surface model files (STEP, STL), produced by a CAD design program such as SolidWorks or Autodesk Inventor. The printing firmware decides the internal structure of the part using the surfaces as boundary conditions, as well as the printing process details, such as the amount of material to be consumed, the tool path (in the case of extruded plastic), and thus the total print time. As the part is designed using CAD software suites, and manufactured with an additive process, complexity comes free. That is, an increase in part complexity will not result in an disproportionate increase in part cost.

Plasma devices offer extreme environments, which often necessitate complicated diagnostic designs that are even more often unique to the limitations of the specific experiment, and on top of that no two experimental plasma devices are exactly alike. Differences in, for example, space available for diagnostic, angle of view to the plasma, plasma density, temperature, and magnetic field, will all provide design limitations unique to the device. Figure D.1 is a good example of AM overcoming an obstacle with ease: a CF mirror mount that holds the mirror exactly perpendicular to the CF window, is height and rotationally-adjustable, and has the capabilities of the two kinematic adjusters inherent to the commercial mirror from THORLABS. AM can offer rapidly-prototyped, increasingly complicated solutions to such limitations (such as figure D.1), and furthermore do not require experienced staff to implement.

D.15.2 Additive manufactured unequal path length, heterodyne interferometer

The compact, isolated nature of the optomechanical pieces in the unequal path length, heterodyne interferometer lends well to monolithic replication (figure D.2). The Monolithic, Unequal Path Length Interferometer (MUPLI) was modeled using Autodesk Inventor, and the mirror faces were aligned using constrictions on construction planes. The angles of the construction planes were manually calculated, propagating from the separation angle of the AOM crystal (figure D.3. The end result is that the pieces seen in figure D.2 can be dragged around by the user, and the alignment remains preserved. This will enable the most compact design, for a two-dimensional optical plane.

The foremost benefit to a AM monolithic interferometer is that the alignment is preserved; there is little to nothing to adjust. Not everything is printed: pieces such as the light source, mirrors and beamsplittters would still come from conventional suppliers. However, the end-user would simply insert the mirrors into the non-adjustable mounts, and the device would be aligned, removing the need for skilled optomechanical time. This removes cost, and not just labor costs, but also component costs. Another benefit to a monolithic interferometer is its capability for expansion. Adding more chords to the diagnostic needs only the time spent with CAD model, and the cost of extra mirrors, and a new print. The laser-sintered 3D printing process provided by ShapeWays was selected as the print provider. The initial design seen in figure D.2 was larger than the upper threshold of ShapeWays' print volume. Therefore, it was decided that a Proof-of-Principle (PoP) design showcasing a working, simple, 3D-aligned, Michelson interferometer would be a cost-efficient endeavor.

D.15.3 Proof-of-Principle interferomter

The first attempt at creating a working monolithic interferometer is seen in figure D.4. This designed failed, as contraction in the printed plastic caused the component mounts to deviate from their press-fit dimensions; some of the mirrors didn't fit. Modifications were made to attempt to fit the mirrors properly, but for a HeNe the room for error is little to none.

Figures D.5 through D.8 display attempts made to compensate for the contraction in the printed mirror mounts. These various standardized mount designs were printed with a varying amount of material surrounding the mount itself. The deviation in mount diameter printed versus diameter specific in Inventor was measured, and incorporated into the CAD model.

The second attempt at a working monolithic interferometer is seen in figure D.9. As you can see, the new mounts were implemented, and they served their function well: the mirrors made a solid, press-fit connection. However, this design failed since another contraction made itself evident: contraction in the lone vertical extension opposite the beamsplitter.

Figure D.10 was the third and final iteration attempting to achieve interference. The vertical extension was stabilized against the beamsplitter mount section, this appeared to be successful. Another design implemented was a beam expansion cavity that expanded the beam by a factor of ten. This allowed the widened laser to hit every mirror (figure D.11), however the design still failed to achieve any indication of interference.

D.15.4 Discussion and Future Work

Even though the third iteration was successful in guiding the laser to each mirror face, the design ultimately failed on a conceptual level. The miniscule étendue of a HeNe laser makes it highly sensitive to any spatial deviations. The only way to make the design work would be to add adjustable components, either commercial or custom. However, this would mean that the interferomter needs to be aligned, which defeats the original purpose of ingrained laser alignment. Some ideas for a PoP design using a single adjustable beamsplitter mount can be seen in figures D.12 and D.13.

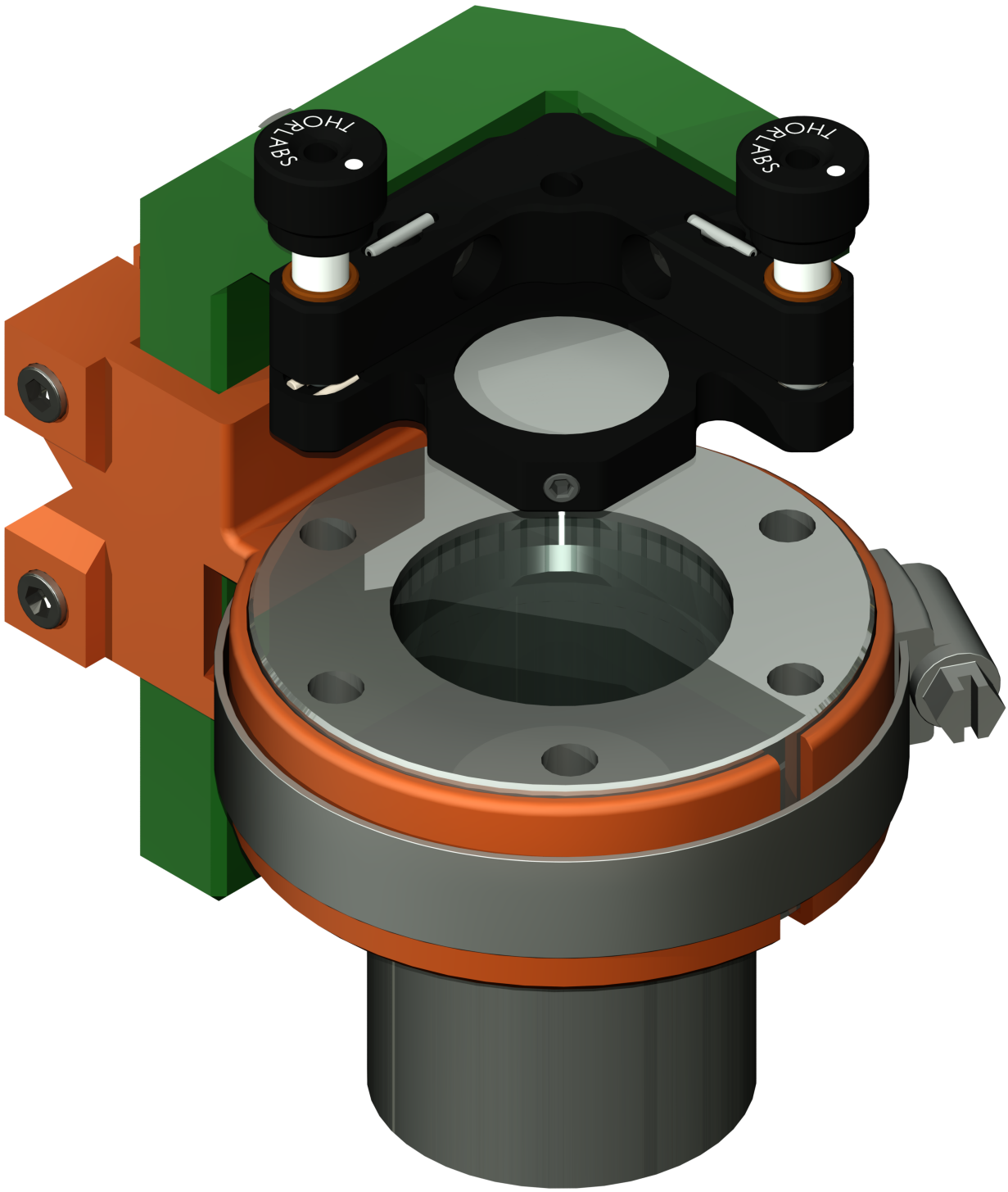

Figure D.1: ConFlat optical mount

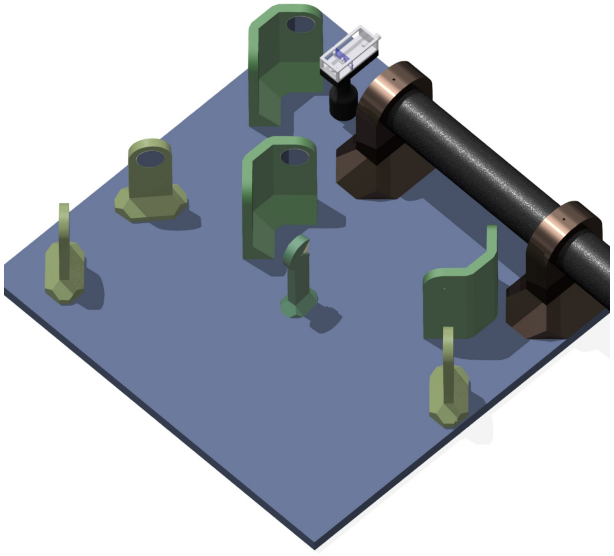

Figure D.2: Monolithic, Unequal Path Length Interferometer (MUPLI) was initially going to replicate the UW interferomter

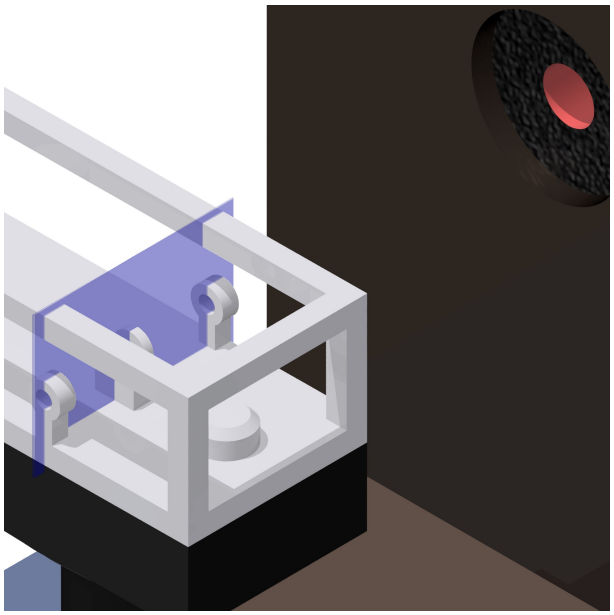

Figure D.3: Bragg separation planes of the AOM seen accurately represented via the visible construction planes.

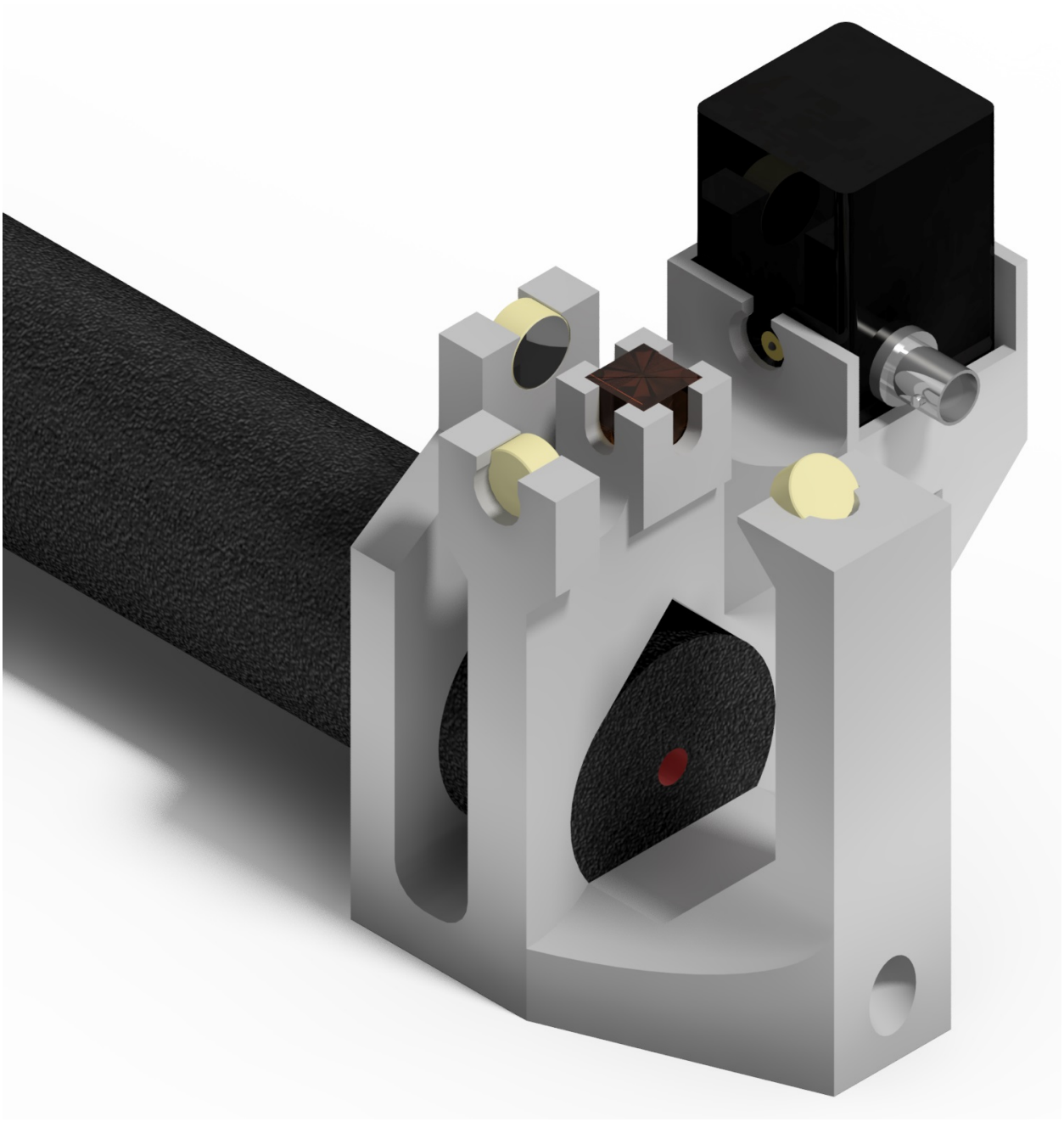

Figure D.4: Micro-Michelson: V1 design. The initial 3-D design. This did not have the print accuracy to guide laser properly to the recombination beamsplitter.

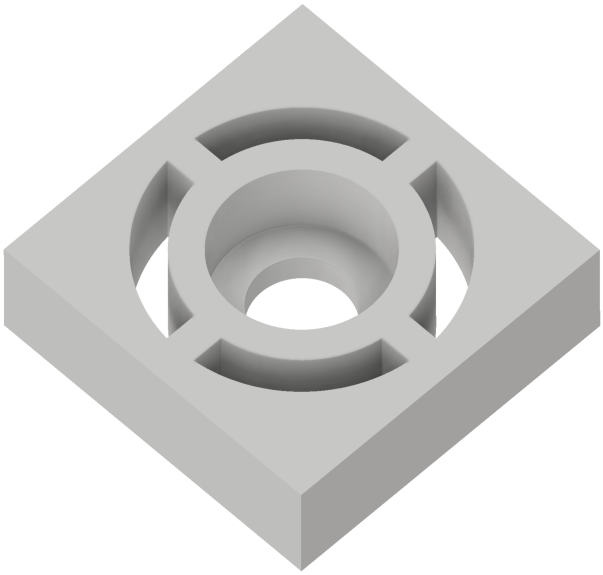

Figure D.5: Contraction testing: Round mount with minimal surrounding material

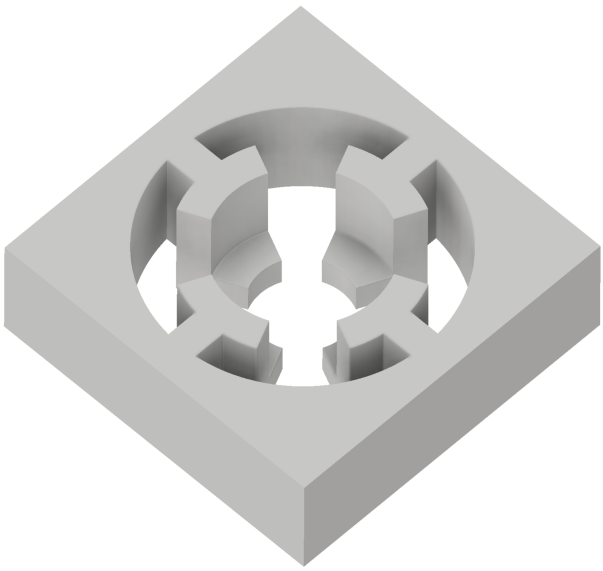

Figure D.6: Contraction testing: Discrete mount with minimal surrounding material

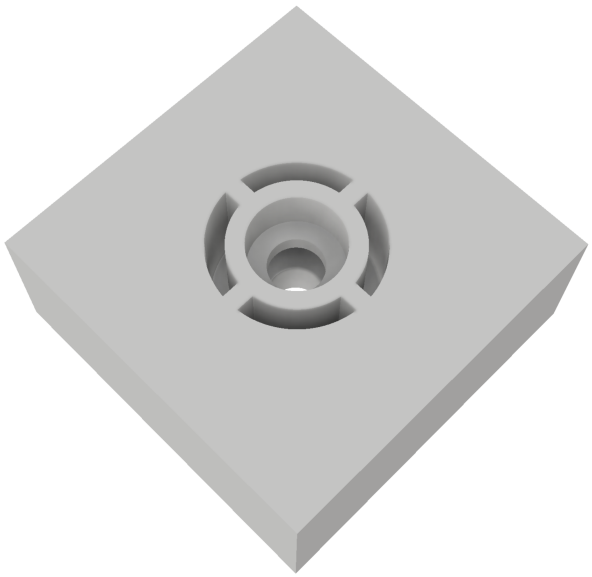

Figure D.7: Contraction testing: Round mount with excessive surrounding material

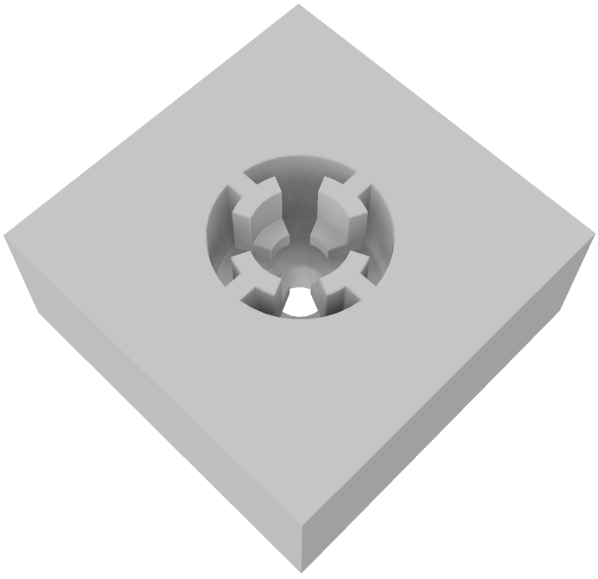

Figure D.8: Contraction testing: Discrete mount with excessive surrounding material

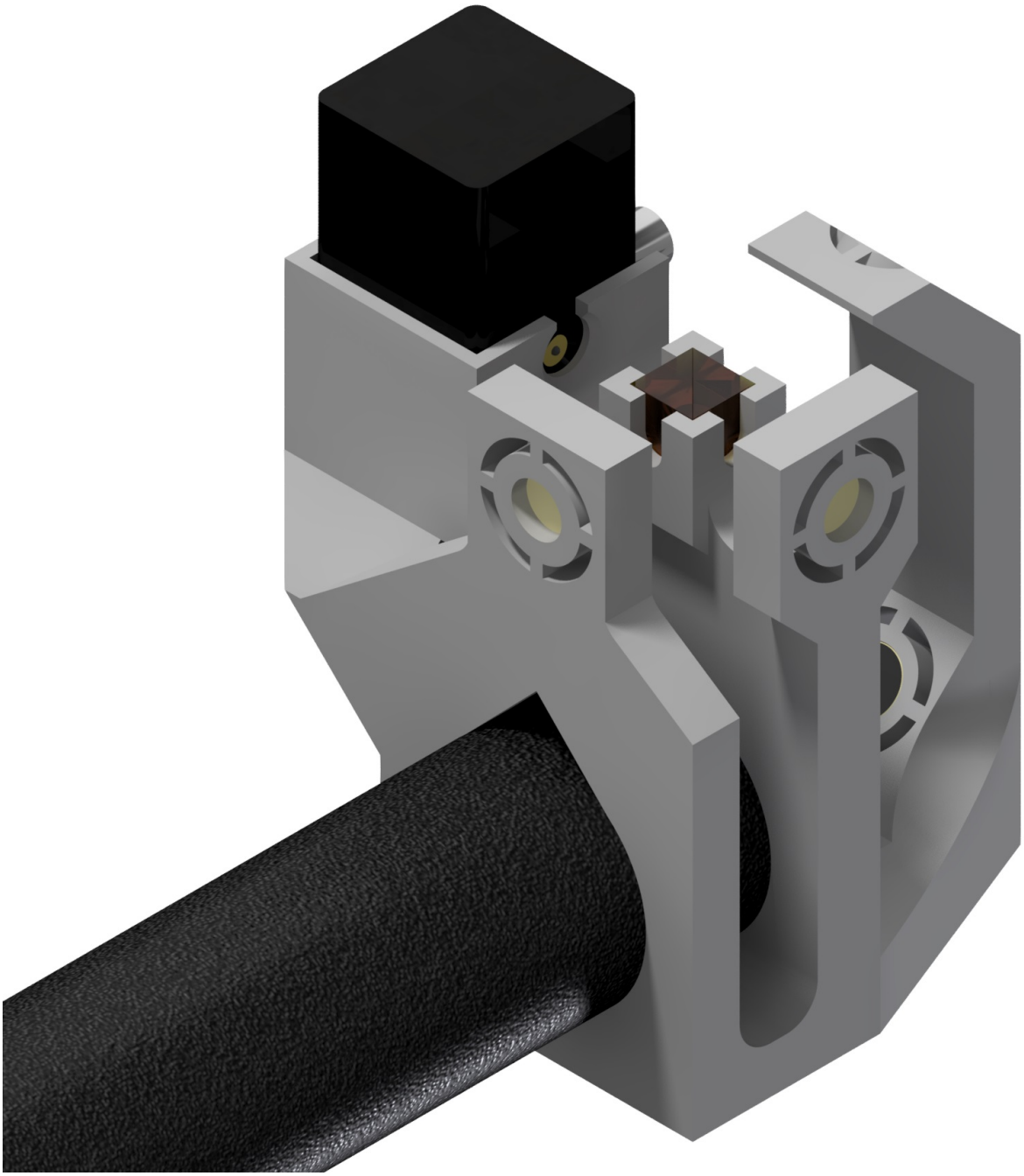

Figure D.9: Micro-Michelson: V2 design. The first iteration on figure D.4. This design incorporated the contraction-calibrated mirror mounts. The small deviations still ruined the laser alignment.

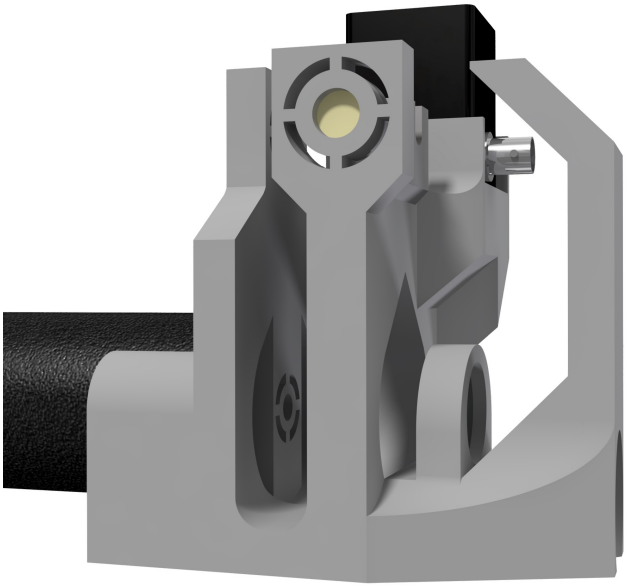

Figure D.10: Micro-Michelson: V3 design. The laser was expanded, and the top section stabilized against contraction. Produces the alignment seen in figure D.11.

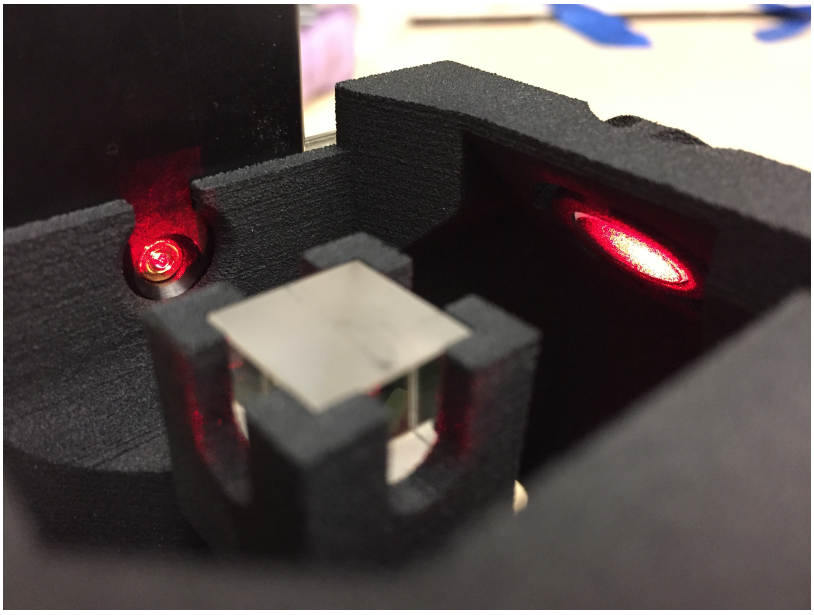

Figure D.11: Micro-Michelson: V3 alignment. Produced from the design seen in figure D.10. While the design did send the laser along the correct paths, we did not see any signature of interference.

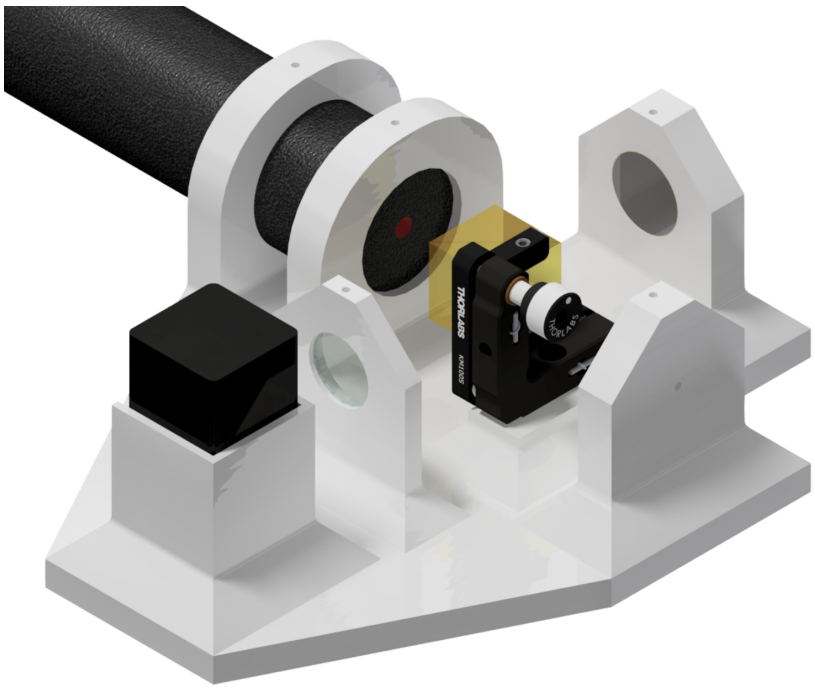

Figure D.12: Hyper compact Michelson design. Note how all angles are 90^o.

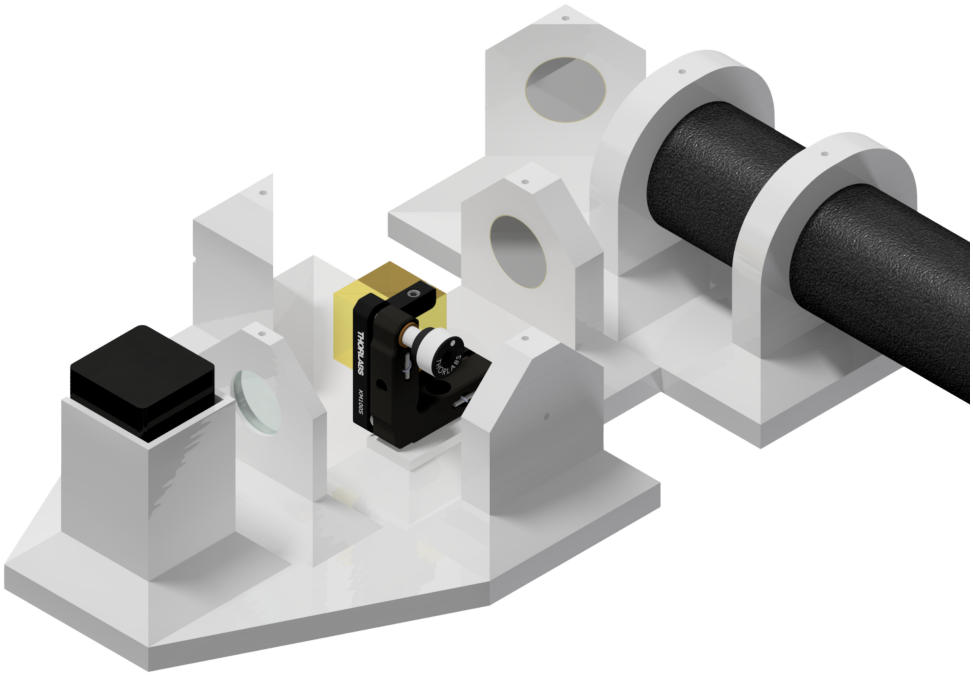

Figure D.13: Compact Michelson design. This design incorporates an angle to test the capability of manufacturing accuracy.